Microbial activity in energy-rich and redox-variable ecosystems

Dissertation

zur Erlangung des Grades eines Doktors der Naturwissenschaften

- Dr. rer. nat. -

am Fachbereich Biologie/Chemie

der Universität Bremen

Marit R. van Erk

August 2021

Die vorliegende Arbeit wurde in der Arbeitsgruppe Mikrosensoren am Max-Planck-Institut für Marine Mikrobiologie in Bremen angefertigt.

1. Gutachter: Dr. Dirk de Beer
2. Gutachter: Dr. Timothy Ferdelman

1. Prüfer: Prof. Dr. Kai Bischof
2. Prüfer: Prof. Dr. Tilmann Harder

Datum des Promotionskolloquiums: 14.09.2021

Diese zur Veröffentlichung erstellte Version der Dissertation enthält Korrekturen

What we know is a drop, what we don't know is an ocean

Isaac Newton

Table of Contents

I. Introduction

Chapter 1: Introduction

II. Manuscripts

III. Discussion

Chapter 6: Discussion and future perspectives

Acknowledgements 159

Appendices

Summary

Microbial mineralization in intertidal sandy sediments plays an essential role in coastal carbon cycling. Surface sediments in these dynamic systems frequently switch between oxic and anoxic conditions depending on factors such as tides and waves. Additionally, they are occasionally subjected to the sudden, high deposition of organic material. When the production rate of the reduced products of anaerobic degradation is higher than the transport rate of oxygen into the sediments, reduced intermediates can accumulate and eventually be exported from the sediments. The aim of this study was to improve the understanding of the response of microbial activity to dynamics in electron donor and acceptor availability, particularly of anaerobic microbial degradation of the organic material.

In Chapter 2, a sandy beach on the island of Helgoland was explored, which regularly receives large depositions of kelp debris. A combination of in situ and laboratory microsensing, ^{35}S radiotracer incubations, porewater and sediment analyses, and molecular analyses was used to address the impact of kelp deposition on microbial mineralization and community composition in underlying sandy sediments. The sedimentary biogeochemical conditions on the beach were distinct, with high concentrations of nutrients, dissolved organic and inorganic carbon, and a low pH. Kelp deposition shaped the microbial community, which is optimized for the use of kelp material. The community could immediately degrade kelp upon deposition, which fostered high production rates of reduced products. As these rates were higher than the transport rate of oxygen into the sediments, sulfide accumulated and was exported from the sediments. The export of sulfide to the sea led to the development of a diverse community of filamentous sulfide-oxidizing bacteria.

As Chapter 2 highlighted that the microbial community in sediments associated with kelp deposits must be highly specialized to be able to deal with the complex organic material in kelp, Chapter 3 aimed to illuminate the adaptation of microbial communities in these sediments to the degradation of kelp-derived carbohydrate substrates. Oxygen microsensor and ^{35}S radiotracer methods showed strong increases in aerobic respiration and sulfate reduction rates after the addition of specific carbohydrates. The community was indeed specialized to the degradation of kelp-derived carbohydrates. Remarkably, kelp-derived polysaccharides often led to higher aerobic respiration rates than monomers. Monosaccharide analysis and microarray analysis were used to determine the substrate pools in sediments. Respiration rates were up two orders of

magnitude higher than in reference sediments, though substrate pools were approximately equal. Thus, substrate turnover rates are much higher on beaches with regular kelp deposition, where microbial communities are more active and are specialized in the carbohydrates they often encounter.

Chapter 4 focused on illuminating the effect of transient oxygen exposure on the efficiency of microbial mineralization in an intertidal sandflat in the Wadden Sea. This included testing the hypothesis that reactive oxygen species (ROS) are present in high concentrations in intertidal permeable sediments and control microbial mineralization rates. We incubated sediment slurries that transitioned from oxic to anoxic conditions and slurries that were anoxic throughout the incubation period. Furthermore, we measured hydrogen peroxide concentrations in porewater. Sulfate-reducing bacteria in intertidal permeable sediments are frequently exposed to oxygen. Yet, this did not select for sulfate-reducing bacteria that perform sulfate reduction in the presence of oxygen. Whereas oxygen inhibited sulfate reduction, the sulfate-reducing bacteria were not eliminated by oxygen, but sulfate reduction instantly resumed after oxygen was depleted. The presence of oxygen even boosted subsequent sulfate reduction in the anoxic period. This could be related to oxygen-stimulated hydrolysis of macromolecules during the oxic period. High levels of ROS were found in the porewater of the intertidal flat. ROS are detrimental for microorganisms, as they are able to degrade cellular components and thus lead to cell death. Indeed, removal of ROS in slurry incubations led to strongly increased microbial mineralization rates. This study highlights the contradictory effects of redox shifts on mineralization efficiency, with the presence of oxygen increasing efficiency of subsequent anaerobic processes, even though ROS appeared to inhibit mineralization.

In Chapter 5, a sulfide-oxidizing community forming egg-shaped sulfur structures on top of a hot smoker in the deep-sea was studied. Hydrodynamics around such structures are dominated by diffusion, contrary to the advection-dominated system of Chapter 2. Both studied systems are characterized by input of reduced material in an oxic ecosystem, and are therefore out of thermodynamic equilibrium. Comparison between the systems described in Chapter 2 and Chapter 5 aimed to further illuminate the oxidative side of the sulfur cycle in the two contrasting energy-rich redox-variable systems. Different environmental conditions, including hydrodynamics, select for specific sulfide-oxidizing communities and morphologies. The mixing of sulfide into turbulent oxygenated seawater led to the development of filamentous mats of sulfide-oxidizing bacteria growing on rocks at the low tide waterline of the beach (Chapter 2). This attachment

prevents the sulfide-oxidizing bacteria from being washed away, and the filamentous structure allows them to make optimal use of the dynamic conditions of the turbulent seawater. On the other hand, the egg-shaped gelatinous sulfur structure produced by sulfide-oxidizing bacteria (Chapter 5) might result from the narrow overlap of oxygen and sulfide which are provided from the same direction.

Overall, this study shows that changes in the availability of electron donors and acceptors, and thus redox dynamics, have a large effect on microbial activity. Large influxes of organic material result in a system that is out of thermodynamic equilibrium, and exports reduced compounds towards the sea. Microbial communities are optimized for these conditions, and can directly access the available organic material, while also being able to make use of the reduced compounds that result from microbial mineralization. Sulfide-oxidizing bacteria at the low tide waterline are adapted to the especially dynamic conditions of this environment. While the production of ROS reduces microbial mineralization, the presence of oxygen should not only be seen as an inhibitor of anaerobic microbial mineralization, but also as crucial to the production of electron donors available at the start of anoxia. This study therefore highlights the importance of spatio-temporal dynamics in electron donor and acceptor availability for microbial activity.

Zusammenfassung

Die mikrobielle Mineralisierung in sandigen Sedimenten der Gezeitenzone spielt eine wesentliche Rolle im küstennahen Kohlenstoffkreislauf. Oberflächensedimente in diesen dynamischen Systemen wechseln in Abhängigkeit von Faktoren wie Gezeiten und Wellen häufig zwischen oxischen und anoxischen Bedingungen. An den sandigen Küsten kommt es zudem durch Stürme oder andere Umwelteinflüsse zu unregelmäßigen großen Anlandungen und Ablagerung von organischem Material. Im Sediment sammeln sich reduzierte Zwischenprodukte an und werden daraus transportiert, wenn die Produktionsrate von Reduktanten des anaeroben Abbaus höher ist als die Transportrate von Sauerstoff in das Sediment. Das Ziel dieser Studie war es, das Verständnis der Reaktion mikrobieller Aktivität auf solche Dynamiken bei der Verfügbarkeit von Elektronendonatoren und -akzeptoren zu verbessern, vor allem bezogen auf den anaeroben mikrobiellen Abbau des organischen Materials.

In Kapitel 2 wurde ein Sandstrand auf der Insel Helgoland untersucht, an dem regelmäßig große Ablagerungen von Kelp auftreten. Um die Auswirkungen der Kelpablagerung auf die mikrobielle Mineralisierung und die Zusammensetzung der Gemeinschaft in den darunter liegenden sandigen Sedimenten zu untersuchen, wurden in und ex situ Mikrosensormessungen, in Kombination mit ^{35}S-Radioaktivtracer-Inkubationen, Porenwasser- und Sedimentanalysen sowie molekularen Analysen durchgeführt. Die sedimentären biogeochemischen Bedingungen am Strand zeichneten sich vor allem durch hohe Nährstoffkonzentrationen mit gelöstem organischem und anorganischem Kohlenstoff, sowie einem niedrigen pH-Wert aus. Die Ablagerung von Kelp führt zu der Etablierung einer mikrobiellen Gemeinschaft, die auf die Zersetzung von Kelpmaterial spezialisiert ist. Diese mikrobielle Gemeinschaft konnte Kelp bei der Ablagerung sofort abbauen, was zu hohen Produktionsraten von Reduktanten führte. Das Übermaß an Reduktanten im Vergleich zur Sauerstofftransportrate in die Sedimente, führte zu einer Anreicherung von Sulfid, welches aus den Sedimenten exportiert wurde. Der Export von Sulfid ins Meer führte zur Entwicklung einer vielfältigen Gemeinschaft von filamentösen sulfidoxidierenden Bakterien.

Während Kapitel 2 verdeutlicht, dass die mikrobielle Gemeinschaft in Sedimenten in Verbindung mit Kelpablagerungen hochspezialisiert sein muss, um mit komplexem organischem Material umgehen zu können, zielte Kapitel 3 darauf ab, die Anpassung mikrobieller Gemeinschaften in diesen Sedimenten an den Abbau von aus Kelp stammenden Kohlenhydratsubstraten näher zu beschreiben. Sauerstoff-Mikrosensormessungen und ^{35}S-Radioaktivtracer-Methoden zeigten

starke Zunahmen der aeroben Atmung und der Sulfatreduktionsraten nach Zugabe spezifischer Kohlenhydrate. Die mikrobielle Gemeinschaft war demnach tatsächlich auf den Abbau von aus Kelp gewonnenen Kohlenhydraten spezialisiert. Bemerkenswerterweise führten Inkubationen mit im Kelp vorkommenden Polysacchariden oft zu höheren aeroben Atmungsraten als die mit Monomeren. Zur Bestimmung der Substratzusammensetzung in Sedimenten wurden Monosaccharid-Analysen und Microarray-Analysen verwendet. Sowohl die aerobe Atmung als auch die Sulfatreduktionsrate waren zwei Größenordnungen höher als in Referenzsedimenten, obwohl die Substratzusammensetzung ähnlich war. Der Substratumsatz an Stränden mit regelmäßiger Kelpablagerung ist viel höher, da dort mikrobielle Gemeinschaften aktiver sind und auf die Kohlenhydrate spezialisiert sind, denen sie häufig begegnen.

In Kapitel 4 wurden die Auswirkungen einer vorübergehenden Sauerstoffexposition auf die Effizienz der mikrobiellen Mineralisierung in einer Sandbank im Wattenmeer untersucht und beschrieben. Dies beinhaltete das Testen der Hypothese, dass reaktive Sauerstoffspezies (ROS) in hohen Konzentrationen in durchlässigen Sedimenten der Gezeitenzone vorhanden sind, und diese die mikrobiellen Mineralisierungsraten kontrollieren. Wir inkubierten Sediment-Schlammgemisch, welches erst oxisch und dann anoxisch wurde, und Sediment-Schlammgemisch, welches während der gesamten Inkubationszeit anoxisch war. Darüber hinaus wurde die Wasserstoffperoxidkonzentrationen im Porenwasser gemessen. Sulfatreduzierende Bakterien in durchlässigen Sedimenten der Gezeitenzone sind häufig Sauerstoff ausgesetzt. Dies selektierte jedoch nicht für Bakterien, die zur Sulfatreduktion in Gegenwart von Sauerstoff fähig sind. Während Sauerstoff die Sulfatreduktion hemmte, wurden die sulfatreduzierenden Bakterien nicht durch Sauerstoff eliminiert, sondern die Sulfatreduktion wurde sofort wieder aufgenommen, nachdem der Sauerstoff aufgebraucht war. Die Anwesenheit von Sauerstoff verstärkte sogar die anschließende Sulfatreduktion in der anoxischen Phase. Diese Beobachtung erklärt sich wahrscheinlich durch die sauerstoffstimulierte Hydrolyse von Makromolekülen während der oxischen Phase. Im Porenwasser des Wattenmeeres wurden hohe ROS-Vorkommen gemessen. ROS sind für Mikroorganismen schädlich, da es zelluläre Bestandteile abbauen kann und somit zum Zelltod führt. Tatsächlich führte die Entfernung von ROS in Inkubationen von Sediment-Schlammgemisch zu stark erhöhten mikrobiellen Mineralisierungsraten. Diese Studie unterstreicht den ambivalenten Effekt von Redoxverschiebungen auf die Mineralisierungseffizienz, wobei die Anwesenheit von Sauerstoff die Effizienz nachfolgender anaerober Prozesse erhöht, ROS jedoch und einen großen negativen Einfluss auf mikrobielle Prozesse aufweisent.

In Kapitel 5 wurde eine sulfidoxidierende Gemeinschaft untersucht, die eiförmige Schwefelstrukturen auf Schwarzen Rauchern in der Tiefsee bildet. Die Hydrodynamik um solche Strukturen von Diffusion dominiert, im Kontrast zum advektionsdominierten System von Kapitel 2. Beide untersuchten Systeme zeichnen sich durch den Eintrag von reduziertem Material in ein oxisches Ökosystem aus und befinden sich daher außerhalb des thermodynamischen Gleichgewichts. Der Vergleich zwischen den in Kapitel 2 und Kapitel 5 beschriebenen Systemen zielte darauf ab, die oxidative Seite des Schwefelzyklus in den beiden kontrastierenden energiereichen Redox-Variablen-Systemen zu verdeutlichen. Verschiedene Umweltbedingungen, einschließlich Hydrodynamik, selektieren für spezifische sulfidoxidierende Gemeinschaften und Morphologien. Der Eintrag von Sulfid in turbulentes sauerstoffreiches Meerwasser führte zur Entwicklung von fadenförmigen Matten aus sulfidoxidierenden Bakterien, die auf Felsen an der Ebbe-Wasserlinie des Strandes wachsen (Kapitel 2). Diese Mattenbildung verhinderte, dass die sulfidoxidierenden Bakterien weggespült werden, denn durch die fadenförmige Struktur können sie die dynamischen Bedingungen des turbulenten Meerwassers optimal nutzen. Eine andere Strategie ist die der sulfidoxidierenden Bakterien (Kapitel 5), welche eine eiförmige gallertartige Schwefelstruktur erzeugen, die aus der engen Überlappung von Sauerstoff und Sulfid resultieren.

Insgesamt zeigt diese Studie, dass Veränderungen in der Verfügbarkeit von Elektronendonatoren und -akzeptoren und damit die Redoxdynamik einen großen Einfluss auf die mikrobielle Aktivität haben. Große Zuflüsse an organischem Material führen zu einem System außerhalb des thermodynamischen Gleichgewichts, das reduzierte Verbindungen in Richtung Meer exportiert. Spezielle mikrobielle Gemeinschaften sind für diese Bedingungen angepasst und können direkt auf das organische Material zugreifen und gleichzeitig die reduzierten Verbindungen nutzen, die aus der mikrobiellen Mineralisierung resultieren. Sulfidoxidierende Gemeinschaften an der Ebbe-Wasserlinie sind an die besonders dynamischen Bedingungen dieser Umgebung angepasst. Während die Produktion von ROS die mikrobielle Mineralisierung reduziert, sollte die Anwesenheit von Sauerstoff nicht nur als Inhibitor für die anaerobe mikrobielle Mineralisierung angesehen werden, sondern stellt vielmehr Elektronendonatoren zu Beginn der Anoxie bereit. Diese Studie unterstreicht daher die Bedeutung der räumlich-zeitlichen Dynamik bei der Verfügbarkeit von Elektronendonatoren und -akzeptoren für die mikrobielle Aktivität.

I. Introduction

1.1 Microbial mineralization of organic material in marine sediments

Carbon is the central element of all organic compounds, and its biogeochemical cycling in marine sediments is coupled to that of many other elements via both biotic and abiotic processes. Marine sediments are supplied with organic compounds produced via photosynthesis in the surface ocean and in photic sediments. In addition, terrestrial organic material can reach the ocean via for instance river input. Heterotrophic microorganisms degrade this organic material for energy generation. Microbial mineralization of organic material is controlled by thermodynamics, kinetics and mass transport of both substrates and electron acceptors. Thermodynamics predicts if a reaction is theoretically possible under certain conditions, i.e. if a reaction would provide enough energy for life, where the available energy yield must be high enough to synthesize ATP (Schink 1997, Bethke et al. 2011). Thermodynamics is evaluated by a reaction's Gibbs free energy, which expresses the energetic yield of a reaction. Only reactions with a negative Gibbs free energy are thermodynamically feasible. In heterotrophic degradation, more negative Gibbs free energy indicates more energy is released per molecule of carbon oxidized, and results in a higher growth yield and possibly even rate. Thermodynamics predicts if a process is possible, but not if it really happens or how fast it can proceed. In contrast, reaction kinetics dictates the actual rates of reactions. Many factors specific to a particular place and time control kinetics, such as the number of catalysts (enzymes or microbial cells), temperature, salinity, microbial growth rates and microbial affinities to the substrate, and substrate and product concentrations. The kinetics of a process can only be poorly constrained for complex redox cascades, and quantification requires empirical measurements. Finally, microbial mineralization can only take place if its reactants encounter one another, a process regulated by mass transport.

The limiting step in the microbial mineralization of organic material is often considered to be hydrolysis (Arnosti 2004). Organic molecules with high molecular weight must first be hydrolysed before they can be taken up (Weiss et al. 1991, Reintjes et al. 2017). Hydrolysis converts high molecular weight compounds to smaller organic molecules such as oligosaccharides, amino acids, and long-chain fatty acids, and is thus the first step of the mineralization of macromolecular compounds in marine sediments. Hydrolysis products are further broken down through fermentation, in which organic compounds serve both as a source and sink of electrons, forming hydrogen and short chain fatty acids such as acetate. To perform hydrolysis, microorganisms must contain the correct enzymes. Enzymes are substrate- and bond-specific. Thus, a large set of enzymes is needed to degrade even one complex molecule. As the diversity of organic

compounds in marine systems is also large, exponentially more enzymes are needed to degrade a substantial portion of these molecules.

The degradation of complex organic material under anoxic conditions requires the interaction of many metabolic processes that are not encoded in single organisms (Figure 1). Products of hydrolysis and fermentation are substrates for downstream terminal degradation processes to carbon dioxide and water, e.g. sulfate reduction (Canfield et al. 2005). The activity of microorganisms performing the downstream processes thus depends on that of hydrolysing and fermenting bacteria. Within marine sediments, concentrations of the fermentation products hydrogen and volatile fatty acids are generally low, resulting from the tight relationship between fermentation and the terminal oxidation process, for example sulfate reduction (Wellsbury and Parkes 1995, Hoehler et al. 1998). Changes in environmental conditions such as temperature increases or physical disturbance can disrupt the balance between fermentation and the terminal oxidation process (Arnosti et al. 2005, Finke and Jørgensen 2008). These disruptions can lead to higher rates of fermentation compared to the terminal oxidation processes and therefore to an accumulation of hydrogen and volatile fatty acids (Finke and Jørgensen 2008).

Heterotrophic degradation of organic material can occur via several electron acceptors, i.e. oxygen, nitrate, Fe(III), Mn(IV), sulfate, or via methanogenesis. The importance of the individual electron acceptors depends on conditions such as the supply rate of organic material and electron acceptors. Oxygen concentrations in seawater are relatively low (around 250 μM), and oxygen is therefore usually depleted within the first few millimeters to centimeters of marine sediment (Glud 2008). Sulfate concentrations are much higher (28 mM). Sulfate reduction can account for 50% of the degradation of organic material in coastal sediments (Jørgensen 1982a). The electron acceptors Fe(III) and Mn(IV) occur in solid-phase and therefore differ from the other electron acceptors in the redox cascade. The rate of Fe(III) and Mn(IV) reduction is determined by, amongst others, local mineralogy (Burdige et al. 1992, Bonneville et al. 2004). Depending on the dominant mineral available, Fe(III) reduction can be more or less favorable than sulfate reduction under the same environmental conditions (Thamdrup et al. 1994, Thamdrup 2000).
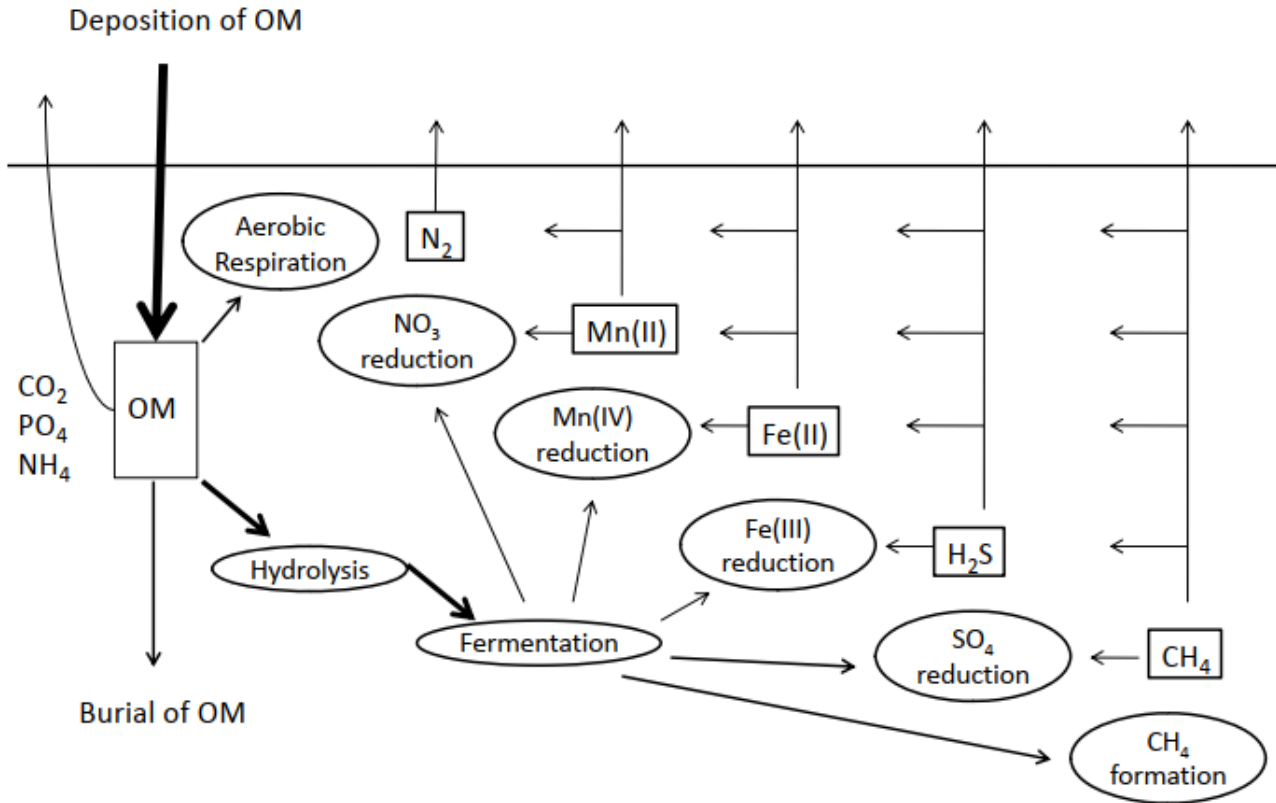
Figure 1: Pathways of degradation of organic material in marine sediments. Ovals represent processes. Rectangles represent reduced products from the reaction, and are placed above the reaction. These products can subsequently diffuse upwards and be oxidized by electron acceptors higher in the sequence, as indicated by the arrows. Taken from Middelburg and Levin (2009).

In the classical view of early diagenesis in marine sediments, organic material is ultimately degraded in steps via a sequence of these electron acceptors (Froelich et al. 1979) (Figure 1), as these reactions all have a different energy yield. The standard Gibbs free energy becomes less negative, thus less thermodynamically favorable, going from aerobic respiration to methanogenesis (Table 1). These distinct energy yields are the basis for sediment stratification over time and with depth into zones characterized by a dominant electron acceptor, i.e. the "redox cascade" (Froelich et al. 1979). The electron acceptor highest in the sequence is used until depletion, after which the next electron acceptor takes over. The final energy yield of these reactions further depends on the composition of the organic material and the type and concentration of intermediates (Arndt et al. 2013). However, this ideal thermodynamics-based model is often insufficient to explain observations in the environment, namely overlapping zones or a reversed order of the dominant electron acceptor. For example, sulfate reduction occurred in

the presence of oxygen in a marine microbial mat (Visscher et al. 1992), aerobic denitrification in permeable sandy sediments (Gao et al. 2010), and sulfate reduction can precede iron reduction (Postma and Jakobsen 1996). These observations illustrate that the final outcome of competition between microorganisms and their redox processes depends not only on thermodynamics.

Table 1: *The standard Gibbs free energy (ΔG^0) of the oxidation of organic material coupled to different electron acceptors. Taken from Middelburg (2019), based on Berner (1980).*

Degradation pathway	Reaction	ΔG^0 (kJ mol^{-1} of CH_2O)
Aerobic respiration	$CH_2O + O_2 \Leftrightarrow CO_2 + H_2O$	−475
Denitrification	$CH_2O + 0.8\ NO_3^- \Leftrightarrow 0.4\ N_2 + 0.8\ HCO_3^- + 0.2\ CO_2 + 0.6\ H_2O$	−448
Manganese oxide reduction	$CH_2O + 3\ CO_2 + 2\ MnO_2 + H_2O \Leftrightarrow 2\ Mn^{2+} + 4\ HCO_3^-$	−349
Iron(hydr)oxide reduction	$CH_2O + 7\ CO_2 + 4\ Fe(OH)_3 \Leftrightarrow 4\ Fe^{2+} + 8\ HCO_3^- + 3\ H_2O$	−114
Sulfate reduction	$CH_2O + 0.5\ SO_4^{2-} \Leftrightarrow 0.5\ H_2S + HCO_3^-$	−77
Methanogenesis	$CH_2O \Leftrightarrow 0.5\ CO_2 + 0.5\ CH_4$	−58

The degradation of organic material results in the production of reduced products, e.g. Fe^{2+}, sulfide and methane, produced via iron reduction, sulfate reduction, and methanogenesis, respectively. These reduced products are reoxidized within the sediments (Berner 1980) in zones where more favorable electron acceptors are still available (Figure 1). Ultimately, oxygen oxidizes all remaining reduced products. Thus, when all cycles are coupled, the total sediment oxygen consumption is an indicator for total sedimentary mineralization (Canfield et al. 1993a). Oxygen consumption in marine sediments thus occurs via both aerobic respiration and abiotic and biotic reoxidation of the reduced products of anaerobic degradation of organic material (Glud 2008). This latter process can dominate over aerobic resirpation, for example in *Beggiatoa* mats where the majority of oxygen consumption is used for sulfide oxidation (Jørgensen 1982b).

Reoxidation reactions and the tight coupling between fermentation and terminal oxidation processes can result in low concentrations of reaction intermediates. Their steady-state concentrations reflect the balance between production and consumption. Turnover of reaction intermediates can lead to so-called "cryptic" cycles, where concentrations of compounds that are continuously turned over are too low to be measured. For example, rapid reoxidation of sulfide

can hide active sulfate reduction. Cryptic sulfur cycling has been demonstrated in both the water column and sediments (Canfield et al. 2010, Holmkvist et al. 2011). In the Chilean oxygen minimum zone, sulfide concentrations are very low, although an active sulfur cycling community exists. In this environment, coupling of the sulfur and nitrogen cycle leads to the rapid reoxidation of sulfide. Despite the low dissolved sulfide concentrations, sulfate reduction can be responsible for a third of the total carbon mineralization, demonstrating the importance of cryptic cycling (Canfield et al. 2010). In marine sediments of the Aarhus Bay, Denmark, a cryptic sulfur cycle was suggested below the sulfate-methane transition zone, where sulfate is usually absent or present in only low concentrations. The sulfide in the deep sediment is oxidized by Fe(III) minerals, leading to a range of intermediates and finally sulfate (Holmkvist et al. 2011). Furthermore, cryptic iron and methane cycling exists (Berg et al. 2016, Beulig et al. 2019). Although not apparent, cryptic cycling can be very important in biogeochemical element cycles and the coupling between them. Thus, pool sizes in marine sediments are not representative for process rates.

1.2 Microbial communities and transport processes in intertidal sediments

Sandy sediments were regarded as not very active in terms of mineralization, because the content of organic material and bacterial numbers are generally low (Jickells and Rae 1997, Llobet-Brossa et al. 1998). Sediment in coastal areas consists of 50 to 70% of sand (Emery 1968). The dominant mode of transport in these permeable sandy sediments is advection rather than diffusion. This is due to sand´s substantially higher permeability. On the centimeter- to decimeter-scale, pressure-driven advective transport of organic material and electron acceptors is much faster than their concentration-driven diffusional transport. The view that sandy sediments are not active sites of mineralization changed when it was revealed that fast advective exchange of dissolved and particulate compounds between the water column and sediments allows for high rates of organic matter turnover (Huettel and Rusch 2000, Rusch and Huettel 2000). Permeable intertidal sediments serve as biocatalytic filters that can maintain high rates of mineralization (De Beer et al. 2005).

The community in coastal sandy sediments is dominated by bacteria, with only minor proportions of archaea and eukaryotes (Musat et al. 2006). Despite the continuous exchange of porewater, communities in seawater and sediment significantly differ (Rusch et al. 2003). The majority of the community in sediments is associated with sand grains. Cell abundances in porewater are only

0.2% of sand grain-associated cell numbers (Rusch et al. 2003, Gobet et al. 2012). This attachment to sand grains prevents microorganisms from being washed off of the sediment, and explains the low exchange of sedimentary bacterial communities with the water column. Dominant members of the sedimentary community are *Planctomycetes*, *Bacteroidetes*, *Gammaproteobacteria* and *Deltaproteobacteria* (Rusch et al. 2003, Musat et al. 2006, Lenk et al. 2011, Gobet et al. 2012). Both the *Planctomycetes* and the *Bacteroidetes* are presumably heterotrophic organisms that are able to degrade complex macromolecules. Members of the *Deltaproteobacteria* and *Gammaproteobacteria* in intertidal sediments can perform sulfate reduction and sulfide oxidation, respectively (Lenk et al. 2011).

Transport in intertidal environments occurs via advection and mixing by waves, tides, storms and animal activity. This combination makes intertidal sandy sediments extremely dynamic and selects for a community that is adapted to rapid environmental changes. Redox conditions in surface intertidal sediments transition between oxic and anoxic conditions. During high tide, oxygen can penetrate several centimeters, while during low tide, oxygen can be completely consumed in surface sediments (Jansen et al. 2009). Thus, a strong selection pressure exists for the ability to survive both of these conditions (Marchant et al. 2017). Furthermore, due to deep advection and sediment mixing by tidal and wave action, the microbial community is homogeneous within the top few centimeters of intertidal sandy sediment (Musat et al. 2006). Sulfate-reducing bacteria are present in the oxic zone, while typical aerobic organisms occur in deep, predominantly anoxic, sediment layers (Musat et al. 2006). Consequently, the microbial communities inhabiting surface sediments have to adapt to large spatial and temporal heterogeneity and mechanical and oxidative stress induced by transport processes.

1.3 Reactive oxygen species

Reactive oxygen species (ROS) such as superoxide ($O_2^{\cdot-}$), hydrogen peroxide (H_2O_2) and the hydroxyl radical ($OH^{\cdot}$) are important for controlling activity and growth of sedimentary communities. ROS are highly reactive molecules. They are both detrimental and required for life. Microorganisms can use ROS for e.g. nutrient acquisition (Rose et al. 2005) , pathogen resistance (Armoza-Zvuloni et al. 2016) and as signaling molecules (Aguirre et al. 2005). However, at detrimental concentrations ROS have the potential to damage enzymes or destroy biomolecules of anaerobic organisms (Imlay 2013). Organisms can regulate the ROS concentrations within their cells via ROS-removing enzymes (Fridovich 1998) such as superoxide dismutase and

catalase. Superoxide is converted by superoxide dismutase to hydrogen peroxide and oxygen (reaction 1), while hydrogen peroxide is converted by catalase to water and oxygen (reaction 2):

$$2O_2^{\cdot-} + 2H^+ \rightarrow H_2O_2 + O_2 \quad (1)$$

$$2H_2O_2 \rightarrow 2H_2O + O_2 \qquad (2)$$
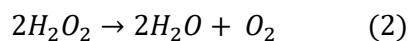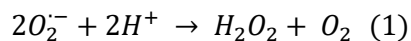
ROS can be produced via a variety of biotic and abiotic processes (Hansel and Diaz 2021). Biotic ROS formation includes both intracellular and extracellular processes, such as byproduction in metabolic processes (Fridovich 1998). Especially abiotic reactions forming ROS can be of importance in intertidal environments. These reactions could involve oxygen, reduced iron and sulfide. When in contact with reduced metals, hydrogen peroxide can be converted to the hydroxyl radical, which can degrade most organic molecules (Imlay 2013, Trusiak et al. 2018). ROS formation further occurs by oxidation of sulfide and Fe(II) (Burns et al. 2010, Murphy et al. 2016), and reactions with pyrite (Borda et al. 2001). These abiotic reactions could make intertidal sediments particularly important environments for ROS production, as oxygen and iron and sulfide are actively cycled and often encounter one another. The iron cycle is also intimately linked to the sulfur cycle, making the dynamics and formation of ROS in intertidal environments extremely complex.

1.4 Iron and sulfur cycling in marine sediments

Dissimilatory sulfate reduction is the main anaerobic pathway for the oxidation of organic material in marine sediments (Jørgensen 1982a). A diverse group of organisms is able to perform sulfate reduction, most of which are bacteria (Jørgensen et al. 2019). The majority of these sulfate-reducing bacteria belong to the *Deltaproteobacteria* (Wasmund et al. 2017). Sulfate-reducing bacteria are able to use a wide spectrum of low molecular weight fermentation products and thus depend on the activity of organisms performing hydrolysis and fermentation. In marine sediments, acetate is an important substrate, as can be propionate, butyrate and hydrogen (Sørensen et al. 1981). Sulfate reduction rates depend on the concentration of degradable organic material and temperature (Al-Raei et al. 2009). Sulfide that diffuses down into deeper sediments can react with iron to form iron sulfides (Berner 1984), or with organic material to form sulfidized organic material (Dale et al. 2009), but the majority of sulfide is oxidized within the sediments.

In contrast to sulfate reduction, the electron acceptor in iron reduction, Fe(III), is in the solid phase. It is not very soluble under marine conditions, and is therefore mainly present in minerals or clays.

Iron-reducing bacteria can outcompete sulfate-reducing bacteria for the same substrates (Lovley and Phillips 1987). Iron reduction can be important in environments with extensive bioturbation, relatively low organic carbon input, and relatively high solid-phase iron concentrations (Burdige 1993). Here, bioturbation transports iron sulfides to the oxic zone, thereby exposing iron sulfides to oxygen, leading to oxidation and formation of iron oxides. These iron oxides are subsequently reduced via oxidation of organic material. This efficient recycling of iron, where iron can be cycled at least 100 times before permanent burial (Thamdrup 2000), increases the importance of iron reduction in organic matter oxidation (Canfield et al. 1993b). Several genera within the bacteria and archaea perform microbial iron reduction (Thamdrup 2000), such as *Geobacter* and *Shewanella*. Iron reduction can also be performed by some sulfate-reducing bacteria (Lovley 1991). The main pathway of abiotic iron reduction of iron oxides is reaction with sulfide (Thamdrup 2000). Iron reduction produces soluble Fe^{2+}, which can be transported upward and oxidized by electron acceptors higher in the redox cascade via both biotic and abiotic processes. Under pH conditions typical of marine sediments, abiotic iron oxidation will outcompete biotic iron oxidation (Nealson 1997). Under conditions typical for the surface ocean, iron oxidation by oxygen is extremely fast (Millero et al. 1987), but when oxygen concentrations and pH are low, abiotic iron oxidation is slow (Roekens and Van Grieken 1983, Morgan and Lahav 2007). Downward transport of Fe^{2+} can lead to formation of FeS and eventually pyrite (Berner 1984). Furthermore, Fe^{2+} can be used as electron source during anoxic photosynthesis (Widdel et al. 1993).

The iron and sulfur cycles in marine sediments are tightly coupled. Sulfide can react with both Fe(III) minerals and Fe^{2+}, producing sulfur intermediates such as elemental sulfur and eventually leading to production of FeS and pyrite (Canfield et al. 1992). The reaction between sulfide and iron oxides is a surface-controlled process. Sulfide is oxidized at the mineral surface of the iron oxide mineral, which produces elemental sulfur and releases Fe^{2+} into solution. Fe^{2+} can subsequently react with additional sulfide to form iron sulfides (Poulton et al. 2004). The reactivity of iron minerals depends on their mineralogy, with iron oxides being much more reactive than iron silicates (Canfield et al. 1992), and different Fe(III) minerals are associated with a different energy yield (Arndt et al. 2013). The high reactivity of iron oxides can lead to sulfide depletion in zones of intense sulfate reduction. Pyrite represents a major sink for both iron and sulfur and is stable over long timescales, although it is unstable when in contact with oxygen (Bottrell and Newton 2006). Therefore, sulfide only builds up in sediments after the reactive iron oxides are depleted and converted to FeS and pyrite (Canfield et al. 1992).

1.5 Sulfide oxidation in the marine environment

Oxidation of sulfide in marine sediments occurs by a variety of abiotic and biotic processes. Sulfide oxidation is usually restricted to the upper sediment, and related to the presence of favorable electron acceptors such as oxygen, nitrate, manganese oxides, and iron oxides (Thamdrup et al. 1994). Sulfide that diffuses towards the sediment surface can be oxidized within the sediments, or may be oxidized on the sediment surface by mats of large sulfur bacteria. Sulfide is rarely oxidized directly to sulfate, but rather to intermediates, such as elemental sulfur, thiosulfate, and polysulfides. These intermediates can then be oxidized further, reduced, or disproportionated. The final product of sulfide oxidation is determined by the oxidant used, the type of the reaction (biotic or abiotic), and for biotic reactions by the microorganisms involved (Jørgensen et al. 2019).

In most environments, the rates of biotic sulfide oxidation exceed those of abiotic sulfide oxidation (Luther III et al. 2011). Yet, competition between these two processes also occurs, especially when abiotic sulfide oxidation occurs via reaction with Fe(III). The outcome of competition is highly dependent on the iron mineral involved, as the reactivity of iron minerals towards sulfide varies greatly with mineralogy. Reaction rate constants differ by several orders of magnitude between the reactive ferrihydrite and the much less reactive sheet silicates (Canfield et al. 1992).

Sulfide oxidation is performed by a diverse group of microorganisms, with a large diversity in the *Alpha-*, *Epsilon-* and *Gammaproteobacteria* (Wasmund et al. 2017). Most sulfide oxidizers are metabolically versatile and can oxidize and reduce various intermediate sulfur species, such as elemental sulfur, thiosulfate, and sulfite (Wasmund et al. 2017). Reaction products can be used for further reactions or can be excreted from the cell (Wirsen et al. 2002). Marine sediments contain many different sulfide oxidizers, although some are confined to narrow niches. Examples of widely distributed sulfide oxidizers are the *Campylobacteriales*, *Arcobacteria*, *Sulfurovum/Sulfurimonas*, *Woeseiaceae/JTB225*, and *Acidiferrobacteraceae* (Wasmund et al. 2017).

Spatial separation of sulfide and oxygen in marine sediments occurs when alternative compounds such as nitrate, oxidize sulfide. Aerobic sulfide oxidizers in these environments must evolve strategies that enable them to bridge this separation. Such strategies include electrogenic sulfur oxidation, intracellular storage of alternative oxidants and/or reductants such as nitrate and

elemental sulfur, and mobility. Electrogenic sulfur oxidation is performed by so-called "cable bacteria", which have special electrogenic pili that allow them to thrive in environments where oxygen and sulfide are spatially separated. They couple sulfide oxidation to oxygen reduction via electronic currents through their pili, or "cables", over centimeter-long distances (Nielsen et al. 2010, Bjerg et al. 2018). Other sulfide oxidizers, the *Beggiatoaceae*, form thick mats on top of sulfidic sediments and oxidize sulfide with oxygen when it is available, or with nitrate that is stored in their vacuoles when oxygen is not available (McHatton et al. 1996, Preisler et al. 2007).

In marine sediments, sulfide is usually oxidized before it reaches the sediment surface, or is buried. Although the presence of free sulfide in the sediment surface or overlying water is not a common phenomenon, it is characteristic of some environments. Well-known examples are hot vents, where smokers release reduced compounds such as sulfide, Fe^{2+} and methane to the water column. In addition, diffusive flow through the sediment (hydrothermal seepage) occurs (Teske et al. 2014). Other marine environments in which free sulfide is present in the sediment surface or bottom water are those with high sulfate reduction rates that exceed sulfide removal rates within the sediments due to large inputs of degradable organic material. For example, whale falls and wood falls in the deep sea and "black spots" in intertidal sediments are all environments where large amounts of organic material are deposited and reduced material leaks out of the sediment (Böttcher et al. 1998, Treude et al. 2009, Bienhold et al. 2013). Also deposition of kelp detritus on beaches is an example of such a system, where large depositions of organic material become available to the intertidal microbial community.

1.6 Kelp deposition in intertidal sandy sediments

Forests of kelp, brown macroalgae, occur along virtually all temperate hard bottom coasts (Dayton 1985, Rafaelli and Hawkins 1985). Kelp holdfasts can be detached from the seafloor by physical forcing during storm events or other physical stresses. Transport of this material can occur over kilometer-long distances (Wernberg and Filbee-Dexter 2018), leading to further fragmentation and deposition on the coastline. The deposition of kelp detritus inputs enormous amounts of degradable organic material to the intertidal zone. Masses of up to 2200 kg wet weight per meter of strandline per year were reported for a South African sandy beach (Stenton-Dozey 1983). Here, the material is prone to degradation by the coastal community.

Underwater forests of kelp are among the most productive ecosystems in the world (Mann 1973) and are characterized by high biomasses. A biomass of 16 kg m^{-2} for the genus *Laminaria* was reported (Mann 1972). Kelp exhibits rapid seasonal growth, with net production rates as high as 1750 g carbon m^{-2} yr^{-1}, which is higher than in terrestrial tropical rain forests (Mann 1973). During growth and senescence kelp releases particulate and dissolved organic material, which provides a carbon source for associated organisms such as benthic and planktonic invertebrates. The kelp forest community is therefore highly productive (Mann 1973).

Kelp-derived carbon forms the basis of food webs, and is found throughout all trophic levels (Duggins et al. 1989). Bacteria play a dominant role in the degradation of kelp on sandy beaches. The dry weight of bacteria is 3 times higher than that of macro- and of meiofauna (Koop and Griffiths 1982), and the biomass produced by heterotrophs on beaches with kelp deposits is mainly bacterial (Koop et al. 1982). Although the biomass of macro- and meiofauna is relatively low, these organisms have an important role in making material available for microbial degradation. They physically fragment the kelp, thereby increasing the surface area of the substrate for bacteria (Koop and Griffiths 1982).

The deposition and subsequent degradation of kelp detritus on beaches represents an important coupling between the ocean and nearshore environments. Beaches, usually environments with low contents of organic material, can sustain high mineralization rates, and release dissolved organic carbon and nutrients back to the sea (Dugan et al. 2011). The extent of accumulation of degradation intermediates and products will depend on factors such as the period organic material resides in the habitat (which can be very short due to relocation by the tides), the transport of both electron acceptors and donors, and the presence of suitable microorganisms.

1.7 Polysaccharide degradation

The main compounds that become available to the intertidal community after kelp deposition are carbohydrates. Although the composition of kelp differs by species and furthermore depends on environmental conditions and season, carbohydrates always make up a high proportion of the dry weight (up to 84%) (Schiener et al. 2015). The main carbohydrate, the structural carbohydrate alginate, can represent up to 40% of the dry weight. Other abundant components of the carbohydrate pool are cellulose (8%), laminarin (7-11%), mannitol (12-19%) (Schiener et al. 2015) and fucoidan (<1% in *Laminaria*, but up to 23% in other species) (Usov et al. 2001, Deniaud-

Bouët et al. 2014). Other compounds such as proteins (3-15% of kelp dry weight (Schiener et al. 2015)) represent a much lower proportion.

Carbohydrates include polysaccharides, oligosaccharides, disaccharides and monosaccharides. Polysaccharides such as alginate, laminarin and fucoidan that are abundant in kelp consist of a series of monosaccharides connected via glycosidic bonds. Polysaccharides can form complex structures (examples from a selection of polysaccharides that are present in macroalgae in Figure 2). An extremely large variety of polysaccharides exist in nature, much larger than the variety of other organic compounds such as proteins and nucleic acids. One polysaccharide can consist of many types of monosaccharides (heteropolysaccharide). But even polysaccharides consisting of one type of monosaccharide (homopolysaccharides) can vary greatly in structure. Two glucose monosaccharides, for example, can be linked via α- or β- glycosidic bonds at 6 different locations of the molecule, thus forming 12 structurally different disaccharides. With increasing length of the molecule, the diversity increases exponentially (Arnosti et al. 2021). Additionally, polysaccharides can have many different groups attached as side branches.
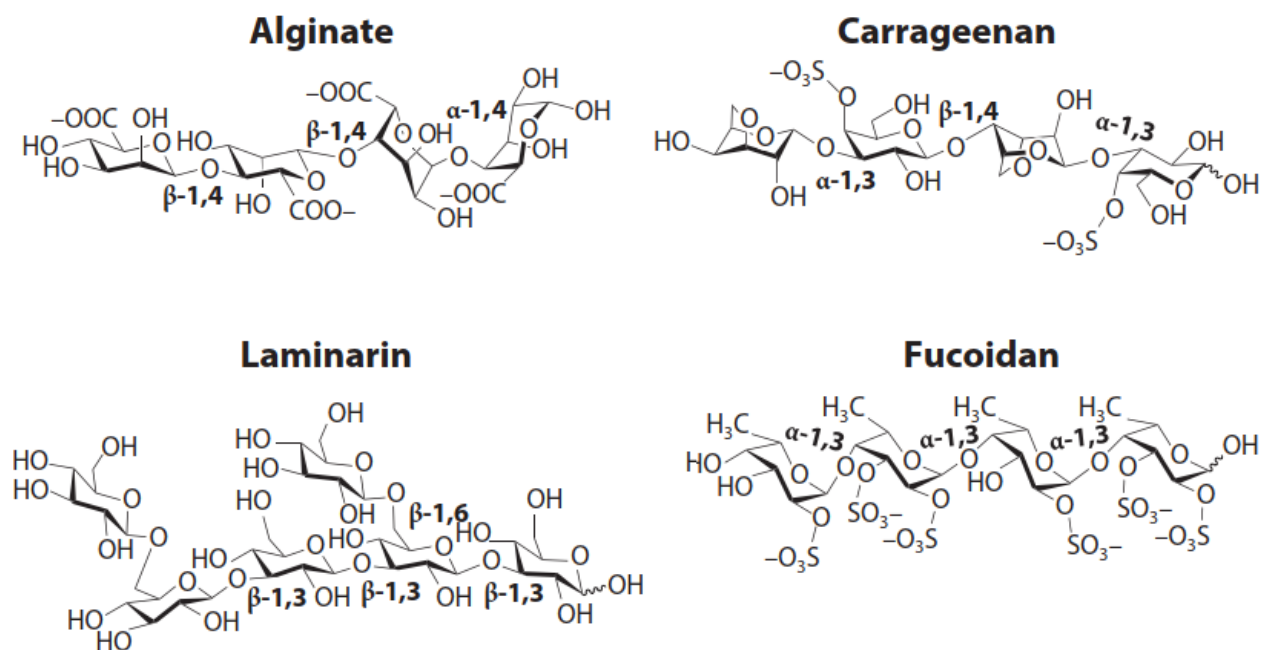

Figure 2: Structures of a selection of polysaccharides that are present in macroalgae (taken from Arnosti et al. (2021)). Used with permission of Annual Reviews, Inc., from The Biogeochemistry of Marine Polysaccharides: Sources, Inventories, and Bacterial Drivers of the Carbohydrate Cycle, Annual Reviews, Inc., 13, 2021; permission conveyed through Copyright Clearance Center, Inc.

The large structural complexity and variety of polysaccharides are a challenge for the heterotrophic microorganisms in marine sediments. Polysaccharide-degrading enzymes of heterotrophic organisms have a structural specificity, therefore for complex polysaccharides heterotrophic organisms must possess a large variety of enzymes. Alternatively, several steps performed by a consortium of microorganisms are needed to completely degrade a complex polysaccharide. Polysaccharides are degraded by so-called carbohydrate active enzymes (CAZymes). These enzymes are part of gene clusters called PULs, which furthermore contain proteins that can sense, bind, transport and hydrolyse the polysaccharides (Bjursell et al. 2006). This clustering couples all the proteins and enzymes that are needed for a specific polysaccharide linkage, thus makes the degradation more efficient (Martens et al. 2009). A CAZyme can be specific for one particular linkage in a polysaccharide molecule, thus often a large group of CAZymes is active to degrade one molecule. Organisms specialized for fucoidan degradation, for example, contain hundreds of different enzymes to break down the molecule (Sichert et al. 2020). CAZymes are divided into families, which are grouped based on the amino acid sequence of the enzyme, with the number of defined families rapidly expanding (>300 families in the database CAZy in 2013; http://www.cazy.org (Lombard et al. 2014)). Two important classes that contain CAZyme families for degradation of polysaccharides are the glycoside hydrolyases (GHs) and polysaccharide lyases (PLs). Another form of enzyme that cleaves polysaccharides are the sulfatases. Sulfatases are also substrate specific and cleave the sulfate group of sulfated polysaccharides from the polysaccharide backbone (Hettle et al. 2018). GHs, PLs, and sulfatases can be endo-acting or exo-acting. Endo-acting enzymes act on linkages midchain of the polysaccharide backbone, which produces oligosaccharides. Exo-acting enzymes on the other hand cleave monosaccharides or disaccharides from the ends of the backbone. Microorganisms shown to be able to degrade polysaccharides in the marine environment include members of *Bacteroidetes* (Fernández-Gómez et al. 2013), *Gammaproteobacteria* (Sarmento et al. 2016), *Planctomycetes* (Lage and Bondoso 2014) and *Verrucomicrobia* (Martinez-Garcia et al. 2012). The large structural variety and complexity of kelp-derived polysaccharides and the wide range of enzymes needed to degrade them provides a challenge for microorganisms in intertidal sediments underlying deposits of kelp detritus.

1.8 Aims of the study

The overall aim of this study was to improve the understanding of microbial activity in energy-rich systems with high dynamics in the availability of electron donors and acceptors. Intertidal permeable sediments and hydrothermal vent systems are such systems, Here, reduced compounds such as sulfide accumulate. Free sulfide at the sediment-water interface or in overlying waters is not common in marine environments, as sulfide is usually oxidized before it reaches the sediment surface, or is buried. However, in environments in which the electron acceptor requirement is higher than its transport rate into sediments, sulfide can accumulate and eventually escape sediments. Similarly, sulfide is emitted into oxygenated seawater by hot smokers at the seafloor.

In this study three of these systems are addressed, for which the export of sulfide has different sources and mechanisms:

1. an intertidal sandy beach on the island of Helgoland, Germany, where sulfidic sediments develop as a result of high and sudden input of degradable kelp (Figure 3A,B);

2. the intertidal sandflat Janssand, Germany, where deep porewater transport occurs, leading to formation of sulfidic seeps when the deep porewater flow reaches the sediment surface (Billerbeck et al. 2006) (Figure 3C,D);

3. the hydrothermal vent system Guaymas Basin, Mexico, a location where sulfide is released by hot smokers, and by hydrothermal seepage through the sediment
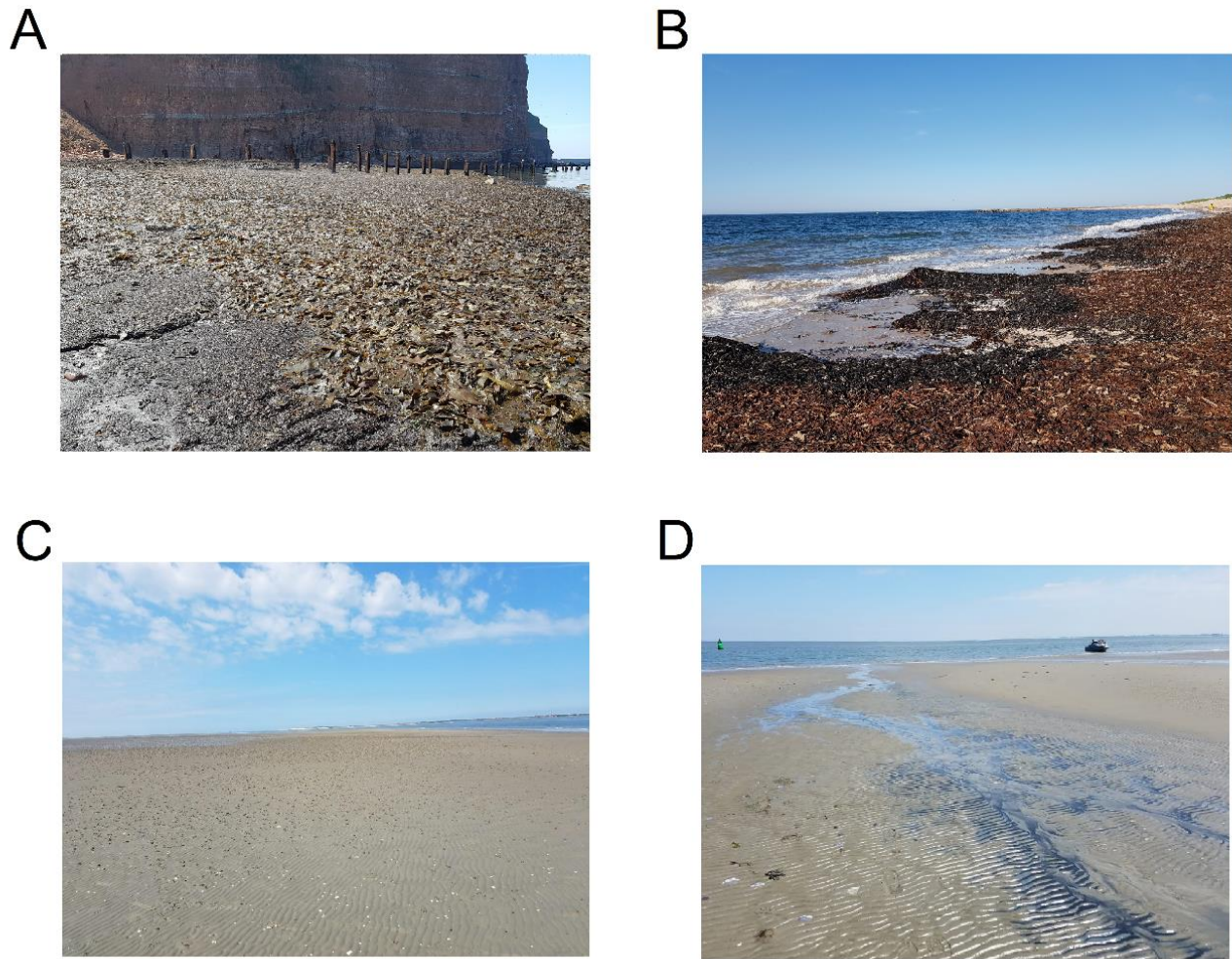
Figure 3: *Intertidal sandy beach on the island of Helgoland, Germany, with depositions of kelp debris in May 2018 (A and B); intertidal sandlfat Janssand, Germany (C), and the sulfidic seeps on Janssand (D). Image courtesy: A: Van Erk et al. (2020); B: Marit R. van Erk; C and D: Olivia M. Bourceau*

Three main questions were addressed in this study, for which the objectives, hypotheses and approaches are discussed below:

1. How do sudden high pulses of complex organic material influence the anaerobic degradation processes in intertidal sediments?

2. How do switches between oxic and anoxic conditions in highly active sediments influence mineralization processes? Does the oxidation of the exported reductants lead to ROS formation, and does ROS inhibit microbial processes?

3. How do contrasting environmental conditions influence the sulfide-oxidizing communities?

1. How do sudden high pulses of complex organic material influence the anaerobic degradation processes in intertidal sediments?

The first objective was to understand how kelp deposition on beaches influences the microbial mineralization processes (Chapter 2), and the availability of kelp-derived organic compounds and products of mineralization in the sediments (Chapters 2 and 3). We hypothesized that sudden deposition of enormous amounts of degradable organic material such as kelp debris would strongly enhance anaerobic decomposition, as the oxygen concentration in seawater is relatively low (~250 µM). Thus, we expected that rates of microbial degradation are strongly enhanced, and dominant degradation pathways are different from those in reference sediments without kelp deposition. Furthermore, intermediates and reduced products such as sulfide and methane would be produced in large amounts. These hypotheses were tested by comparing a beach with regular kelp deposition (kelp-beach) with a second beach on Helgoland where kelp deposition does not occur (reference beach). The main focus was on the sulfur cycle and the fate of sulfide within this environment, as sulfate reduction is important in coastal sediments (Jørgensen 1982a), and high sulfide concentrations have toxic effects (Bagarinao 1992). We analyzed porewater and sediment compositions, and performed radiotracer (^{35}S) incubations and in situ and laboratory microsensor measurements (Chapter 2). Furthermore, we analyzed monosaccharides and polysaccharides in the kelp-beach sediments, and compared these results with reference beach sediments, and kelp fragments (Chapter 3).

The second objective was to determine how microbial communities in intertidal sediment are shaped for the degradation of regular deposited kelp. Kelp is a mixture of compounds that are labile and more recalcitrant. Kelp deposition likely leads to a shift in the community to organisms able to use the specific complex polysaccharides within the kelp. We hypothesize that the

microbial community in kelp-beach sediments is optimized to degrade the kelp material. Microbial communities in intertidal sediments subjected to regular kelp deposition often encounter polysaccharides derived from kelp. Polysaccharides need to be hydrolysed first to sizes small enough to be transported into the cell (Weiss et al. 1991, Reintjes et al. 2017), and sulfate-reducing bacteria depend on the activity of hydrolysers and fermenters for their substrates. We addressed the objective using 16S rRNA analysis of seawater and sediment samples from the kelp-beach and reference beach of Helgoland. We also used radiotracer (^{35}S) incubations to address whether the terminal respiration pathway of sulfate reduction is able to directly respond to kelp deposition (Chapter 2), which would imply that hydrolysis and fermentation are also already active.

Furthermore, we hypothesized that the community would be adapted to specific substrates derived from kelp. We therefore expected that in response to the presence of these substrates rates of aerobic respiration as well as sulfate reduction would be higher compared to those in sediments that do not encounter these substrates. We also hypothesized that polysaccharides that are not present in kelp will not be degraded as fast, as microorganisms might not have the necessary capacities. These hypotheses were tested by laboratory microsensor oxygen consumption measurements and radiotracer (^{35}S) incubations, in which polysaccharides that are present and not present in kelp were added to sediments from the kelp-beach and a reference beach on Helgoland (Chapter 3).

2. How do switches between oxic and anoxic conditions in highly active sediments influence mineralization processes? Does the oxidation of the exported reductants lead to ROS formation, and does ROS inhibit microbial processes?

The first objective was to test the impact of transient oxygenation on anaerobic respiration in intertidal permeable surface sediments of the intertidal sandflat Janssand in the Wadden Sea (Chapter 4). Intertidal sediments are extreme environments for microorganisms due to their dynamic nature in both time and space. Factors such as advection, patchy deposition of organic material, and animal activity make these systems heterogeneous. Oxygen penetration depths and sulfate reduction rates are variable (De Beer et al. 2005, Al-Raei et al. 2009), depending on the transport processes within the sediments: advection, diffusion, bioturbation and bioirrigation, and sediment mixing. These processes transport both organic material and electron acceptors into and out of the sediments. During low tide, oxygen can disappear completely, whereas during tidal

inundation oxygen penetrates a few centimeters into the sediment (De Beer et al. 2005, Jansen et al. 2009). This makes redox conditions within surface sediments variable, likely selecting for organisms that are able to adapt to these conditions. These expectations are based on the observations that anaerobes in the upper sediment maintain high rates of anaerobic respiration, such as dissimilatory nitrate reduction (Marchant et al. 2014) despite variable redox conditions and regular oxygen input.

We expected that sulfate reduction would continue during oxic periods, as an environment that fluctuates multiple times a day between oxic and anoxic conditions would exert a strong selective pressure for sulfate-reducing bacteria capable of coping with oxygen. Sulfate-reducing bacteria capable of respiring in the presence of oxygen were observed previously in cyanobacterial mats (Visscher et al. 1992). However, this would require an adaptation, as in their active state, reduced enzymes with iron cofactors that are involved in sulfate reduction become irreversibly damaged by oxygen and then release ROS leading to cell death (Imlay 2013, Rabus et al. 2013). We tested this hypothesis in Chapter 4. We incubated sediment slurries over an oxic-anoxic period. Furthermore, we incubated sediment slurries that were anoxic from the start. We measured oxygen consumption, sulfate reduction, hydrogen concentrations and Fe^{2+} concentrations throughout the incubation period.

The second objective was to address if ROS play a role in microbial mineralization in intertidal permeable sediments. As surface sediments of the Janssand intertidal sandflat regularly switch between oxic and anoxic conditions and have very active iron and sulfur cycling, we expected that ROS will be produced in this system. Oxygen can easily come in contact with reduced iron and sulfide, producing ROS. ROS could abiotically increase carbon mineralization via hydrogen peroxide, which can induce the Fenton reaction when in contact with reduced iron, producing the hydroxyl radical. The hydroxyl radical is a very strong oxidant of organic material (Imlay 2013, Trusiak et al. 2018). Therefore, we tested if ROS can also affect biomineralization. First, we investigated if ROS are indeed present in Janssand sediments. The potential effect of ROS on biomineralization was addressed by the addition of the ROS-removing enzymes catalase and superoxide dismutase to sediment slurries, in which oxygen concentration, sulfate reduction, hydrogen concentrations and Fe^{2+} concentrations were measured over the course of the incubation.

3. How do contrasting environmental conditions influence the sulfide-oxidizing communities?

Free sulfide that escapes from the sediment surface is rare in the marine environment, and is restricted to special conditions where the rate of supply of oxidants is lower than the rate of sulfide production and upward transport. Based on the local characteristics of the environment, sulfide-oxidizing communities differ. I studied sulfide-oxidizing communities in two especially contrasting environments where free sulfide is transported into oxygenated seawater: the low tide waterline of the beach with kelp deposition on Helgoland (Chapter 2), where filaments are attached to rocks at the low waterline, and communities on top of a hot smoker in the Guaymas Basin, where a conspicuous smooth and transparent egg-shaped structure was formed (Chapter 5). The hypothesis was that the large differences in hydrodynamics and availability of oxygen and sulfide select for specific types of sulfide oxidation. I synthesize the knowledge gain from studying these sulfide oxidizing communities in the general discussion (Chapter 6).

1.9 References

Aguirre, J., M. Ríos-Momberg, D. Hewitt & W. Hansberg (2005). Reactive oxygen species and development in microbial eukaryotes. *Trends Microbiol,* 13, 111-118.

Al-Raei, A. M., K. Bosselmann, M. E. Böttcher, B. Hespenheide & F. Tauber (2009). Seasonal dynamics of microbial sulfate reduction in temperate intertidal surface sediments: controls by temperature and organic matter. *Ocean Dyn,* 59, 351-370.

Armoza-Zvuloni, R., A. Schneider & Y. Shaked (2016). Rapid hydrogen peroxide release during coral-bacteria interactions. *Front Mar Sci,* 3, 124.

Arndt, S., B. B. Jørgensen, D. E. LaRowe, J. J. Middelburg, R. D. Pancost & P. Regnier (2013). Quantifying the degradation of organic matter in marine sediments: A review and synthesis. *Earth Sci Rev,* 123, 53-86.

Arnosti, C. (2004). Speed bumps and barricades in the carbon cycle: substrate structural effects on carbon cycling. *Mar Chem,* 92, 263-273.

Arnosti, C., N. Finke, O. Larsen & S. Ghobrial (2005). Anoxic carbon degradation in Arctic sediments: microbial transformations of complex substrates. *Geochim Cosmochim Acta,* 69, 2309-2320.

Arnosti, C., M. Wietz, T. Brinkhoff, J.-H. Hehemann, D. Probandt, L. Zeugner & R. Amann (2021). The biogeochemistry of marine polysaccharides: sources, inventories, and bacterial drivers of the carbohydrate cycle. *Ann Rev Mar Sci,* 13, 81-108.

Bagarinao, T. (1992). Sulfide as an environmental factor and toxicant: tolerance and adaptations in aquatic organisms. *Aquat Toxicol,* 24, 21-62.

Berg, J. S., D. Michellod, P. Pjevac, C. Martinez-Perez, C. R. T. Buckner, P. F. Hach, C. J. Schubert, J. Milucka & M. M. M. Kuypers (2016). Intensive cryptic microbial iron cycling in the low iron water column of the meromictic Lake Cadagno. *Environ Microbiol,* 18, 5288-5302.

Berner, R. A. (1980). Early diagenesis: a theoretical approach. Princeton University Press.

Berner, R. A. (1984). Sedimentary pyrite formation: an update. *Geochim Cosmochim Acta,* 48, 605-615.

Bethke, C. M., R. A. Sanford, M. F. Kirk, Q. Jin & T. M. Flynn (2011). The thermodynamic ladder in geomicrobiology. *Am J Sci,* 311, 183-210.

Beulig, F., H. Røy, S. E. McGlynn & B. B. Jørgensen (2019). Cryptic CH_4 cycling in the sulfate-methane transition of marine sediments apparently mediated by ANME-1 archaea. *ISME J,* 13, 250-262.

Bienhold, C., P. P. Ristova, F. Wenzhöfer, T. Dittmar & A. Boetius (2013). How deep-sea wood falls sustain chemosynthetic life. *PLoS ONE* 8, e53590.

Billerbeck, M., U. Werner, L. Polerecky, E. Walpersdorf, D. De Beer & M. Huettel (2006). Surficial and deep pore water circulation governs spatial and temporal scales of nutrient recycling in intertidal sand flat sediment. *Mar Ecol Prog Ser,* 326, 61-76.

Bjerg, J. T., H. T. S. Boschker, S. Larsen, D. Berry, M. Schmid, D. Millo, P. Tataru, F. J. R. Meysman, M. Wagner, L. P. Nielsen & A. Schramm (2018). Long-distance electron transport in individual, living cable bacteria. *Proc Natl Acad Sci U S A,* 115, 5786-5791.

Bjursell, M. K., E. C. Martens & J. I. Gordon (2006). Functional genomic and metabolic studies of the adaptations of a prominent adult human gut symbiont, *Bacteroides thetaiotaomicron*, to the suckling period. *J Biol Chem,* 281, 36269-26279.

Bonneville, S., P. Van Cappellen & T. Behrends (2004). Microbial reduction of iron(III) oxyhydroxides: effects of mineral solubility and availability. *Chem Geol,* 212, 255-268.

Borda, M. J., A. R. Elsetinow, M. A. Schoonen & D. R. Strongin (2001). Pyrite-induced hydrogen peroxide formation as a driving force in the evolution of photosynthetic organisms on an Early Earth. *Astrobiology,* 1, 283-288.

Böttcher, M. E., B. Oelschläger, T. Höpner, H.-J. Brumsack & J. Rullkötter (1998). Sulfate reduction related to the early diagenetic degradation of organic matter and "black spot" formation in tidal sandlfats of the German Wadden Sea (southern North Sea): stable isotope (^{13}C, ^{34}S, ^{18}O) and other geochemical results. *Org Geochem,* 29, 1517-1530.

Bottrell, S. H. & R. J. Newton (2006). Reconstruction of changes in global sulfur cycling from marine sulfate isotopes. *Earth Sci Rev,* 75, 59-83.

Burdige, D. J. (1993). The biogeochemistry of manganese and iron reduction in marine sediments. *Earth Sci Rev,* 35, 249-284.

Burdige, D. J., S. P. Dhakar & K. H. Nealson (1992). Effects of manganese oxide mineralogy on microbial and chemical manganese reduction. *Geomicrobiol J,* 10, 27-48.

Burns, J. M., P. S. Craig, T. J. Shaw & J. L. Ferry (2010). Multivariate examination of Fe(II)/Fe(III) cycling and consequent hydroxyl radical generation. *Environ Sci Technol,* 44, 7226-7231.

Canfield, D. E., R. Raiswell & S. H. Bottrell (1992). The reactivity of sedimentary iron minerals toward sulfide. *Am J Sci,* 292, 659-683.

Canfield, D. E., B. B. Jørgensen, H. Fossing, R. Glud, J. Gundersen, N. B. Ramsing, B. Thamdrup, J. W. Hansen, L. P. Nielsen & P. O. J. Hall (1993a). Pathways of organic carbon oxidation in three continental margin sediments. *Mar Geol,* 113, 27-40.

Canfield, D. E., B. Thampdrup & J. W. Hansen (1993b). The anaerobic degradation of organic matter in Danish coastal sediments: Iron reduction, manganese reduction, and sulfate reduction. *Geochim Cosmochim Acta,* 57, 3867-3883.

Canfield, D. E., E. Kristensen & B. Thamdrup (2005). Aquatic Geomicrobiology. Elsevier.

Canfield, D. E., F. J. Stewart, B. Thamdrup, L. De Brabendere, T. Dalsgaard, E. F. Delong, N. P. Revsbech & O. Ulloa (2010). A cryptic sulfur cycle in oxygen-minimum-zone waters off the Chilean coast. *Science,* 330, 1375-1378.

Dale, A. W., V. Brüchert, M. Alperin & P. Regnier (2009). An integrated sulfur isotope model for Namibian shelf sediments. *Geochim Cosmochim Acta,* 73, 1924-1944.

Dayton, P. K. (1985). Ecology of kelp communities. *Annu Rev Ecol Syst,* 16, 215-245.

De Beer, D., F. Wenzhöfer, T. G. Ferdelman, S. E. Boehme, M. Huettel, J. E. E. Van Beusekom, M. E. Böttcher, N. Musat & N. Dubilier (2005). Transport and mineralization rates in North Sea sandy intertidal sediments, Sylt-Rømø Basin, Wadden Sea. *Limnol Oceanogr,* 50, 113-127.

Deniaud-Bouët, E., N. Kervarec, G. Michel, T. Tonon, B. Kloareg & C. Hervé (2014). Chemical and enzymatic fractionation of cell walls from Fucales: insights into the structure of the extracellular matrix of brown algae. *Ann Bot,* 114, 1203-1216.

Dugan, J. E., D. M. Hubbard, H. M. Page & J. P. Schimel (2011). Marine macrophyte wrack inputs and dissolved nutrients in beach sands. *Estuaries Coast,* 34, 839-850.

Duggins, D. O., C. A. Simenstad & J. A. Estes (1989). Magnification of secondary production by kelp detritus in coastal marine ecosystems. *Science,* 245, 170-173.

Emery, K. O. (1968). Relict sediments on continental shelves of world. *Am Assoc Pet Geol Bull,* 52, 445-464.

Fernández-Gómez, B., M. Richter, M. Schüler, J. Pinhassi, S. G. Acinas, J. M. González & C. Pedrós-Alió (2013). Ecology of marine Bacteroidetes: a comparative genomics approach. *ISME J,* 7, 1026-1037.

Finke, N. & B. B. Jørgensen (2008). Response of fermentation and sulfate reduction to experimental temperature changes in temperate and Arctic marine sediments. *ISME J,* 2, 815-829.

Fridovich, I. (1998). Oxygen toxicity: a radical explanation. *J Exp Biol,* 8, 1203-1209.

Froelich, P. N., G. P. Klinkhammer, M. L. Bender, N. A. Luedtke, G. R. Heath, D. Cullen, P. Dauphin, D. Hammond, B. Hartman & V. Maynard (1979). Early oxidation of organic matter in pelagic sediments of the eastern equatorial Atlantic: suboxic diagenesis. *Geochim Cosmochim Acta,* 43, 1075-1090.

Gao, H., F. Schreiber, G. Collins, M. M. Jensen, J. E. Kostka, G. Lavik, D. de Beer, H.-Y. Zhou & M. M. M. Kuypers (2010). Aerobic denitrification in permeable Wadden Sea sediments. *ISME J,* 4, 417-426.

Glud, R. N. (2008). Oxygen dynamics of marine sediments. *Mar Biol Res,* 4, 243-289.

Gobet, A., S. I. Böer, S. M. Huse, J. E. E. Van Beusekom, C. Quince, M. L. Sogin, A. Boetius & A. Ramette (2012). Diversity and dynamics of rare and of resident bacterial populations in coastal sands. *ISME J,* 6, 542-553.

Hansel, C. M. & J. M. Diaz (2021). Production of extracellular reactive oxygen species by marine biota. *Ann Rev Mar Sci,* 13, 177-200.

Hettle, A. G., C. Vickers, C. S. Robb, F. Liu, S. G. Withers, J.-H. Hehemann & A. B. Boraston (2018). The molecular basis of polysaccharide sulfatase activity and a nomenclature for catalytic subsites in this class of enzyme. *Structure,* 26, 747-758.

Hoehler, T. M., M. J. Alperin, D. B. Albert & C. S. Martens (1998). Thermodynamic control on hydrogen concentrations in anoxic sediments. *Geochim Cosmochim Acta,* 62, 1745-1756.

Holmkvist, L., T. G. Ferdelman & B. B. Jørgensen (2011). A cryptic sulfur cycle driven by iron in the methane zone of marine sediment (Aarhus Bay, Denmark). *Geochim Cosmochim Acta,* 75, 3581-3599.

Huettel, M. & A. Rusch (2000). Transport and degradation of phytoplankton in permeable sediment. *Limnol Oceanogr,* 45, 534-549.

Imlay, J. A. (2013). The molecular mechanisms and physiological conseqeuences of oxidative stress: lessons from a model bacterium. *Nat Rev Microbiol,* 11, 443-454.

Jansen, S., E. Walpersdorf, U. Werner, M. Billerbeck, M. E. Böttcher & D. De Beer (2009). Functioning of intertidal flats inferred from temporal and spatial dynamics of O_2, H_2S and pH in their surface sediment. *Ocean Dyn,* 59, 317-332.

Jickells, T. D. & J. E. Rae (1997). Biogeochemistry of intertidal sediments. In *Biogeochemistry of intertidal sediments,* eds. T. D. Jickells & J. E. Rae, 1-15. Cambridge University Press.

Jørgensen, B. B. (1982a). Mineralization of organic matter in the sea bed - the role of sulphate reduction. *Nature,* 296, 643-645.

Jørgensen, B. B. (1982b). Ecology of the bacteria of the sulphur cycle with special reference to anoxic-oxic interface environments. *Philos Trans R Soc Lond B,* 298, 543-561.

Jørgensen, B. B., A. J. Findlay & A. Pellerin (2019). The biogeochemical sulfur cycle of marine sediments. *Front Microbiol,* 10, 849.

Koop, K. & C. L. Griffiths (1982). The relative significance of bacteria, meio- and macrofauna on an exposed sandy beach. *Mar Biol,* 66, 295-300.

Koop, K., R. C. Newell & M. I. Lucas (1982). Biodegradation and carbon flow based on kelp (*Ecklonia maxima*) debris in a sandy beach microcosm. *Mar Ecol Prog Ser,* 7, 315-326.

Lage, O. M. & J. Bondoso (2014). Planctomycetes and macroalgae, a striking association. *Front Microbiol,* 5, 267.

Lenk, S., J. Arnds, K. Zerjatke, N. Musat, R. Amann & M. Mußmann (2011). Novel groups of *Gammaproteobacteria* catalyse sulfur oxidation and carbon fixation in a coastal, intertidal sediment. *Environ Microbiol,* 13, 758-774.

Llobet-Brossa, E., R. Rosselló-Mora & R. Amann (1998). Microbial community composition of Wadden Sea sediments as revealed by fluorescence in situ hybridization. *Appl Environ Microbiol,* 64, 2691-2696.

Lombard, V., H. G. Ramulu, E. Drula, P. M. Coutinho & B. Henrissat (2014). The carbohydrate-active enzymes database (CAZy) in 2013. *Nucleic Acids Res,* 42, D490-D495.

Lovley, D. R. (1991). Dissimilatory Fe(III) and Mn(IV) reduction. *Microbiol Rev,* 55, 259-287.

Lovley, D. R. & E. J. P. Phillips (1987). Competitive mechanisms for inhibition of sulfate reduction and methane production in the zone of ferric iron reduction in sediments. *Appl Environ Microbiol,* 53, 2636-2641.

Luther III, G. W., A. J. Findlay, D. J. MacDonald, S. M. Owings, T. E. Hanson, R. A. Beinart & P. R. Girguis (2011). Thermodynamics and kinetics of sulfide oxidation by oxygen: a look at inorganically controlled reactions and biologically mediated processes in the environment. *Front Microbiol,* 2, 62.

Mann, K. H. (1972). Ecological energetics of the seaweed zone in a marine bay on the Atlantic coast of Canada. I. Zonation and biomass of seaweeds. *Mar Biol,* 12, 1-10.

Mann, K. H. (1973). Seaweeds: their productivity and strategy for growth. *Science,* 182, 975-981.

Marchant, H. K., G. Lavik, M. Holtappels & M. M. M. Kuypers (2014). The fate of nitrate in intertidal permeable sediments. *PLoS One,* 9, e104517.

Marchant, H. K., S. Ahmerkamp, G. Lavik, H. E. Tegetmeyer, J. Graf, J. M. Klatt, M. Holtappels, E. Walpersdorf & M. M. M. Kuypers (2017). Denitrifying community in coastal sediments performs aerobic and anaerobic respiration simultaneously. *ISME J,* 11, 1799-1812.

Martens, E. C., N. M. Koropatkin, T. J. Smith & J. I. Gordon (2009). Complex glycan catabolism by the human gut microbiota: the *Bacteroidetes* Sus-like paradigm. *J Biol Chem,* 284, 24673-24677.

Martinez-Garcia, M., D. M. Brazel, B. K. Swan, C. Arnosti, P. S. G. Chain, K. G. Reitenga, G. Xie, N. J. Poulton, M. L. Gomez, D. E. D. Masland, B. Thompson, W. K. Bellows, K. Ziervogel, C.-C. Lo, S. Ahmed, C. D. Gleasner, C. J. Detter & R. Stepanauskas (2012). Capturing single cell genomes of active polysaccharide degraders: an unexpected contribution of *Verrucomicrobia*. *PLoS ONE,* 7, e35314.

McHatton, S. C., J. P. Barry, H. W. Jannasch & D. C. Nelson (1996). High nitrate concentrations in vacuolate, autotrophic marine Beggiatoa spp. *Appl Environ Microbiol,* 62, 954-958.

Middelburg, J. J. (2019). Marine carbon biogeochemistry: a primer for earth system scientists. Springer Nature, 118.

Middelburg, J. J. & L. A. Levin (2009). Coastal hypoxia and sediment biogeochemistry. *Biogeosciences,* 6, 1273-1293.

Millero, F. J., S. Sotolongo & M. Izaguirre (1987). The oxidation kinetics of Fe(II) in seawater. *Geochim Cosmochim Acta,* 51, 793-801.

Morgan, B. & O. Lahav (2007). The effect of pH on the kinetics of spontaneous Fe(II) oxidation by O_2 in aqueous solution - basic principles and a simple heuristic description. *Chemosphere,* 68, 2080-2084.

Murphy, S. A., S. Meng, B. M. Solomon, D. M. C. Dias, T. J. Shaw & J. L. Ferry (2016). Hydrous ferric oxides in sediment catalyze formation of reactive oxygen species during sulfide oxidation. *Front Mar Sci,* 3, 227.

Musat, N., U. Werner, K. Knittel, S. Kolb, T. Dodenhof, J. E. E. Van Beusekom, D. De Beer, N. Dubilier & R. Amann (2006). Microbial community structure of sandy intertidal sediments in the North sea, Sylt-Rømø Basin, Wadden Sea. *Syst Appl Microbiol,* 29, 333-348.

Nealson, K. H. (1997). Sediment bacteria: who's there, what are they doing, and what's new? *Annu Rev Earth Planet Sci,* 25, 403-434.

Nielsen, L. P., N. Risgaard-Petersen, H. Fossing, P. B. Christensen & M. Sayama (2010). Electric currents couple spatially separated biogeochemical processes in marine sediment. *Nature,* 463, 1071-1074.

Postma, D. & R. Jakobsen (1996). Redox zonation: equilibrium constraints on the Fe(III)/SO_4-reduction interface. *Geochim Cosmochim Acta,* 60, 3169-3175.

Poulton, S. W., M. D. Krom & R. Raiswell (2004). A revised scheme for the reactivity of iron (oxyhydr)oxide minerals towards dissolved sulfide. *Geochim Cosmochim Acta,* 68, 3703-3715.

Preisler, A., D. De Beer, A. Lichtschlag, G. Lavik, A. Boetius & B. B. Jørgensen (2007). Biological and chemical sulfide oxidation in a *Beggiatoa* inhabited marine sediment. *ISME J,* 1, 341-353.

Rabus, R., T. A. Hansen & F. Widdel (2013). Dissimilatory sulfate- and sulfur-reducing prokaryotes. In *The prokaryotes: prokaryotic physiology and biochemistry,* eds. E. Rosenberg, E. F. DeLong, S. Lory, E. Stackebrandt & F. Thompson, 309-404.

Rafaelli, D. & S. J. Hawkins (1985). Intertidal ecology. Springer Science & Business Media, 356.

Reintjes, G., C. Arnosti, B. M. Fuchs & R. Amann (2017). An alternative polysaccharide uptake mechanism of marine bacteria. *ISME J,* 11, 1640-1650.

Roekens, E. J. & R. Van Grieken (1983). Kinetics of iron(II) oxidation in seawater of various pH. *Mar Chem,* 13, 195-202.

Rose, A. L., T. P. Salmon, T. Lukondeh, B. A. Neilan & T. D. Waite (2005). Use of superoxide as an electron shuttle for iron acquisition by the marine cyanobacterium *Lyngbya majuscula*. *Environ Sci Technol,* 39, 3708-3715.

Rusch, A. & M. Huettel (2000). Advective particle transport into permeable sediments - evidence from experiments in an intertidal sandflat. *Limnol Oceanogr,* 45, 525 - 533.

Rusch, A., M. Huettel, C. E. Reimers, G. L. Taghon & C. M. Fuller (2003). Activity and distribution of bacterial populations in Middle Atlantic Bight shelf sands. *FEMS Microbiol Ecol,* 44, 89-100.

Sarmento, H., C. Morana & J. M. Gasol (2016). Bacterioplankton niche partitioning in the use of phytoplankton-derived dissolved organic carbon: quantity is more important than quality. *ISME J,* 10, 2582-2592.

Schiener, P., K. D. Black, M. S. Stanley & D. H. Green (2015). The seasonal variation in the chemical composition of the kelp species *Laminaria digitata*, *Laminaria hyperborea*, *Saccharina latissima* and *Alaria esculenta*. *J Appl Phycol,* 27, 363-373.

Schink, B. (1997). Energetics of syntrophic cooperation in methanogenic degradation. *Microbiol Mol Biol Rev,* 61, 262-280.

Sichert, A., C. H. Corzett, M. S. Schechter, F. Unfried, S. Markert, D. Becher, A. Fernandez-Guerra, M. Liebeke, T. Schweder, M. F. Polz & J.-H. Hehemann (2020). Verrucomicrobia use hundreds of enzymes to digest the algal polysaccharide fucoidan. *Nat Microbiol,* 5, 1026-1039.

Sørensen, J., D. Christensen & B. B. Jørgensen (1981). Volatile fatty acids and hydrogen as substrates for sulfate-reducing bacteria in anaerobic marine sediment. *Appl Environ Microbiol,* 42, 5-11.

Stenton-Dozey, J. M. E. 1983. Stranded kelp: its fauna and influence on sandy beach energetics. University of Cape Town.

Teske, A., A. V. Callaghan & D. E. LaRowe (2014). Biosphere frontiers of subsurface life in the sedimented hydrothermal system of Guaymas Basin. *Front Microbiol,* 5, 362.

Thamdrup, B. (2000). Bacterial manganese and iron reduction in aquatic sediments. In *Advances in microbial ecology,* ed. B. Schink, 41-84. Springer, Boston, MA.

Thamdrup, B., H. Fossing & B. B. Jørgensen (1994). Manganese, iron and sulfur cycling in a coastal marine sediment, Aarhus Bay, Denmark. *Geochim Cosmochim Acta,* 58, 5115-5129.

Treude, T., C. R. Smith, F. Wenzhöfer, E. Carney, A. F. Bernardino, A. K. Hannides, M. Krüger & A. Boetius (2009). Biogeochemistry of a deep-sea whale fall: sulfate reduction, sulfide efflux and methanogenesis. *Mar Ecol Prog Ser,* 382, 1-21.

Trusiak, A., L. A. Treibergs, G. W. Kling & R. M. Cory (2018). The role of iron and reactive oxygen species in the production of CO_2 in arctic soil waters. *Geochim Cosmochim Acta,* 224, 80-95.

Usov, A. I., G. P. Smirnova & N. G. Klochkova (2001). Polysaccharides of algae: 55. Polysaccharide composition of several brown algae from Kamchatka. *Russ J Bioorg Chem,* 27, 395-399.

Van Erk, M. R., D. V. Meier, T. Ferdelman, J. Harder, I. Bussmann, & D. De Beer (2020). Kelp deposition changes mineralization pathways and microbial communities in a sandy beach. *Limnology and Oceanography*, 65, 3066-3084.

Visscher, P. T., R. A. Prins & H. Van Gemerden (1992). Rates of sulfate reduction and thiosulfate consumption in a marine microbial mat. *FEMS Microbiol Lett,* 86, 283-293.

Wasmund, K., M. Mußmann & A. Loy (2017). The life sulfuric: microbial ecology of sulfur cycling in marine sediments. *Environ Microbiol Rep,* 9, 323-344.

Weiss, M. S., U. Abele, J. Weckesser, W. Welte, E. Schiltz & G. E. Schulz (1991). Molecular architecture and electrostatic properties of a bacterial porin. *Science,* 254, 1627-1630.

Wellsbury, P. & R. J. Parkes (1995). Acetate bioavailability and turnover in an estuarine sediment. *FEMS Microbiol Ecol,* 17, 85-94.

Wernberg, T. & K. Filbee-Dexter (2018). Grazers extend blue carbon transfer by slowing sinking speeds of kelp detritus. *Sci Rep,* 8, 17180.

Widdel, F., S. Schnell, S. Heising, A. Ehrenreich, B. Assmus & B. Schink (1993). Ferrous iron oxidation by anoxygenic phototrophic bacteria. *Nature,* 362, 834-836.

Wirsen, C. O., S. M. Sievert, C. M. Cavanaugh, S. J. Molyneaux, A. Ahmad, L. T. Taylor, E. F. DeLong & C. D. Taylor (2002). Characterization of an autotrophic sulfide-oxidizing marine *Arcobacter* sp. that produces filamentous sulfur. *Appl Environ Microbiol,* 68, 316-325.

II. Manuscripts

Overview of Chapters

Chapter 2: Kelp deposition changes mineralization pathways and microbial communities in a sandy beach

Marit R. van Erk; Dimitri V. Meier; Timothy Ferdelman; Jens Harder; Ingeborg Bussmann; Dirk de Beer

Status: published in Limnology and Oceanography (2020)

Chapter 3: **Microbial communities in intertidal permeable sediments are optimized for the degradation of kelp polysaccharides**

Marit R. van Erk; Silvia Vidal-Melgosa; Dirk de Beer

Status: summary of preliminary results, further experiments planned

Chapter 4: Reactive oxygen species affect mineralization processes in permeable intertidal flats

Marit R. van Erk; Olivia M. Bourceau; Chyrene Moncada; Subhajit Basu; Colleen M. Hansel; Dirk de Beer

Status: in preparation

Chapter 5: Conspicuous smooth and white egg-shaped sulfur structures on a deep-sea hydrothermal vent formed by sulfide-oxidizing bacteria

Marit R. van Erk; Viola Krukenberg; Pia Bomholt Jensen; Sten Littmann, Dirk de Beer

Status: accepted in Microbiology Spectrum

Kelp deposition changes mineralization pathways and microbial communities in a sandy beach

Marit R. van Erk[1,*], Dimitri V. Meier[1,a], Timothy Ferdelman[1], Jens Harder[1], Ingeborg Bussmann[2], Dirk de Beer[1]

[1]Max Planck Institute for Marine Microbiology, Bremen, Germany

[2]Alfred Wegener Institute, Helmholtz Centre for Polar and Marine Research, Helgoland, Germany

[a]Present address: Division of Microbial Ecology, Centre for Microbiology and Environmental Systems Science, University of Vienna, Vienna, Austria

*corresponding author

Check for updates

Kelp deposition changes mineralization pathways and microbial communities in a sandy beach

Marit R. van Erk [iD],[1]* **Dimitri V. Meier,**[1,a] **Timothy Ferdelman,**[1] **Jens Harder,**[1] **Ingeborg Bussmann,**[2] **Dirk de Beer**[1]
[1]Max Planck Institute for Marine Microbiology, Bremen, Germany
[2]Alfred Wegener Institute, Helmholtz Centre for Polar and Marine Research, Helgoland, Germany

Abstract

We investigated the impact of kelp deposition on the geochemistry and microbial community composition of beach sands on the island of Helgoland (North Sea). The composition of the microbial community at a beach with regular kelp deposition appeared shaped by this regular input of organic material, as indicated by significantly higher proportions of aerobic degraders, fermenters, and sulfur cycling microorganisms. Rapid degradation of deposited kelp by this community leads to high levels of dissolved organic and inorganic carbon and nutrients, a lower pH and anoxia. Aerobic respiration, fermentation, Fe- and SO_4^{2-} reduction, and methanogenesis were strongly enhanced, with SO_4^{2-} reduction being the main process in kelp degradation. SO_4^{2-} reduction rates increased 20- to 25-fold upon addition of kelp. The main route of electrons from kelp to SO_4^{2-} was not via CO and H_2, as expected, but via organic fermentation products. O_2 supply by the tides was not sufficient and reduced intermediates escaped from the sediment with tidal water retraction. The resulting extremely high levels of free sulfide (>10 mmol L^{-1}) lead to abundant filamentous growth of sulfur-oxidizing bacteria largely composed of a rare O_2-adapted *Sulfurovum* lacking the expected denitrification genes. Our results show that regular kelp deposition strongly enhances the thermodynamic disequilibrium in the beach sand habitat, leading to a dramatic enhancement of the sulfur cycle.

Large amounts of organic material consisting mainly of macroalgae and seagrasses are regularly deposited on shores. Kelps, or brown macroalgae, need a hard substrate on which to attach, and occur along all temperate shores (Mann 1973). Kelp beds can attain high rates of production and form a large pool of biomass (Mann 1973). Physical forcing of storms and waves causes the sessile kelp plants to become detached. The detached kelp may subsequently be carried ashore, and form layers of up to several meters thick on shores nearby rocky seafloors. Rates of annual kelp deposition were estimated to be between 1.2×10^6 and 1.8×10^6 kg wet weight along a 1 km strandline in South Africa (Koop and Field 1980). Such large accumulations of organic material in the marine realm are sporadic but locally dramatic, and the sequence of events that follows

sudden pulses of organic material is complex and of great interest to microbial ecologists and biogeochemists. Another example of such a pulse biogeochemical impact is the arrival of a whale carcass on the sea floor (Treude et al. 2009). Such an input of degradable organic material results in unusually high levels of organic substrates, intermediates, and degradation products. Degradation will depend on arrival of and colonization by degrading organisms, transport rates of degradation products, and the period the organic material resides in the habitat (i.e., relocation of kelp by tides).

Macroalgal deposits on beaches are classified as biogeochemical hotspots as they are metabolically very active, with high CO_2 fluxes demonstrating elevated respiration rates (Rodil et al. 2019). Studies focusing on the effects of increased amounts of organic material within sandy sediments found surface sediments to be anoxic, and dissolved reduced sulfur concentrations and SO_4^{2-} reduction to be enhanced (Böttcher et al. 1997). This further highlights the enhanced metabolic activity of sandy sediments characterized by large depositions of organic material.

Kelp deposits are a source of dissolved organic carbon (DOC) and nutrients. The release of leachates to the sediments was shown by high concentrations of DOC in associated sediments, exceeding concentrations in offshore kelp beds. The released DOC can be used rapidly within the sediments (Koop

Additional Supporting Information may be found in the online version of this article.

[a]Present address: Division of Microbial Ecology, Centre for Microbiology and Environmental Systems Science, University of Vienna, Vienna, Austria

et al. 1982). Mineralization of kelp detritus on beaches leads to the export of nutrients to the sea. A significant correlation between intertidal dissolved inorganic and organic nitrogen (DIN and DON) concentrations and deposit biomass was found (Dugan et al. 2011). These authors also found DIN concentrations in surf zone waters to correlate with deposit biomass and intertidal DIN concentrations, suggesting that deposits cause the release of DIN to the sediments, which is subsequently partly exported to the surf zone water. Beaches with kelp deposits could therefore be important sites of biogeochemical activity for nearshore communities (Dugan et al. 2011).

Sandy beach sediments are characterized by low contents of organic material compared to muddy sediments (Jickells and Rae 1997), and heterotrophic organisms within sandy beach sediments are thus dependent on the input of allochthonous organic material. Kelp-derived carbon was found throughout nearshore food webs (Duggins et al. 1989). Besides being a food source, kelp deposits provide a habitat and shelter against predation and environmental conditions to a variety of organisms (Colombini et al. 2000). Deposits increase the density and species richness of communities (Colombini and Chelazzi 2003). Invertebrate consumers fragment the kelp material and thereby make the material available to bacteria (Colombini and Chelazzi 2003).

Bacteria are the key decomposers of the kelp deposits and the further mineralization occurs via a complex set of microbial processes. Kelp dry biomass is rich in polysaccharides, such as alginic acid, laminarin, mannans, and fucoidan (Usov et al. 2001). Therefore, degradation likely involves the hydrolysis of polymers, fermentation of hydrolysis products, and aerobic and anaerobic oxidation processes. The largest fraction of biomass associated with kelp deposits is microbial, being about three times that of macro- and meiofauna (Koop and Griffiths 1982). Over 90% of the kelp-derived leachates is used by bacteria, and a large fraction (23–27%) of kelp carbon is converted to bacterial carbon, with the remainder rapidly being mineralized by bacteria (Koop et al. 1982). A positive relationship between DIN concentrations below deposits and bacterial diversity further supports the role of bacteria as key decomposers of the deposits (Rodil et al. 2019). Remarkably, no detailed biogeochemical studies on degradation within kelp deposits on sandy beaches, including analyses on the release of substances, microbial processes, and associated microbial communities, have been performed. Here, we report on such a study carried out on a North Sea beach.

We hypothesize that the microbial communities associated with kelp deposits are different from the normal coastal communities within sandy intertidal sediments. In normal early diagenesis, mass transfer of organic material and electron acceptors to the cells limits turnover rates, as advectional exchange of electron acceptors between oxygenated seawater (the source of electron acceptors, e.g., O_2, NO_3^-, SO_4^{2-}) and sediment is limited. This leads to a vertical stratification of processes, the redox cascade, in a typical sequence of electron acceptors (O_2, NO_3^-, Mn(IV), Fe(III), SO_4^{2-}, and CO_2) dictated by the energy gain related to the different processes (Froelich et al. 1979). The reduction processes are coupled to reoxidation of the reduced products (Berner 1980). In general, microorganisms in early diagenesis are limited by one or several compounds, and microbial communities are thus thought to be specialized in slow growth and to have a high affinity to limiting substrates (Chen et al. 2017). SO_4^{2-} reduction is an important process in marine sediments, as it can account for 50% of the remineralization of organic material in coastal sediments (Jørgensen 1982).

Conditions in sediments below kelp deposits are expected to be different from steady-state depositional environments. Mineralization processes after sudden inputs of large amounts of organic material are ultimately controlled by kinetics, which in turn depend on the presence of the optimal microbial consortia, substrate quality, pH, temperature, and other microenvironmental factors. The batch-wise input of a large amount of readily degradable material will favor fast-growing organisms, and leads to high levels of intermediates, e.g., fermentation products. The short deposition time may favor facultative anaerobes, but not allow for full development of the anaerobic processes that are common in diffusion-controlled sediments.

An interesting route for stimulating SO_4^{2-} reduction could be via the intermediates CO and H_2. Formation of CO occurs from organic material, likely polyphenols, under oxic conditions by abiotic processes (Conrad and Seiler 1985). The formation of CO in intertidal environments is thus likely an aerobic process. CO can biologically react with water to produce H_2: $CO + 2H_2O \rightarrow HCO_3^- + H_2 + H^+$ (Parshina et al. 2010). The produced H_2 could be an important substrate for SO_4^{2-} reduction. This is a possible scenario in the intertidal zone with fluctuating O_2 conditions. Alternatively, CO can be used directly as electron donor in SO_4^{2-} reduction.

Sandy beaches consist of permeable sediments in which advection plays a major role. Advection efficiently transports organics and electron acceptors from the water column into the sediments, however, only by hydraulic forcing.

We investigated the hypotheses that the degradation rates are strongly enhanced and degradation follows other pathways than on beaches without kelp. Specifically, we expected that CO and H_2 may be important intermediates, and export from the sediments of intermediates and products of anaerobic processes occurs. The hypotheses were tested using porewater and sediment analyses, radiotracer (^{35}S) incubations and in situ microsensor measurements, as well as microbial community composition analysis and selective population-resolved genomic potential analysis.

Materials and methods

Site description

Helgoland is a small archipelago in the German Bight, southeast North Sea (54°11′ N; 7°53′ E). It lies approximately

60 km off the German coast and consists of two islands: the main island (Hauptinsel) to the west (1 km^2) and the smaller Düne to the east (0.7 km^2). The tidal regime of Helgoland is semidiurnal, with an average tidal range of 2.3 m. Around Helgoland, the sublittoral hard-bottom sediment is covered by brown seaweeds: mainly *Laminaria digitata*, *Laminaria hyperborea*, *Saccharina latissima*, and *Desmarestia aculeata* (Pehlke and Bartsch 2008), of which the first three are kelp species, and have leaves that are up to over a meter in length. Two sandy beaches on the main island were selected as sampling locations: the North Beach, hereafter referred to as kelp-beach, and a reference beach (Fig. 1). An area of 1 km^2 of the kelp forest is located north of the kelp-beach (Uhl et al. 2016), the main source for huge masses of kelp deposits on this beach. Deposition happens often but irregular, with highest deposition rates occurring during and directly after storms. Sampling for biogeochemical analyses was conducted in November 2017, May 2018, October 2018, and August 2019 (Table 1), during low to incoming tide in water-saturated sediments. The microbial community composition was assessed using samples obtained in October 2015, and total cell counts were determined from July 2019 samples.

Sediment properties

Sediments for porosity, total organic carbon (TOC), and solid-phase Fe determinations were sampled in situ using cut-off syringes. Sampling was conducted within the upper 10 cm, in 2 cm intervals. Sediments for TOC determination were freeze-dried, and sediments for Fe determination were stored at −20°C. Sediment density was determined from the wet weight of a known volume of sediment. Porosity was calculated using the weight loss upon drying to constant weight at 60°C. For TOC determination, freeze-dried sediments (0.5–1.0 g) were ground and homogenized. Sediments were then decalcified using 10% HCl, and freeze-dried. The TOC concentration was determined in duplicate on 40–50 mg of sediment using a continuous-flow elemental analyzer (Thermofinnigan Flash EA 2000) coupled to an isotope ratio mass spectrometer (Delta V plus). For solid-phase Fe(III) and Fe(II) determination, Fe was extracted from about 0.5 g of wet sediment using 5 mL of 0.5 mol L^{-1} HCl (0.5 h). Supernatants were then analyzed spectrophotometrically using the ferrozine method (Viollier et al. 2000).

Porewater extraction and analysis

Porewater extraction and filtration were conducted in the field using Rhizon samplers (Rhizosphere Research Products, average pore size 0.15 μm). Sampling was conducted in 2 cm intervals from 0 to 12 cm depth (kelp-beach November 2017), 0 to 14 cm depth (reference beach November 2017), and 0 to 10 cm depth (May and October 2018). In November 2017, extracted kelp-beach porewater at 10 and 12 cm depth was only sufficient for DOC analyses. The first mL of porewater was discarded. Seawater was collected in 50 mL tubes and Rhizon sampling was conducted from these tubes as described for porewater sampling. After extraction and filtration,
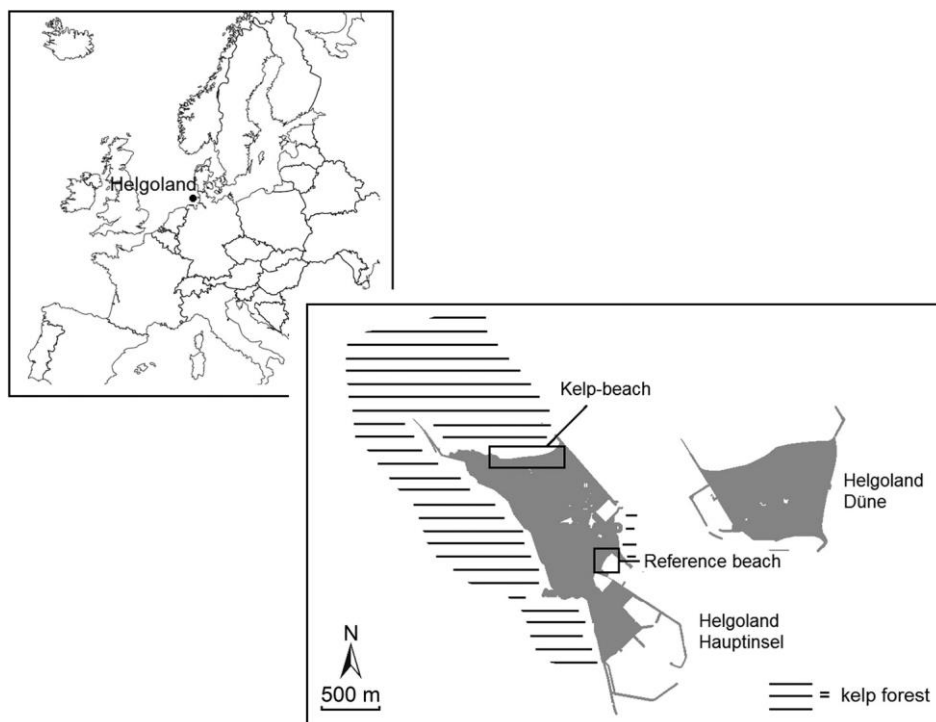

Fig. 1. Location of the two study sites (kelp-beach and reference beach), including the location of the kelp forest (Uhl et al. 2016).

Table 1. Parameters measured during the different field campaigns. Crosses (X) denote that measurements were done during that campaign. Dashes (—) denote that measurements were not done during that campaign or that data is not shown. TOC, Total organic carbon; DOC, Dissolved organic carbon; P_i, Inorganic phosphorus; DIC, Dissolved inorganic carbon; S^{2-}_{tot}, Total sulfide; SRR, SO_4^{2-} reduction rate.

Parameter	November 2017	May 2018	October 2018	August 2019
Sediment parameters				
Porosity	—	—	X	—
TOC	—	—	X	—
Fe(III) and Fe(II)	—	—	X	—
Porewater parameters				—
DOC	X	—	—	—
Nutrients ($NO_3^- + NO_2^-$, NH_4^+, P_i)	X	X	—	—
DIC	—	—	X	—
SO_4^{2-}	—	X	—	—
Sulfide	—	X	—	—
Cl^-	—	X	—	—
Fe^{2+}	—	—	X	—
Microsensor parameters				—
O_2	—	X	—	—
pH	—	X	—	—
S^{2-}_{tot}	—	X	—	—
Gases				—
CH_4	—	X	—	—
N_2O	—	X	—	—
CO	X	X	—	—
H_2	X	X	—	—
Rates and fluxes				—
SRR	—	—	X	—
O_2 flux/O_2 consumption	—	X	—	X

porewater was directly subsampled from the syringe using a sampling cup attached to the side-outlet of a 3-way stopcock that was between the syringe and the Rhizon sampler. Porewater was transferred to combusted glass vials for DOC and to centrifuge tubes for nutrient ($NO_3^- + NO_2^-$, NH_4^+, and inorganic phosphorus [P_i]) determinations. Both the glass vials and centrifuge tubes were stored at $-20°C$. For dissolved inorganic carbon (DIC) determination, 2 mL glass vials (Zinsser Analytic) were filled without headspace, and stored at $4°C$. Porewater was fixed with ZnAc in Eppendorf tubes and stored at $4°C$ for sulfide, SO_4^{2-}, and Cl^- determination. For Fe^{2+} determination, porewater was fixed using ferrozine in semimicro cuvettes and stored at $4°C$.

Concentrations of DOC were measured by high temperature catalytic oxidation using a DIMATOC® 2010 K1 analyzer, with potassium hydrogen phthalate as standard. Nutrients were analyzed photometrically with a continuous-flow analyzer (BQuAAtro39 analyzer, Seal Analytic), using a variant of a method described previously (Grasshoff et al. 1999). The DIC concentrations were determined using a flow injection system (Hall and Aller 1992). Both SO_4^{2-} and Cl^- concentrations were determined by ion chromatography (Metrohm

930 Compact IC Flex). Dissolved sulfide (H_2S, HS^-, S^{2-}) was analyzed spectrophotometrically using the methylene blue method (Cline 1969). The Fe^{2+} concentrations were determined spectrophotometrically within 3 d after sampling using the ferrozine method (Viollier et al. 2000).

Microsensor measurements

Depth profiles were measured in situ at different locations on the kelp-beach and the reference beach. Microsensors for O_2, pH, and H_2S were mounted on a manually operated micromanipulator attached to a heavy stand. The readings were made directly from the displays of the battery-powered amplifier (H_2S, pH) or from the laptop (O_2). Measurements were conducted in water-saturated sediments. Measurements could only be done at low tide or during the first minutes upon inundation. The sites on the kelp-beach were exposed during low tide for approximately 8 h d^{-1}.

O_2 was recorded using micro-optodes (OXROB10, Pyroscience GmbH, Germany), connected to a FirestingO$_2$ meter (Pyroscience GmbH, Germany) and a laptop with the Pyroscience software. The sensors were calibrated using 1 mol L^{-1} Na ascorbate solution (0% saturation) and

air-saturated water (100% saturation) and signals were corrected for temperature and salinity to calculate the O_2 concentrations. Salinity was measured using a refractometer. The H_2S microsensors were prepared as described previously (Jeroschewski et al. 1996). The multiple-point calibration was conducted in the on-site laboratory by stepwise addition of known amounts of a 1 mol L^{-1} Na_2S solution to acidified (pH < 2) seawater. The steel needle enforced pH microsensors, obtained from Microelectrodes Inc (Bedford, USA), were calibrated in standard buffers. The pH and H_2S concentrations were used to calculate total sulfide (S^{2-}_{tot}) as described previously (Jeroschewski et al. 1996), using a pK of 6.6 or 6.7, depending on the in situ porewater temperature and seawater salinity (Millero et al. 1988).

The diffusive O_2 fluxes were calculated from the O_2 gradients using Fick's first law of one-dimensional diffusion. The effective diffusion coefficient (D_e) of O_2 in the sediment was obtained by multiplying the molecular diffusion coefficient of O_2 (D_0) with the porosity of the sediment (Kühl et al. 1996). The D_0 was corrected for the in situ porewater temperature and salinity (Li and Gregory 1974). For kelp-beach sediments, D_e was equal to 5.04×10^{-10} m^2 s^{-1}, and for reference beach sediments, D_e was equal to 4.68×10^{-10} m^2 s^{-1}.

Volumetric O_2 consumption rates were determined by percolating oxygenated seawater through kelp-beach and reference beach sediments. Surface sediments and seawater were sampled in August 2019 on both beaches, and stored cooled at 4°C until use within 3 d after sampling. Sediments were homogenized and large pieces of kelp and large grains were removed by sieving. The homogenized sediments were carefully added to sediment cores (5.3 cm diameter) that were filled with seawater. The bottom stopper of the core was fitted with a valve. Porewater O_2 concentrations were tracked with O_2 micro-optodes positioned at 2 cm depth. Approximately 50 mL of aerated seawater was percolated through the sediments by outflow through the valve. The sediment cores contained sufficient seawater to allow for a layer of overlying seawater to remain after percolation. An air pump induced continuous water movement in this overlying layer of seawater. The O_2 decrease after percolation was used to calculate the volumetric O_2 consumption rate. Conversion from volume of porewater to volume of sediment occurred by multiplication with the sediment porosity. To determine the areal O_2 consumption rate, the volumetric rate was multiplied with the in situ O_2 penetration depth measured in May 2018 (kelp-beach low tide = 0 cm; kelp-beach incoming tide = 0.8 cm; reference beach = 3.6 cm).

Gas analysis

Sediment was collected in situ using cut-off syringes. Sampling was conducted to a depth of 10 cm, in 2 cm intervals. For CH_4 and N_2O analysis, 3 mL of sediment was transferred to a serum vial containing 3 mL 5 mol L^{-1} NaOH. Serum vials were closed with a butyl rubber stopper and aluminum crimp

seal, shaken, and stored at 4°C. Headspace CH_4 and N_2O concentrations were analyzed with a gas chromatograph (GC 2014, Shimadzu) equipped with a flame ionization detector (FID) for CH_4 and an electron capture detector (ECD) for N_2O. Calibration was done with 2, 10, and 100 ppm standards (Air Liquide) for CH_4 and with 1 and 5 ppm standards (Microsense, Denmark) for N_2O. For CO and H_2 analysis, 0.5 mL of sediment was transferred to Exetainers (November 2017) or to Exetainers containing 0.5 mL 20% (w/v) $ZnCl_2$ (May 2018). Samples for CO and H_2 analysis were shaken and analyzed within 3 h by gas chromatography (Peak Performer 1 RCP 910-Series). Calibration was done with 20 and 100 ppm standards (Air Products) for CO and with 100 and 500 ppm standards (Air Products) for H_2.

CO, H_2, and O_2 evolution in experiments

Two 100 mL serum vials were filled with 10 mL of artificial seawater (pH 8.2, salinity 32) and equilibrated to the incubation temperature of 15°C. Pieces of 1×1 cm from the middle of *Laminaria hyperborea* leaves were cut out, and about 5 g of these pieces were added to each vial, which were then closed with a butyl rubber stopper and aluminum crimp seal, and incubated in the dark on a horizontal shaker. At selected time points, headspace samples for CO and H_2 analysis were taken using a gas and pressure tight syringe and were directly measured (see above). During incubation, the pressure inside the vials changed as the withdrawal of aliquots was not replaced. Headspace O_2 concentrations were measured continuously using Oxygen Sensor Spots (OXSP5, Pyroscience GmbH) glued to the inner side of the vial. The sensor spots were calibrated using a 2-point calibration with N_2 gas (0%) and O_2-saturated air (100%). Only O_2 concentrations from the time points at which CO and H_2 sampling was conducted are shown.

SO_4^{2-} reduction rates
SO_4^{2-} reduction rates within kelp-beach and reference beach sediments

The SO_4^{2-} reduction rates (SRR) were determined on 3 mL sediment samples that were collected using cut-off syringe cores, in 2 cm intervals, from 0 to 10 cm depth. On the kelp-beach, sediments were sampled both below and next to kelp deposits. Syringe cores with sediments were transported cooled and in the dark to the laboratory. There, ^{35}S tracer was added to anoxic seawater, and 3 mL of this tracer-containing seawater was percolated through the syringe core. This addition was equivalent to 200 kBq $^{35}SO_4^{2-}$ per sample. Sediments were incubated at room temperature in the dark for 6 h. To stop the reaction, sediment samples were transferred to 6 mL 20% (w/v) ZnAc and stored at −20°C. The pool of reduced ^{35}S was separated from the pool of unreacted ^{35}S ($^{35}SO_4^{2-}$) by cold acidic Cr^{2+} distillation (Røy et al. 2014). Radioactivity was determined by scintillation counting (Perkin-Elmer Tri-Carb 4910 TR; Ultima-Gold Scintillation cocktail) and SRR were calculated as described previously (Røy et al. 2014).

SO_4^{2-} reduction rates in experiments

In order to assess the influence of kelp deposition on SRR, SRR were determined in syringe cores with either only kelp, sediment-only from the kelp-beach, or kelp plus sediment from the kelp-beach, each in four replicates. In the experiments, either 0.5 g of kelp, 3 mL of sediment, or 0.5 g of kelp plus 3 mL of sediment was used. Sediments comprised a mixture of the top 10 cm of kelp-beach sediments. To mimic beach conditions, the sediments were exposed to air at 4°C until use 2 d later. Intact *Laminaria hyperborea* plants were sampled from fresh kelp deposits on the kelp-beach in parallel to the sediment sampling, and stored at 4°C until use 2 d later. The kelp fragments were cut from the middle of *Laminaria hyperborea* leaves. Kelp fragments were mixed with the sediments. The samples were incubated and SRR were determined as described above.

Microbial community composition
Collection of water, sediment, and white filaments

Water was collected from the beaches, harbors and promenades around the main island of Helgoland with a bucket and filtered on 0.22 μm pore-size polyethersulfone filters (47 mm diameter, Millipore). The filters were frozen at −20°C and stored until further analysis. Sediment cores were collected at the kelp-beach and reference beach. At the kelp-beach, cores were taken from the sediment at the low tide waterline and from sediment below a kelp deposit. From each layer 0.4 g of sediment was frozen at −20°C for DNA extraction. At the low tide waterline of the kelp-beach, pieces of green algae completely covered with white filaments were collected in 15 mL tubes and stored at −20°C until further processing.

DNA extraction

DNA was extracted from a quarter of a polyethersulfone filter, corresponding to ca. 0.4 g of sediment or ca. 0.1 g of white filaments, using the MoBio PowerSoil DNA extraction kit (MoBio, Carlsbad) with an additional Proteinase K digestion and heating at 65°C step as described previously (Meier et al. 2017).

16S rRNA amplification, sequencing, and analysis

For a detailed description of the 16S rRNA amplification, sequencing, and analysis, see Supplementary Materials and Methods.

Metagenome sequencing and analysis

For a detailed description of the sequencing, assembly, binning, and annotation, see Supplementary Materials and Methods.

Fluorescence in situ hybridization

Frozen white filaments were thawed on ice and immediately fixed with 1.5% formaldehyde in 1× PBS (pH = 7.4) at 4°C overnight. Fixed material was filtered on a 0.22 μm polycarbonate filter (Millipore). The filter was excessively flushed with 1× PBS to remove the remaining formaldehyde. For fluorescence in situ hybridization (FISH), filter slices were incubated with fluorescently double-labeled oligonucleotide probes in a 35% formamide containing hybridization buffer for 3 h at 46°C. The GAM42a probe (Manz et al. 1992) labeled with two Atto-488 fluorochromes was used to detect *Gammaproteobacteria* cells, and a mix of SFO1112 and SFO1210 probes (McNichol et al., https://osf.io/yts4p/, accessed on 18 July 2020) labeled with two Atto-594 fluorochromes to detect *Sulfurovum* cells. Visualization was done on an Axioplan epifluorescence microscope (Zeiss).

Total cell counts

Sampling was conducted at 6 locations on the kelp-beach (3 locations below kelp deposits, 3 locations next to kelp deposits), and 2 locations on the reference beach. Samples were obtained from 0 to 2, 2 to 4, 5 to 7, and 9 to 11 cm depth. A volume of 0.5 mL of sediment was fixed using 1 mL of 2% formaldehyde for 1–1.5 h at room temperature. Samples were then centrifuged, the supernatant removed, and replaced by 1 mL 1:1 ethanol:1× PBS. Samples were again centrifuged, the supernatant removed, and 1 mL 1:1 ethanol:1× PBS added. The samples were stored at −20°C until further use. Ultrasonication was used to remove cells from the sediment (3× 30 s at 20% power). After each round, 1 mL of supernatant was removed and replaced by 1 mL 1:1 ethanol:1× PBS. Supernatant was stored at −20°C. A volume of 50 μL of supernatant was filtered on polycarbonate membrane filters (pore size of 0.2 μm). Cells on the filter were stained with DAPI. Cell counting was conducted under an epifluorescence microscope.

Nucleotide sequence accession numbers

All sequence data have been deposited in the European Nucleotide Archive under project number PRJEB36085.

Results
Description of the sampling sites

The kelp-beach and reference beach consisted of predominantly sandy sediments, mixed with gravel and stones. Sediments from the kelp-beach occasionally had a dark-gray appearance. The porosity was 0.28 ± 0.08 for kelp-beach and 0.26 ± 0.08 for reference beach sediments, respectively. The unexpectedly low porosity for sands could be due to the presence of small air bubbles in the sediments. The average TOC content in kelp-beach sediments is slightly higher than in reference beach sediments ($0.04\% \pm 0.02\%$ ($n = 24$) vs. $0.02\% \pm 0.01\%$ ($n = 19$), equal to 61.9 g C m^{-2} vs. 26.2 g C m^{-2} after integration over the sample depth of 0–10 cm). Both values are remarkably low and not statistically different.

Kelp deposits occurred on the kelp-beach during all field campaigns; however, the amount of material in the deposits was variable in time and space (Fig. 2a,b). In November 2017,
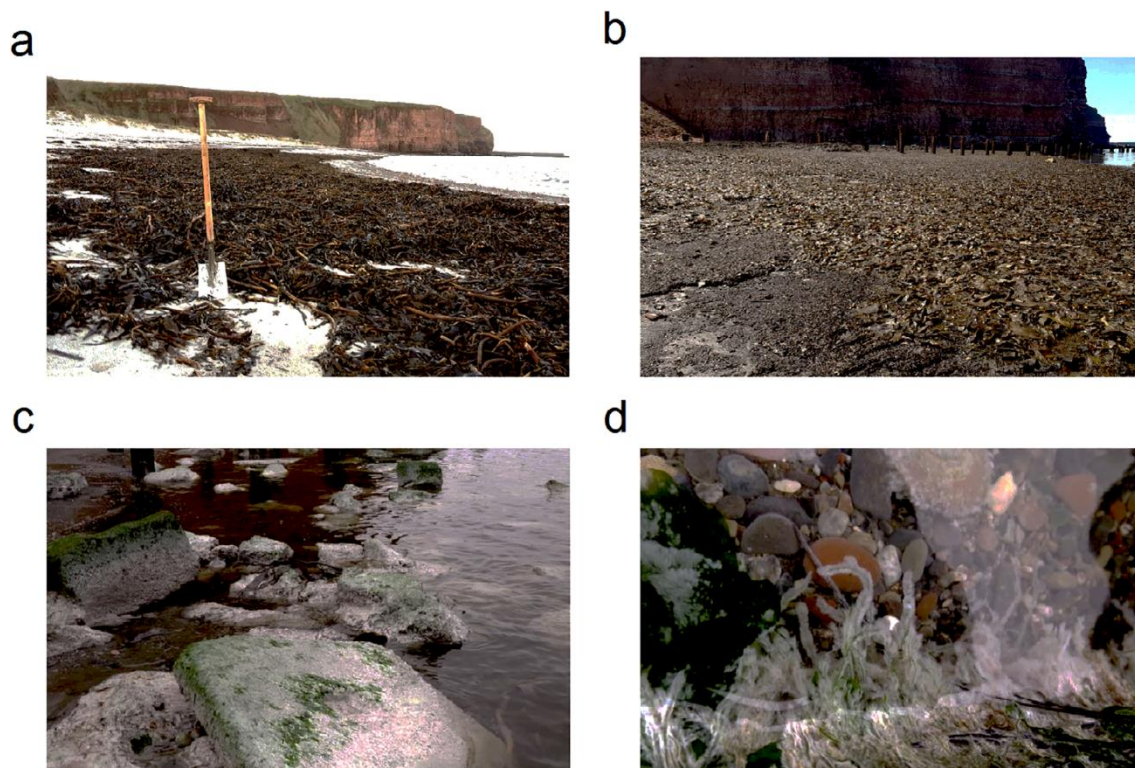
Fig. 2. The kelp-beach with dominantly *Laminaria* deposits in November 2017 (**a**) and May 2018 (**b**). White filaments covering green algae on rocks at the low tide waterline of the kelp-beach in October 2015, in overview (**c**) and in close-up (**d**).

October 2018, July 2019, and August 2019, kelp deposits were patchy and mainly occurred close to the edges of the beach, while relatively small amounts were present at the center of the beach. In October 2015 and May 2018, kelp covered the whole beach, with 15 m wide, 0.5 m thick deposits. Kelp was partially fragmented to pieces of down to lengths of centimeters to several decimeters. The deposits were usually inhabited by kelp flies and the beach was occasionally pervaded by an intense sulfidic smell. Kelp fragments were buried down to at least 30 cm in the sediment. The investigated deposits were inundated during high tide and exposed during low tide. In October 2015, green algae on rocks at the low tide waterline of the sea adjacent to the kelp-beach were completely covered with a bloom of white filaments (Fig. 2c,d). Close to the low tide waterline, the outflowing porewater was milky and had a strong sulfidic smell. During this field campaign, the weather was very calm with nearly no wind and waves. On the reference beach, kelp deposits were absent during all field campaigns.

In situ geochemical analyses

Concentrations of degradation products of organic material were elevated within sediments from the kelp-beach, but were highly variable and within the depth layer investigated, no trend could be observed. In November 2017, DOC was elevated by approximately 5 mmol L^{-1} and DIC by 10 mmol L^{-1} in

October 2018 (Fig. 3a,b). In May 2018, SO_4^{2-} concentrations were ~15 mmol L^{-1} lower in kelp-beach sediments compared to reference beach sediments (Fig. 3c), and depleted in equal extent compared to seawater (average kelp-beach seawater SO_4^{2-} concentration is 23.2 ± 2.3 mmol L^{-1}, that of reference beach seawater is 26.3 ± 0.3 mmol L^{-1}). These lower concentrations are not due to dilution with freshwater, since porewater Cl^- concentrations were similar to those of seawater. Indeed, sulfide levels were strongly elevated relative to reference beach porewater levels (by about 10 mmol L^{-1}) (Fig. 3d), indicating conversion of SO_4^{2-} to sulfide. The levels of DIC, SO_4^{2-}, and sulfide correspond roughly with the stoichiometry of SO_4^{2-} reduction by the oxidation of organic material:

$$2CH_2O + SO_4^{2-} \rightarrow H_2S + 2HCO_3^-,$$
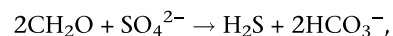
where per mol of reduced SO_4^{2-} 1 mol of sulfide and two moles of DIC are produced. In sediments from the reference beach, no sulfide was detected (Fig. 3d). Sulfide was present in 9 out of 13 seawater samples from seawater adjacent to the kelp-beach in May 2018, taken at times when microsensor measurements were made, in concentrations between 0.05 and 4.27 mmol L^{-1}.

Fe(II) was the dominant form of solid-phase Fe in kelp-beach sediments. Conversely, Fe(III) was the main form of solid-phase Fe in reference beach sediments (Table 2). In sediments from the kelp-beach, solid-phase, Fe(III) was thus
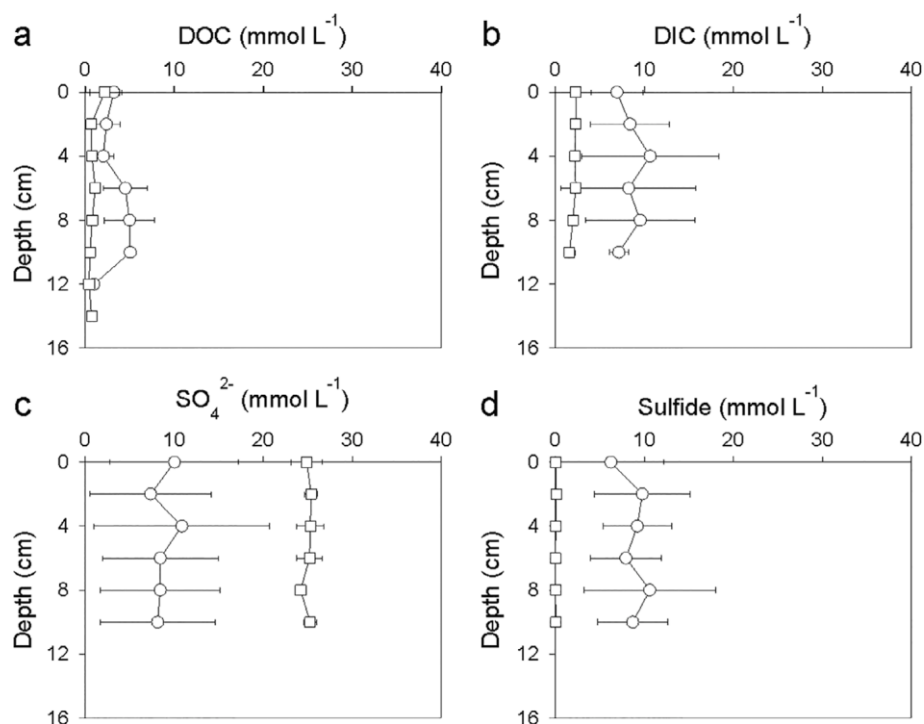
Fig. 3. Dissolved organic carbon (DOC; **a**), dissolved inorganic carbon (DIC; **b**), SO_4^{2-} (**c**) and sulfide (**d**) within porewaters from the kelp-beach ($\circ$) and the reference beach ($\square$).

quantitatively reduced to Fe(II), while in the reference beach sediments net Fe(III) reduction did not occur, at least was much slower than Fe(II) oxidation. Dissolved Fe was negligible, compared to the concentrations of solid-phase Fe (Table 2).

Concentrations of the nutrients NH_4^+ and P_i were elevated in porewater of kelp-beach sediments, likely due to kelp biomass degradation. P_i could furthermore have been released by minerals during their reduction. On the other hand, $NO_3^- + NO_2^-$ concentrations were reduced (Fig. 4), probably due to denitrification driven by kelp degradation. These features were mainly occurring during periods with relatively high amounts of deposited kelp (May 2018), and were less

pronounced in November 2017, when kelp deposits were not that extensive. Denitrification was furthermore indicated by higher N_2O concentrations in kelp-beach sediments (Table 2). Sediments from the kelp-beach also had slightly elevated CH_4 concentrations, indicating methanogenesis (Table 2). Nutrient and DOC concentrations were occasionally high in seawater adjacent to the kelp-beach (data not shown), with maximum concentrations of 2400, 30, 85, and 1300 μmol L^{-1} for NH_4^+, $NO_3^- + NO_2^-$, P_i, and DOC, respectively. These concentrations are 1 to 2 orders of magnitude higher than average concentrations in seawater adjacent to the reference beach for NH_4^+, $NO_3^- + NO_2^-$, and P_i (May 2018), and 5 times higher for DOC.

Table 2. Solid-phase Fe (Fe(II) and Fe(III)) and dissolved Fe (Fe^{2+}), N_2O, CH_4, CO and H_2 concentrations for sediments from the kelp-beach and sediments from the reference beach. Values are averages over separate profiles, since no trend with depth or location on the beaches was evident.

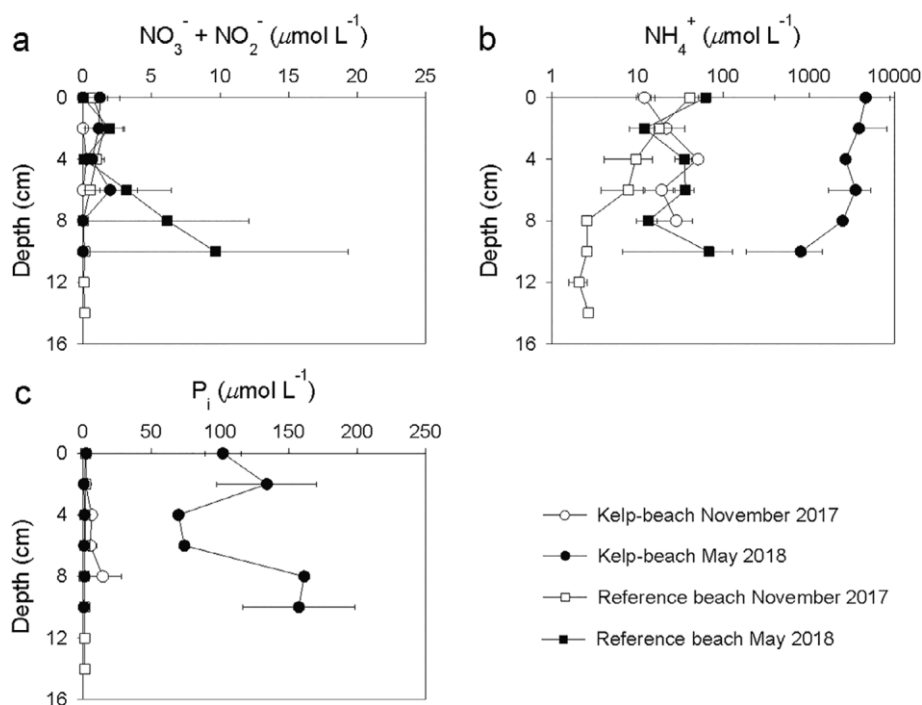|	November 2017		May 2018		October 2018	
	Kelp-beach	Reference beach	Kelp-beach	Reference beach	Kelp-beach	Reference beach
Fe(III) (mmol L^{-1} sed)					17.44 ± 56.40	9.25 ± 1.95
Fe(II) (mmol L^{-1} sed)					127.02 ± 128.81	0.62 ± 0.19
Fe^{2+} (μmol L^{-1} sed)					4.47 ± 4.05	0.86 ± 0.08
N_2O (μmol L^{-1} sed)			0.46 ± 0.39	0.13 ± 0.19		
CH_4 (μmol L^{-1} sed)			4.69 ± 4.36	1.58 ± 1.53		
CO (μmol L^{-1} sed)	0.18 ± 0.15	0.09 ± 0.07	1.34 ± 0.99	0.51 ± 0.50		
H_2 (μmol L^{-1} sed)	0.79 ± 0.52	0.53 ± 0.13	0.50 ± 0.22	0.33 ± 0.06		

Fig. 4. Porewater $NO_3^- + NO_2^-$ (**a**), NH_4^+ (**b**), and inorganic phosphorus (Pi; **c**) concentrations from sediments of the kelp-beach in November 2017 (○) and May 2018 (●) and from sediments of the reference beach in November 2017 (□) and May 2018 (■).

In situ microsensor measurements in kelp-beach sediments show highly dynamic O_2 and pH profiles in response to the tides (Fig. 5). During low tide, O_2 is depleted within sediments from the kelp-beach (both below and next to the kelp deposits). Conversely, during high tide, O_2 quickly penetrates the surface sediments by hydraulic forcing. Thus, high diffusive O_2 fluxes exist in sediments covered by, or next to, kelp deposits (4.2×10^{-8} and 2.1×10^{-8} mol m^{-2} s^{-1}). The volumetric O_2 consumption rate was 3.3×10^{-4} mol m^{-3} s^{-1}, which would result in an areal O_2 consumption rate of 2.7×10^{-6} mol m^{-2} s^{-1}. During low tide, O_2 did not penetrate the sediments and O_2 consumption had thus stopped. The pH values during low tide were low, reaching minima of around 6.7. Seawater coverage quickly elevated the pH in the upper 2.5 cm, indicating rapid water exchange. The top 3.5 cm of reference beach sediments stayed oxic at low tide, and the pH values remained close to those in seawater (7.9). The diffusive O_2 flux in reference beach sediments was 2.7×10^{-10} mol m^{-2} s^{-1}, which was 2 orders of magnitude lower than the diffusive O_2 fluxes in kelp-beach sediments. The volumetric O_2 consumption rate was 3.6×10^{-5} mol m^{-3} s^{-1}, which is one order of magnitude lower than for kelp-beach sediments. This would result in an areal O_2 consumption rate of 1.3×10^{-6} mol m^{-2} s^{-1}, which is 2 times lower than in kelp-beach sediments.

The porewater S^{2-}_{tot} concentrations are extremely high within surface sediments from the kelp-beach, reaching maxima of more than 15 mmol L^{-1} during low tide (Fig. 5). These levels are comparable to dissolved total sulfide levels measured

by porewater extraction (Fig. 3d). It should be noted that calculations of S^{2-}_{tot} from pH and H_2S profiles are inaccurate in dynamic conditions, because the alignment of pH and H_2S profiles is uncertain. The S^{2-}_{tot} concentrations are below detection limit within sediments from the reference beach. No H_2S was detected in reference beach sediments. The low pH, high diffusive O_2 fluxes and O_2 consumption rates, and high S^{2-}_{tot} levels in kelp-beach sediments indicate high rates of fermentation, aerobic respiration, and SO_4^{2-} reduction.

Both CO and H_2 concentrations were elevated within sediments from the kelp-beach compared to sediments from the reference beach (Table 2). The CO concentrations were highest in May 2018, whereas H_2 concentrations were highest in November 2017.

CO and H_2 evolution in laboratory experiments

Net CO and H_2 formation only occurred in incubations with kelp, and their concentrations were inversely correlated to O_2 concentrations (Fig. 6). When O_2 was present in the headspace, CO was quickly produced. After around 200 h of incubation, when O_2 concentrations were as low as 12 μmol L^{-1}, net production ceased. The CO concentration at that time was 37 μmol L^{-1}. Importantly, no further change in CO concentration was observed during the anoxic phase. Net H_2 production, on the other hand, mainly occurred at low O_2 concentrations. The majority of H_2 production occurred after 72 h, when O_2 concentrations were below 26 μmol L^{-1}. Both CO and H_2 could thus be produced from degrading kelp. Net
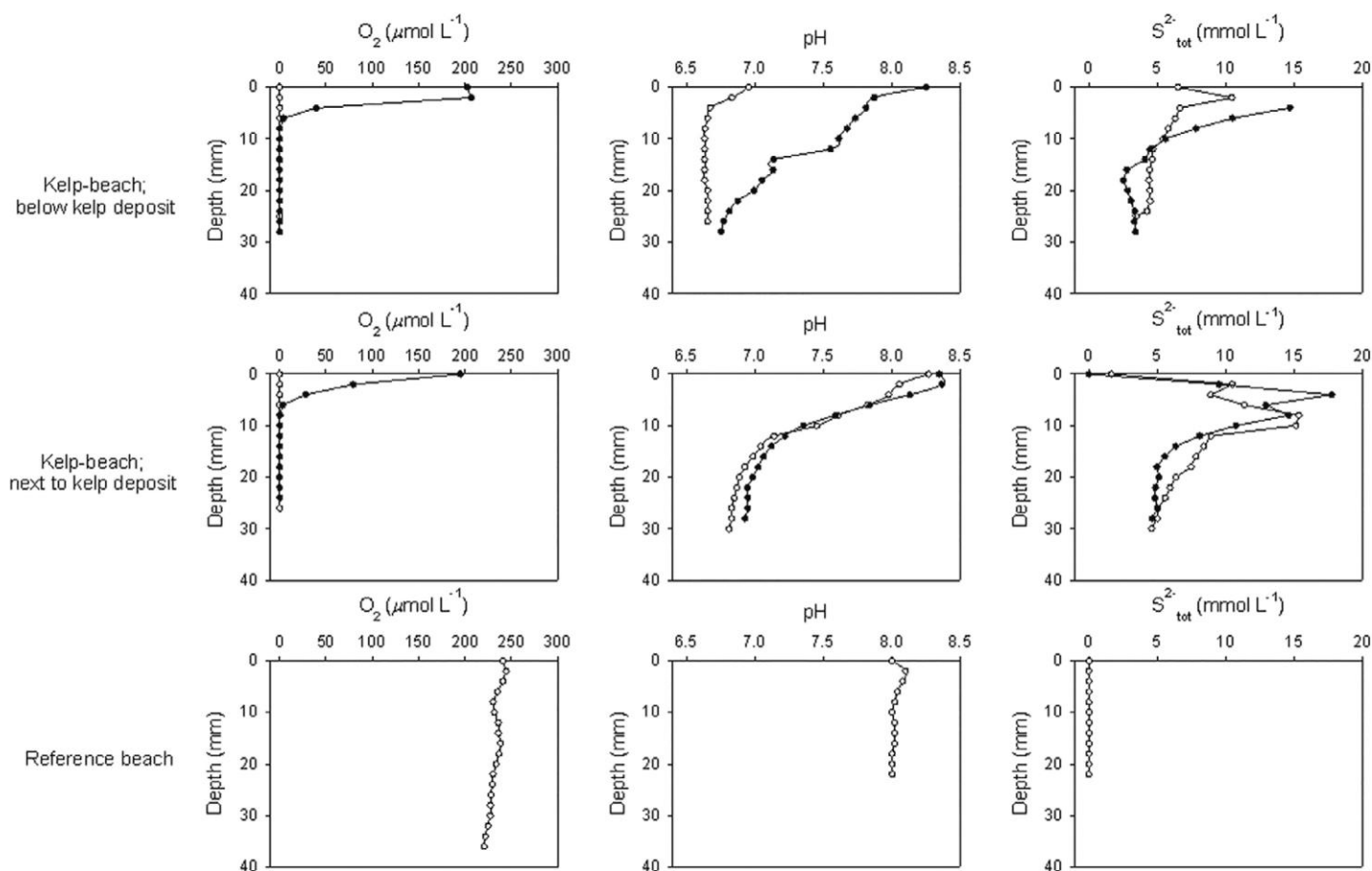
Fig. 5. O_2 (left panels), pH (middle panels) and total sulfide (S^{2-}_{tot}; right panels) microprofiles within kelp-beach sediments (top and middle panels) and within reference beach sediments (bottom panels) during low tide (o) and incoming tide (●). The top panels show profiles within sediments below kelp deposits and the middle panels profiles within sediments next to kelp deposits. Incoming tide profiles refer to the moment when seawater starts to cover the site, while during low tide, the sites are exposed.

CO production mainly occurs under high O_2 conditions, while low O_2 conditions are needed for significant H_2 accumulation. No significant net production of either CO or H_2 took place within the kelp-free controls.

Calculated production rates within artificial seawater were converted to production rates within sediment using the porosity of kelp-beach sediment. Sedimentary net production of CO occurred with a rate of $1.22 \times 10^{-7} \pm 0.24 \times 10^{-7}$ mol m^{-3} s^{-1} during the first 6 h of incubation. Net H_2 production rates were determined during the period of fastest increase (120–264 h). During this period, sedimentary net H_2 production was $1.13 \times 10^{-8} \pm 0.27 \times 10^{-8}$ mol m^{-3} s^{-1}.

SO$_4^{2-}$ reduction rates

The SRR was extremely variable in the kelp-beach sediments, as reflected in the large standard deviation (Table 3). The lack of a clear trend with depth or location (below deposits vs. next to deposits) reflected a heterogeneous distribution of kelp fragments. Rates varied with 2 orders of magnitude within individual depth profiles and between depth
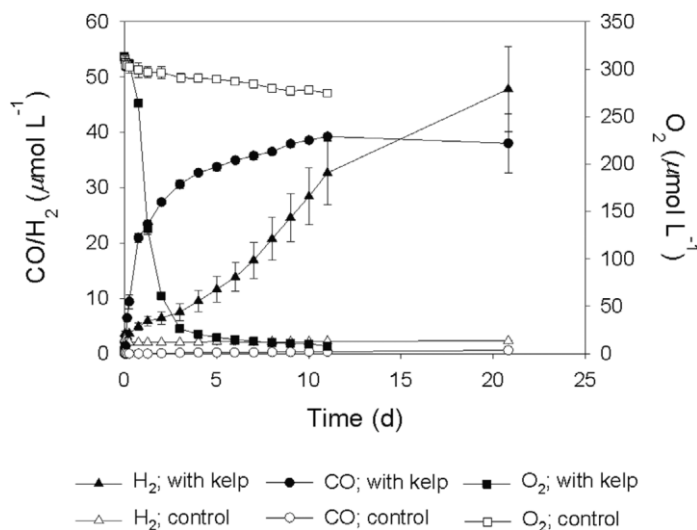

Fig. 6. H_2 (triangles), CO (circles) and O_2 (squares) concentrations within incubations with kelp (filled symbols) and within controls (open symbols).

profiles (Table 3). All rates for sediments from the reference beach were below the minimum detection limit of 2.46×10^{-9} mol m^{-3} s^{-1} (Table 3).

The average SRR in sediments from the kelp-beach was $3.77 \times 10^{-6} \pm 6.34 \times 10^{-6}$ mol m^{-3} s^{-1} (Table 3; median was 1.25×10^{-6} mol m^{-3} s^{-1}). The SO$_4^{2-}$ turnover time was 13 d, as calculated by dividing the depletion of SO$_4^{2-}$ per volume sediment (15 mol depletion m^{-3} porewater $\times$ porosity of 0.28 = 4.2 mol depletion m^{-3} sediment) by the average SRR of 3.77×10^{-6} mol m^{-3} s^{-1}.

Addition of kelp leaf fragments to kelp-beach sediments led to a 20- to 25-fold increase in SRR. In treatments with only kelp, no SO$_4^{2-}$ reduction occurred (average counts over the 4 treatments is below the minimum detection limit), and in treatments with only sediment SRR are low (average $0.31 \times 10^{-6} \pm 0.12 \times 10^{-6}$ mol m^{-3} s^{-1}; median 0.26×10^{-6} mol m^{-3} s^{-1}). Only the mixture of kelp leaf fragments and sediment leads to a direct stimulation of SRR, resulting in an average rate of $7.06 \times 10^{-6} \pm 2.49 \times 10^{-6}$ mol m^{-3} s^{-1} (median of 8.12×10^{-6} mol m^{-3} s^{-1}). The SO$_4^{2-}$ turnover time calculated using the average SRR from this experiment (7.06×10^{-6} mol m^{-3} s^{-1}) and the 4.2 mol depletion m^{-3} sediment is 7 d.

Microbial community composition

In order to assess the effect of kelp deposition on the microbial community composition, we performed 16S rRNA gene amplicon sequencing of the DNA extracted from different sediment layers from the kelp-beach and the reference beach. Additionally, we sequenced the white filaments growing on green algae on rocks at the kelp-beach low tide waterline and samples of seawater from the beaches and harbors around the main island of Helgoland. An overview of the sequencing efforts can be found in Supplementary Information (Table S1).

We clustered the samples based on the similarity of their microbial community composition on SWARM-generated OTU level (Fig. 7). All samples clustered based on the sample type and location they were coming from.

In general, the community in kelp-beach sediment differed from that in reference beach sediment by showing higher average proportions of the fermenters, such as *Clostridia* (4% compared to 0.3%), *Fusobacteria* (3.4% compared to 0.8%), *Kiritimatiellaeota* (4.2% compared to 0.2%), *Gracilibacteria* (2.3%

compared to 0.05%), *Spirochaetes* (3% compared to 0.3%), the SO$_4^{2-}$ reducing *Deltaproteobacteria* (13% compared to 8%), and the sulfide-oxidizing *Epsilonbacteraeota* (17% compared to 3%) (Fig. 7). In the three deepest layers of kelp-beach sediments, the methanogenic archaea *Methanolobus* was present, albeit in very low proportion (0.02–0.04%).

For samples next to kelp deposits, a clear shift of the microbial community composition with depth was apparent (Fig. 7). With depth *Epsilonbacteraeota* (consisting of *Sulfurovum* and *Sulfurimonas*) dramatically decreased (from 40% to 4.5%), while *Deltaproteobacteria*, *Bacteroidetes*, *Clostridia*, *Fusobacteria*, *Kiritimatiellaeota*, and *Spirochaetes* increased (all together from 23% to 49%; Fig. 7).

No trend with depth and only little variation in microbial community was detectable in samples from below kelp deposits. The proportion of *Desulfobacteraceae* (*Deltaproteobacteria*) sequences was constant with depth (12% $\pm$ 2%). Proportions of *Clostridia*, *Kiritimatiellaeota*, *Gracilibacteria*, and *Spirochaetes* were higher than in reference beach samples but lower than in the kelp-beach sediment from next to a deposit. The sediment samples taken below a kelp deposit also had increased proportions of *Thiotrichaceae* sequences (10%) and the highest proportions of *Bacteroidetes* (24%).

The community of the white filaments had a higher similarity to that of sediment samples from below kelp deposits than to the communities of reference sediment and seawater (Fig. 7). The communities of the white filaments were dominated by *Thiotrichaceae* (on average 32%) and *Sulfurovum* (on average 39%) sequences, with only small proportions of *Bacteroidetes* (on average 4%), *Gracilibacteria* (on average 4.8%), and *Alphaproteobacteria* (on average 4%). The *Thiotrichaceae* and *Sulfurovum* sequences were also found in all other samples, but in lower relative abundances (not higher than 7.5% and 21%, respectively). *Sulfurimonas* sequences which were co-occurring with *Sulfurovum* in all other samples (Fig. 7) were absent from the samples of the white filaments. Interestingly, the two OTUs constituting the large part of *Sulfurovum* sequences in the white filaments (on average 27%) and the sediment under the kelp deposit (on average 5.8%) were only found in very low relative abundance in all other samples (not higher than 3.8%). The most abundant *Sulfurovum* OTU in the sediment samples from next to a kelp

Table 3. SO$_4^{2-}$ reduction rate (SRR) for sediments from the kelp-beach and the reference beach and from the kelp deposition simulation experiment with sediment from the kelp-beach. Also shown are the minimum and maximum rates for kelp-beach sediments. SRR within reference beach sediments was below the minimum detection limit (2.46×10^{-9} mol m^{-3} s^{-1}).

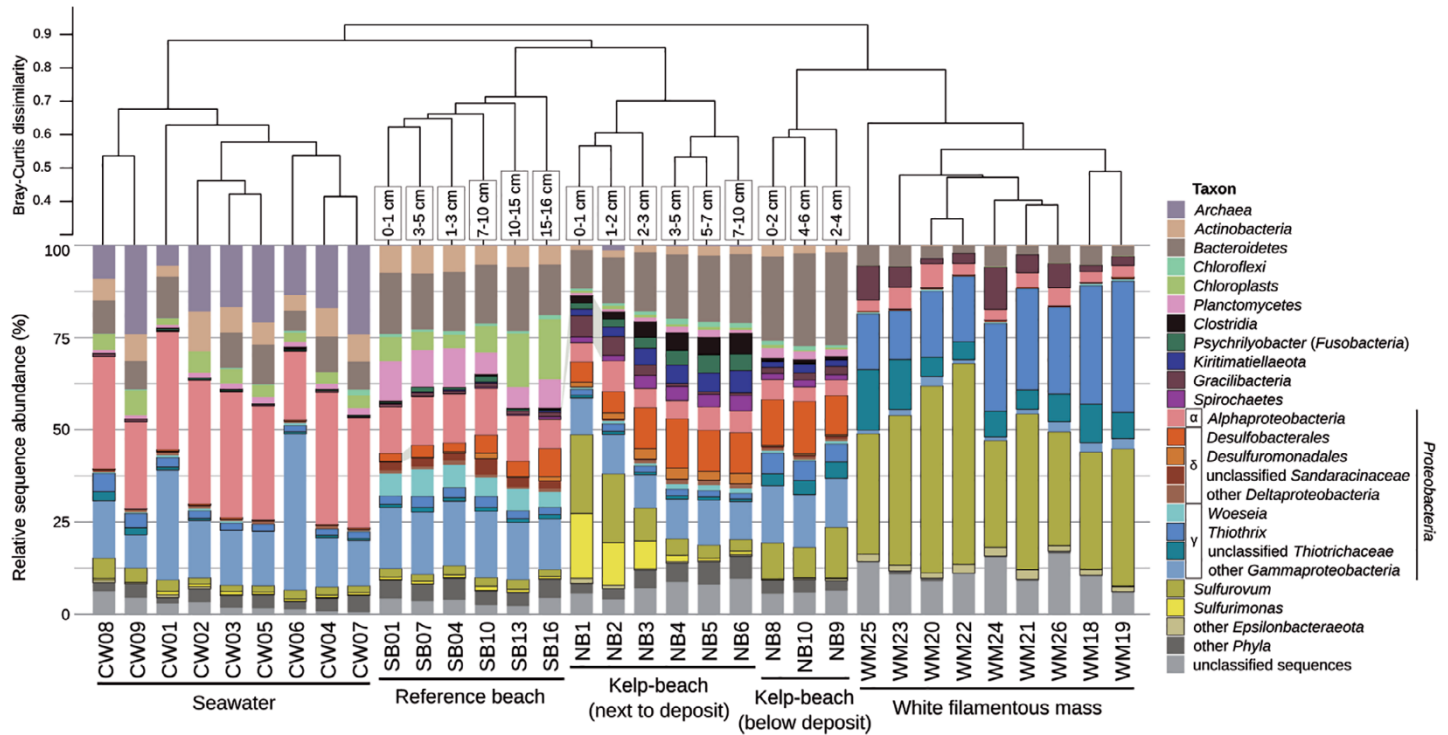|	Average SRR (mol m^{-3} s^{-1})	Maximum SRR (mol m^{-3} s^{-1})	Minimum SRR (mol m^{-3} s^{-1})
Kelp-beach	$3.77 \times 10^{-6} \pm 6.34 \times 10^{-6}$	2.23×10^{-5}	2.05×10^{-7}
Reference beach	Below minimum detection limit	—	—
Experiment			
Sediment	$0.31 \times 10^{-6} \pm 0.12 \times 10^{-6}$		
Kelp plus sediment	$7.06 \times 10^{-6} \pm 2.49 \times 10^{-6}$		

Fig. 7. Microbial community composition based on 16S rRNA gene amplicon sequences. Samples were clustered based on their community composition according to a Bray–Curtis dissimilarity matrix. For the sediment samples the depth in cm is indicated above the bars.

deposit and in the reference beach samples did not surpass 0.6% in the sediment under the kelp and white filaments.

Detection of *Sulfurovum* by FISH

We performed FISH with a *Gammaproteobacteria*-specific probe (GAM42a) and *Sulfurovum*-specific probe mix (SFO1112 and SFO1210, McNichol et al., https://osf.io/yts4p/, accessed on 18 July 2020). We could detect both groups growing as filaments directly next to each other, attached to green algae on rocks at the low tide waterline (Fig. 8), thus within the oxic seawater environment.

Genomic potential of filamentous biomass

We sequenced three metagenomes of the white filaments and performed metagenomic binning to obtain population genomes (bin metrics in Supplementary Information, Table S1). Our assembly is representing over 69% of the raw reads based on read mapping. Over 84% of the assembled metagenome is in bins with over 50% completeness and less than 10% contamination (based on CheckM analysis).

We obtained a total of six *Sulfurovaceae* (according to GTDB classification) population genomes (81–99% completeness, 1–5% contamination) and compared their genomic potential to other published *Sulfurovum* genomes and metagenomic bins (Fig. 9). The potential for oxidizing reduced sulfur species (sulfide: quinone reductase and SOX system encoding genes) as well as the potential for CO_2-fixation via reductive

tricarboxylic acid cycle was present in all genomes. The difference with published *Sulfurovum* genomes with respect to the basic energy generation metabolism seemed to occur on the electron acceptor side. Our genomes lack the genes for NO-forming nitrite reductase and nitric- and nitrous-oxide reductases. Thus, these aerobic sulfur oxidizers cannot perform denitrification.

Another difference was the presence of a low-affinity Cytochrome C oxidase (aa3, Type A2), which was not found in most of the other genomes, except *Sulfurovum* sp. isolated from marine sediment, *Sulfurovum* genome from a surface biofilm in the Frassassi caves, a mine drainage run-off metagenomic bin and in one of the hydrothermal genomes. However, all *Sulfurovum* genomes also encoded genes for the high-affinity Type-C (cbb3) terminal oxidase.

Another gene unique to the Helgoland bins was encoding a Ferritin-like antioxidant protein hinting at an increased ability of tolerating exposure to O_2.

Total cell counts

The amount of cells on the kelp-beach was not much higher than on the reference beach ($2.18 \times 10^8 \pm 5.33 \times 10^7$ cells cm^{-3} sediment compared to $1.82 \times 10^8 \pm 2.63 \times 10^7$ cells cm^{-3} sediment). Considering the big difference in rates of microbially mediated processes, this small difference in cell numbers suggests that the microbial community at the kelp-beach is more active.
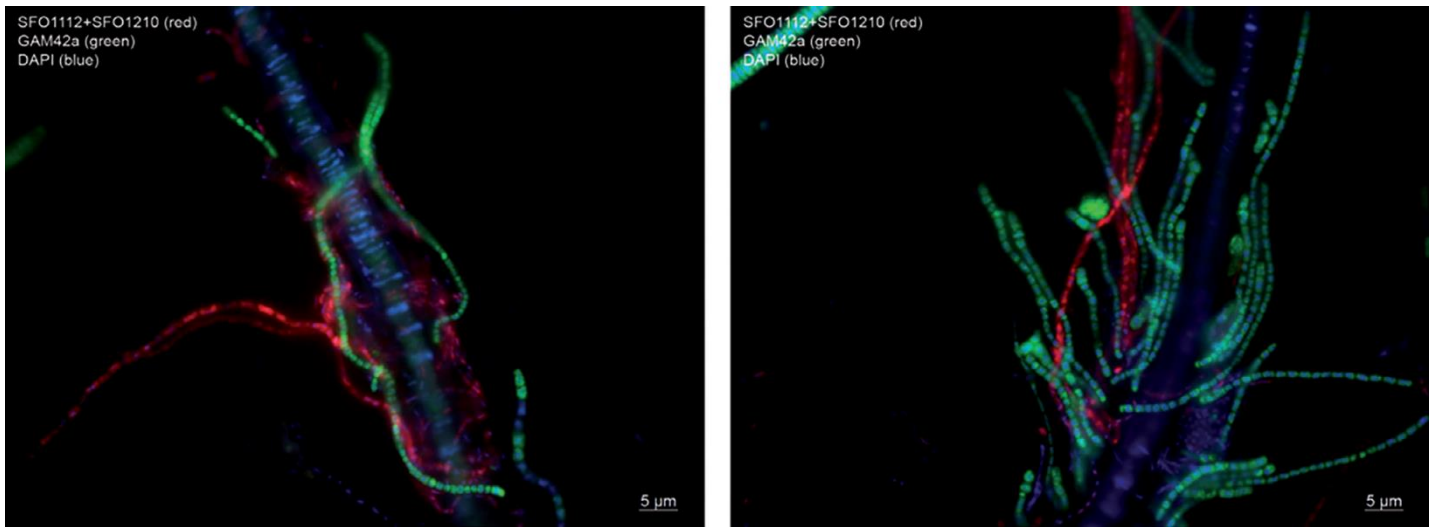
Fig. 8. Fluorescent microscopy images of sulfur-oxidizing bacterial filaments attached to the green algae. The cells are labeled with *Gammaproteobacteria*- (GAM42a; in green), and *Sulfurovum*-specific (SFO1112 + SFO1210; in red) rRNA probes. DAPI signals are shown in blue.
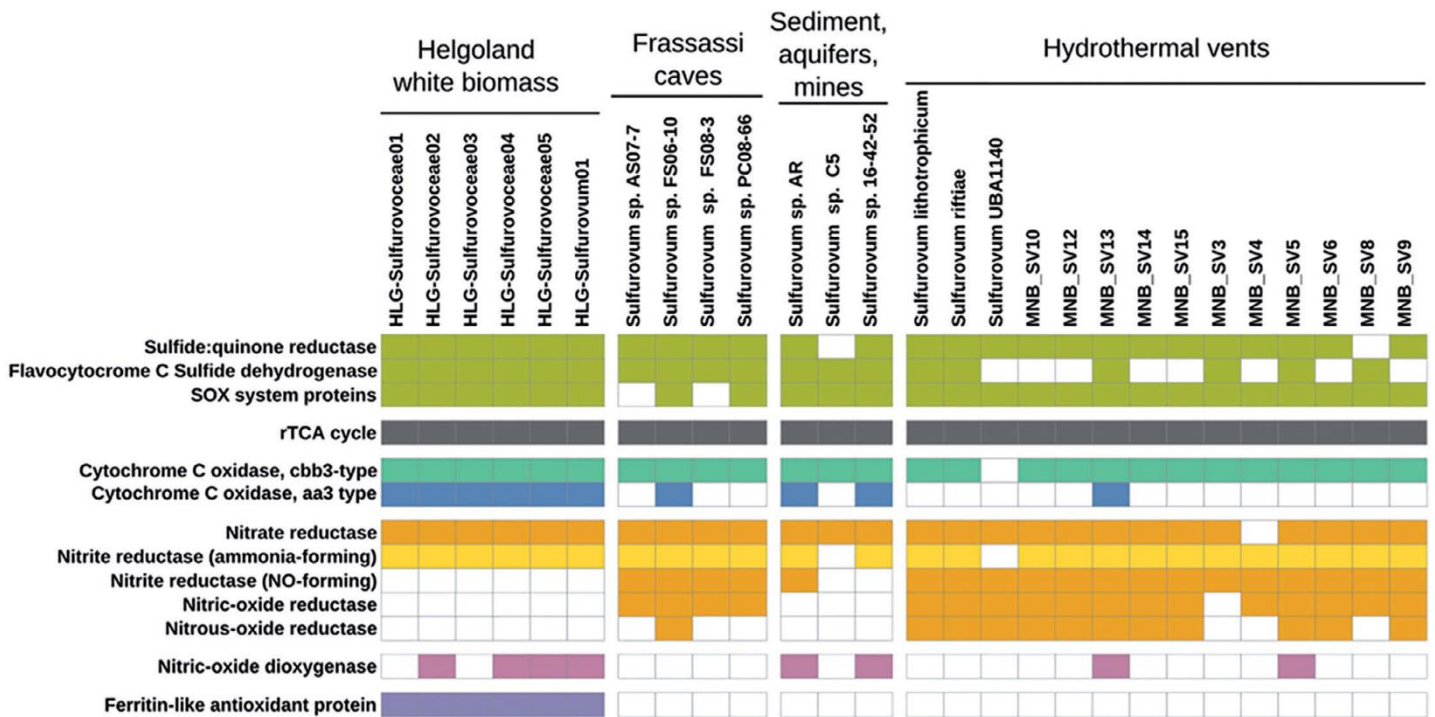
Fig. 9. Basic genomic potential of the *Sulfurovum*-related bins in comparison to other sequenced *Sulfurovum* genomes and metagenomic bins (Meier et al. 2017), with project accession number PRJEB15554. The comparison was mainly based on presence-absence of orthologous clusters based on Egg-NOG annotation and cross-checked with the other annotation sources: BLAST vs. (point behind the s) Uniprot, RAST, Pfam. For the *Sulfurovum* UBA1140 genome genes were predicted and annotated de-novo. All annotations can be found in Supplementary Information (Table S3).

Discussion

Kelp deposits that are not swept back out to sea by the next tide become partly buried, decomposed, and eventually heterogeneously distributed as fragments over the beach surface and within the sediment. Burial of kelp fragments thus leads to mixing of fresh and decayed organic material. Kelp fragments are composed of both labile and refractory compounds, which are degraded at different rates. Intertidal zones are dynamic systems, in which changes in hydration, temperature and salinity can be large and fast. All these factors will lead to

a high variability in decomposition rates. Laboratory measured rates must therefore be seen as approximates of rates occurring in situ.

Kelp deposition is the main factor in shaping the composition and function of the microbial communities at the kelp-beach and the main cause of the observed differences between the two studied beaches. The sediment characteristics were nearly identical (Supplementary Information, Table S2), and can thus not be the main determinant for the different geochemistries. The dominant winds around Helgoland are west-southwesterly (Siegismund and Schrum 2001), and the residual currents are north–south oriented (von Haugwitz et al. 1988). The kelp-beach faces northwest and the reference beach southeast. The kelp-beach is adjacent to rocky seafloor covered with kelp forests (Uhl et al. 2016). The reference beach does not face a large kelp forest (Uhl et al. 2016) and wind and current directions are not oriented toward the beach. Therefore, the kelp-beach is regularly covered with kelp, while the reference beach is not, thus kelp deposits are the main determinant for the distinct geochemistry of the kelp-beach.

Although the heterogeneity of the sediments was reflected in the geochemical data that showed very large standard deviations and scattered trends with depth, our data demonstrated that the presence of kelp deposits strongly enhanced microbial degradation processes. Furthermore, the release of reduced material was so large that it cannot be oxidized locally, driving a sulfuretum in the adjacent sea. Such phenomena are restricted to beaches near rocky coasts, as kelp needs a hard substrate to attach. This study extends the knowledge on mineralization pathways of kelp deposited on beaches, as it combines both geochemical and microbial community data, and shows that kelp deposition leads to unique conditions. Especially, the high SO_4^{2-} reduction can induce high concentrations of free sulfide, even in the oxic parts of the ecosystem. This in turn leads to a distinct microbial community within sediments and on solid surfaces in the adjacent sea. Fragmentation by physical forces and macro- and meiofauna will facilitate and stimulate the subsequent microbial processes, of which hydrolysis, fermentation, aerobic respiration, Fe reduction, and SO_4^{2-} reduction will be discussed sequentially.

Hydrolysis and fermentation processes

Elevated DOC levels plus the strongly enhanced consumption of electron acceptors indicated that hydrolysis was active and extremely fast. Active fermentation was demonstrated by the low pH, much lower than can be explained by CO_2 production during aerobic respiration alone. CO_2calc is a program for calculations on the DIC system, which relates a suite of relevant input parameters to determine the concentration and speciation of the DIC system. CO_2calc v. 2.1.0 (Robbins et al. 2010) was used to assess the change in pH as a result of CO_2 production by aerobic respiration. First, the total CO_2 concentration in the kelp-beach porewaters was calculated to

be 2.23 mmol kg^{-1}. Subsequently, the pH was calculated for a situation in which all O_2 is consumed and thus an equal amount of CO_2 is released. This total removal of O_2 and thus increase in CO_2 equals 0.21 mmol kg^{-1}, leading to a new total CO_2 concentration of 2.44 mmol kg^{-1}. Input of this new total CO_2 concentration resulted in a pH value of 7.58, which is thus the value that is induced by aerobic respiration. As porewater may be more strongly buffered than seawater, the actual decrease by respiration may even be overestimated. SO_4^{2-} reduction will not lead to a further decrease (Soetaert et al. 2007). Furthermore, sulfide oxidation will not be of importance, as the sediments are anoxic. Hence, the only process that can drive the pH down to 6.7 is the production of organic acids by fermentation.

Elevated hydrolysis and fermentation within kelp-beach sediments is furthermore supported by the higher abundances of polymer hydrolysers like *Bacteroidetes* and fermenters like various *Clostridiales*, *Psychrilyobacter*, *Kiritimatiellaeota*, and *Spirochaetes* (see https://lpsn.dsmz.de, accessed on 18 July 2020) in kelp-beach sediments.

SO_4^{2-} reducing bacteria cannot use complex and large organic molecules, and these kelp-derived molecules must thus first be hydrolysed and fermented to e.g., volatile fatty acids and H_2. Fermentation is therefore an important intermediate process in this environment, as SO_4^{2-} reduction occurs extensively.

The pathway of electron transport from fermentation to SO_4^{2-} reduction via DOC was considered to be significant, since fermentation occurred intensively, and DOC concentrations in porewaters were high (up to 8.9 mmol L^{-1}).

Aerobic respiration

It appeared to be difficult to determine aerobic respiration reliably, as the transport mechanisms could not well be constrained. The O_2 fluxes determined from the profiles assuming diffusion as transport process underestimated the aerobic respiration, as also advective transport will occur. Conversely, the areal O_2 consumption rates determined from the volumetric rates and the penetration depth overestimated the aerobic respiration, as the sediments were homogenized and sieved, hence also strongly reduced deeper sediments, that normally would not be in contact with O_2 were taken into the calculation. Furthermore, in situ, the kelp deposits could physically restrict advective transport of seawater and thereby O_2 into the sediments, leading to a lower penetration depth. O_2 only penetrated the kelp-beach sediments during inundation. Thus, the rates were corrected for the inundation time of 16 h d^{-1}. The diffusive O_2 flux was 2.8×10^{-8} mol m^{-2} s^{-1} (below a kelp deposit) and the areal O_2 consumption rate was 1.8×10^{-6} mol m^{-2} s^{-1}.

Diffusive O_2 fluxes within kelp-beach sediments were enhanced by two orders of magnitude compared to reference beach sediments, and the areal O_2 consumption rate is 1.4 times higher, which results in rapid depletion of O_2. During low tide, O_2 penetration was low, while during high tide O_2

penetrated the sediments by hydrodynamic forcing (Werner et al. 2006). Therefore, aerobic respiration could only occur during high tide.

The O_2 microprofiles were measured during a period with extensive kelp deposits (~0.5 m thick and covering a large part of the beach surface), and aerobic respiration rates were thus likely relatively high compared to rates during other times of the year. Based on the microbial community composition profile, the microorganisms likely responsible for fast O_2-consumption were *Bacteroidetes*, which are known to degrade complex plant- or algae-derived sugar polymers (see https://lpsn.dsmz.de, accessed on 18 July 2020) and sulfide-oxidizing *Epsilonbacteraeota*, which were present in very high relative abundances in upper sediment layers. These microbial clades showed massively increased relative sequence abundances in kelp-beach sediments compared to reference beach sediments.

Aerobic respiration can be a proxy for the sum of all mineralization processes occurring within sediments (Canfield et al. 1993), as O_2 is used in aerobic respiration and in the reoxidation of the products of anaerobic respiration (e.g., Fe^{2+}, H_2S, CH_4). In this study, this is clearly not the case. Reduced intermediates escape to the atmosphere and the sea, as evidenced by a strong sulfidic smell, the presence of sulfide oxidizers at the low tide waterline, and the occasionally high concentrations of nutrients, DOC, and sulfide in seawater. Also CH_4 is expected to escape from the sediments to the atmosphere. These reduced products of anaerobic respiration are thus not reoxidized locally by O_2 and aerobic respiration does not represent the sum of all mineralization processes.

Fe reduction

The Fe chemistry of the kelp-beach was completely different from that of the reference beach. In kelp-beach sediments, Fe(III) is converted to Fe^{2+}, which may subsequently precipitate as FeS and FeS_2. The Fe cycling is thus tightly linked to SO_4^{2-} reduction. Our extraction method does not extract the Fe(II) present as FeS_2, and the pool of Fe(II) within the sediments is thus underestimated. The absence of Fe(III) below kelp deposits points to a very strong Fe reduction potential. The regular physical forcing by storms will expose these reduced sediments to O_2 resulting in reoxidation of the Fe sulfides. Fe reduction is probably not an important process in kelp degradation, but its role as sulfide scavenger makes the process important in this environment.

SO_4^{2-} reduction

The composition of the microbial community in kelp-beach sediments appears optimized for efficient kelp degradation. The sediment below a kelp deposit as well as deeper layers of sediments next to a deposit showed increased relative proportions of SO_4^{2-} reducing deltaproteobacterial clades such as *Desulfobacterales* and *Desulfuromonadales* (see https://lpsn.dsmz.de, accessed on 18 July 2020) indicating an

enhancement of SO_4^{2-} reduction induced by the kelp-derived organic material. This community composition is likely driven by regular sudden depositions of kelp, and enables rapid and efficient hydrolysis of large amounts of organic material, leading to stimulated SO_4^{2-} reduction. Only the mixing of kelp fragments into sediment, however, results in high SRR. SO_4^{2-} reduction was absent in treatments with only kelp (Table 3). Thus, the stimulation of SO_4^{2-} reduction is not driven by microorganisms on the kelp itself, but by the microbial community in kelp-beach sediments.

Consistent with bacterial distributions and the kelp deposition simulation experiments, the in situ SRR were greatly stimulated by the presence of kelp deposits. The average SRR were comparable to SRR reported for sandy intertidal sediments with high contents of organic material (Kristensen et al. 2000), but also exhibited variability in volumetric rates of up to one order of magnitude around the average (Table 3). We observed an average depletion of about 15 mmol L^{-1} SO_4^{2-} in the kelp-beach sediment porewaters relative to the reference beach (Fig. 3c). Approximately 13 d would be required to deplete SO_4^{2-} by this amount given the average SRR observed for the kelp-beach sediments. This appears to be longer than the expected residence time of porewaters for beach sediments (2–8 d) as reported for Catalina Island (Colbert et al. 2008), which is also surrounded by kelp beds. Our reported SRR may, therefore, be underestimated. The SRR were determined in October 2018, when both kelp availability and temperatures were significantly lower than in May 2018, the period of the SO_4^{2-} and sulfide measurements. Higher temperatures and availability of degradable organic material lead to higher SRR in marine surface sediments (Kristensen et al. 2000). The kelp deposition simulation experiments yielded SO_4^{2-} turnover times of only 7 d. Moreover, under conditions where sulfide oxidation can occur, especially in the presence of Fe oxides formed upon sediment oxygenation during mixing and porewater advection events (both in situ and in the incubation experiments), rapid sulfide oxidation may lead to substantial underestimation of SRR (Moeslund et al. 1994).

Methanogenesis

It is generally accepted that methanogens are outcompeted by SO_4^{2-} reducers, due to competition for H_2 and acetate (Sansone and Martens 1982). As indicated by slightly elevated CH_4 concentrations, deposition of kelp fragments, and thus degradable organic material, relieves methanogens from competition. High DOC concentrations in porewater (up to 8.9 mmol L^{-1}) show that indeed sufficient substrate is available. Supporting the occurrence of methanogenesis, we have found sequences of likely methylotrophic methanogenic *Methanolobus* archaea (see https://lpsn.dsmz.de, accessed on 18 July 2020), but only in the three deepest layers of sediment of the kelp-beach.

Aerobic respiration vs. SO_4^{2-} reduction rates

The ratio of aerobic respiration rates and SRR is relevant as aerobic processes can remove the products of anaerobic degradation, like sulfide. The uncertainty of the areal O_2 consumption rates complicates the assessment which process is most important. The aerobic processes only can occur during high tide, but SO_4^{2-} reduction continued during low tide, as SO_4^{2-} was never depleted. The estimation of the areal SRR from our measurements within the top 10 cm (3.8×10^{-7} mol m^{-2} s^{-1}) strongly underestimated the areal SRR, as SO_4^{2-} reduction occurred probably even to 1 m depth (the level of the low water line), hence the areal SRR may be underestimated by an order of magnitude. Previously, high SRR were found to occur to the level of the low water line in an intertidal sand flat, below which the rates decreased (Schutte et al. 2019). The areal SRR was 13.4 times higher than diffusive O_2 fluxes, but 4.6 times lower than areal O_2 consumption rates. However, as the areal SRR were probably about 10 times underestimated, the areal SRR may have been an order of magnitude higher than the areal O_2 consumption rates.

Also, the leakage of reduced products either next to, or through the oxygenated surface sediments, indicates that SO_4^{2-} reduction could be more important than found previously in intertidal flats and sandy beaches of the North Sea (Werner et al. 2006). We conclude that organic carbon remineralization in kelp deposits on sandy beaches is primarily driven by SO_4^{2-} reduction, and not aerobic respiration.

CO and H_2 dynamics

Higher concentrations of both CO and H_2 in kelp-beach compared to reference beach sediments indicate a production related to kelp decomposition. Our laboratory experiment showed that net CO formation from kelp mainly occurs when O_2 is available, as expected (Conrad and Seiler 1985). Therefore, the process of CO production is only of potential importance during high tide, which is when O_2 penetrates into the sediments. Net H_2 production only occurs when conditions are anoxic, thus during low tide. However, whereas CO was indeed formed under oxic conditions, it was not consumed during the subsequent anoxic phase (Fig. 6). The absence of anaerobic CO consumption indicates that the H_2 is probably not originating from CO disproportionation. Instead, the H_2 measured in the sediments is likely formed by fermentation processes. Sequences of microorganisms related to known H_2-producing fermenters like *Psychrilyobacter* (see https://lpsn.dsmz.de, accessed on 18 July 2020) were detected in increased relative abundances in kelp-beach sediments. The pathway to SRR via CO is likely not of major importance, since even if all O_2 would be used for CO production, this would not be able to fuel the very high SRR we measured.

Reduced compounds in the environment

Reduced compounds accumulate in kelp-beach sediments during low tide. During these periods of exposure, there is no advective input of oxygenated seawater. O_2 is quickly depleted, and concentrations of DOC, DIC, sulfide, S^{2-}_{tot}, N_2O, CH_4, and the nutrients NH_4^+ and P_i are high. We cannot explain the low TOC content of the kelp-beach sediment, which is almost equal to that of the reference beach sediments. The biodegradability of the TOC in kelp-beach sediment must have been much higher than that of the TOC in reference beach sediment. Although sulfide concentrations are high, they are lower than expected based on the stoichiometry of SO_4^{2-} reduction. The observed decrease of SO_4^{2-} concentrations of about 15 mmol L^{-1} would lead to the production of an equal amount of sulfide. However, sulfide concentrations reach average concentrations of about 10 mmol L^{-1}. Since we proposed that SO_4^{2-} reduction is the dominant process removing SO_4^{2-} from the porewaters, the discrepancy between SO_4^{2-} depletion and sulfide accumulation is likely caused by removal of the produced sulfide. Several processes could be responsible for the sulfide removal. One is the production of Fe sulfides, which are indeed present in elevated concentrations within kelp-beach sediments. Also, sulfide-oxidizing *Sulfurimonas*, *Sulfurovum*, and *Thiotrichaceae* occur in higher abundances within kelp-beach sediments than in reference beach sediments. Surprising is the large abundance of *Sulfurimonas* and *Sulfurovum* that are typical inhabitants of hydrothermal vent systems (Inagaki et al. 2004; Mino et al. 2017).

Sulfide that is not removed from the sediments by Fe sulfide precipitation or reoxidation escapes the sediments and reaches the atmosphere or sea. Incomplete removal of sulfide led to an intense sulfidic smell and the detection of sulfide within adjacent seawater, which enabled massive filamentous growth of sulfur-oxidizing bacteria on green algae on rocks at the low tide waterline. Surprisingly, these white filaments were not only made up of sulfur-oxidizing *Gammaproteobacteria* known from terrestrial and coastal environments (Salman et al. 2013), but also *Epsilonbacteraeota* from the family of *Sulfurovaceae*. The FISH analysis showed that both were exhibiting filamentous morphology and were growing directly next to each other. Sulfur-oxidizing *Epsilonbacteraeota* like *Sulfurovaceae* are mostly known from micro-oxic and anoxic habitats (Nakagawa et al. 2005; Meyer et al. 2013). Filamentous growth of *Sulfurovaceae* was also observed in sulfidic streams of Frassassi caves (Hamilton et al. 2015). However, in all these environments, they were found to oxidize reduced sulfur compounds via denitrification or aerobic respiration by means of high-affinity cbb3-type terminal oxidases adapted to low O_2 concentrations. The carbon fixation pathway utilized by *Epsilonbacteraeota* (reductive tricarboxylic acid cycle) is considered to be O_2 sensitive due to involvement of ferredoxins that can be oxidized easily (Campbell et al. 2006). It was very surprising to find these organisms abundantly growing on surfaces exposed to high O_2 concentrations. Remarkable is also that they have lost the genetic capacity for denitrification, which must be an adaptation to the oxic environment. Notably, the species (OTUs) forming the

white filaments did not surpass 1% relative abundance in the sediments. Instead, sediment samples were dominated by other *Sulfurovaceae* species, which are probably more adapted to low O_2 environments.

Kelp deposition enriches a rare sulfur-oxidizing *Sulfurovaceae* species adapted to oxic environments. A brief analysis of the genomic potential and comparison to other *Sulfurovaceae* genomes showed that the genomes of filament-forming *Sulfurovaceae* populations encoded low-affinity aa3-type terminal oxidases absent from the vast majority of reference genomes. As also no denitrification genes were found, these filament-forming *Sulfurovaceae* species are adapted to aerobic respiration at high O_2 concentrations. A gene unique to the Helgoland genomes was encoding an anti-oxidative protein, hinting at further unique adaptation to high O_2 levels. All denitrification genes (e.g., for nitric- and nitrous-oxide reductases) found in the metagenome were associated to *Gammaproteobacteria*. However, the Helgoland *Sulfurovum* genomes encoded a NO-detoxifying dioxygenase. This might be a hint that although they cannot denitrify themselves, they might be adapted to co-exist with NO-evolving incomplete denitrifyers.

The microbial community composition showed clear stratification by depth only in the kelp-beach sediments, yet not underneath the deposits themselves. As typically in sediments, the microbial community stratification seems to reflect the different O_2 levels with SO_4^{2-} reducers and anaerobic organisms more abundant in the lower and sulfide oxidizers and aerobic microorganisms more abundant in the upper layers. While the lack of stratification at the reference beach is likely caused by high permeability and resulting oxygenation of the sediment combined with low respiration rates, underneath the kelp the lack of stratification is likely caused by the lack of O_2 penetrating the sediment from above.

Further research is needed in order to elucidate the main substrates for SO_4^{2-} reducers. One of the steps would be to focus on obtaining a more detailed view of the heterotrophic microorganisms associated with kelp-beach sediments, and investigate who are the specialized kelp degraders present. It would furthermore be of importance to find the hydrolysis products, and test their effects on aerobic respiration and SO_4^{2-} reduction.

Conclusions

Although sandy beaches are very dynamic systems with fast and large changes in hydration, temperature and salinity, the intense degradation of kelp deposits leads to distinct changes in biogeochemical conditions and microbial community composition in the underlying sandy sediments. The major processes driving these changes are highly increased fermentation and SO_4^{2-} reduction. We found that the sum of degradation processes in sandy sediments is not reflected in the total respiration rate, as these sediments are an open system where reduced compounds are washed out before they are completely oxidized. The export of intermediates and sulfide from kelp deposits leads to a spatial separation of SO_4^{2-} reduction and sulfide oxidation. The described conditions select for a microbial community composition that is highly optimized for degradation of large amounts of kelp. It is ready to instantly start kelp degradation and able to efficiently utilize the resulting large amounts of reduced compounds.

References

Berner, R. A. 1980. Early diagenesis: A theoretical approch. Princeton Univ. Press.

Böttcher, M. E., A. Rusch, T. Höpner, and H.-J. Brumsack. 1997. Stable sulfur isotope effects related to local intense sulfate reduction in a tidal sandflat (southern North Sea): Results from loading experiments. Isotopes Environ. Health Stud. **33**: 109–129. doi:10.1080/10256019808036363

Campbell, B. J., A. S. Engel, M. L. Porter, and K. Takai. 2006. The versatile ε-proteobacteria: Key players in sulphidic habitats. Nat. Rev. Microbiol. **4**: 458–468. doi:10.1038/nrmicro1414

Canfield, D. E. et al. 1993. Pathways of organic carbon oxidation in three continental margin sediments. Mar. Geol. **113**: 27–40, doi: 10.1016/0025-3227(93)90147-N

Chen, J. and others. 2017. Impacts of chemical gradients on microbial community structure. ISME J. **11**: 920–931, doi: 10.1038/ismej.2016.175

Cline, J. D. 1969. Spectrophotometric determination of hydrogen sulfide in natural waters. Limnol. Oceanogr. **14**: 454–458. doi:10.4319/lo.1969.14.3.0454

Colbert, S. L., W. M. Berelson, and D. E. Hammond. 2008. Radon-222 budget in Catalina Harbor, California: 2. Flow dynamics and residence time in a tidal beach. Limnol. Oceanogr. **53**: 659–665. doi:10.4319/lo.2008.53.2.0659

Colombini, I., A. Aloia, M. Fallaci, G. Pezzoli, and L. Chelazzi. 2000. Temporal and spatial use of stranded wrack by the macrofauna of a tropical sandy beach. Mar. Biol. **136**: 531–541. doi:10.1007/s002270050713

Colombini, I., and L. Chelazzi. 2003. Influence of marine allochthonous input on sandy beach communities. Oceanogr. Mar. Biol. Annu. Rev. **41**: 115–159.

Conrad, R., and W. Seiler. 1985. Characteristics of abiological carbon monoxide formation from soil organic matter, humic acids, and phenolic compounds. Environ. Sci. Technol. **19**: 1165–1169. doi:10.1021/es00142a004

Dugan, J. E., D. M. Hubbard, H. M. Page, and J. P. Schimel. 2011. Marine macrophyte wrack inputs and dissolved nutrients in beach sands. Estuaries Coasts **34**: 839–850. doi:10.1007/s12237-011-9375-9

Duggins, D. O., C. A. Simenstad, and J. A. Estes. 1989. Magnification of secondary production by kelp detritus in coastal marine ecosystems. Science **245**: 170–173. doi:10.1126/science.245.4914.170

Froelich, P. N., and others. 1979. Early oxidation of organic matter in pelagic sediments of the eastern equatorial Atlantic: Suboxic diagenesis. Geochim. Cosmochim. Acta **43**: 1075–1090. doi:10.1016/0016-7037(79)90095-4

Grasshoff, K., K. Kremling, and M. Ehrhardt. 1999. Methods of seawater analysis. New York: Wiley.

Hall, P. O. J., and R. C. Aller. 1992. Rapid, small-volume, flow injection analysis for ΣCO_2, and NH_4^+ in marine and freshwaters. Limnol. Oceanogr. **37**: 1113–1119. doi:10.4319/lo.1992.37.5.1113

Hamilton, T. L., D. S. Jones, I. Schaperdoth, and J. L. Macalady. 2015. Metagenomic insights into S(0) precipitation in a terrestrial subsurface lithoautotrophic ecosystem. Front. Microbiol. **5**: 756. doi:10.3389/fmicb.2014.00756

Inagaki, F., K. Takai, K. H. Nealson, and K. Horikoshi. 2004. *Sulfurovum lithotrophicum* gen. nov., sp. nov., a novel sulfur-oxidizing chemolithoautotroph within the *ε-Proteobacteria* isolated from Okinawa trough hydrothermal sediments. Int. J. Syst. Evol. Microbiol. **54**: 1477–1482. doi:10.1099/ijs.0.03042-0

Jeroschewski, P., C. Steuckart, and M. Kühl. 1996. An amperometric microsensor for the determination of H_2S in aquatic environments. Anal. Chem. **68**: 4351–4357. doi:10.1021/ac960091b

Jickells, T. D., and J. E. Rae. 1997. Biogeochemistry of intertidal sediments, p. 1–15. *In* T. D. Jickells and J. E. Rae [eds.], Biogeochemistry of intertidal sediments. Cambridge University Press.

Jørgensen, B. B. 1982. Mineralization of organic matter in the sea bed—The role of sulphate reduction. Nature **296**: 643–645. doi:10.1038/296643a0

Koop, K., and J. G. Field. 1980. The influence of food availability on population dynamics of a supralittoral isopod, *Ligia dilatata* brandt. J. Exp. Mar. Biol. Ecol. **48**: 61–72. doi:10.1016/0022-0981(80)90007-6

Koop, K., and C. L. Griffiths. 1982. The relative significance of bacteria, meio- and macrofauna on an exposed sandy beach. Mar. Biol. **66**: 295–300. doi:10.1007/BF00397035

Koop, K., R. C. Newell, and M. I. Lucas. 1982. Biodegradation and carbon flow based on kelp (*Ecklonia maxima*) debris in a sandy beach microcosm. Mar. Ecol. Prog. Ser. **7**: 315–326. doi:10.3354/meps007315

Kristensen, E., J. Bodenbender, M. H. Jensen, H. Rennenberg, and K. M. Jensen. 2000. Sulfur cycling of intertidal Wadden Sea sediments (Konigshafen, Island of Sylt, Germany): Sulfate reduction and sulfur gas emission. J. Sea Res. **43**: 93–104. doi:10.1016/S1385-1101(00)00007-1

Kühl, M., R. N. Glud, H. Ploug, and N. B. Ramsing. 1996. Microenvironmental control of photosynthesis and photosynthesis-coupled respiration in an epilithic cyanobacterial biofilm. J. Phycol. **32**: 799–812. doi:10.1111/j.0022-3646.1996.00799.x

Li, Y.-H., and S. Gregory. 1974. Diffusion of ions in sea water and in deep-sea sediments. Geochim. Cosmochim. Acta **38**: 703–714. doi:10.1016/0016-7037(74)90145-8

Mann, K. H. 1973. Seaweeds: Their productivity and strategy for growth. Science **182**: 975–981. doi:10.1126/science.182.4116.975

Manz, W., R. Amann, W. Ludwig, M. Wagner, and K.-H. Schleifer. 1992. Phylogenetic oligodeoxynucleotide probes for the major subclasses of proteobacteria: Problems and solutions. Syst. Appl. Microbiol. **15**: 593–600. doi:10.1016/S0723-2020(11)80121-9

Meier, D. V., P. Pjevac, W. Bach, S. Hourdez, P. R. Girguis, C. Vidoudez, R. Amann, and A. Meyerdierks. 2017. Niche partitioning of diverse sulfur-oxidizing bacteria at hydrothermal vents. ISME J. **11**: 1545–1558. doi:10.1038/ismej.2017.37

Meyer, J. L., N. H. Akerman, G. Proskurowski, and J. A. Huber. 2013. Microbiological characterization of post-eruption "snowblower" vents at axial seamount, Juan de Fuca ridge. Front. Microbiol. **4**: 153. doi:10.3389/fmicb.2013.00153

Millero, F. J., T. Plese, and M. Fernandez. 1988. The dissociation of hydrogen sulfide in seawater. Limnol. Oceanogr. **33**: 269–274. doi:10.4319/lo.1988.33.2.0269

Mino, S. and others. 2017. Endemicity of the cosmopolitan mesophilic chemolithoautotroph *Sulfurimonas* at deep-sea hydrothermal vents. ISME J **11**: 909–919, doi:10.1038/ismej.2016.178

Moeslund, L., B. Thamdrup, and B. B. Jørgensen. 1994. Sulfur and iron cycling in a coastal sediment: Radiotracer studies and seasonal dynamics. Biogeochemistry **27**: 129–152. doi:10.1007/BF00002815

Nakagawa, S., K. Takai, F. Inagaki, H. Hirayama, T. Nunoura, K. Horikoshi, and Y. Sako. 2005. Distribution, phylogenetic diversity and physiological characteristics of epsilon-*Proteobacteria* in a deep-sea hydrothermal field. Environ. Microbiol. **7**: 1619–1632. doi:10.1111/j.1462-2920.2005.00856.x

Parshina, S. N., J. Sipma, A. M. Henstra, and A. J. M. Stams. 2010. Carbon monoxide as an electron donor for the biological reduction of sulphate. Int. J. Microbiol. **2010**: 319527–319529. doi:10.1155/2010/319527

Pehlke, C., and I. Bartsch. 2008. Changes in depth distribution and biomass of sublittoral seaweeds at Helgoland (North Sea) between 1970 and 2005. Climate Res. **37**: 135–147. doi:10.3354/cr00767

Robbins, L. L., M. E. Hansen, J. A. Kleypas, and S. C. Meylan. 2010. CO2calc: A user-friendly seawater carbon calculator for Windows, Mac OS X, and iOS (iPhone). U.S. Geological Survey Open-File Report: 2010–1280, p. 17.

Rodil, I. F., M. Lastra, J. López, A. P. Mucha, J. P. Fernandes, S. V. Fernandes, and C. Olabarria. 2019. Sandy beaches as biogeochemical hotspots: The metabolic role of macroalgal wrack on low-productive shores. Ecosystems **22**: 49–63. doi:10.1007/s10021-018-0253-1

Røy, H., H. S. Weber, I. H. Tarpgaard, T. G. Ferdelman, and B. B. Jørgensen. 2014. Determination of dissimilatory sulfate reduction rates in marine sediment via radioactive ^{35}S tracer. Limnol. Oceanogr. Methods **12**: 196–211. doi:10.4319/lom.2014.12.196

Salman, V., J. V. Bailey, and A. Teske. 2013. Phylogenetic and morphologic complexity of giant sulphur bacteria. Antonie Van Leeuwenhoek **104**: 169–186. doi:10.1007/s10482-013-9952-y

Sansone, F. J., and C. S. Martens. 1982. Volatile fatty acid cycling in organic-rich marine sediments. Geochim. Cosmochim. Acta **46**: 1575–1589. doi:10.1016/0016-7037(82)90315-5

Schutte, C. A., S. Ahmerkamp, C. S. Wu, M. Seidel, D. de Beer, P. L. M. Cook, and S. B. Joye. 2019. Biogeochemical dynamics of coastal tidal flats, p. 407–440. *In* G. M. E. Perillo, E. Wolanski, D. R. Cahoon, and C. S. Hopkinson [eds.], Coastal wetlands: An integrated ecosystem approach. Elsevier.

Siegismund, F., and C. Schrum. 2001. Decadal changes in the wind forcing over the North Sea. Climate Res. **18**: 39–45. doi:10.3354/cr018039

Soetaert, K., A. F. Hofmann, J. J. Middelburg, F. J. R. Meysman, and J. Greenwood. 2007. The effect of biogeochemical processes on pH. Mar. Chem. **105**: 30–51. doi:10.1016/j.marchem.2006.12.012

Treude, T., C. R. Smith, F. Wenzhöfer, E. Carney, A. F. Bernardino, A. K. Hannides, M. Krüger, and A. Boetius. 2009. Biogeochemistry of a deep-sea whale fall: Sulfate reduction, sulfide efflux and methanogenesis. Mar. Ecol. Prog. Ser. **382**: 1–21. doi:10.3354/meps07972

Uhl, F., I. Bartsch, and N. Oppelt. 2016. Submerged kelp detection with hyperspectral data. Remote Sens. (Basel) **8**: 487. doi:10.3390/rs8060487

Usov, A. I., G. P. Smirnova, and N. G. Klochkova. 2001. Polysaccharides of algae: 55. Polysaccharide composition of several brown algae from Kamchatka. Russ. J. Bioorg. Chem. **27**: 395–399. doi:10.1023/A:1012992820204

Viollier, E., P. W. Inglett, K. Hunter, A. N. Roychoudhury, and P. van Cappellen. 2000. The ferrozine method revisited: Fe(II)/Fe(III) determination in natural waters. Appl. Geochem. **15**: 785–790. doi:10.1016/S0883-2927(99)00097-9

von Haugwitz, W., H. K. Wong, and U. Salge. 1988. The mud area southeast of Helgoland: A reflection seismic study. Mitt. Geol.-Paläont. Inst. Univ. Hamburg **65**: 409–422.

Werner, U., M. Billerbeck, L. Polerecky, U. Franke, M. Huettel, J. E. E. van Beusekom, and D. de Beer. 2006. Spatial and temporal patterns of mineralization rates and oxygen distribution in a permeable intertidal sand flat (Sylt, Germany). Limnol. Oceanogr. **51**: 2549–2563. doi:10.4319/lo.2006.51.6.2549

Conflict of Interest

None declared.

Microbial communities in intertidal permeable sediments are optimized for the degradation of kelp polysaccharides

Marit R. van Erk[1], Silvia Vidal-Melgosa[1,2], Dirk de Beer[1]

[1]Max Planck Institute for Marine Microbiology, Bremen, Germany
[2]University of Bremen, Center for Marine Environmental Sciences, MARUM, Bremen, Germany

Summary of preliminary results, further experiments planned

This version has not been seen by all authors

Abstract

We investigated the potential adaptation of microbial communities in sandy intertidal sediments to kelp-derived carbohydrate substrates. Oxygen microsensor and radiotracer (^{35}S) methods were used to determine which substrates boost the dominant respiration pathways in this intertidal environment, i.e. aerobic respiration and sulfate reduction. Our results show that both aerobic respiration and sulfate reduction directly increase by addition of carbohydrates. Respiration rates were strongly stimulated by carbohydrates present in kelp (fucoidan, mannitol, alginate, laminarin). Carbohydrates not present in kelp (agar, carrageenan, glycogen) provoked a much lower response. Thus, the communities in the sand were specialized to degrade the specific mix of carbohydrates from kelp. Moreover, often polysaccharides from kelp provoked higher aerobic respiration rates than low molecular weight substrates (glucose, acetate, fructose). This could indicate bacterial selfish uptake of polysaccharides. Kelp-derived substrates were transported deep into the sediments, at least to 20 cm depth. Aerobic respiration and sulfate reduction rates were up to two orders of magnitude higher in these highly active sediments than in reference sites without kelp deposition, however the saccharide pool sizes were nearly equal. Hence, turnover rates of organic matter are much higher than on reference sites. Thus, the microbial communities in sandy intertidal sediments with kelp deposition are adapted to instantly use kelp biomass.

Introduction

Intertidal sediments bordering kelp forests are prone to sudden and large depositions of kelp detritus, which provide energy substrates for the microbial communities in the beach sediments. Forests of kelp, brown macroalgae, are highly productive environments that occur along many temperate hard-bottom coasts (Mann 1973, Steneck et al. 2002). Storms and wave action can detach kelp from the seafloor and bring kelp fragments towards the shore. Here, deposition leads to high concentrations of degradable organic matter (Krumhansl and Scheibling 2012). These wrack deposits are biogeochemical hot spots with increased CO_2 fluxes (Coupland et al. 2007). Microorganisms are the main degraders of kelp-derived organic matter in intertidal sediments (Koop and Griffiths 1982, Koop et al. 1982). Kelp carbon is an important constituent of the food web, with contributions in several trophic levels (Duggins and Estes 1989, Tallis 2009, Queirós et al. 2019).

The kelp dry biomass is primarily composed of carbohydrates (Schiener et al. 2015). The carbohydrate composition of kelp depends on many factors such as species, environmental factors, maturity, and season (Zimmerman and Kremer 1986, Murakami et al. 2011, Schiener et al. 2015, Forbord et al. 2020). The main carbohydrate in kelp is alginate, while laminarin, mannitol and fucoidan are also substantial constituents (Usov et al. 2001, Schiener et al. 2015). Carbohydrates in macroalgae have different biological roles, such as to provide structural support or to serve as energy storage. After kelp deposition, carbohydrates become available to intertidal communities via fragmentation and/or release in mucilage (Linley et al. 1981). Since carbohydrates are quantitatively important constituents of kelp (up to 84% of the dry weight (Schiener et al. 2015)), they are likely to play an important role in carbon turnover in intertidal permeable sediments subjected to kelp deposition.

Carbohydrates are a significant fraction of dissolved and particulate organic carbon (DOC and POC) in seawater and sediments (Hedges 1992, Hedges et al. 2001, Eglinton and Repeta 2006, Hansell 2013). The main carbohydrate producers in the ocean are microalgae and macroalgae. Carbohydrates consist of polysaccharides, oligosaccharides, disaccharides and monosaccharides. Polysaccharides consist of multiple linked monosaccharides that cannot be taken up by bacteria directly. Instead, polysaccharide uptake requires partial hydrolysis to sizes sufficiently small to be transported across the cell membrane (Weiss et al. 1991, Reintjes et al. 2017). Hydrolysis is thus the first step in polysaccharide degradation. Extracellular enzymes are

substrate specific, and therefore the capability to utilize different carbohydrate substrates is determined by the repertoire of genes coding for carbohydrate-degrading enzymes present in the genomes of the microbial community. The complete breakdown of large and/or complex substrates requires many different enzymes. Enzyme production and activity is tightly regulated via the presence of the particular substrate, and via end-product inhibition. Changes in substrate availability lead to active responses of bacterial enzyme production and enzyme activity (Boetius and Lochte 1996, Böer et al. 2009, Thornton et al. 2010).

The degradability of organic matter does not only depend on the structure of the substrate, but also on the capability of the microbial community to degrade it. Differences in degradation of the same substrate exist between pelagic and benthic environments (Arnosti 2000), onshore and offshore environments (D'Ambrosio et al. 2014), and biogeographic areas (Arnosti et al. 2011).

The range of substrates present in an environment shapes the microbial community. When different carbohydrates are available in an environment, communities with associated carbohydrate-degrading enzymes targeting those substrates can use them as energy source, overgrowing other microbes whose genomes do not contain the enzymes to target the substrates. Organisms may specialize on the production of specific enzymes. As producing extracellular enzymes represents an energy cost, organisms may not focus on substrates that are not common in their habitat. This results for example in differences of degradability of substrates between benthic and pelagic communities in the oligotrophic deep-sea. Communities in the deep-sea sediment could degrade refractory compounds readily, but a lag did exist for more labile compounds which are already degraded within the water column, and therefore usually do not reach the sediment (Boetius and Lochte 1994). Also, a lower diversity of substrates available for microbial communities in high-latitude environments leads to the capacity to access a more limited range of substrates than low-latitude microbial communities (Arnosti et al. 2011).

Anaerobic respiration occurs via a chain of reactions involving a consortium of microorganisms (Gottschalk 1986): hydrolysis, fermentation, and the terminal respiration process to CO_2. One example of anaerobic respiration is sulfate reduction, where sulfate-reducing bacteria depend on the activity of hydrolytic and fermentative bacteria. Hydrolysis is often seen as the limiting step, but this is not always the case (Arnosti 2004).

Sandy beaches are proposed locations of intensified degradation of recalcitrant compounds (Misic and Fabiano 2005). Around 5% of single isolated strains from the surface layer (0-1 cm) of a sandy beach showed potential enzymatic activity of phosphatases, esterases, lipases, proteases and glucosidases (Mudryk and Podgórska 2006). The degradation of lipids, proteins, and DNA was most common, but also glycolysis of complex carbohydrates is a source of energy (Podgórska and Mudryk 2003, Misic and Harriague 2007, Mudryk et al. 2011). Sandy intertidal sediments are low in bacterial numbers and organic matter content compared to their muddy counterparts (Jickells and Rae 1997, Llobet-Brossa et al. 1998), but are highly active (De Beer et al. 2005). Advection dominates in these sediments, leading to high input of electron acceptors and dissolved and particulate organic matter and high degradation rates (Huettel and Rusch 2000). Sandy intertidal sediments are extremely dynamic environments, caused by processes as advection, storms and waves. Redox conditions change on short timescales, so does organic matter availability (Huettel and Rusch 2000, Werner et al. 2006, Jansen et al. 2009). The community in sandy sediments must be adapted to these dynamics.

Here, we studied the potential adaptation of a beach sand microbial community to regular input of large amounts of degradable organic matter, here in the form of kelp. We hypothesized that the community is adapted to substrates often encountered within the environment. We analyzed the substrates that are present in the sediment and kelp. We used microsensor and radiotracer (^{35}S) methods to determine the influence of specific substrates on aerobic respiration and sulfate reduction, the dominant terminal respiration processes in coastal marine sediments (Jørgensen 1982). Substrates were selected based on their availability in the environment, and their chemical structure.

Material and methods

Sampling

The two sampling locations were on the main island of Helgoland, located around 60 km from the mainland of Germany in the North Sea (54°10´57´N; 7°53´07´E). Sediment, kelp and seawater were sampled during three sampling periods in 2019 and 2020 (August 2019, November 2019, and September 2020) on two beaches. The first beach, hereafter kelp-beach, was located on the northern edge of the island, and was characterized by regular input of large amounts of kelp, mainly *Laminaria* species. During all sampling periods, kelp debris was present on the beach surface, mainly concentrated at the last high waterline. The second beach, hereafter reference

beach, was located on the eastern part of the island and is not characterized by regular large kelp depositions. Sediments on both beaches were permeable, consisting of coarse sands. The samples taken in August 2019 and November 2019 were used for oxygen consumption measurements. Samples taken in September 2020 were used for sulfate reduction rate measurements and total dissolved carbon, dissolved inorganic carbon, and saccharide analyses.

Density and porosity

Density was determined by weighing a known volume of wet sediment. Samples for porosity were dried at 60 °C until constant weight, and porosity calculated using the sediment density and dry weight.

Dissolved carbon measurements

Porewater was sampled at 0 and 4 cm depth in September 2020 at both beaches using Rhizon samplers (average pore size 0.15 μm, Rhizosphere Research Products) on 5 locations, and transferred to 2 mL Zinsser vials (dissolved inorganic carbon; DIC) which were filled without headspace, and to combusted (4 h at 450 °C) glass vials (total dissolved carbon; TDC). Samples were transported cooled to the laboratory in Bremen, where they were stored at 4 °C (DIC) and -20 °C (TDC). DIC was analyzed using flow injection analysis (Hall and Aller 1992). TDC was measured via thermal catalysis using a DIMATOC® 2010 K1, with potassium hydrogen phthalate as standard. Dissolved organic carbon (DOC) was calculated as TDC – DIC.

Monosaccharide quantification and polysaccharide microarray analysis

Carbohydrate extraction

Sediment samples were taken at 0, 4, 8 and 20 cm depth at the kelp-beach on 3 locations, and at 0 and 4 cm depth at the reference beach on 1 location using 15 mL centrifuge tubes. Sediment samples were transported cooled and stored at -20 °C in the laboratory in Bremen. Kelp was sampled from the beach surface and rinsed with tap water in the laboratory on Helgoland, transported cooled and stored at -20 °C in the laboratory in Bremen. A subset of porewater samples from section 'Dissolved carbon measurements' (2 locations at 0 and 4 cm depth, both for the kelp-beach and the reference beach) were also analyzed.

Both sediment and kelp samples were freeze-dried. Freeze-dried kelp was subsequently homogenized and the Alcohol Insoluble Residue procedure was performed on the homogenized

sample. Pure ethanol (99.9% ethanol) was added in a volume 6 times that of the volume of kelp. The sample was then vortexed and rotated for 10 minutes at room temperature, spun down at 4000 rpm for 15 minutes, and the supernatant discarded. This procedure was repeated with chloroform:methanol (1:1) (4 times), and pure acetone. The resulting kelp pellet was left to air dry at room temperature overnight.

Kelp and sediment samples were homogenized using a spatula. For each sample, about 90 mg of freeze-dried sediment or 20 mg of freeze-dried kelp was transferred in triplicates to 2 mL Eppendorf tubes. Carbohydrates from the samples were sequentially extracted with three solvents in the following order: autoclaved MilliQ water, 400 mM EDTA (pH 7.5) and 4 M NaOH with 0.1% w/v $NaBH_4$, which release water soluble, anionic, and water insoluble polysaccharides, respectively. For every 10 mg of sediment sample, 30 µL of solvent was added to the tube (carbohydrate extractions were thus normalized by sample dry weight). In the case of kelp, for every 10 mg of kelp sample 300 µL of solvent was added. After addition of the solvent, the samples were vortexed, placed in a sonication bath for 1 hr and centrifuged at 6000 × g for 15 minutes. The extracts (supernatant) were collected in 1.5 mL Eppendorf tubes and the pellets were re-suspended in the following extraction solvent using the same procedure. All three extractions occurred on the same day.

Monosaccharide analysis
Porewater and the MilliQ extracts for sediment and kelp samples were used for saccharide analysis, which were measured in the form of monosaccharides. Carbohydrates present in the samples were hydrolysed with acid into monosaccharides. This analysis thus includes monosaccharides present as monosaccharides, but also those present as larger saccharides. For sediment MilliQ extracts and porewater samples, 110 µL of the sample was mixed with 110 µL 2 M HCl in a glass ampule. Kelp MilliQ extracts (1 µL) were diluted with MilliQ (499 µL) prior to mixing with 2 M HCl (500 µL) in a glass ampule. Ampules were then incubated at 100 °C for 24 hrs and after the acid hydrolysis samples were stored at 4 °C until analysis. A volume of 200 µL of the acid hydrolysis was dried in a SpeedVac (Christ GmbH) at 37 °C at 1300 rpm for 2.5 hrs. After drying, the samples were resuspended in 100 µL MilliQ (200 µL for kelp samples) and vortexed in a thermoshaker at 25 °C and 1000 rpm. Standard monosaccharide mixtures at different concentrations (from 10 to 1000 µg/L), which were used as reference for identification and quantification, were prepared in 1 M HCl following the same procedure. All samples were then centrifuged at 14800 rpm for 2 minutes, diluted ten-fold, and a volume of 90 µL of the

supernatant was transferred to HPLC vials. Neutral, amino and acidic monosaccharides were quantified using high performance anion exchange chromatography (HPAEC) using a Dionex ICS-5000$^+$ system with pulsed amperometric detection (PAD) equipped with a CarboPac PA10 analytical column (2 × 250 mm) and a CarboPac PA10 guard column (2 × 50 mm). The followed protocol has been described previously (Engel and Händel 2011). System control and data acquisition used Chromeleon v7.2 software (Dionex). Separation of neutral and amino monosaccharides occurred via an isocratic flow of 18 mM NaOH for 20 min. Thereafter, a gradient of 200 mM Na acetate separated the acidic monosaccharides. The dilution series of the standard monosaccharide mixture were used for quantification. Porewater samples were diluted 60-fold with MilliQ water due to the high salinity in these samples.

Carbohydrate microarray analysis

MilliQ, EDTA and NaOH extracts from all sediment samples as well as from the kelp samples were analyzed by carbohydrate microarrays. Each extract (30 µL) was added into a well of a 384-microwell plate diluted 2-fold in printing buffer (55.2% glycerol, 44% water, 0.8% Triton X-100) followed by a further 2-fold dilution in printing buffer. A microarrayer (Sprint, Arrayjet, Roslin, UK) was used to print the plates content onto nitrocellulose membrane with a pore size of 0.45 µm (Whatman). Printing was done at 20 °C and 50% humidity. A printing replicate per each sample was included.

Once microarrays were printed (all being identical and containing all of the extracts), they were blocked for 1 h in phosphate buffered saline (PBS) with 5% (w/v) non-fat milk powder (MPBS). Afterwards each array was individually incubated for 2 h with one of 50 carbohydrate specific monoclonal antibodies (Supp. Figure 1 and Supp. Table 1). All antibodies were diluted 1:10 in MPBS, except the three BS-400 antibodies and CBM3a that were diluted 1:1000 and 10 µg/mL in MPBS, respectively. Arrays were thoroughly washed in PBS and incubated for 2 h with either anti-rat, anti-mouse or anti-His tag secondary antibodies conjugated to alkaline phosphatase diluted 1:5000, 1:5000 or 1:1500, respectively, in MPBS. After thorough washing in PBS, arrays were washed in deionized water and then developed in a solution containing 5-bromo-4-chloro-3-indolylphosphate and nitro blue tetrazolium in alkaline phosphatase buffer (100 mM NaCl, 5 mM $MgCl_2$, 100 mM Tris-HCl, pH 9.5). For data analysis, developed arrays were scanned at 2400 dots per inch and binding signal intensity of each antibody to each sample was quantified using the software Array-Pro Analyzer 6.3 (Media Cybernetics). Per extract the mean antibody signal intensity was calculated and the maximal mean intensity detected in the whole data set was set

to 100 and all other values were normalized accordingly. The highest mean intensity detected was in the EDTA extract from kelp (first dilution) with the antibody BAM10. A cut-off of 5 arbitrary units was applied. Negative controls for the three extraction solvents were included in the print showing no unspecific binding.

Each antibody has a different avidity (overall binding capacity) and thus the signal intensities from different antibodies should not be used to infer different abundances of the corresponding epitopes, but the signal intensity of a single antibody correlates to the relative abundance of the epitope in each extract (because when performing carbohydrate extraction all samples were normalized by sediment weight). As the ratio between sample:solvent was different for the sediment and kelp samples, their signals (absolute number) cannot be compared.

Oxygen consumption

In August, sediment, kelp, and seawater were sampled on the kelp-beach and reference beach and stored in containers at 4 °C in the dark until use. Measurements were conducted in the laboratory on Helgoland, within 2 days after sampling. Large grains were taken out of the sediment to protect the microsensors, and the remaining sediment carefully transferred to core liners with a diameter of 5.3 cm filled with seawater. Core liners had a stopper with a valve at the bottom. Seawater, or seawater with the dissolved substrate of interest, was added on top of the sediment, and 50 mL of oxygen-saturated seawater was pulled out of the core via the valve (adapted from (De Beer et al. 2005)). A small layer of solution was left on top of the sediment during the measurements. Oxygen consumption was measured using an oxygen microsensor (optodes; Pyroscience Research Products) located at 2 cm depth within the sediment. Microsensors were calibrated using saturated seawater (100% saturation) and ascorbate solution (0% saturation). A few cores were made, and before adding the substrates the background (percolated with only seawater) oxygen consumption was measured. In between addition of the different substrates, the sediments were purged with seawater, in order to remove the previous substrate from the porewater. The linear decrease in oxygen concentration at 2 cm depth was used to calculate oxygen consumption. The oxygen consumption for the corresponding background was subtracted from the oxygen consumption after substrate addition (De Beer et al. 2005).

In November, surface sediment, seawater and kelp were sampled on both beaches. Samples were stored in containers, transported cooled to the laboratory in Bremen and stored at 4 °C in the dark until use within 35 days (78 days for mannitol and laminarin). In the laboratory, cores and

microsensors were prepared and oxygen measurements conducted as in August 2019. Unlike in August 2019, for every substrate of interest a new core was prepared, and first a background (percolation with only seawater) measured. Thus, every substrate was measured in a separate core, with its own background. Sediments in the core did thus not encounter another substrate before.

Sulfate reduction rates

Sediment used for sulfate reduction measurements was sampled from the top 2 cm of kelp-beach and reference beach sediment, transported cooled to the laboratory in Bremen, and stored at 4 °C in the dark until use 6-7 days later. Seawater was also sampled, and transported and stored in the same way.

Sediment (3 mL) was added to 5 mL cut-off syringes. Syringes were closed at the bottom with a valve, and placed vertically with the valve facing down. A volume of 3 mL of seawater with ^{35}S radiotracer, or seawater with the dissolved substrate and ^{35}S radiotracer was added on top of the sediment, equal to 250 kBq of $^{35}SO_4^{2-}$ per sample. The added seawater solutions were percolated through the sediment via the valve, and a thin layer was left on top. Samples were incubated in the dark at room temperature for 6 hrs. Samples were taken every 2 hrs from 0 to 6 hrs after start of the incubations for kelp-beach sediment, and after 0 and 6 hrs for reference beach sediment. Incubations were stopped by transferring the content of the syringes to 6 mL of 20% (w/v) ZnAc and storage at -20 °C. All sampling points for each treatment were separate syringes, thus different time points within the time series are replicate syringes. Cold acid-chromium distillation was used to separate the reduced from the unreduced sulfur (Røy et al. 2014). Radioactivity was measured using a scintillation counter (Perkin-Elmer Tri-Carb 4910 TR; Ultima-Gold Scintillation cocktail). Sulfate reduction rates for kelp-beach sediments were determined from the sulfate reduced over time for data points of 2, 4 and 6 hrs after start of the incubation (these represent timepoints during anoxic conditions, see below and 'Results').

To determine the time until anoxia, 12 mL Exetainers (Labco, UK) were filled headspace-free using seawater and 4 mL sediment, in 4 replicates. Sediment and seawater were from the same canisters as used for sulfate reduction measurements. The Exetainers were placed on a roller table, ensuring homogeneous slurries. At selected timepoints, the Exetainers were opened, and an oxygen microsensor quickly inserted. The microsensor was prepared as described previously (Revsbech 1989), and calibrated using saturated seawater (100% saturation), and sodium

ascorbate solution (0% saturation). A trendline was plotted through the data points, and the interception with the 0 μM oxygen concentration axis calculated, the time at which sediments in the Exetainers became anoxic.

Substrates

Substrates were dissolved to a final concentration of 70 mM carbon equivalents in seawater, so that concentrations would be higher than could be used by iron reduction (Chapter 2). The substrates used in oxygen consumption and sulfate reduction measurements were selected based on their structure and presence in kelp. The first class of substrates were low molecular weight substrates, i.e. glucose, acetate and fructose. The substrates glucose and fructose are monosaccharides. Acetate is a short-chain fatty acid. All three are also substrates for sulfate-reducing bacteria (Rabus et al. 2006). The second class were carbohydrates present in kelp. Mannitol is a sugar alcohol, and is an important photosynthate and energy storage compound of kelp (Reed et al. 1985). The other used substrates present in kelp are polysaccharides, i.e. alginate, laminarin and fucoidan. Alginate is the major polysaccharide in brown macroalgae. Alginate is a structural polysaccharide, and consists of the monosaccharides mannuronic acid and guluronic acid. Laminarin is a long-term storage compound, interconverting energy with mannitol (Scheschonk et al. 2019), and consists of a linear glucose-based backbone with glucose branches. Laminarin is extremely abundant in the marine environment, and is produced by a variety of primary producers including diatoms and macroalgae (Becker et al. 2020). The ability to degrade laminarin is abundant in microbes from the marine environment (Arnosti et al. 2011, D'Ambrosio et al. 2014). Fucoidans are sulfated polysaccharides with a fucose-backbone occurring in the kelp cell wall. Fucoidans have a complex and varying structure with many branches and sulfate groups (Deniaud-Bouët et al. 2017). Fucoidan is not universally degraded in marine environments (Arnosti 2000). Organisms need a large repertoire of carbohydrate-degrading enzymes for degradation of fucoidan, thus only highly specialized organisms can degrade fucoidan (Sichert et al. 2020). The third class of substrates contains polysaccharides that are not present in kelp, i.e. glycogen, carrageenan, and agar. Instead, these substrates occur in animals, fungi, bacteria (glycogen), and red algae (carrageenan and agar). Also, kelp was added as small fragments in 70 mM carbon equivalents.

Results

Concentrations of total dissolved carbon (TDC), and dissolved inorganic and organic carbon (DIC and DOC) are higher on the beach with regular kelp deposition (kelp-beach), both at the surface and at 4 cm depth (Table 1).

Table 1: Total dissolved carbon (TDC), dissolved inorganic carbon (DIC) and dissolved organic carbon (DOC) in kelp-beach and reference beach sediment, at 0 and 4 cm depth. Numbers in between brackets are the number of replicates.

	Kelp-beach		Reference beach	
	0 cm	4 cm	0 cm	4 cm
TDC (mmol L^{-1})	4.65 (1)	3.89 ± 0.82 (2)	2.29 ± 0.27 (4)	2.73 ± 0.47 (5)
DIC (mmol L^{-1})	1.70 ± 0.42 (5)	2.20 ± 0.29 (5)	1.33 ± 0.29 (5)	1.79 ± 0.41 (5)
TDC - DIC (=DOC) (mmol L^{-1})	2.13 (1)	1.78 ± 0.95 (4)	0.86 ± 0.44 (4)	0.94 ± 0.39 (5)

The concentration of saccharides in the kelp-beach sediments is 1.5 – 2 times higher than in the reference beach sediments (Table 2). These saccharides represent the total saccharides and include those that were present as larger saccharides in the samples. Total saccharide concentrations in deeper sediments in kelp-beach sediment (4, 8, and 20 cm depth) are higher than concentrations in reference beach sediment (4 cm depth). Total saccharide concentrations for kelp-beach sediments do not show a trend with sediment depth. Glucose is the dominant monosaccharide in all samples. Saccharide concentrations in the porewater were below detection limit, due to the high dilution (60-fold) performed to reduce the high salinity in these samples that would interfere in the chromatographic analysis. In our HPAEC analysis we detected monosaccharide concentrations down to 10 µg/L, thus monosaccharide concentrations in the porewater samples were below 600 µg/L. The contribution of the saccharides to the DOC pool was approximately equal for the kelp-beach at 0 and 4 cm depth and reference beach at 4 cm depth (~60%). The monosaccharide composition of kelp-beach sediment is more similar to reference beach sediment than to kelp detritus (Figure 1).

	Kelp-beach (µg/g)				Reference beach (µg/g)		Kelp (mg/g)
	0 cm	4 cm	8 cm	20 cm	0 cm	4 cm	
Arabinose	4.2 ± 1.1	3.4 ± 1.2	4.1 ± 1.3	5.1 ± 4.3	1.7 ± 0.5	1.7 ± 0.2	0.0 ± 0.0
Fucose	18.4 ± 4.8	14.9 ± 4.3	16.6 ± 5.3	15.1 ± 9.8	7.0 ± 2.1	4.6 ± 0.7	83.5 ± 10.1
Galactosamine	5.0 ± 1.8	4.1 ± 1.4	4.4 ± 1.1	3.1 ± 1.7	3.3 ± 1.4	2.5 ± 0.9	0.0 ± 0.0
Galactose	14.9 ± 4.6	11.2 ± 3.7	13.5 ± 4.0	13.4 ± 10.0	14.7 ± 2.6	10.3 ± 0.7	28.2 ± 3.9
Galacturonic acid	6.8 ± 2.0	5.2 ± 2.1	6.1 ± 1.9	4.9 ± 4.1	1.5 ± 0.5	1.3 ± 0.2	0.8 ± 0.2
Gluconic acid	0.7 ± 0.2	0.5 ± 0.2	0.6 ± 0.5	0.1 ± 0.1	1.0 ± 1.4	0.0 ± 0.0	0.0 ± 0.0
Glucosamine	13.8 ± 3.4	11.4 ± 3.9	12.6 ± 3.8	10.6 ± 7.6	4.2 ± 1.1	3.7 ± 0.4	3.2 ± 0.6
Glucose	104.4 ± 20.0	79.2 ± 22.7	78.9 ± 18.0	79.3 ± 53.6	-	68.4 ± 5.9	510.9 ± 66.1
Glucuronic acid	9.8 ± 2.9	7.5 ± 2.5	9.3 ± 3.2	8.7 ± 5.8	3.0 ± 0.5	2.8 ± 0.2	14.8 ± 0.9
Mannose	21.9 ± 6.4	15.6 ± 4.7	18.6 ± 4.9	14.5 ± 9.7	16.6 ± 3.0	8.6 ± 2.1	12.8 ± 2.4
Mannuronic acid	5.6 ± 1.2	8.5 ± 7.1	4.7 ± 2.3	4.1 ± 2.0	0.9 ± 0.2	1.0 ± 0.1	42.2 ± 3.9
Muramic acid	0.5 ± 0.3	0.6 ± 0.5	0.7 ± 0.5	0.3 ± 0.4	0.0 ± 0.0	0.0 ± 0.0	0.0 ± 0.0
Rhamnose	1.5 ± 0.5	1.2 ± 0.4	1.2 ± 0.4	1.5 ± 1.0	0.3 ± 0.1	0.3 ± 0.1	0.14 ± 0.0
Xylose	12.3 ± 3.4	12.5 ± 7.9	14.0 ± 5.9	24.3 ± 23.7	19.4 ± 2.2	10.6 ± 4.1	8.1 ± 1.3
Total	219.8	175.8	185.3	185.0	73.6	115.8	704.6
Total (excluding glucose)	115.4	96.6	106.4	105.7	-	47.4	193.7

Table 2: Concentration of monosaccharides in reference beach and kelp-beach sediment, and in kelp. Averages are calculated for 1 location in triplicate for reference beach sediment, and for 2 locations in kelp-beach sediments, in duplicate for 0 and 4 cm, and in triplicate for 8 and 20 cm. Concentrations are shown in µg/(g sediment) for kelp-beach and reference beach sediments, and in mg/(g kelp) for kelp. Glucose determination for reference beach sediments at 0 cm depth failed.
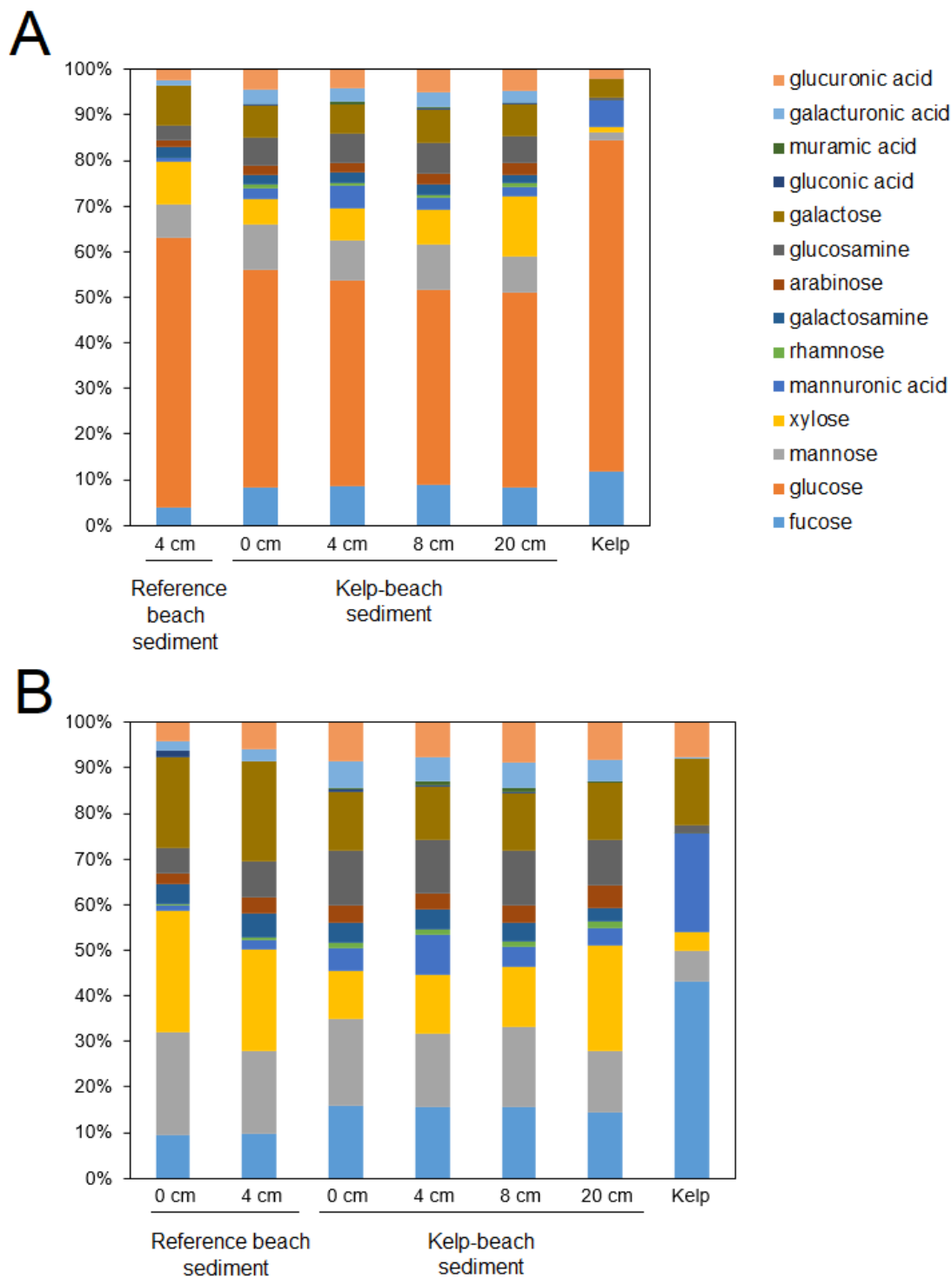
Figure 1: Relative contributions of monosaccharides in reference beach and kelp-beach sediment to the total pool of saccharides (A), and relative contributions of monosaccharides when glucose is excluded (B). Relative contributions were calculated using the average concentrations of Table 2. Glucose determination for reference beach sediments at 0 cm depth failed.

The carbohydrate microarray method, which is semi-quantitative, uses monoclonal antibodies for detection of specific polysaccharides. The microarray analysis shows the presence of the polysaccharides alginate, fucoidan, and laminarin in the kelp sample (Figure 2A), while cellulose was not detected. In the kelp-beach sediments only alginate was detected in the top 4 cm, while in the reference beach sediment none of these polysaccharides was detected (Figure 2B). All antibodies with a detected signal, including the ones with low signals and antibodies that did not bind to any of the samples can be found in Supp. Figure 1 and Supp. Table 1.

Oxygen consumption rates are higher in kelp-beach sediments than in reference beach sediments both in August and in November (Figure 3). Rates for experiments with only seawater (background) were $4.89 \times 10^{-4} \pm 1.26 \times 10^{-4}$ mol m^{-3} s^{-1} (August) and $1.37 \times 10^{-4} \pm 0.58 \times 10^{-4}$ mol m^{-3} s^{-1} (November) in kelp-beach sediments, and $1.18 \times 10^{-4} \pm 0.54 \times 10^{-4}$ mol m^{-3} s^{-1} (August) and $0.34 \times 10^{-4} \pm 0.24 \times 10^{-4}$ mol m^{-3} s^{-1} (November) in reference beach sediments. Background rates were subtracted from the measured oxygen consumption rates after substrate addition, resulting in the rates shown in Figure 3. Addition of kelp leads to the highest rates of oxygen consumption in both seasons for kelp-beach sediments. Rates for substrates that are present in the kelp (mannitol, alginate, fucoidan and laminarin) are higher than rates for polysaccharides not present in kelp (agar, glycogen and carrageenan). Rates for the substrates with lower molecular weight (acetate, glucose and fructose) do not show higher oxygen consumption rates than for carbohydrates from kelp, except for acetate and fructose compared to laminarin in November sediment. Oxygen consumption for alginate is probably underestimated, as alginate was difficult to dissolve, thus likely only the sides of the formed gel were available for the sedimentary community.

A

Kelp

	fucoidan - BAM 1	fucoidan - BAM 2	fucoidan - BAM 4	laminarin - BS-400-2	pectin/alginate - LM7	alginate - BAM6	alginate - BAM7	alginate - BAM8	alginate - BAM9	alginate - BAM10	cellulose - CMB3a
MilliQ water	16	28	16	0	61	15	73	61	62	78	0
EDTA*	0	0	0	0	63	29	50	61	54	50	0
NaOH	6	0	11	27	58	11	65	52	55	61	0

B

Kelp-beach

	fucoidan - BAM1 - EDTA*	fucoidan - BAM2 - EDTA*	fucoidan - BAM4 - EDTA*	laminarin - BS-400-2 - EDTA*	pectin/alginate - LM7 - EDTA*	alginate - BAM6 - EDTA*	alginate - BAM7 - EDTA*	alginate - BAM8 - EDTA*	alginate - BAM9 - EDTA*	alginate - BAM10 - EDTA*	cellulose - CBM3a - NaOH
0 cm	0	0	0	0	0	0	9	0	0	6	0
4 cm	0	0	0	0	0	0	14	0	0	12	0
8 cm	0	0	0	0	0	0	0	0	0	0	0
20 cm	0	0	0	0	0	0	0	0	0	0	0

Reference beach

	fucoidan - BAM1 - EDTA*	fucoidan - BAM2 - EDTA*	fucoidan - BAM4 - EDTA*	laminarin - BS-400-2 - EDTA*	pectin/alginate - LM7 - EDTA*	alginate - BAM6 - EDTA*	alginate - BAM7 - EDTA*	alginate - BAM8 - EDTA*	alginate - BAM9 - EDTA*	alginate - BAM10 - EDTA*	cellulose - CBM3a - NaOH
0 cm	0	0	0	0	0	0	0	0	0	0	0
4 cm	0	0	0	0	0	0	0	0	0	0	0

Figure 2: *Heat maps showing microarray data of selected polysaccharides for kelp samples (A) and sediment samples (B). The polysaccharide recognized by each antibody and the antibody name are depicted at the top of each column, in (B) the extraction solvent is also shown. In (A) data are shown for the three different extraction solvents: autoclaved MilliQ water, EDTA, and NaOH. * EDTA extracts from the kelp sample had high viscosity (which affect the quality of the microarray print) and thus a further two-fold dilution of the extracts is shown compared to the MilliQ water and NaOH extracts. Also a further two-fold dilution for EDTA extracts is shown for the sediment samples for comparison. Signal intensities for kelp show the average of triplicates. Kelp-beach sediment signals are calculated for 2 different locations, and the triplicates of both locations averaged to 1 signal intensity. Reference beach sediment signals are calculated for 1 location, and the triplicates averaged to 1 signal intensity. The highest mean value in the data set was set to 100 and the rest was normalized accordingly having a cut-off of 5 arbitrary units, signals <5 were set to zero.*
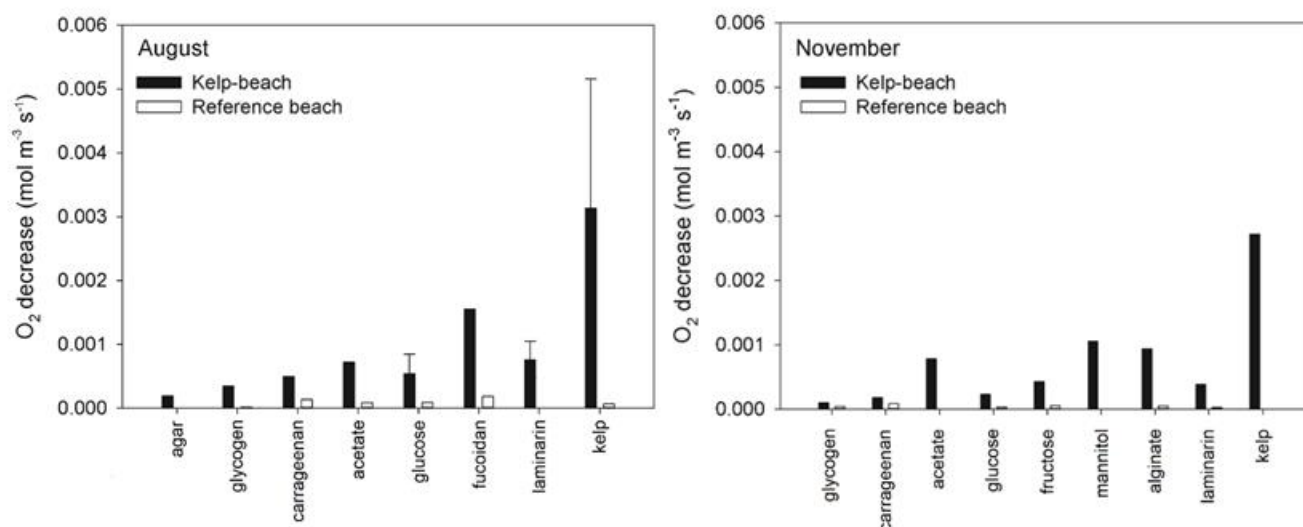
Figure 3: Oxygen consumption rates in kelp-beach sediment (black bars) and reference beach sediment (white bars) in August (left) and November (right). Oxygen consumption rates were calculated by subtracting the measured oxygen consumption rates with the oxygen consumption rates of the background (only seawater). Oxygen consumption in reference beach sediments was in some occasions too small to be visible in the graph.

Sulfate reduced after 6 hrs of incubation is approximately 30 to 160 times higher for kelp-beach than for reference beach sediment (Supp. Table 2). Kelp-beach sediments became anoxic after approximately 1 hr (Supp. Fig. 2). Therefore, sulfate reduction rates were calculated using the timepoints 2, 4 and 6 hrs after start of the incubation, thus only including the timepoints for which the incubation was anoxic. Sulfate reduction rates are higher for substrates present in the kelp, such as mannitol and laminarin, and for kelp itself in kelp-beach sediments (Figure 4). Further, rates are higher for the well-known substrates for sulfate reduction in marine sediments: glucose and acetate. On the contrary, sulfate reduction rates for polysaccharide substrates that are not present in kelp (agar and glycogen) are much lower. The sulfate reduction rate after kelp addition was slightly lower than for the individual polysaccharides in kelp, but higher than for polysaccharides not present in kelp.
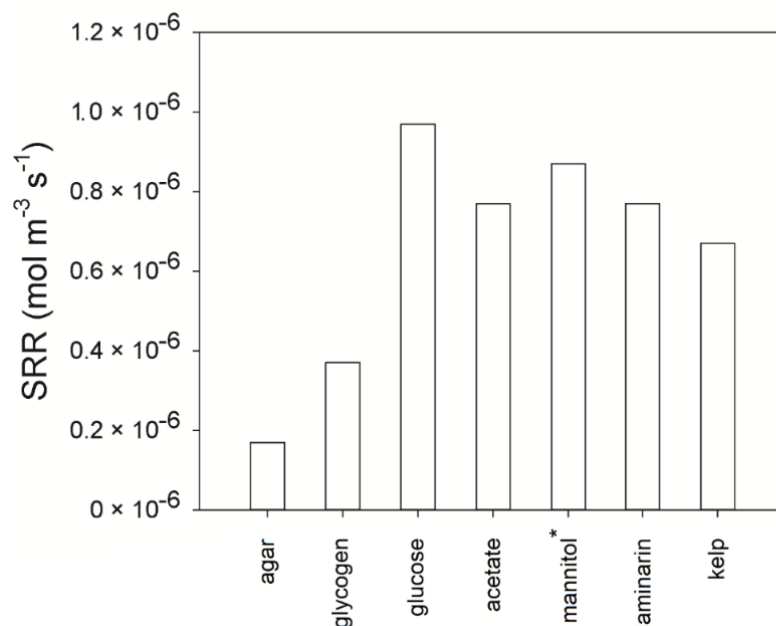
Figure 4: *Sulfate reduction rates (SRR) in kelp-beach sediments between 2 and 6 hrs after start of the incubation, which represent the incubations under anoxic conditions. Sulfate reduction rates were calculated by subtracting the background sulfate reduction rates (only seawater) from the sulfate reduction rates for the substrate treatments. *: sulfate reduction for the substrate mannitol is calculated between 2 and 4 hrs, because the determination of the amount of sulfate reduced failed for the 6 hrs timepoint.*

Discussion

We observed centimeter-large kelp fragments until at least 20 cm depth in the kelp-beach sediments. Also the kelp-derived substrates alginate, mannuronic acid (as monosaccharide or from alginate) and fucose (as monosaccharide or from fucoidan) were present in kelp-beach sediments over this depth. The distribution of kelp material is driven by the deep mixing of kelp fragments and deep advectional transport, as is characteristic for intertidal environments (Billerbeck et al. 2006). These organics are available for degradation by the microbial community, and indeed, DOC and DIC are elevated as compared to the reference beach. This indicates that kelp-derived organic matter is available for the microbial community until deep into the sediments, and degradation of this material does take place. Thus, the microorganisms in the sediment are capable of degrading the specific mix of substrates present in kelp. Fucoidan cannot be easily degraded by non-specialized organisms (Sichert et al. 2020), while we found fucoidan degradation in kelp-beach sediments, which thus indicates the community is tuned to substrates

of kelp. Additions of the polysaccharides of kelp to the reference beach sediments did not provoke such a strong response. As the kelp input in the kelp-beach is much higher than in the reference beach, the oxygen consumption and sulfate reduction rates are indeed much higher. Also, the rates for the kelp-beach sediments could be strongly stimulated by additions of the specific hydrolysis intermediates. However, whereas oxygen consumption and sulfate reduction rates are up to two orders of magnitude higher, the saccharide pool sizes are comparable (1.5 - 2 times higher on the kelp-beach). Thus, pool sizes of organic substrates do not reflect the degradation rates.

Rates of oxygen consumption and sulfate reduction in kelp-beach sediment were very strongly stimulated by carbohydrates that are present in kelp (mannitol, alginate, laminarin, fucoidan), but less by those not present in kelp (glycogen, agar, carrageenan). This strongly indicates that the microbial community in kelp-beach sediments is functionally specialized for organic matter of kelp. Oxygen consumption increased directly after addition of the substrates. Also sulfate reduction showed a quick response to carbohydrates present in kelp. Sulfate reduction in kelp-beach sediments was high and rapidly different between substrates, while in reference beach sediments sulfate reduction remained low after 6 hrs.

The addition of kelp material in the form of kelp fragments led to the highest oxygen consumption rates for kelp-beach sediments. Thus, although kelp was added as fragments and not dissolved like the other substrates, kelp is a readily bioavailable carbon source. With kelp fragments as substrate the whole community degrading the full suite of organics could become active. Besides the substrates added in this study, also other components of kelp such as proteins could increase the respiration rates.

Contrary to expectation, the oxygen consumption rates were often more strongly stimulated by kelp-derived polysaccharides than by the low molecular weight substrates, i.e. glucose, fructose and acetate. Thus, linked monomers (in polymer form) are preferred or lead to equal degradation rates as for the monomer form, as was the case for oxygen consumption after glucose or laminarin addition. Kelp-beach sediments are thus specialized for the use of polysaccharides. Remarkably, these polysaccharides must be more efficiently taken up and metabolized than monosaccharides. The quick response to polysaccharides is counterintuitive, as the hydrolysis step required for polysaccharide degradation is often considered the limiting step in the turnover of high molecular weight organic material (Arnosti 2004). Even if all enzymes required for degradation are

continuously present and/or quickly induced upon presence of the substrates, thus even if the full hydrolysis capacity is present, polysaccharide degradation should be slower than monosaccharide degradation.

Overall, our preliminary data set shows that kelp-derived substrates are transported at least centimeters deep into kelp-beach sediments. The relatively small saccharide pool size of the kelp-beach does not reflect the fast substrate turnover. Microbial communities in kelp-beach sediments are specialized for the use of the substrates derived from kelp, and show preferred use of polysaccharides over monosaccharides.

The quick response to and fast turnover of polysaccharides could be due to direct bacterial uptake referred to as "selfish uptake", which can occur very fast. Selfish uptake was recently discovered as an additional way of polysaccharide use in the marine environment to extracellular enzymatic hydrolysis ("sharing uptake") (Reintjes et al. 2017). During extracellular enzymatic hydrolysis, enzymes are released by the bacterial cell and polysaccharides converted to low molecular weight compounds outside of the cell, which would become available for a broader community. Microorganisms that do not degrade polysaccharides themselves ("scavengers") can also profit from these low molecular weight products, and as they do not invest in extracellular enzymes are more competitive. Instead, during selfish uptake, surface-associated binding proteins and enzymes are used to bind and partially hydrolyse the polysaccharide, and the resulting large oligosaccharides are transported into the periplasm, where they are then further converted to monomers. The benefit for selfish microorganisms is that they do not lose saccharides in the external environment via e.g. diffusion or uptake by scavengers (Reintjes et al. 2017). A considerable fraction of heterotrophic microorganisms in marine environments can conduct selfish uptake, which was shown for e.g. *Bacteroidetes* and *Planctomycetes* (Reintjes et al. 2019). Selfish uptake has been shown for alginate (Thomas et al. 2021), laminarin, and fucoidan (Reintjes et al. 2019). Uptake could be induced within a few minutes, and previous exposure to a substrate can increase the rates of initial uptake (Reintjes et al. 2020), which would be the situation in kelp-beach sediments where deposition of kelp detritus regularly occurs. Kelp-beach microorganisms might be specialized for degradation of polysaccharides via selfish uptake, and stockpile them to avoid competition.

We detected alginate, fucoidan and β-1,3-glucan (laminarin-like structure) in kelp samples with our microarray analysis. In the kelp-beach sediments only alginate was detected, while laminarin

and fucoidan were not detected (Figure 2). No detection of laminarin and fucoidan could be due to low concentrations or due to a partial degradation of these substrates. Note that the microarray approach used in our analysis immobilizes polysaccharides and long oligosaccharides, but not short oligosaccharides and monosaccharides (Pedersen et al. 2012), thus partially degraded polysaccharides would not be detected. Alternatively, it might thus be that laminarin and fucoidan were processed by selfish uptake. Fucoidan is not readily used via external hydrolysis in a range of environments (Arnosti 2000), due to the large amount of enzymes needed and thus only usage by specialized microorganisms (Sichert et al. 2020). However, selfish uptake of fucoidan was observed in environments where extracellular hydrolysis was absent (Reintjes et al. 2019).

Although we hypothesize that selfish uptake could be responsible for the observed preferential use of polysaccharides, this cannot be demonstrated based on this preliminary data set alone. Visualization of the uptake of fluorescently labelled polysaccharides (FLA-PS) by cells in freshly sampled sediments via microscopy could be used to determine if this is indeed the case. Parallel to these measurements, oxygen consumption and sulfate reduction after substrate addition should be measured in these sediments. Furthermore, an increased ratio of dry sediment to extraction solvent may be used to increase the polysaccharide concentration in the extracts, which could result in detection of more substrates by microarray analysis. In addition, higher resolution samples with more locations for the kelp-beach and reference beach need to be analyzed.

Acknowledgements

References

Arnosti, C. (2000). Substrate specificity in polysaccharide hydrolysis: contrasts between bottom water and sediments. *Limnol Oceanogr,* 45, 1112-1119.

Arnosti, C. (2004). Speed bumps and barricades in the carbon cycle: substrate structural effects on carbon cycling. *Mar Chem,* 92, 263-273.

Arnosti, C., A. D. Steen, K. Ziervogel, S. Ghobrial & W. H. Jeffrey (2011). Latitudinal gradients in degradation of marine dissolved organic carbon. *PloS ONE,* 6, e28900.

Becker, S., J. Tebben, S. Coffinet, K. Wiltshire, M. H. Iversen, T. Harder, K.-U. Hinrichs & J.-H. Hehemann (2020). Laminarin is a major molecule in the marine carbon cycle. *PNAS,* 117, 6599-6607.

Billerbeck, M., U. Werner, L. Polerecky, E. Walpersdorf, D. De Beer & M. Huettel (2006). Surficial and deep pore water circulation governs spatial and temporal scales of nutrient recycling in intertidal sand flat sediment. *Mar Ecol Prog Ser,* 326, 61-76.

Böer, S. I., C. Arnosti, J. E. E. Van Beusekom & A. Boetius (2009). Temporal variations in microbial activities and carbon turnover in subtidal sandy sediments. *Biogeosciences* 6, 1149-1165.

Boetius, A. & K. Lochte (1994). Regulation of microbial enzymatic degradation of organic matter in deep-sea sediments. *Mar Ecol Prog Ser,* 104, 299-307.

Boetius, A. & K. Lochte (1996). Effect of organic enrichments on hydrolytic potentials and growth of bacteria in deep-sea sediments. *Mar Ecol Prog Ser,* 140, 239-250.

Coupland, G. T., C. M. Duarte & D. I. Walker (2007). High metabolic rates in beach cast communities. *Ecosystems,* 10, 1341-1350.

D'Ambrosio, L., K. Ziervogel, B. MacGregor, A. Teske & C. Arnosti (2014). Composition and enzymatic function of particle-associated and free-living bacteria: a coastal/offshore comparison. *ISME J,* 8, 2167-2179.

De Beer, D., F. Wenzhöfer, T. G. Ferdelman, S. E. Boehme, M. Huettel, J. E. E. Van Beusekom, M. E. Böttcher, N. Musat & N. Dubilier (2005). Transport and mineralization rates in North Sea sandy intertidal sediments, Sylt-Rømø Basin, Wadden Sea. *Limnol Oceanogr,* 50, 113-127.

Deniaud-Bouët, E., K. Hardouin, P. Potin, B. Kloareg & C. Hervé (2017). A review about brown algal cell walls and fucose-containing sulfated polysaccharides: cell wall context, biomedical properties and key research challenges. *Carbohydr Polym,* 175, 395-408.

Duggins, D. O., C. A. Simenstad & J. A. Estes (1989). Magnification of secondary production by kelp detritus in coastal marine ecosystems. *Science,* 245, 170-173.

Eglinton, T. I. & D. J. Repeta (2006). Organic matter in the contemporary ocean. In *The oceans and marine geochemistry,* ed. H. Elderfield, 145-180. Elsevier.

Engel, A. & N. Händel (2011). A novel protocol for determining the concentration and composition of sugars in particulate and in high molecular weight dissolved organic matter (HMW-DOM) in seawater. *Mar Chem,* 127, 180-191.

Forbord, S., S. Matsson, G. E. Brodahl, B. A. Bluhm, O. J. Broch, A. Handå, A. Metaxas, J. Skjermo, K. B. Steinhovden & Y. Olsen (2020). Latitudinal, seasonal and depth-dependent

variation in growth, chemical composition and biofouling of cultivated *Saccharina latissima* (Phaeophyceae) along the Norwegian coast. *J Appl Phycol,* 32, 2215-2232.

Gottschalk, G. (1986). Regulation of bacterial metabolism. In *Bacterial metabolism,* ed. G. Gottschalk, 178-207. Springer.

Hall, P. O. J. & R. C. Aller (1992). Rapid, small-volume, flow injection analysis for SCO_2, and NH_4^+ in marine and freshwaters. *Limnol Oceanogr,* 37, 1113-1119.

Hansell, D. A. (2013). Recalitrant dissolved organic carbon fractions. *Ann Rev Mar Sci,* 5, 421-445.

Hedges, J. I. (1992). Global biogeochemical cycles: progress and problems. *Mar Chem,* 39, 67-93.

Hedges, J. I., J. A. Baldock, Y. Gélinas, C. Lee, M. Peterson & S. G. Wakeham (2001). Evidence for non-selective preservation of organic matter in sinking marine particles. *Nature,* 409, 801-804.

Huettel, M. & A. Rusch (2000). Transport and degradation of phytoplankton in permeable sediment. *Limnol Oceanogr,* 45, 534-549.

Jansen, S., E. Walpersdorf, U. Werner, M. Billerbeck, M. E. Böttcher & D. De Beer (2009). Functioning of intertidal flats inferred from temporal and spatial dynamics of O_2, H_2S and pH in their surface sediment. *Ocean Dyn,* 59, 317-332.

Jickells, T. D. & J. E. Rae (1997). Biogeochemistry of intertidal sediments. In *Biogeochemistry of intertidal sediments,* eds. T. D. Jickells & J. E. Rae, 1-15. Cambridge University Press.

Jørgensen, B. B. (1982). Mineralization of organic matter in the sea bed - the role of sulphate reduction. *Nature,* 296, 643-645.

Koop, K. & C. L. Griffiths (1982). The relative significance of bacteria, meio- and macrofauna on an exposed sandy beach. *Mar Biol,* 66, 295-300.

Koop, K., R. C. Newell & M. I. Lucas (1982). Biodegradation and carbon flow based on kelp (*Ecklonia maxima*) debris in a sandy beach microcosm. *Mar Ecol Prog Ser,* 7, 315-326.

Krumhansl, K. A. & R. E. Scheibling (2012). Production and fate of kelp detritus. *Mar Ecol Prog Ser,* 467, 281-302.

Linley, E. A. S., R. C. Newell & S. A. Bosma (1981). Heterotrophic utilisation of mucilage released during fragmentation of kelp (*Ecklonia maxima* and *Laminaria pallida*). I. Development of microbial communities associated with the degradation of kelp mucilage. *Mar Ecol Prog Ser,* 4, 31-41.

Llobet-Brossa, E., R. Rosselló-Mora & R. Amann (1998). Microbial community composition of Wadden Sea sediments as revealed by fluorescence in situ hybridization. *Appl Environ Microbiol,* 64, 2691-2696.

Mann, K. H. (1973). Seaweeds: their productivity and strategy for growth. *Science,* 182, 975-981.

Misic, C. & M. Fabiano (2005). Enzymatic activity on sandy beaches of the Ligurian Sea (NW Mediterranean). *Microb Ecol,* 49, 513-522.

Misic, C. & A. C. Harriague (2007). Enzymatic activity and organic substrates on a sandy beach of the Ligurian Sea (NW Mediterranean) influenced by anthropogenic pressure. *Aquat Microb Ecol,* 47, 239-251.

Mudryk, Z., P. Skórczewski, P. Perliński & M. Wielgat (2011). Studies concerning heterotrophic bacteria decomposing macromolecular compounds at two marine beaches. *Oceanol Hydrobiol Stud,* 40, 74-83.

Mudryk, Z. J. & B. Podgórska (2006). Enzymatic activity of bacterial strains isolated from marine beach sediments. *Pol J Environ Stud,* 3, 441-448.

Murakami, K., Y. Yamaguchi, K. Noda, T. Fujii, N. Shinohara, T. Ushirokawa, Y. Sugawa-Katayama & M. Katayama (2011). Seasonal variation in the chemical composition of a marine brown alga, *Sargassum horneri* (Turner) C. Agardh. *J Food Compost Anal,* 24, 231-236.

Pedersen, H. L., J. U. Fangel, B. McCleary, C. Ruzanski, M. G. Rydahl, M.-C. Ralet, V. Farkas, L. Von Schantz, S. E. Marcus, M. C. F. Andersen, R. Field, M. Ohlin, J. P. Knox, M. H. Clausen & W. G. T. Willats (2012). Versatile high resolution oligosaccharide microarrays for plant glycobiology and cell wall research. *J Biol Chem,* 287, P39429-39438.

Podgórska, B. & Z. J. Mudryk (2003). Distribution and enzymatic activity of heterotrophic bacteria decomposing selected macromolecular compounds in a Baltic Sea sandy beach. *Estuar Coast Shelf Sci,* 56, 539-546.

Queirós, A. M., N. Stephens, S. Widdicombe, K. Tait, S. J. McCoy, J. Ingels, S. Rühl, R. Airs, A. Beesley, G. Carnovale, P. Cazenave, S. Dashfield, E. Hua, M. Jones, P. Lindeque, C. L. McNeill, J. Nunes, H. Parry, C. Pascoe, C. Widdicombe, T. Smyth, A. Atkinson, D. Krause-Jensen & P. J. Somerfield (2019). Connected macroalgal-sediment systems: blue carbon and food webs in the deep coastal ocean. *Ecol Monogr,* 89, e01366.

Rabus, R., T. A. Hansen & F. Widdel (2006). Dissimilatory sulfate- and sulfur-reducing prokaryotes. In *The prokaryotes,* eds. M. Dworkin, S. Falkow, E. Rosenberg, K.-H. Schleifer & E. Stackebrandt, 659-768. Springer.

Reed, R. H., I. R. Davison, J. A. Chudek & R. Foster (1985). The osmotic role of mannitol in the Phaeophyta: an appraisal. *Phycologia,* 24, 35-47.

Reintjes, G., C. Arnosti, B. Fuchs & R. Amann (2019). Selfish, sharing and scavenging bacteria in the Atlantic Ocean: a biogeographical study of bacterial substrate utilisation. *ISME J,* 13, 1119-1132.

Reintjes, G., C. Arnosti, B. M. Fuchs & R. Amann (2017). An alternative polysaccharide uptake mechanism of marine bacteria. *ISME J,* 11, 1640-1650.

Reintjes, G., B. M. Fuchs, R. Amann & C. Arnosti (2020). Extensive microbial processing of polysaccharides in the South Pacific Gyre via selfish uptake and extracellular hydrolysis. *Front Microbiol,* 11, 3242.

Revsbech, N. P. (1989). An oxygen microsensor with a guard cathode. *Limnol Oceanogr,* 34, 474-478.

Røy, H., H. S. Weber, I. H. Tarpgaard, T. G. Ferdelman & B. B. Jørgensen (2014). Determination of dissimilatory sulfate reduction rates in marine sediment via radioactive ^{35}S tracer. *Limnol Oceanogr Methods,* 12, 196-211.

Scheschonk, L., S. Becker, J.-H. Hehemann, N. Diehl, U. Karsten & K. Bischof (2019). Arctic kelp eco-physiology during the polar night in the face of global warming: a crucial role for laminarin. *Mar Ecol Prog Ser,* 611, 59-74.

Schiener, P., K. D. Black, M. S. Stanley & D. H. Green (2015). The seasonal variation in the chemical composition of the kelp species *Laminaria digitata*, *Laminaria hyperborea*, *Saccharina latissima* and *Alaria esculenta*. *J Appl Phycol,* 27, 363-373.

Sichert, A., C. H. Corzett, M. S. Schechter, F. Unfried, S. Markert, D. Becher, A. Fernandez-Guerra, M. Liebeke, T. Schweder, M. F. Polz & J.-H. Hehemann (2020). Verrucomicrobia

use hundreds of enzymes to digest the algal polysaccharide fucoidan. *Nat Microbiol,* 5, 1026-1039.

Steneck, R. S., M. H. Graham, B. J. Bourque, D. Corbett, J. M. Erlandson, J. A. Estes & M. J. Tegner (2002). Kelp forest ecosystems: biodiversity, stability, resilience and future. *Environ Conserv,* 29, 436-459.

Tallis, H. (2009). Kelp and rivers subsidize rocky intertidal communities in the Pacific Northwest (USA). *Mar Ecol Prog Ser,* 389, 85-96.

Thomas, F., N. Le Duff, T.-D. Wu, A. Cébron, S. Uroz, P. Riera, C. Leroux, G. Tanguy, E. Legeay & J.-L. Guerquin-Kern (2021). Isotopic tracing reveals single-cell assimilation of a macroalgal polysaccharide by a few marine Flavobacteria and Gammaproteobacteria. *ISME J*, 15, 3062-3075.

Thornton, D. C. O., S. M. Kopac & R. A. Long (2010). Production and enzymatic hydrolysis of carbohydrates in intertidal sediment. *Aquat Microb Ecol,* 60, 109-125.

Usov, A. I., G. P. Smirnova & N. G. Klochkova (2001). Polysaccharides of algae: 55. Polysaccharide composition of several brown algae from Kamchatka. *Russ J Bioorg Chem,* 27, 395-399.

Weiss, M. S., U. Abele, J. Weckesser, W. Welte, E. Schiltz & G. E. Schulz (1991). Molecular architecture and electrostatic properties of a bacterial porin. *Science,* 254, 1627-1630.

Werner, U., M. Billerbeck, L. Polerecky, U. Franke, M. Huettel, J. E. E. Van Beusekom & D. De Beer (2006). Spatial and temporal patterns of mineralization rates and oxygen distribution in a premeable intertidal sand flat (Sylt, Germany). *Limnol Oceanogr,* 51, 2549-2563.

Zimmerman, R. C. & J. N. Kremer (1986). In situ growth and chemical composition of the giant kelp, *Macrocystis pyrifera*: response to temporal changes in ambient nutrient availability. *Mar Ecol Prog Ser,* 27, 277-285.

Supplementary Information

Microbial communities in intertidal permeable sediments are optimized for the degradation of kelp polysaccharides

Marit R. van Erk[1], Silvia Vidal-Melgosa[1,2], Dirk de Beer[1]

[1]Max Planck Institute for Marine Microbiology, Bremen, Germany

[2]University of Bremen, Center for Marine Environmental Sciences, MARUM, Bremen, Germany

Content
1. Supplementary Figure 1
2. Supplementary Figure 2
3. Supplementary Table 1
4. Supplementary Table 2

A

Kelp

	BAM1	BAM2	BAM4	LM7	LM16	CBM3a	BS-400-2	BS-400-3	LM26	INRA-AX1	LM23	JIM13	BAM6	BAM7	BAM8	BAM9	BAM10
MilliQ water	16	28	16	61	11	0	0	0	37	16	17	15	15	73	61	62	78
EDTA*	5	0	0	9	0	0	0	0	12	0	0	0	0	11	12	17	23
NaOH	6	0	11	58	0	0	27	16	0	7	0	0	11	65	52	55	61

B

Kelp-beach

	BAM1 - EDTA*	BAM2 - EDTA*	BAM4 - EDTA*	LM7 - EDTA*	LM16 - EDTA*	CBM3a - NaOH	BS-400-2 - EDTA*	BS-400-3 - EDTA*	LM26 - EDTA*	INRA-AX1 - EDTA*	LM23 - EDTA*	JIM13 - EDTA*	BAM6 - EDTA*	BAM7 - EDTA*	BAM8 - EDTA*	BAM9 - EDTA*	BAM10 - EDTA*
0 cm	0	0	0	0	0	0	0	0	0	0	0	0	0	9	0	0	6
4 cm	0	0	0	0	0	0	0	0	0	0	0	0	0	14	0	0	12
8 cm	0	0	0	0	0	0	0	0	0	0	0	0	0	0	0	0	0
20 cm	0	0	0	0	0	0	0	0	0	0	0	0	0	0	0	0	0

Reference beach

	BAM1 - EDTA*	BAM2 - EDTA*	BAM4 - EDTA*	LM7 - EDTA*	LM16 - EDTA*	CBM3a - NaOH	BS-400-2 - EDTA*	BS-400-3 - EDTA*	LM26 - EDTA*	INRA-AX1 - EDTA*	LM23 - EDTA*	JIM13 - EDTA*	BAM6 - EDTA*	BAM7 - EDTA*	BAM8 - EDTA*	BAM9 - EDTA*	BAM10 - EDTA*
0 cm	0	0	0	0	0	0	0	0	0	0	0	0	0	0	0	0	0
4 cm	0	0	0	0	0	0	0	0	0	0	0	0	0	0	0	0	0

C

BAM1	Un-sulfated epitope present in sulfated fucan
BAM2	Sulfated epitope present in sulfated fucan
BAM4	Sulfated epitope present in sulfated fucan
LM7	Non-blockwise partially methyl-esterified homogalacturonan
LM16	Galactosyl residue(s) on rhamnogalacturonan I
CBM3a	Cellulose
BS-400-2	$(1{\rightarrow}3)$-β-D-glucan
BS-400-3	$(1{\rightarrow}3)(1{\rightarrow}4)$-$\beta$-D-glucan
LM26	Branched $(1,6$-Gal$)(1{\rightarrow}4)$-β-D-galactan
INRA-AX1	$(1{\rightarrow}4)$-β-D-xylan/arabinoxylan
LM23	Xylosyl residues
JIM13	Arabinogalactan protein glycan
BAM6	Alginate - mannuronate-rich epitope
BAM7	Alginate - mannuronate-guluronate
BAM8	Alginate - mannuronate-guluronate
BAM9	Alginate - mannuronate-guluronate
BAM10	Alginate - mannuronate-guluronate

Supp. Figure 1: *Heat maps showing the microarray results in kelp and sediment samples. Data from a selection of antibodies for kelp extracts are shown in (A). (B) shows the signal detected with these antibodies in the kelp-beach and reference beach sediment samples. (C) shows the recognized epitope structures for each of these antibodies. In (A) results are shown for the three different extraction solvents: autoclaved MilliQ water, EDTA, and NaOH. *Due to the high viscosity, the EDTA samples are 2 times more diluted compared to the MilliQ water and NaOH extractions. Signal intensities show the average of triplicates, with signals <5 set to zero. Kelp-beach sediment signals are calculated for 2 different locations, and the triplicates of both locations averaged to 1 signal intensity. Reference beach sediment signals are calculated for 1 location, and the triplicates averaged to 1 signal intensity.*
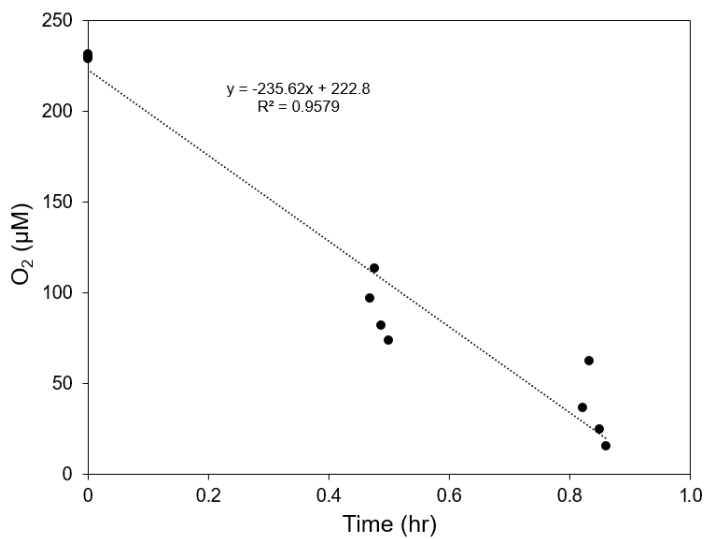
Supp. Figure 2: *Oxygen concentrations in Exetainers filled with kelp-beach sediment and seawater, for 4 replicates.*

Supp. Table 1: *Probes with signals close to the cut-off (<5) and tested probes that did not show binding to any of the samples.*

Antibodies where values close to the cut-off were detected in only one of the triplicates.

LM28	Glucuronoxylan
LM11	(1→4)-β-D-xylan/arabinoxylan
MAC207	Arabinogalactan protein glycan
LM21	(1→4)-β-D-(galacto)(gluco)mannan

Antibodies that did not bind to any of the samples. Polysaccharide epitopes recognized by the antibodies are listed as well.

BAM3	Possibly sulfated epitope present in sulfated fucan
JIM5	Partially methyl-esterified/de-esterified HG
JIM7	Partially methyl-esterified HG
LM18	Partially methyl-esterified/de-esterified HG
LM19	Partially methyl-esterified/de-esterified HG
LM20	Partially methyl-esterified HG
LM8	Xylogalacturonan
INRA-RU2	Rhamnogalacturonan I backbone
INRA-RU1	Rhamnogalacturonan I backbone
LM13	Linearised (1→5)-α-L-arabinan
LM5	(1→4)-β-D-galactan
LM6	(1→5)-α-L-arabinan
LM6-M	(1→5)-α-L-arabinan
BS-400-4	(1→4)-β-D-(galacto)(gluco)mannan
LM22	(1→4)-β-D-(galacto)(gluco)mannan
LM15	Xyloglucan (XXXG motif)
LM25	(1→4)-β-D-mannan
LM30	Arabinogalactan protein glycan
LM10	(1→4)-β-D-xylan
JIM4	Arabinogalactan protein glycan
JIM8	Arabinogalactan protein glycan
JIM15	Arabinogalactan protein glycan
JIM16	Arabinogalactan protein glycan
JIM20	Extensin
LM1	Extensin
LM2	β-linked GlcA in arabinogalactan protein
LM12	Epitope containing ferulic acid
LM14	Arabinogalactan protein glycan
BAM11	Alginate - mannuronate-guluronate

Supp. Table 2: *Sulfate reduced (in mol m^{-3} sed) after 6 hrs of incubation for reference beach and kelp-beach sediment for the background (seawater) and after addition of substrates. *: Sulfate reduced after 4 hrs, because the determination of sulfate reduced failed for the 6 hrs timepoint.*

	Reference beach	Kelp-beach
Seawater	0.02×10^{-2}	1.33×10^{-2}
Glucose	0.36×10^{-2}	21.20×10^{-2}
Agar	0.03×10^{-2}	4.57×10^{-2}
Acetate	0.28×10^{-2}	15.20×10^{-2}
Mannitol*	0.23×10^{-2}	9.00×10^{-2}
Laminarin	0.40×10^{-2}	16.5×10^{-2}
Glycogen	0.07×10^{-2}	8.53×10^{-2}
Kelp	0.44×10^{-2}	12.7×10^{-2}

Reactive oxygen species affect mineralization processes in permeable intertidal flats

Marit R. van Erk*[,a], Olivia M. Bourceau*[,a], Chyrene Moncada[a], Subhajit Basu[a],
Colleen M. Hansel[b], Dirk de Beer[a]

[a]Max Planck Institute for Marine Microbiology, Bremen, Germany
[b]Department of Marine Chemistry and Geochemistry, Woods Hole Oceanographic Institution,
Woods Hole, Massachusetts, USA

* *These authors contributed equally*

Manuscript in preparation

This version has not been seen by all authors

Abstract

Intertidal permeable sediments are crucial for organic matter remineralization. In these sediments reactive oxygen species (ROS) may be abundant because of a shifting oxic-anoxic interface and intense iron-sulfur cycling. We investigated the effect of transient oxygenation on microbial degradation processes in surface intertidal sediments by incubating slurries that transitioned from oxic to anoxic conditions. Removal of ROS strongly increased rates of aerobic respiration, sulfate reduction and hydrogen accumulation. Further, extracted porewaters showed high concentrations of the ROS hydrogen peroxide below the oxic zone. We conclude that ROS were formed in the sediments, and subsequently moderated microbial mineralization process rates. Sulfate reducers were completely inhibited in the oxic period, yet sulfate reduction resumed immediately upon anoxia. Remarkably, oxygen exposure before anoxia boosted the subsequent sulfate reduction rates, possibly by stimulating hydrolysis of organic material. This study demonstrates the strong effects of ROS on the biogeochemistry of intertidal sediments.

Introduction

The depth to which oxygen penetrates into intertidal permeable sediment varies according to tides, currents, storms, and bioturbation[1]. The oxic zone can shift between several cm to several mm deep multiple times a day[2]. Nevertheless, anaerobes in the upper sediment maintain high rates of sulfate reduction, dissimilatory nitrate reduction, fermentation, and other anaerobic processes[3-5]. The high rates of carbon and nitrogen remineralization make these sediments biocatalytic filters[1,6], essential for the functioning of the shallow water ecosystems.

Intertidal permeable sediments frequently switch between oxic and anoxic conditions[2], and have active sulfur and iron cycling. As a consequence, intertidal permeable sediments have the potential to produce reactive oxygen species (ROS), short-lived oxygen-containing intermediates with lifetimes of seconds to hours, including superoxide, hydrogen peroxide and hydroxyl radical. ROS are formed by a variety of photochemical, abiotic, and biotic processes[7]. Biotic formation occurs both intracellularly and extracellularly as a byproduct of metabolic and other physiological mechanisms[8]. In addition to photochemical pathways, a number of light-independent abiotic processes can lead to ROS formation, including oxidation of sulfide and ferrous iron (Fe^{2+})[9,10], as well as anaerobic reactions with pyrite[11]. Intracellular ROS can damage cell components such as DNA, proteins, and lipids via a range of oxidative processes[12], and thus be detrimental to microorganisms at elevated levels. However, both intracellular and extracellular ROS also have beneficial roles, including pathogen resistance[13], nutrient acquisition[14], microbial growth[15], and as signaling molecules[16], amongst others. As such, ROS levels are strictly controlled by degrading enzymes[8], such as superoxide dismutase, which converts superoxide to hydrogen peroxide, and catalase, which converts hydrogen peroxide to oxygen and water. Also, electron donor-driven mechanisms actively degrade ROS, such as reactions with metals and organic material[17].

Consequently, ROS may play an unappreciated role in the biogeochemistry of dynamic coastal sediments. In particular, during disturbance events and at oxic-anoxic interfaces, elevated ROS levels in intertidal permeable sediments can be expected, which will have potentially substantial impacts on the activity and growth of the resident microbiota[18-20]. Here, we tested the hypothesis that high levels of ROS can develop in intertidal permeable sediments and thereby control biomineralization rates. Specifically, we measured hydrogen peroxide concentrations in sediment porewater and investigated the effect of enzymatic removal of ROS on anaerobic respiration.

Also, the impact of transient oxygenation on anaerobic respiration in intertidal permeable sediments was tested.

Impact of reactive oxygen species on respiration

Removal of hydrogen peroxide and superoxide via additions of catalase and superoxide dismutase, respectively, substantially increased the rates of oxygen consumption, sulfate reduction, and Fe^{2+} and hydrogen accumulation (Fig. 1). This effect was not simply due to the addition of protein as a carbon or nitrogen substrate, as incubations with a comparable amount of inert (i.e. non-ROS degrading) bovine serum albumin (BSA) did not have a stimulating effect on these biogeochemical process rates. Enzymatic reactions with superoxide dismutase and catalase both lead to production of oxygen. Superoxide dismutase is involved in dismutation of superoxide to hydrogen peroxide and oxygen (reaction 1), while catalase is involved in hydrogen peroxide decay to water and oxygen (reaction 2). Despite the enzymatic production/recycling of oxygen, oxygen consumption was approximately four times faster in incubations containing catalase and superoxide dismutase pointing to ROS as a control on aerobic respiration in these sediments (Fig. 1A).

$$2O_2^{\cdot-} + 2H^+ \; \rightarrow \; H_2O_2 + \; O_2 \;\; (1)$$

$$2H_2O_2 \rightarrow 2H_2O + \; O_2 \qquad (2)$$
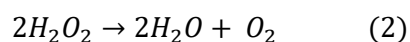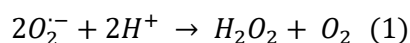
Sulfate reduction was faster (~30%) in the presence of catalase and superoxide dismutase (Fig. 1B). The combination of catalase and superoxide dismutase had the most pronounced effect. Superoxide dismutase alone had no effect, although this does not necessarily mean that superoxide does not impact the rate of sulfate reduction. In the absence of catalase, any positive effect of removing superoxide on the resident sulfate-reducing community may be masked by the negative effect of increasing hydrogen peroxide (reaction 1).

Hydrogen and Fe^{2+} accumulation rates were much higher in the presence of catalase alone and combined catalase and superoxide dismutase (Fig. 1C,1D), where Fe^{2+} accumulation could not be explained by possible release of Fe^{2+} from the catalase molecule, which would only lead to a Fe^{2+} concentration of 0.5 µM (each catalase molecule contains 4 iron atoms). This reconciles

previous observations that catalase additions significantly increase the rate of fermentation in cultures[21,22], but reveals a previously unknown constraint of ROS on fermentation in marine sediments. Addition of catalase alone and combined catalase and superoxide dismutase disrupted the tight balance between hydrogen production by fermentation and consumption by sulfate reduction that is common in marine sediments[23], so that hydrogen accumulated. In situ, hydrogen concentrations are low (0.03 ± 0.01 nmol cm^{-3} sed (9.8 ± 3.9 nmol L^{-1} porewater) in July 2020 and 0.04 ± 0.01 nmol cm^{-3} sed (13.1 ± 2.1 nmol L^{-1} porewater) in March 2021), without trends with depth. Hydrogen in sediments can derive from fermentation, and possibly via H_2S reacting with iron sulfide (Wächterhäuser reaction)[24,25], or N_2 fixation. Inhibiting sulfate reduction with molybdate[26] (Supp. Fig. S1A) resulted in 22 times higher rates of hydrogen accumulation than in untreated sediment during the anoxic period (Supp. Fig. S2A,B). This indicates that hydrogenotrophic sulfate reduction is active in these sediments, confirming predictions based on metagenomics analyses[27]. However, hydrogen fuels only a minor proportion of the sulfate reduction, as the highest hydrogen accumulation rate (with molybdate addition) was 20 times lower than the sulfate reduction rate (Supp. Fig. S3).
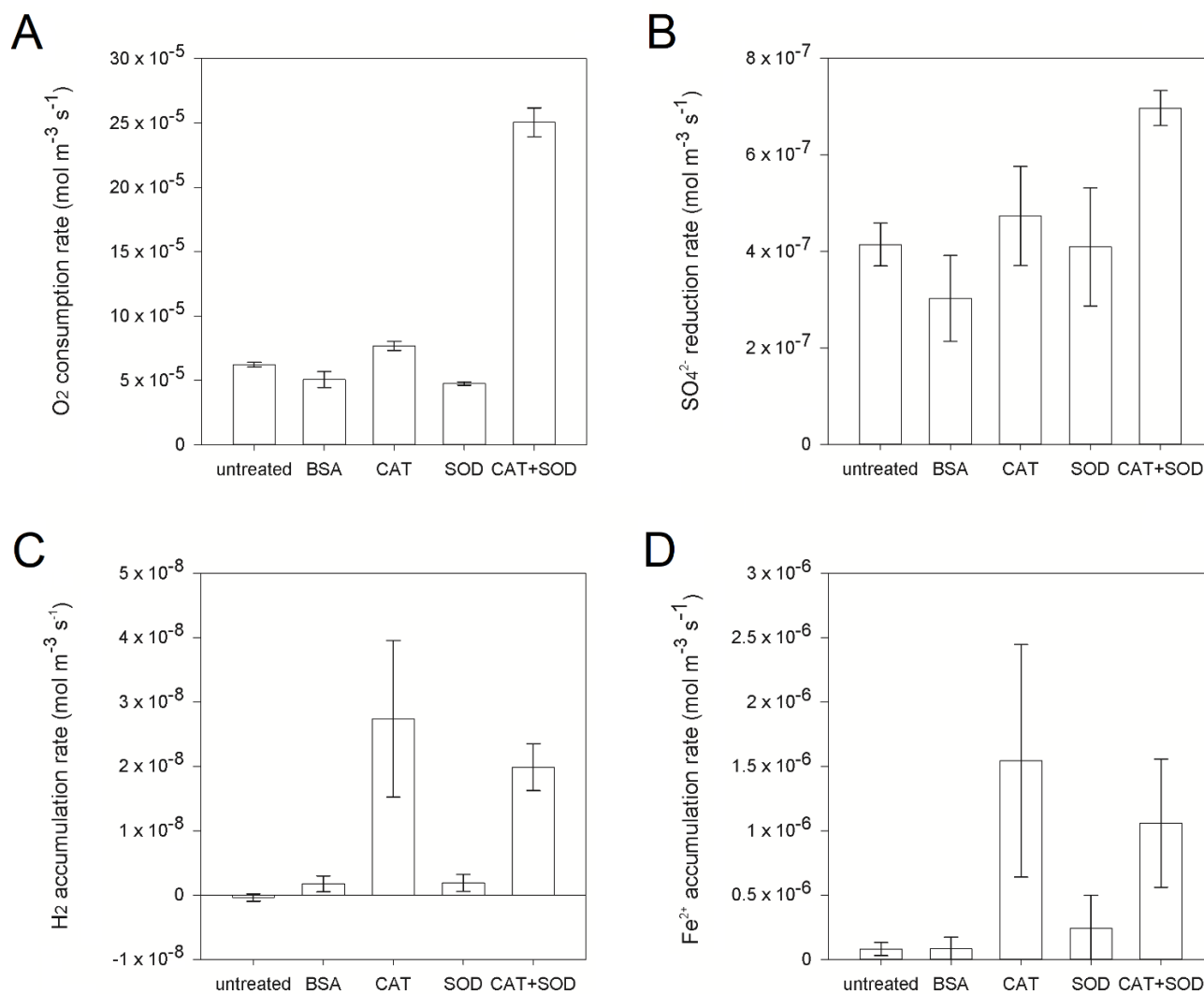
Figure 1: *The influence of reactive oxygen species (ROS) on respiration rates for untreated slurries and slurries treated with BSA, catalase (CAT), superoxide dismutase (SOD), and a combination of CAT and SOD (CAT+SOD), from sediments collected June 15th. **A:** oxygen consumption, **B:** sulfate reduction, **C:** hydrogen accumulation, **D:** Fe^{2+} accumulation. Sulfate reduction, hydrogen accumulation and Fe^{2+} accumulation rates were calculated for the anoxic period of the incubation. Error bars represent standard error of the slope.*

Hydrogen peroxide in intertidal sediments

Microprofiles of hydrogen peroxide, measured with a novel microsensor, show the presence of hydrogen peroxide in anoxic sediment (Fig. 2). The microsensors that were used contained ferrozine in their electrolyte, and do not have interference with Fe^{2+}. Steady-state levels were elevated in comparison to many environmental systems[28-30]. Further, injection of oxygen-saturated seawater at depths that are usually hydrogen peroxide-free led to hydrogen peroxide production (Supp. Fig. S4). Maximum hydrogen peroxide production, determined from the microprofiles using a diffusion-reaction model, was 1×10^{-4} mol m^{-3} s^{-1} (Supp. Fig. S5), which is much higher than in tidal pools, soil waters, aquifers, and brackish and freshwater ponds[28,30-32]. A second increase in hydrogen peroxide production below 4 cm depth might be related to the abiotic dark production of hydrogen peroxide via pyrite[11], as the transition from brown to dark, iron sulfide containing sediments, was between 4 and 5 cm depth. The sediments are indeed iron-rich, with concentrations of 9.7 ± 1.8 and 2.2 ± 0.6 µmol g^{-1} sed in surface sediments (0-2 cm depth) in May and July 2020, and 3.8 ± 0.3 µmol g^{-1} sed in deep sediment (10-14 cm depth) in July 2020.
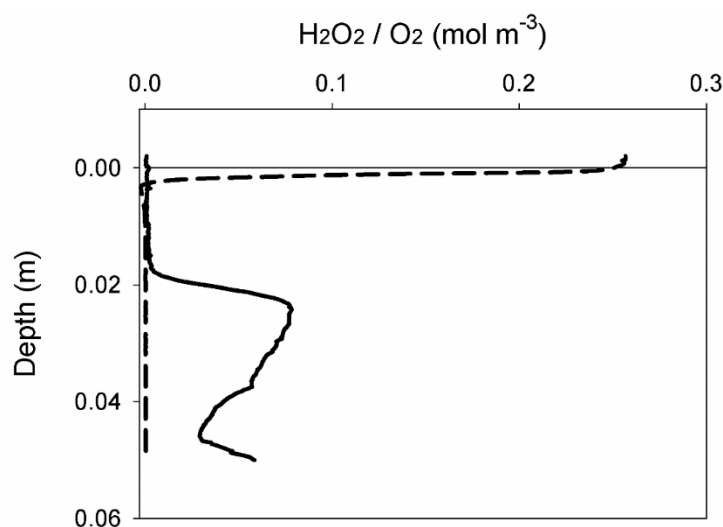
Figure 2: *Steady-state microprofiles of O_2 and H_2O_2.*

The presence of hydrogen peroxide was confirmed using a chemiluminescence technique. Hydrogen peroxide was measured in a parallel sediment core to that in which microsensor measurements were conducted (Supp. Fig S6A), and in porewater extracted by Rhizons on the flat (Supp. Fig S6B), which was directly fixed with ferrozine to prevent reaction with iron before analysis. Absolute concentrations differ from those in microprofiles, probably due to sampling

artefacts and loss during storage between sampling and analysis. As the samples measured using chemiluminescence were not fixed with acid, loss of hydrogen peroxide could have occurred between sampling and analysis a few hours later.

Anaerobic respiration after transient oxygenation

While undetectable in the oxic period of incubations, sulfate reduction resumed instantly after oxygen depletion in both surface sediment subject to daily re-oxygenation (0-2 cm depth) and deeper permanently anoxic sediment (10-14 cm depth) during all sampling campaigns (Fig. 3A, Supp. Fig. S1B,C,D). Rapid sulfide oxidation to sulfate could not explain the absence of sulfate reduction during the oxic period, as it was also not detected by the silver wire method (Fig. 3B). That is the method of choice for detecting aerobic sulfate reduction since sulfide binds instantly and irreversibly to silver[33]. Incomplete sulfide reoxidation to sulfur intermediate oxidation states, e.g. via reactions with iron oxides, would also have been detected by the radiochemical sulfate reduction method used[34]. Thus, sulfate reduction was controlled by oxygen, yet we suspect that the sulfate reducers were not killed, but inactive. In their active state, reduced enzymes with iron cofactors that are involved in sulfate reduction become irreversibly damaged by oxygen, and then release ROS leading to cell death[12,35]. An environment that fluctuates multiple times per day between oxic and anoxic conditions exerts a strong selective pressure for sulfate reducers capable of coping with oxygen. This pressure appears not to select for sulfate reducers capable of respiring in the presence of oxygen, as has been found in cyanobacterial mats[36].
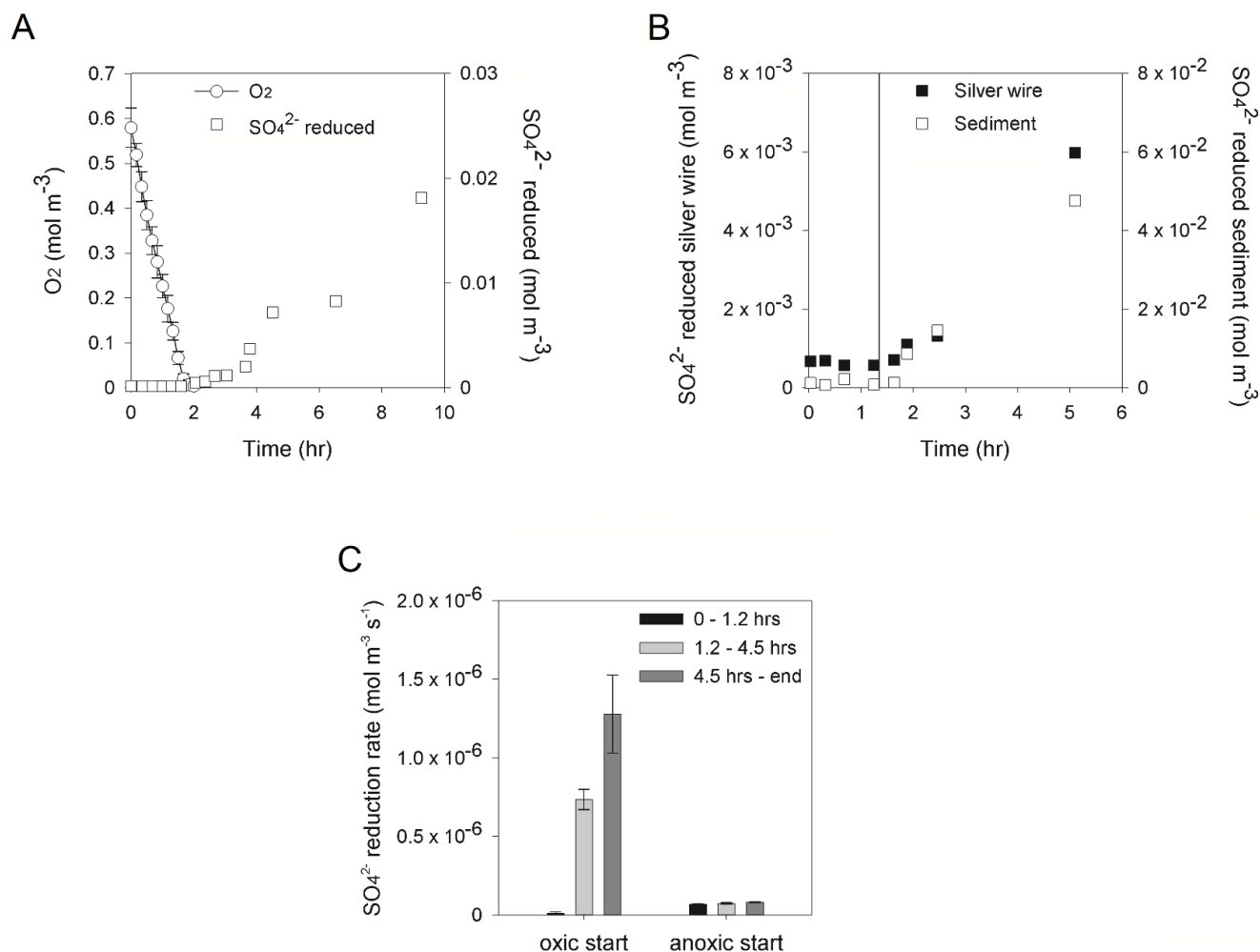
Figure 3: Influence of oxygen on respiration. **A:** *Oxygen concentrations (circles) and reduced sulfur (squares) in slurries over an oxic-anoxic transition. Slurries were from sediment collected on May 25th 2020. Oxygen concentrations are an average of 3-4 Exetainers, resampled over the course of the incubation. Error bars represent standard deviation,* **B:** *Radiolabeled reduced sulfur bound to a silver wire (filled squares), or to the sediment in the same incubation vial (open squares) in incubations including a silver wire over an oxic-anoxic transiton. For all sulfate reduction measurements each point corresponds to a separate incubation vial. The vertical line represents the transition to anoxic conditions,* **C:** *The sulfate reduction rate in slurries at three different periods during incubation shown for two treatments. Oxic incubations started oxic and became anoxic within 1.2 hrs, while anoxic incubations were anoxic for the whole incubation period. Black bars represent the sulfate reduction rate in the first 1.2 hrs of incubation, which corresponds to the oxic period in the transiently oxic incubations. Light grey bars represent the sulfate reduction rate between 1.2 and 4.5 hrs of incubation, dark grey bars represent the sulfate reduction rate from 4.5 hrs of incubation until the end of the incubation (23 - 25 hrs). Error bars represent standard error of the slope.*

Changes in hydrogen levels were minor in the first 24 hrs of incubation, with levels remaining below 1 nmol cm^{-3} sed (Supp. Fig. S7A,B,C). Neither Fe^{2+} (Supp. Fig. S8A,B) nor methane accumulation was observed after anoxia. Fe^{2+} accumulation started after more than 10 hrs, while methane concentrations stayed constant at 1.39 ± 0.25 nmol cm^{-3} sed during the first 24 hrs. While this lag period could indicate that fermenters, iron reducers, and methanogens are more sensitive to oxygenation than sulfate reducers, this is unlikely given that these communities are regularly exposed to oxygen. Instead, reduced iron and methane are likely rapidly reoxidized by pools of electron acceptors, such as Fe(III) and manganese[37], until these pools are exhausted[38]. Also sulfide was scavenged by these pools of oxidants as it could not be detected, despite the occurrence of sulfate reduction.

While ROS limited the rate of anaerobic respiration in the anoxic period, transient oxygenation itself substantially boosted subsequent anaerobic respiration in incubations of surface sediment incubated either anoxically or with a transient oxic period (Fig. 3C). This is contrary to expectations that oxygenation is damaging to anaerobic communities, especially through the production of ROS. Possibly, oxygen is required for the initial hydrolysis of macromolecules in sediments, which is often considered the limiting step of carbon turnover[39]. Alternatively, abiotic mineralization by ROS[28,40] that are produced during the oxic period produced lower-weight molecules that could then be used during the anoxic period.

Implications for respiration in intertidal sediments

Here, we show that removal of extracellular ROS within intertidal permeable sediments substantially boosted the rates of oxygen consumption, sulfate reduction, and Fe^{2+} and hydrogen accumulation (Fig. 4). Biotic carbon turnover by aerobic respiration and sulfate reduction increased 4 times in slurries treated with a combination of catalase and superoxide dismutase (Supp. Table S1). Aerobic respiration and sulfate reduction together are responsible for most of the mineralization in coastal sediments[41], so factors limiting these processes have the potential to directly impact the effectiveness of sands as biocatalytic filters. We propose that ROS reduced biotic mineralization either through changing the availability of organic carbon or through direct oxidative stress. While this study points to the likely importance of ROS in marine sediment biogeochemistry, the extent of the impact of ROS requires in situ measurements of these compounds over space and time. Yet, to date, there is only very limited data on the potential for ROS formation in marine sediments and their in situ distribution[9,18], thereby limiting a clear

understanding of the importance of ROS in sediment biogeochemistry. The relevance of ROS will undoubtedly be amplified in fluctuating redox environments as observed here. In fact, frequent shifts between oxic and anoxic conditions in intertidal flats should not be considered as an inhibitor of anaerobic processes. Anaerobes in intertidal sediments endure daily oxygen exposure because they are handsomely rewarded with electron donors at the beginning of the anoxic period.
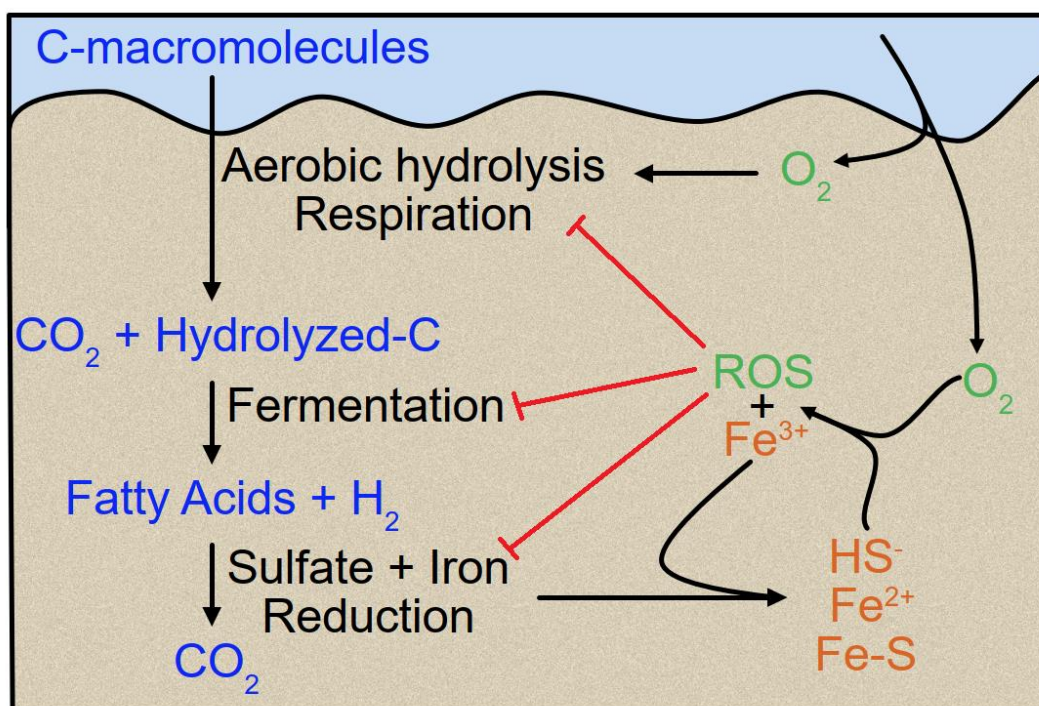

Figure 4: Flow diagram of the proposed effects of reactive oxygen species (ROS) in intertidal sands. Arrows represent transport and production processes. Red lines represent limiting effects. Organic material in the form of macromolecules is transported into the sediments. Hydrolysis and fermentation convert these molecules into e.g. fatty acids and hydrogen, which are substrates for sulfate and iron reducers. Also, oxygen is transported into the sediments where it can come in contact with reduced sulfide and iron, resulting in amongst others Fe^{3+} and ROS. ROS influence biotic reactions with organic material. Sulfate- and iron reduction are limited either indirectly via fermentation, or directly, which is not further assessed in this study.

Methods

Sampling

Sediments were collected in the German Wadden Sea from the backbarrier area behind the island of Spiekeroog, on the intertidal sandflat Janssand (53°44'25.51"N, 7°41'28.63"E)[42-44]. The flat is subjected to advective flushing according to the tides, which are semi-diurnal and have a tidal range of ~2 meters. The flat is inundated at high tide and exposed for ~6 hrs around low tide. Samples were collected from the upper, sandy part of the flat during low tide on five occasions over three seasons, May 15th, June 15th, July 28th, October 8th, 2020, and March 18th, 2021. The upper part of the flat has a porosity of 0.33, a mean grain size of 176 μm, and a permeability of ~7.2 × 10^-12 m^2 [42,43]. Sediment was scrapped from the upper 2 cm and transferred into a canister and covered with seawater. Deeper sediments and depth profiles were collected with core liners. Seawater was collected adjacent to the flat. On March 18th, 2021, porewater samples were sampled in situ for Fe^{2+} and hydrogen peroxide measurements using Rhizons (Rhizosphere Research Products, The Netherlands). Sediment cores were sampled using core liners for oxygen and hydrogen peroxide measurements.

Incubation set up

All incubations were carried out in 6 mL gas-tight vials, hereafter called Exetainers (Labco, UK) that were filled without headspace, with 2 cm^3 sediment and 4 mL seawater. During incubation, all Exetainers were placed in light-impermeable roller tanks and inverted every 30 seconds, to allow thorough slurry mixing. Except for the incubations in October, all incubations were started on the same day as the sediment was sampled. In October, sediment and seawater were stored at 4 °C for six days before incubations started. In the incubations with an anoxic start, seawater was equilibrated with a nitrogen atmosphere and Exetainers were filled in an anoxic hood that had a nitrogen-carbon dioxide (9:1) atmosphere. For all other incubations, Exetainers were filled on a lab bench after sediment was thoroughly mixed, and seawater was shaken to bring to equilibrium with the air. For all measurements except oxygen, Exetainers were destructively sampled, so each timepoint represents a separate individual Exetainer.

Depending on the experiment, incubations were untreated, or amended with 28 mM sodium molybdate, 1500 U/mL catalase, 217 U/mL superoxide dismutase, a combination of 217 U/mL superoxide dismutase and 1500 U/mL catalase, or 0.5 mg/mL bovine serum albumin (BSA). The BSA treatment served as a control for the enzyme treatment, to allow separation of the effects of

enzymatic activity from the effect of added protein. Separate Exetainers were used to measure sulfate reduction, hydrogen accumulation, and methane accumulation, depending on the experiment. When total sulfate, sulfide and dissolved iron were measured, these were measured from the supernatant of the hydrogen Exetainers.

Oxygen consumption measurements

Oxygen concentrations were measured repeatedly from a series of 3-4 Exetainers which were quickly opened at regular intervals to allow insertion of a Clark-type oxygen microsensor produced in-house[45]. When this process introduced a bubble to the Exetainer headspace, the Exetainer was discarded. Oxygen microsensors were calibrated against air-saturated seawater and anoxic sodium ascorbate.

One linear trend line per treatment was plotted through the individual measurements of the Exetainers, and its intersection with an oxygen concentration of zero µM was calculated, which was defined as the transition between oxic and anoxic conditions. For each trend line, the standard error of the slope was calculated.

Sulfate reduction rate measurements

Sulfate reduction was determined according to Røy et al. 2014[34]. 250 kBq of ^{35}S-SO_4^{2-} were added to each Exetainer used for sulfate reduction measurements. Incubations were stopped by transferring the entire content of the Exetainers to 6 mL 20% (w/v) ZnAc and then stored at -20 °C until distillation. Reduced sulfur was distilled from samples using a cold acid-chromium distillation within 2 months. All bioactive extracellular sulfur, except for sulfate, should be captured in this fraction. Radioactivity in the distilled sulfur fraction was determined with a scintillation counter (Perkin-Elmer Tri-Carb 4910 TR; using Ultima-Gold Scintillation cocktail). Sulfate reduction rates were calculated by plotting a linear trend line through the individual measurements of the anoxic period, and for each trend line, the standard error of the slope was calculated.

In October 2020, sulfate reduction was also determined as above with the inclusion of a silver wire twice the length of the Exetainer, to increase sensitivity to oxic sulfate reduction[33]. Exetainers were sampled as above, with a higher resolution during the oxic period. The silver wire was then cleaned twice in 50 mM sodium sulfate, then radioactivity was determined using a scintillation counter.

Hydrogen measurements

At each timepoint during the incubation, a 2 mL headspace was created in an Exetainer using nitrogen gas by removing 2 mL supernatant. The Exetainer was shaken vigorously for 2 minutes to allow for headspace equilibration, then 1 mL of the headspace was injected into a gas chromatograph (Peak Performer RCP 910-Series, Peak Laboratories, USA) using a gas- and pressure-tight syringe. The gas chromatograph was calibrated against a 100 ppm hydrogen standard (Air Products, Germany). Hydrogen accumulation rates were calculated by plotting a linear trend line through the individual points, and for each trend line, the standard error of the slope was calculated.

Dissolved iron, sulfide and sulfate measurements

The supernatant that was replaced by N_2 during headspacing from the Exetainers for hydrogen determination was used to measure dissolved iron and sulfate. Immediately after removing supernatant using a syringe, the syringe was connected to a 0.2 µm PTFE filter. The first 0.5 mL from the syringe was transferred directly into 0.1 mL 5% (w/v) ZnAc for subsequent sulfide and/or sulfate analysis. 1 mL from the remaining volume was added directly to 0.1 mL ferrozine for subsequent dissolved iron measurements. Dissolved iron was measured spectrophotometrically. Porewater samples collected on March 18th, 2021 were transferred to cuvettes and measured using the same spectrophotometric method. Dissolved iron was measured using the ferrozine method[46]. Sulfate was measured using an ion chromatograph (Metrohm 920 Compact IC Flex, Metrohm AG, Switzerland) with a zinc trap, calibrated against a standard curve of a sulfate standard. Sulfide was measured spectrophotometrically[47].

Methane measurements

Slurries in Exetainers used for methane analysis were fixed using 200 µL saturated $ZnCl_2$ solution, and stored upside-down until analysis. A headspace of 2 mL was created using helium gas, and 500 µL headspace was injected in a gas chromatograph using a gas- and pressure-tight syringe. The gas chromatograph was calibrated against a 100 ppm methane standard (Air Liquide, Germany).

Solid-phase iron extraction

Solid-phase acid volatile iron was extracted from sediments in May and July 2020. Samples of 10-50 mg taken from the sediment surface (0-2 cm depth), or from a depth of 10-14 cm in a freshly sliced core, were quickly transferred to 0.5 M HCl and allowed to react for 0.5 hrs. The extract

was then immediately filtered through 0.2 µm PTFE syringe filters and analyzed spectrophotometrically using the ferrozine method[46].

Hydrogen peroxide sensor

The hydrogen peroxide sensor consisted of an etched 50 µm-thick platinum anode plated with platinum chloride (8% $PtCl_4$ in MilliQ water), an etched 100 µm-thick platinum guard, and a thick platinum reference. The anode, guard, and reference were mounted in a glass casing, with the sensing anode at a distance of ca. 50 µm from the tip. The tip diameter of the outer capillary had a diameter of 25-30 µm and a tip opening of 10 µm. Before mounting the electrodes, the tip of the outer capillary was sealed by a thin polyurethane membrane (D6, kindly provided by Anders Tjell, TU Graz, Austria). The membrane was dissolved in tetrahydrofuran (50 mg mL^{-1}) and applied by shortly immersing the capillary in the solution that is kept in the tip of a Pasteur pipette and left to cure overnight. The membrane was applied under microscopic guidance. The membrane separated the electrolyte from the seawater but was permeable for hydrogen peroxide. After mounting the electrodes in the casing, the sensor was filled with electrolyte, a borate/potassium chloride buffer (50 mM borate, 3 M potassium chloride and 490 µM ferrozine), with pH 9. Sensor performance is described in the Supplementary Information.

The sensor was connected to a picoammeter and polarized at +700 mV until a stable current was obtained, which happened normally within an hour. The medium in which the sensor was used was connected to an external reference electrode. The sensors were calibrated before use in a stirred beaker with filtered seawater to which aliquots of stabilized 3% hydrogen peroxide were added.

Hydrogen peroxide microsensor measurements

Steady-state hydrogen peroxide microprofiles were measured using the new hydrogen peroxide microsensor (see "*Hydrogen peroxide sensor*", Supplementary Information, Supp. Table S2, Supp. Fig. S9,S10) in sediment cores collected March 18th, 2021. Parallel oxygen microprofiles were measured using an oxygen microsensor as described previously[45]. The interface between the overlying water column and sediment was set at depth zero. The water column was continuously stirred to ensure a well-mixed column and a constant boundary layer. The oxygen microsensor was 2-point calibrated (air and 1 M Na-ascorbate pH 11). The hydrogen peroxide microsensor was calibrated by incremental addition of a 3% hydrogen peroxide solution to seawater. Microprofiles were measured using a motor-equipped micromanipulator, controlled by

a laptop on which also the data were acquired.

Production of hydrogen peroxide was calculated using the steady-state depth profile. Fluxes were calculated by multiplying the effective molecular diffusion coefficient ($D_{eff} = 1.08 \times 10^{-8}$ m^2 s^{-1}) with the concentration gradient, where $D_{eff} = D_0(1.13 \times 10^{-9}$ m^2 s$^{-1}) \times$ porosity^{-2}. Conversion (production or consumption) was then calculated using the change in flux over depth.

The potential influence of oxygen on hydrogen peroxide production was assessed by addition of oxygen-saturated seawater to hydrogen peroxide-free sediment. A needle connected to a syringe filled with the seawater was inserted into the sediment, and the seawater was slowly injected. Microprofiles were measured after injection. Parallel microprofiling of oxygen ensured that profiling was conducted where the seawater was injected.

Hydrogen peroxide chemiluminescent measurements

Hydrogen peroxide concentrations from sediment porewater were determined in a FeLume system[48,49], essentially a circular flowcell with a photomultiplier placed directly on top to detect the photons from a chemiluminescent reaction in the flowcell. The flowcell and detector combination were placed in a black box to protect against light interference. Hydrogen peroxide is proportional to the amount of photons produced by the chemiluminescent reaction with 10-methyl-9-(p-formylphenyl)-acridinium carboxylate trifluoromethanesulfonate (AE) under alkaline conditions[48,49]. The analysis was carried out in a flow-injection mode. Reagent solutions were prepared in 18.2MΩ-cm MilliQ water with analytical grade reagents. A pH 3 phosphate buffer with freshly 2 μM AE reagent served as the sample carrier solution. A 6-way injector valve with 50 μL sample loop was used to inject the samples and standards in the carrier stream. Both carrier stream and a 0.1 M sodium carbonate solution (pH 11.3) were pumped using a peristaltic pump (Gilson Minipuls 3) at flow-rates of 2 mL/min into the flowcell. Directly upon mixing the carrier flow and the alkaline buffer the chemiluminescent reaction started.

Catalase (10 U/mL) was added to AE and carbonate reagents to remove background hydrogen peroxide. The reagents with added catalase were left for a couple of hours which helped to obtain a stable baseline for the assay. For calibration, standard solutions (0.5–50 μM) of hydrogen peroxide were prepared in 0.22 μm aged filtered seawater collected from the sampling area. Following extraction, porewater samples were immediately injected into the running FeLume. The response time to obtain a chemiluminescent peak was ~15 seconds after the injection. Standards

were injected periodically during the assays, to check for drift. Hydrogen peroxide standards with added catalase (100 U/mL) were also injected to confirm disappearance of the signal during the assay.

Porewaters contain high concentrations of Fe^{2+} (Supp. Fig. S11). Oxidation of Fe^{2+} during sampling and analysis can lead to hydrogen peroxide generation. To prevent such interference by Fe^{2+}, we added ~200 µM ferrozine to the sampling syringe while drawing 2-3 mL of porewater using a Rhizon sampler (Rhizosphere Research Products, The Netherlands). Ferrozine was also added to the reagents and standards at similar concentrations to prevent any bias. Ferrozine does not have any effect on the hydrogen peroxide concentrations[48].

Hydrogen distributions

In July 2020 and March 2021 cores were taken from the upper flat using core liners with 1 cm ports drilled into the side every 2 cm. On the sand flat (or in the harbor in March 2021), 12 mL Exetainers were filled with 10 mL 35% (w/v) NaCl solution (6 mL Exetainers with 4 mL 35% (w/v) NaCl solution in March 2021), in a modification of the procedure outlined in Lin et al. 2012[50]. Between 0 and 12 cm depth, 2 cm^3 of sediment were removed from the cores every 2 cm via the ports using cut-off syringes and transferred into the Exetainers. Exetainers were capped without headspace. Four Exetainers served as controls and were filled with 35% (w/v) NaCl solution to account for any hydrogen produced during transport. Immediately upon returning to the home laboratory in Bremen (~3 hrs later) 2 mL of the water phase of each Exetainer was replaced with nitrogen gas. After equilibration, headspace hydrogen concentrations were measured using a gas chromatograph (see "Hydrogen measurements"). The hydrogen present in the control Exetainers was subtracted from the amounts in the Exetainers with sediment added, after correcting for the slightly increased water volume in the control Exetainers.

Carbon turnover

Carbon turnover rates for untreated slurries and slurries treated with a combination of catalase and superoxide dismutase were used to assess the influence of ROS on carbon turnover in the sediments. Carbon turnover was calculated using the aerobic respiration and sulfate reduction rates for slurries from sediment collected on June 15th. Linear trend lines were plotted through the individual oxygen measurements and reduced sulfate measurements for untreated slurries, and slurries treated with a combination of catalase and superoxide dismutase. For sulfate reduction rates, only the anoxic period of the incubations was used. A stoichiometry of sulfate:carbon of

1:2, and of oxygen:carbon of 138:106 was used to convert these rates to carbon turnover rates. As sulfate reduction is the dominant anaerobic pathway in coastal marine sediments[41], summed carbon turnover rates derived from aerobic respiration and sulfate reduction are a reliable estimation of the total carbon turnover rate via biotic respiration.

Acknowledgements

References

1   Huettel, M., Berg, P. & Kostka, J. E. Benthic exchange and biogeochemical cycling in permeable sediments. *Annu. Rev. Mar. Sci.* **6**, 23-51 (2014).

2   Jansen, S. *et al.* Functioning of intertidal flats inferred from temporal and spatial dynamics of O_2, H_2S and pH in their surface sediment. *Ocean Dyn.* **59**, 317-332 (2009).

3   Marchant, H. K., Lavik, G., Holtappels, M. & Kuypers, M. M. M. The fate of nitrate in intertidal permeable sediments. *PLoS One* **9**, e104517 (2014).

4   Al-Raei, A. M., Bosselmann, K., Böttcher, M. E., Hespenheide, B. & Tauber, F. Seasonal dynamics of microbial sulfate reduction in temperate intertidal surface sediments: controls by temperature and organic matter. *Ocean Dyn.* **59**, 351-370 (2009).

5   Kessler, A. J. *et al.* Bacterial fermentation and respiration processes are uncoupled in anoxic permeable sediments. *Nat. Microbiol.* **4**, 1014-1023 (2019).

6   de Beer, D. *et al.* Transport and mineralization rates in North Sea sandy intertidal sediments, Sylt-Rømø Basin, Wadden Sea. *Limnol. Oceanogr.* **50**, 113-127 (2005).

7   Hansel, C. M. & Diaz, J. M. Production of extracellular reactive oxygen species by marine biota. *Annu. Rev. Mar. Sci.* **13**, 177-200 (2021).

8   Fridovich, I. Oxygen toxicity: a radical explanation. *J. Exp. Biol.* **201**, 1203-1209 (1998).

9   Murphy, S. A. *et al.* Hydrous ferric oxides in sediment catalyze formation of reactive oxygen species during sulfide oxidation. *Front. Mar. Sci.* **3**, 227 (2016).

10   Burns, J. M., Craig, P. S., Shaw, T. J. & Ferry, J. L. Multivariate examination of Fe(II)/Fe(III) cycling and consequent hydroxyl radical generation. *Environ. Sci. Technol.* **44**, 7226-7231 (2010).

11   Borda, M. J., Elsetinow, A. R., Schoonen, M. A. & Strongin, D. R. Pyrite-induced hydrogen peroxide formation as a driving force in the evolution of photosynthetic organisms on an Early Earth. *Astrobiology* **1**, 283-288 (2001).

12   Imlay, J. A. The molecular mechanisms and physiological consequences of oxidative stress: lessons from a model bacterium. *Nat. Rev. Microbiol.* **11**, 443-454 (2013).

13   Armoza-Zvuloni, R., Schneider, A. & Shaked, Y. Rapid hydrogen peroxide release during coral-bacteria interactions. *Front. Mar. Sci.* **3**, 124 (2016).

14   Rose, A. L., Salmon, T. P., Lukondeh, T., Neilan, B. A. & Waite, T. D. Use of superoxide as an electron shuttle for iron acquisition by the marine cyanobacterium *Lyngbya majuscula*. *Envion. Sci. Technol.* **39**, 3708-3715 (2005).

15   Hansel, C. M., Diaz, J. M. & Plummer, S. Tight regulation of extracellular superoxide points to its vital role in the physiology of the globally relevant *Roseobacter* clade. *mBio* **10**, e02668-18 (2019).

16   Aguirre, J., Ríos-Momberg, M., Hewitt, D. & Hansberg, W. Reactive oxygen species and development in microbial eukaryotes. *Trends. Microbiol.* **13**, 111-118 (2005).

17   Zinser, E. R. The microbial contribution to reactive oxygen species dynamics in marine ecosystems. *Environ. Microbiol. Rep.* **10**, 412-427 (2018).

18   Dias, D. M. C. *et al.* Production of reactive oxygen species in the rhizosphere of a *Spartina*-dominated salt marsh systems. *Aquat. Geochem.* **22**, 573-591 (2016).

19   Imlay, J. A. Where in the world do bacteria experience oxidative stress? *Environ. Microbiol.* **21**, 521-530 (2019).

20   Abele, D., Groβpietsch, H. & Pörtner, H. O. Temporal fluctuations and spatial gradients of environmental P_{O2}, temperature, H_2O_2 and H_2S in its intertidal habitat trigger enzymatic antioxidant protection in the capitellid worm *Heteromastus filiformis*. *Mar. Ecol. Prog. Ser.* **163**, 179-191 (1998).

21   Gilliland, S. E. & Speck, M. L. Biological response of lactic *Streptococci* and *Lactobacilli* to catalase. *Appl. Microbiol.* **17**, 797-800 (1969).

22   Collins, E. B. & Aramaki, K. Production of hydrogen peroxide by *Lactobacillus acidophilus*. *J. Dairy Sci.* **63**, 353-357 (1980).

23   Finke, N. & Jørgensen, B. B. Response of fermentation and sulfate reduction to experimental temperature changes in temperate and Arctic marine sediments. *ISME J.* **2**, 815-829 (2008).

24   Rickard, D. & Luther III, G. W. Kinetics of pyrite formation by the H_2S oxidation of iron (II) monosulfide in aqueous solutions beween 25 and 125 °C: The mechanism. *Geochim. Cosmochim. Acta* **61**, 135-147 (1997).

25   Thiel, J., Byrne, J. M., Kappler, A., Schink, B. & Pester, M. Pyrite formation from FeS and H_2S is mediated through microbial redox activity. *Proc. Natl. Acad. Sci. U S A* **116**, 6897-6902 (2019).

26   Peck Jr., H. D. The ATP-dependent reduction of sulfate with hydrogen in extracts of *Desulfovibrio desulfuricans. Proc. Natl. Acad. Sci. U S A* **45**, 701-708 (1959).

27   Dyksma, S., Pjevac, P., Ovanesov, K. & Mussmann, M. Evidence for H_2 consumption by uncultured *Desulfobacterales* in coastal sediments. *Environ. Microbiol.* **20**, 450-461 (2018).

28   Trusiak, A., Treibergs, L. A., Kling, G. W. & Cory, R. M. The role of iron and reactive oxygen species in the production of CO_2 in arctic soil waters. *Geochim. Cosmochim. Acta* **224**, 80-95 (2018).

29   Hopwood, M. J., Rapp, I., Schlosser, C. & Achterberg, E. P. Hydrogen peroxide in deep waters from the Mediterranean Sea, South Atlantic and South Pacific Oceans. *Sci. Rep.* **7**, 43436 (2017).

30   Zhang, N. *et al.* Water table fluctuations regulate hydrogen peroxide production and distribution in unconfined aquifers. *Environ. Sci. Technol.* **54**, 4942-4951 (2020).

31   Abele-Oeschger, D., Tüg, H. & Röttgers, R. Dynamics of UV-driven hydrogen peroxide formation on an intertidal sandflat. *Limnol. Oceanogr.* **42**, 1406-1415 (1997).

32   Zhang, T., Hansel, C. M., Voelker, B. M. & Lamborg, C. H. Extensive dark biologcial production of reactive oxygen species in brackish and freshwater ponds. *Environ. Sci. Technol.* **50**, 2983-2993 (2016).

33   Cohen, Y., Klug, M. J. & Reddy, C. A. Oxygenic photosynthesis, anoxygenic photosynthesis, and sulfate reduction in cyanobacterial mats. *Curr. Perspect. Microb. Ecol. Am. Soc. Microbiol. Wash. DC*, 435-441 (1984).

34   Røy, H., Weber, H. S., Tarpgaard, I. H., Ferdelman, T. G. & Jørgensen, B. B. Determination of dissimilatory sulfate reduction rates in marine sediment via radioactive ^{35}S tracer. *Limnol. Oceanogr. Methods* **12**, 196-211 (2014).

35   Rabus, R., Hansen, T. A. & Widdel, F. in *The Prokaryotes: Prokaryotic Physiology and Biochemistry* (eds E. Rosenberg *et al.*) 309-404 (Springer Berlin Heidelberg, 2013).

36   Visscher, P. T., Prins, R. A. & van Gemerden, H. Rates of sulfate reduction and thiosulfate consumption in a marine microbial mat. *FEMS Microbiol. Lett.* **86**, 283-293 (1992).

37   Bosselmann, K. *et al.* Iron-sulfur-manganese dynamics in intertidal surface sediments of the North Sea. *Ber. Forschungsz. Terramare* **12**, 32-35 (2003).

38   Fenchel, T. M. & Jørgensen, B. B. in *Adv. Microb. Ecol.* Vol. 1 (ed M. Alexander) 1-58 (Springer, Boston, MA, 1977).

39   Arnosti, C. Speed bumps and barricades in the carbon cycle: substrate structural effects on carbon cycling. *Mar. Chem.* **92**, 263-273 (2004).

40   Chen, C., Hall, S. J., Coward, E. & Thompson, A. Iron-mediated organic matter decomposition in humid soils can counteract protection. *Nat. Commun.* **11**, 2255 (2020).

41   Jørgensen, B. B. Mineralization of organic matter in the sea bed—the role of sulphate reduction. *Nature* **296**, 643-645 (1982).

42   Billerbeck, M., Werner, U., Bosselmann, K., Walpersdorf, E. & Huettel, M. Nutrient release from an exposed intertidal sand flat. *Mar. Ecol. Prog. Ser.* **316**, 35-51 (2006).

43   Billerbeck, M. *et al.* Surficial and deep pore water circulation governs spatial and temporal scales of nutrient recycling in intertidal sand flat sediment. *Mar. Ecol. Prog. Ser.* **326**, 61-76 (2006).

44   Røy, H., Lee, J. S., Jansen, S. & de Beer, D. Tide-driven deep pore-water flow in intertidal sand flats. *Limnol. Oceanogr.* **53**, 1521-1530 (2008).

45   Revsbech, N. P. An oxygen microsensor with a guard cathode. *Limnol. Oceanogr.* **34**, 474-478 (1989).

46   Viollier, E., Inglett, P. W., Hunter, K., Roychoudhury, A. N. & Van Cappellen, P. The ferrozine method revisited: Fe(II)/Fe(III) determination in natural waters. *Appl. Geochem.* **15**, 785-790 (2000).

47   Cline, J. D. Spectrophotometric determination of hydrogen sulfide in natural waters. *Limnol. Oceanogr.* **14**, 454-458 (1969).

48   Cooper, W. J., Moegling, J. K., Kieber, R. J. & Kiddle, J. J. A chemiluminescence method for the analysis of H_2O_2 in natural waters. *Mar. Chem.* **70**, 191-200 (2000).

49   King, D. W. *et al.* Flow injection analysis of H_2O_2 in natural waters using acridinium ester chemiluminescence: method development and optimization using a kinetic model. *Anal. Chem.* **79**, 4169-4176 (2007).

50   Lin, Y.-S. *et al.* Towards constraining H_2 concentration in subseafloor sediment: A proposal for combined analysis by two distinct approaches. *Geochim. Cosmochim. Acta* **77**, 186-201 (2012).

Supplementary Information

Reactive oxygen species affect mineralization processes in permeable intertidal flats

Marit R. van Erk[*,a], Olivia M. Bourceau[*,a], Chyrene Moncada[a], Subhajit Basu[a],

Colleen M. Hansel[b], Dirk de Beer[a]

[a]Max Planck Institute for Marine Microbiology, Bremen, Germany

[b]Department of Marine Chemistry and Geochemistry, Woods Hole Oceanographic Institution, Woods Hole, Massachusetts, USA

These authors contributed equally

Content

1. Supplementary Information hydrogen peroxide sensor

2. Supplementary Figures 1 - 11

3. Supplementary Tables 1 - 2

Supplementary Information hydrogen peroxide sensor

The hydrogen peroxide sensor consisted of an etched 50 μm-thick platinum anode plated with platinum chloride (8% $PtCl_4$ in MilliQ water), an etched 100 μm-thick platinum guard, and a thick platinum reference. The anode, guard and reference were mounted in a glass casing, with the sensing anode at a distance of ca 50 μm from the tip. The tip of the outer capillary had a diameter of 25-30 μm and a tip opening of 10 μm. Before mounting the electrodes, the tip of the outer capillary was sealed by a thin polyurethane membrane (D6, kindly provided by Anders Tjell, TU Graz, Austria). The membrane was dissolved in tetrahydrofuran (50 mg/mL) and applied by shortly immersing the capillary in the solution that is kept in the tip of a Pasteur pipette and left to cure overnight. The membrane was applied under microscopic guidance. The membrane separated the electrolyte from the seawater but was permeable for hydrogen peroxide. After mounting the electrodes in the casing, the sensor was filled with electrolyte, a borate/potassium chloride buffer (50 mM borate, 3 M potassium chloride and 490 μM ferrozine), with pH 9.

The selectivity was assessed by addition of potentially interfering compounds (ammonium, nitrate, formate, acetic acid, ascorbate, and Fe^{2+} (Fe^{2+} additions tested at pH 3). The response of the sensor was assessed for incremental additions of these compounds, and for hydrogen peroxide (3% hydrogen peroxide stock solution). Sensitivity was defined as the slope of the linear trend line. The sensitivity for hydrogen peroxide was 9×10^{-5} pA μM^{-1}. Interference (in %) was calculated as: sensitivity interfering compound/sensitivity $H_2O_2 \times 100$ (Supp. Table S2; Supp. Fig. S9).

When no ferrozine was added to the electrolyte, the sensor had strong interference with Fe^{2+}. Sensors with ferrozine in the electrolyte had no response to Fe^{2+}. The ferrozine-filled sensor was used for our measurements. The sensor was connected to a picoammeter and polarized at +700 mV until reaching a stable current, which happened normally within an hour. The medium in which the sensor was used was connected to an external reference electrode. The sensors were calibrated before use in a stirred beaker with filtered seawater to which aliquots of stabilized 3% hydrogen peroxide were added. The response time was <3 seconds. The sensor was very stable and not noise sensitive. The sensitivity was 2×10^{-4} pA μM^{-1} (Supp. Fig. S10). The response to hydrogen peroxide was linear within the range of 0.5 μM to 4.3 mM (Supp. Fig. S10), the highest concentration tested. The sensor was slightly light-sensitive. The shelf lifetime of the sensor was a few weeks. With use in anoxic sediments the sensitivity quickly goes down after a while.
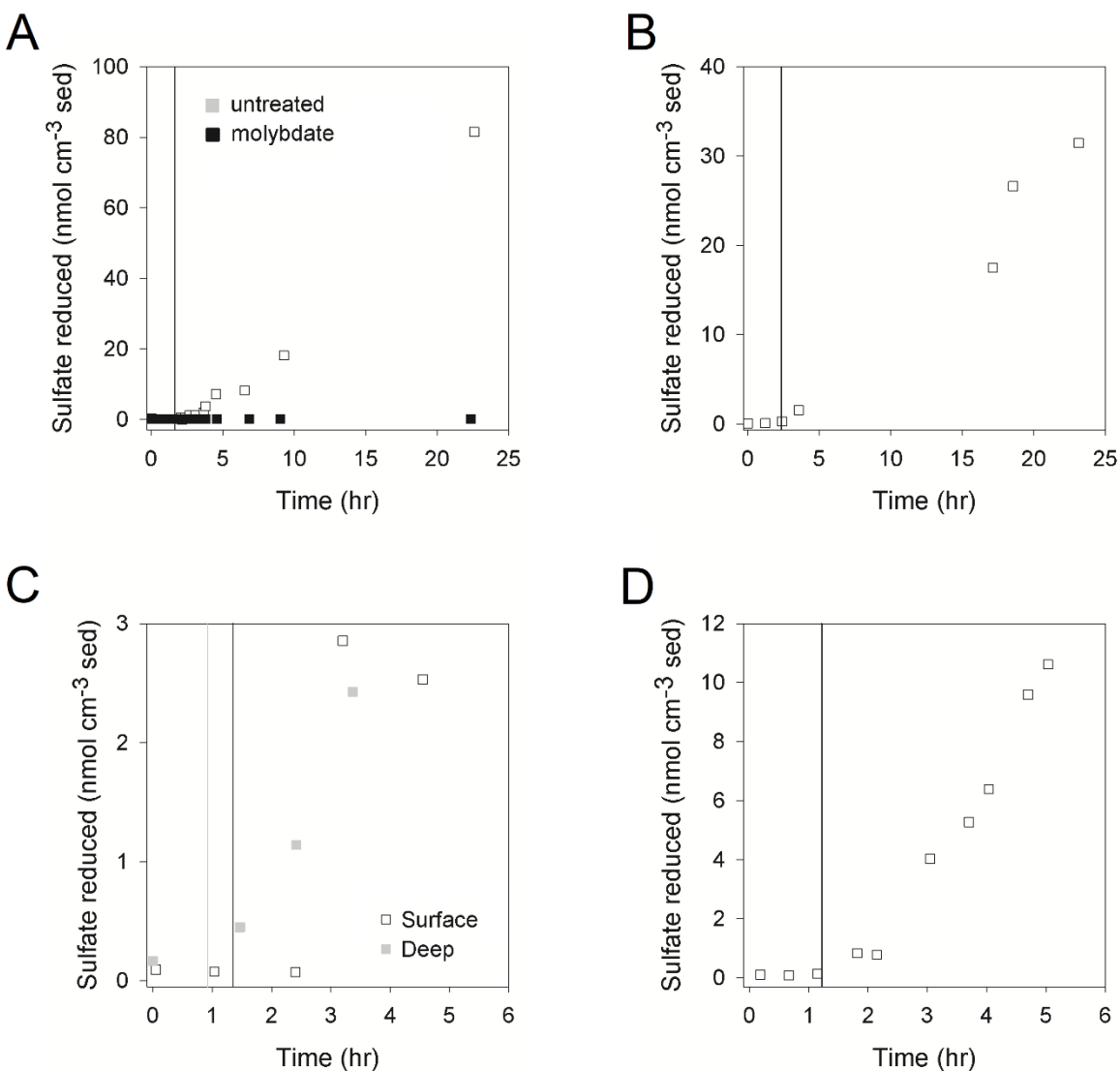
Figure S1: *Reduced sulfate in slurries over an oxic-anoxic transition. The vertical lines indicate the transition from oxic to anoxic conditions.* ***A:*** *Slurries from surface sediments (open squares) and surface sediments treated with molybdate (filled squares), collected May 25th. Untreated and molybdate-treated slurries became anoxic at the same time,* ***B:*** *Slurries from surface sediments collected June 15th,* ***C:*** *Slurries from surface (0-2 cm depth) and deep (10-14 cm depth) sediments collected July 28th. The black vertical line represents the transition to anoxic conditions for surface sediments, the grey line that for deep sediments,* ***D:*** *Slurries from surface sediments collected October 8th.*
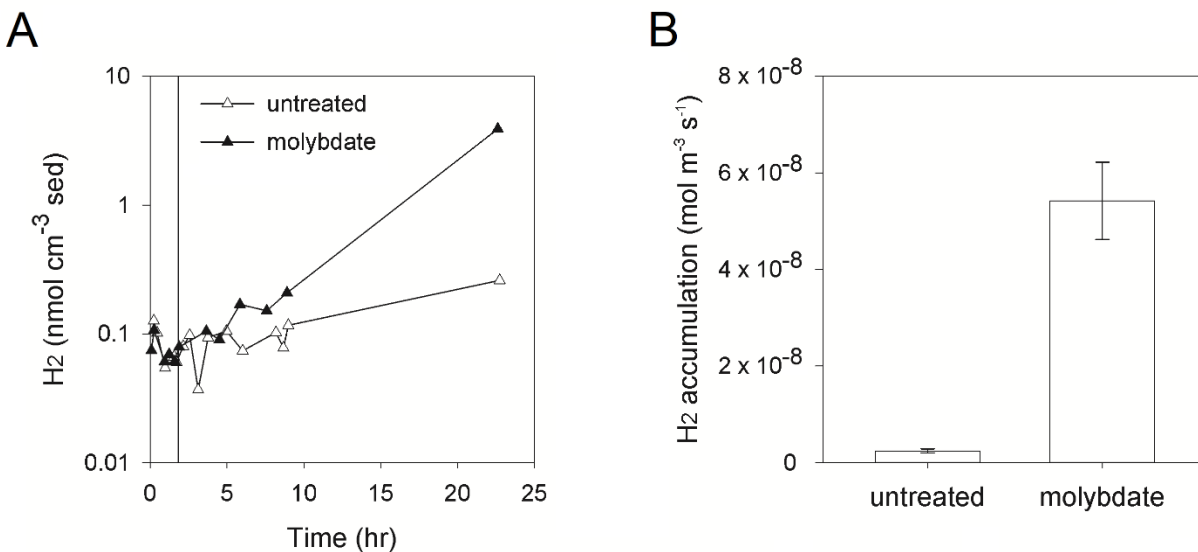
Figure S2: *Hydrogen accumulation.* **A:** *Hydrogen concentrations in slurries over an oxic-anoxic transition with (filled triangles) and without (open triangles) molybdate, an inhibitor for sulfate reduction, plotted against a log scale. Slurries were from sediment collected May 25th, 2020. The vertical line indicates the point where slurries became anoxic, which was the same for untreated and molybdate-treated slurries,* **B:** *Hydrogen accumulation after slurries turned anoxic for slurries with and without (untreated) molybdate. Hydrogen accumulation was calculated from the anoxic period of Fig S2A. Error bar represents standard error of the linear trend line.*
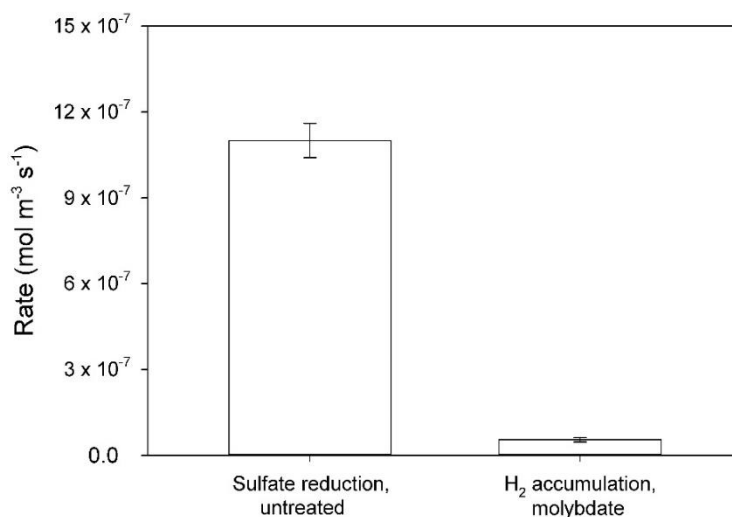
Figure S3: *Rates of sulfate reduction and hydrogen accumulation for the anoxic period of untreated slurries. The sulfate reduction rate was calculated from the anoxic period of Fig S1A. The hydrogen accumulation rate was calculated from the anoxic period of Fig S2A. Error bars represent standard error of the linear trend line.*
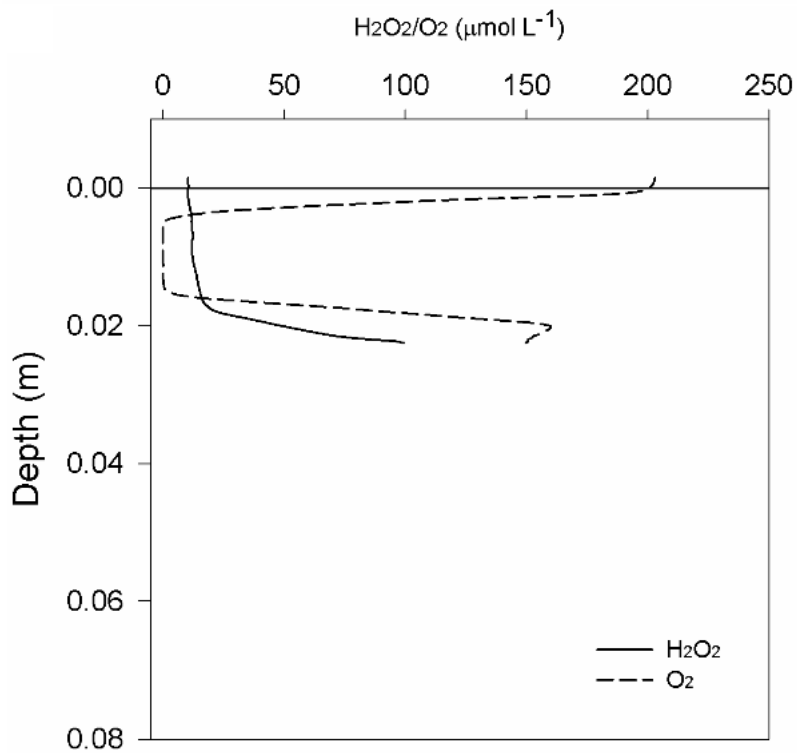
Figure S4: *Hydrogen peroxide dynamics in sediment cores. Microsensor depth profiles of hydrogen peroxide and oxygen within a sediment core. Profiles were measured after injection of oxygen-saturated seawater at a sediment depth where both hydrogen peroxide and oxygen were undetected (around 0.015 m depth; see Fig 2) on March 18th.*
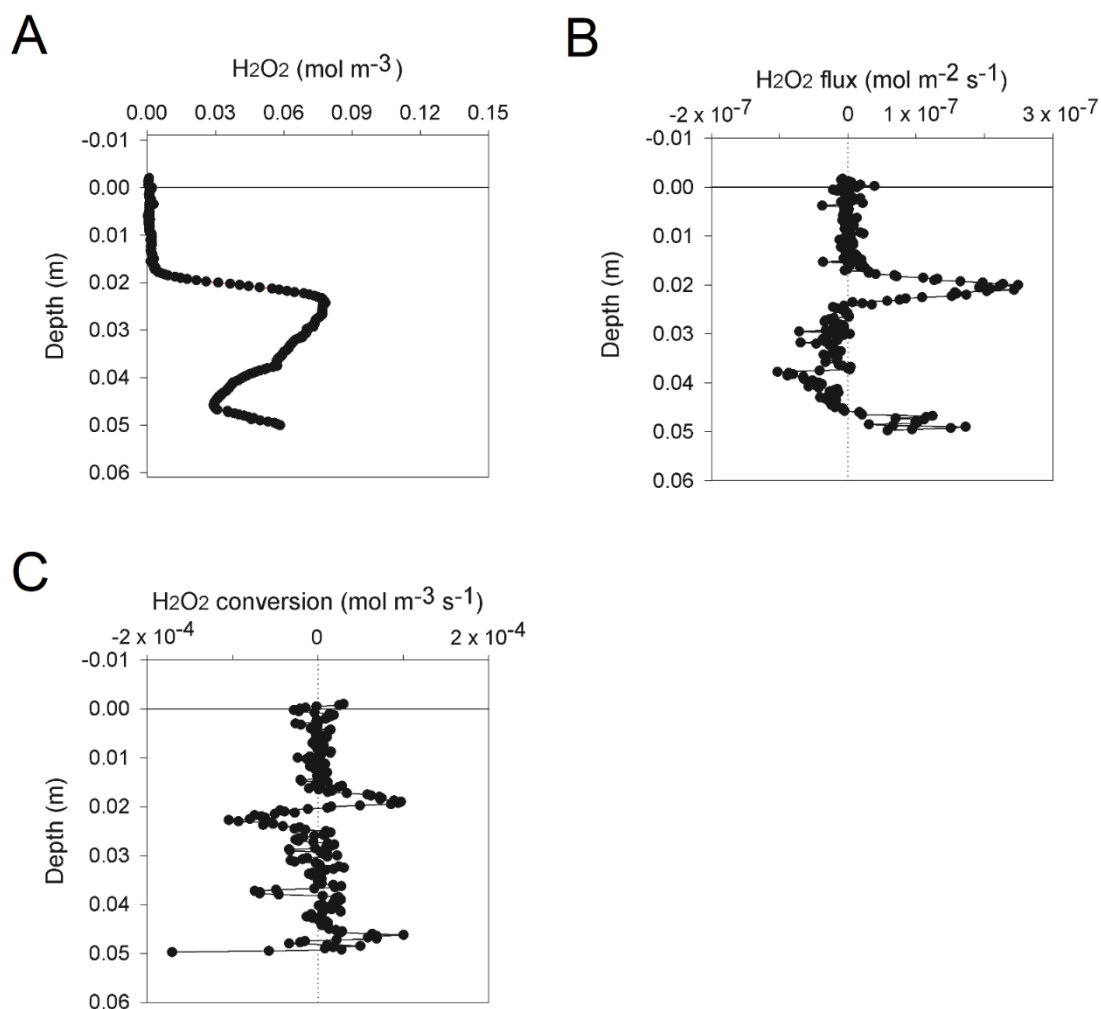
*Figure S5: Concentrations, fluxes and conversion rates of hydrogen peroxide in a sediment core. All are from the same sediment core, collected March 18th 2021. **A:** Steady-state depth profile of hydrogen peroxide, the same depth profile as shown in Fig 2, **B:** Hydrogen peroxide calculated from the steady-state depth profile of Fig S5A. Positive values indicate upward fluxes, negative values downward fluxes, **C:** Hydrogen peroxide conversion within a sediment core, calculated from the hydrogen peroxide fluxes of Fig S5B. Positive values indicate production, negative values consumption.*
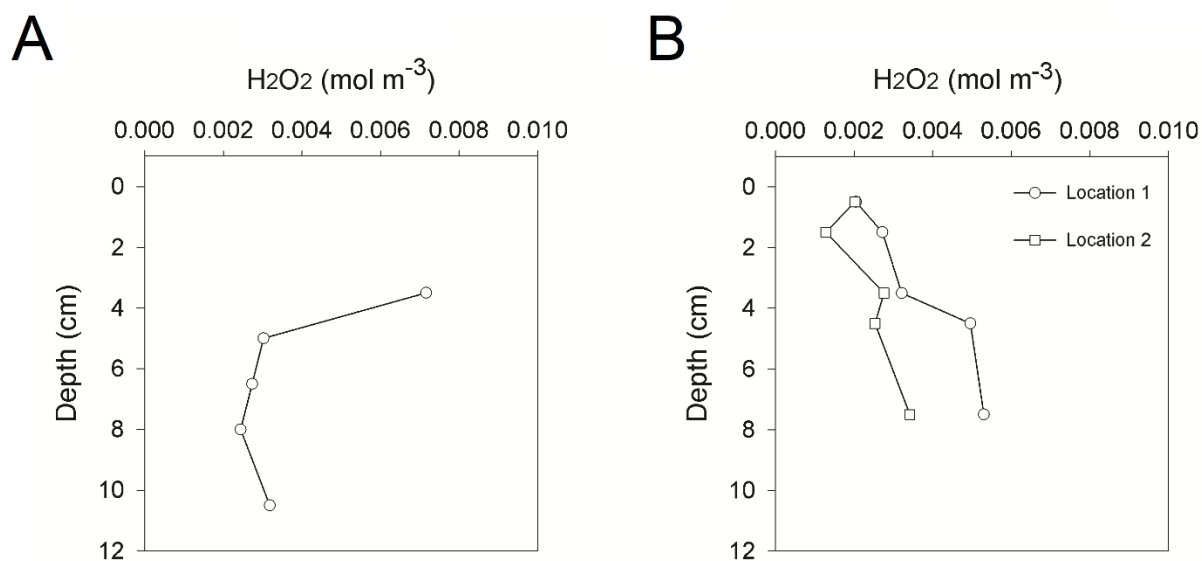
Figure S6: *Hydrogen peroxide concentrations in intertidal permeable sediment.* ***A:*** *Hydrogen peroxide concentrations measured in porewater from a sediment core using a chemiluminescent technique. No measurements were conducted above 4 cm depth, due to an absence of openings in the core through which sampling with Rhizons occurred in this depth interval,* ***B:*** *Hydrogen peroxide concentrations measured in porewater extracted with Rhizons on the flat from 2 locations using a chemiluminescent technique.*
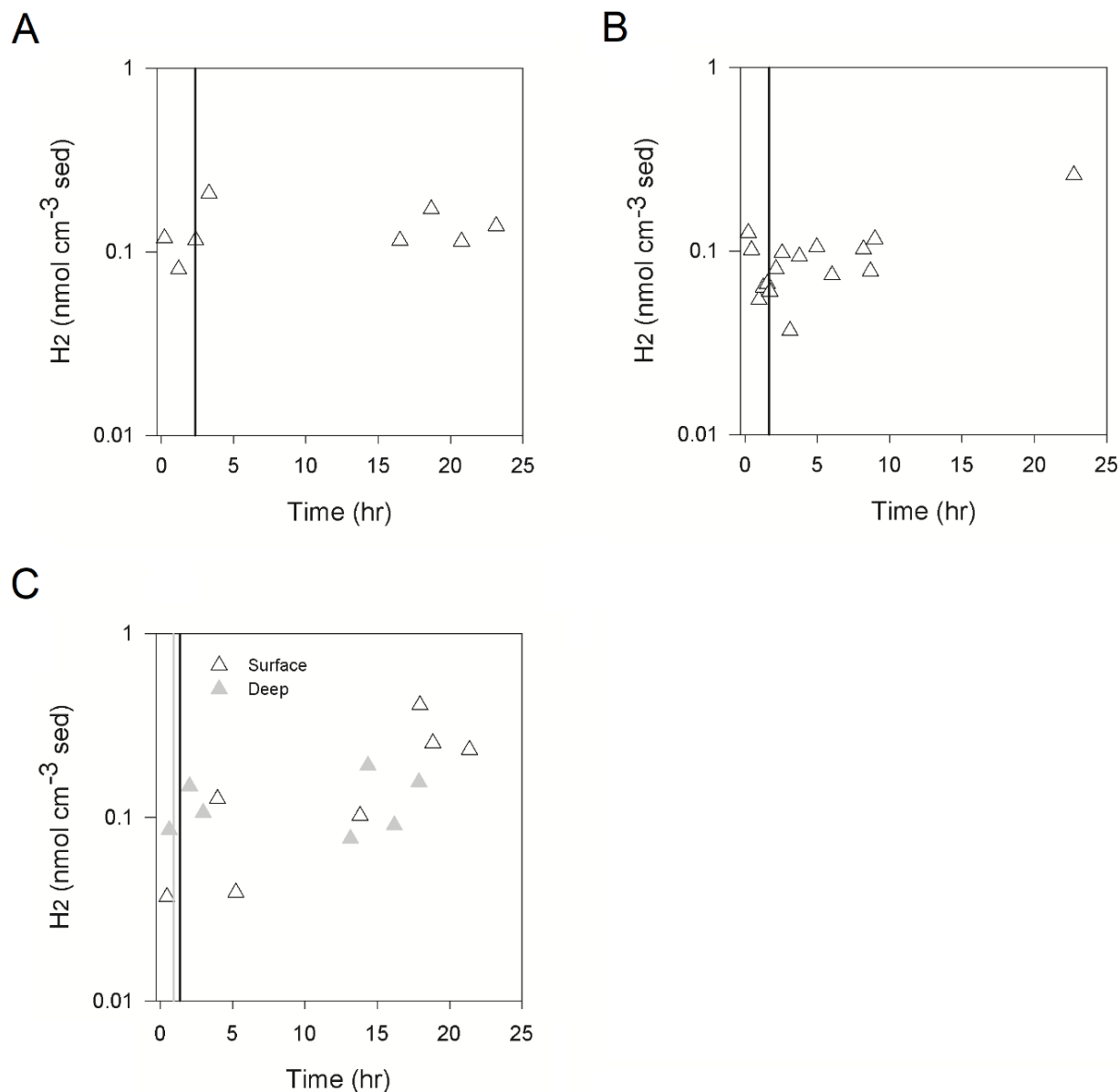
*Figure S7: Hydrogen concentrations in slurries over an oxic-anoxic transition. The vertical lines indicate the transition from oxic to anoxic conditions, **A:** Hydrogen concentrations for sediments collected June 15th, **B:** Hydrogen concentrations for sediments collected May 25th, **C:** Hydrogen concentrations in slurries for surface (0-2 cm depth; open triangles) and deep (10-14 cm depth; grey triangles) sediments collected July 28th. The black vertical line represents the transition to anoxic conditions for surface sediments, the grey line that for deep sediments.*
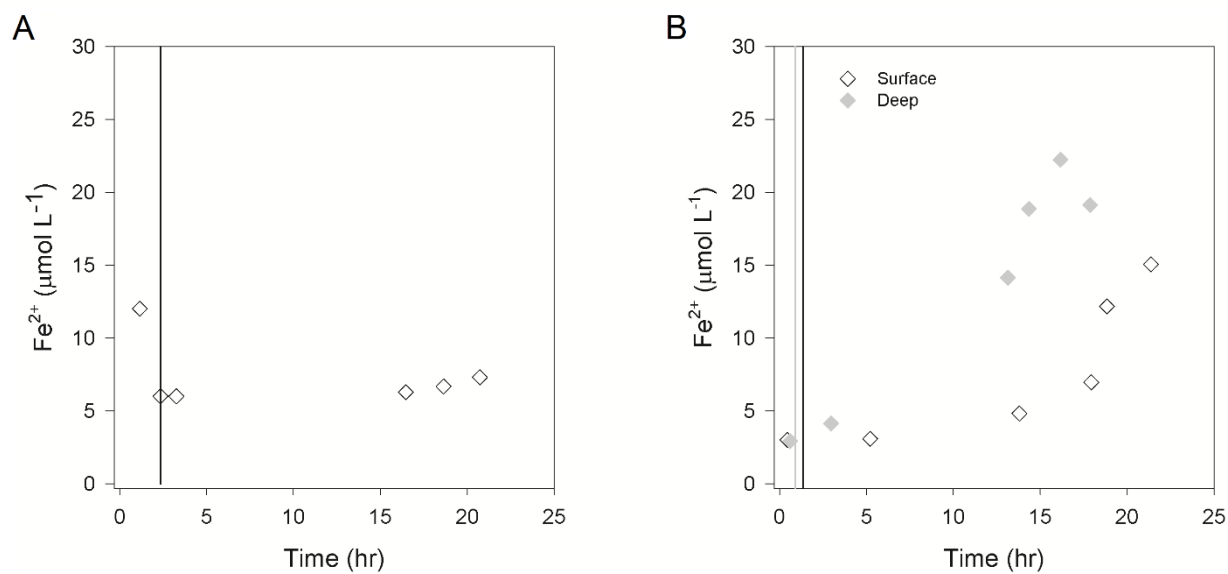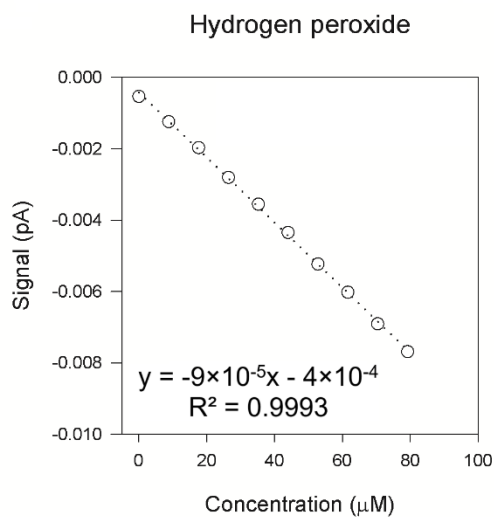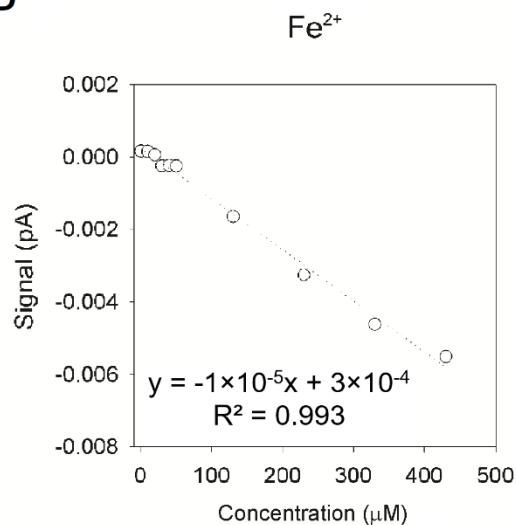
Figure S8: Fe^{2+} concentrations in slurries over an oxic-anoxic transition. The vertical lines indicate the transition from oxic to anoxic conditions, **A:** Slurries from surface sediments collected June 15th, **B:** Slurries from surface and deep sediments collected July 28th. The black vertical line is the transition to anoxic conditions for surface sediments, the grey line for deep sediments.
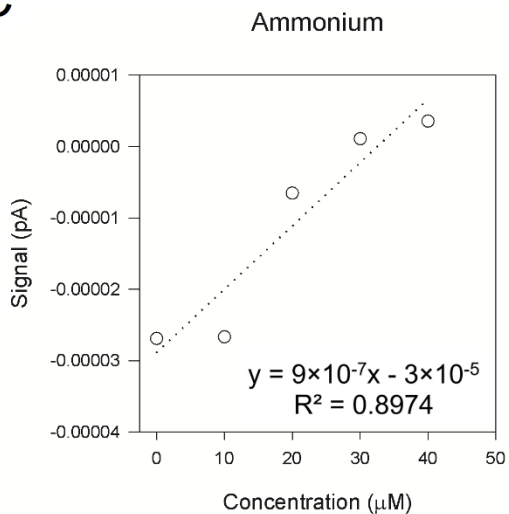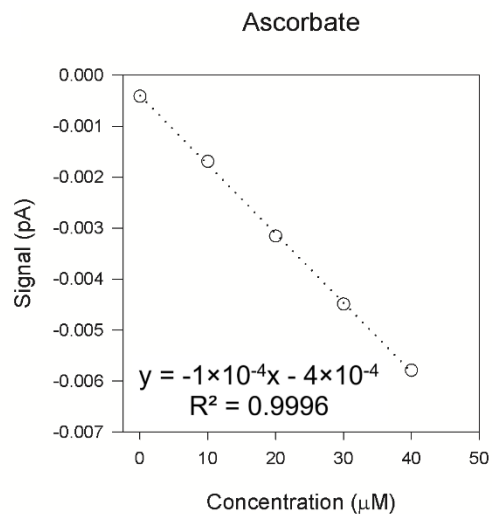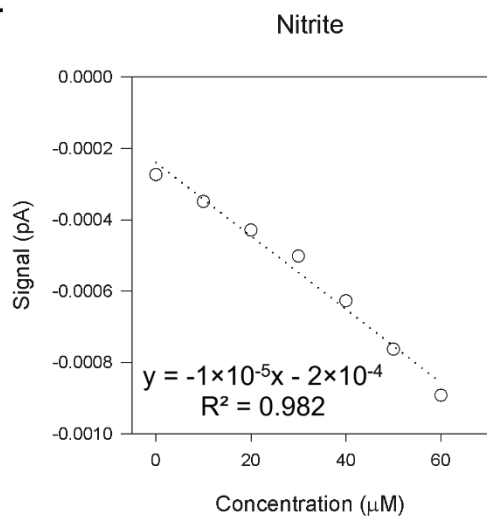
G

Acetic acid

$$y = -5 \times 10^{-7}x - 3 \times 10^{-4}$$
$$R^2 = 0.1022$$

Signal (pA) vs Concentration (μM)

H

Formate

$$y = 1 \times 10^{-6}x - 2 \times 10^{-4}$$
$$R^2 = 0.8501$$
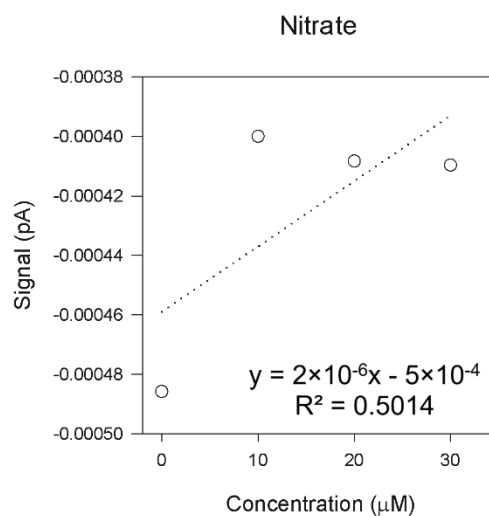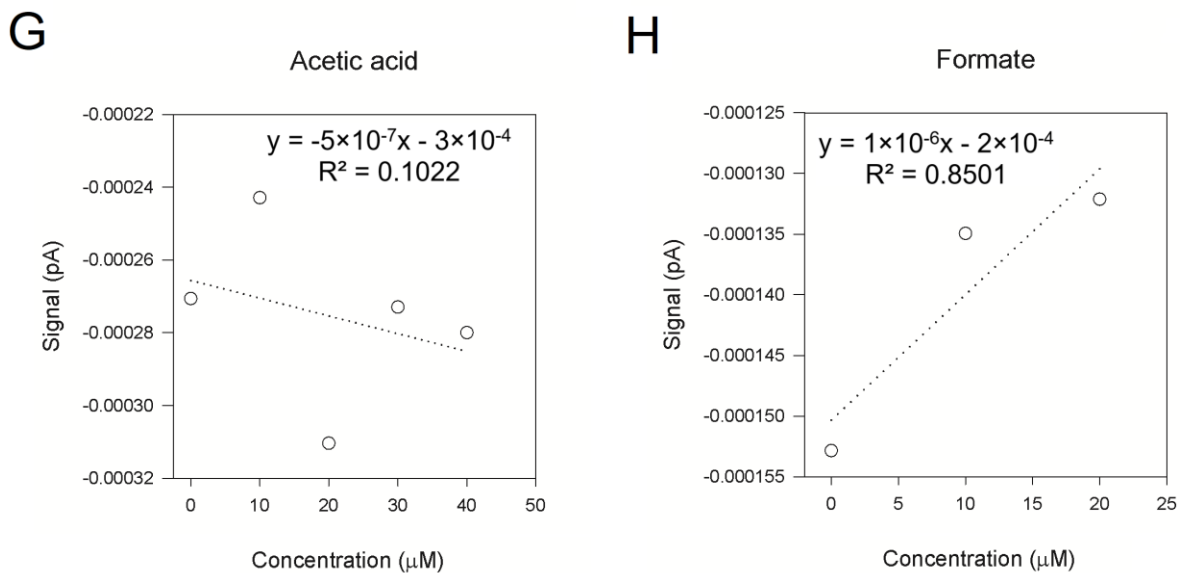
Signal (pA) vs Concentration (μM)

Figure S9: *Response of the hydrogen peroxide sensor to various interfering compounds. **A:** Hydrogen peroxide, **B:** Ferrous iron (Fe^{2+}), **C:** Ammonium, **D:** Ascorbate, **E:** Nitrite, **F:** Nitrate, **G:** Acetic acid, **H:** Formate.*

Hydrogen peroxide

$$y = -2 \times 10^{-4}x - 2.7 \times 10^{-3}$$
$$R^2 = 0.9995$$

Signal (pA) vs Concentration (μM)

Hydrogen peroxide

$$y = -2 \times 10^{-4}x - 1.8 \times 10^{-3}$$
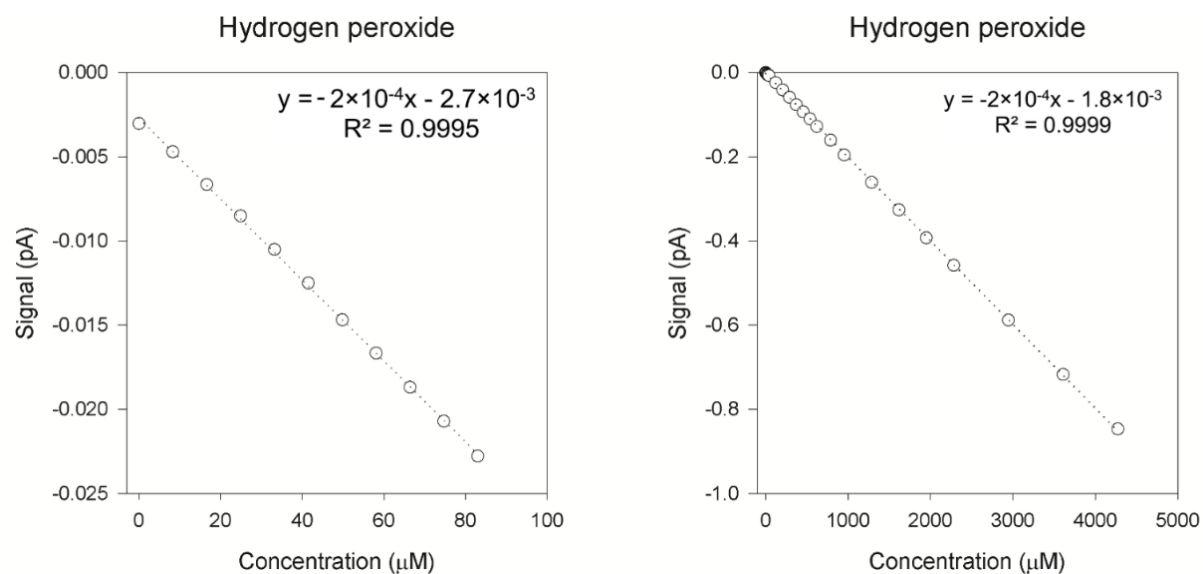$$R^2 = 0.9999$$

Signal (pA) vs Concentration (μM)

Figure S10: *Examples of calibrations of the hydrogen peroxide sensor with ferrozine in the electrolyte, for two different concentration ranges.*
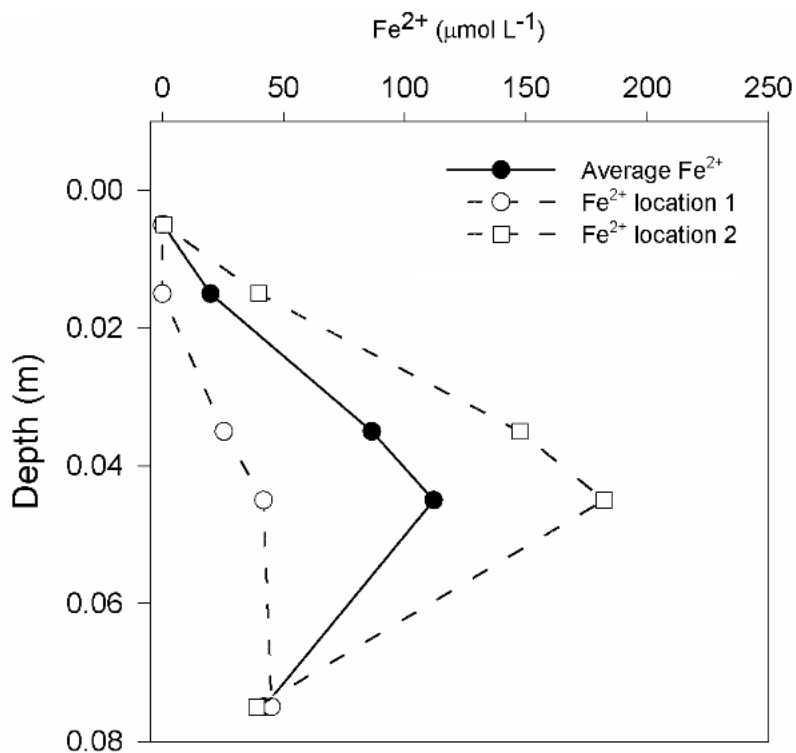
Figure S11: *Dissolved Fe^{2+} concentrations measured at two locations (open circles) on March 18th. Also the average of the two cores is shown (filled circles). Porewater was collected in situ using Rhizons, and directly fixed in the attached syringe using ferrozine. A subsample of the porewater was used for the chemiluminescence measurements of Fig S6B.*

Table S1: *Carbon turnover in untreated slurries and slurries treated with a combination of catalase and superoxide dismutase (CAT+SOD). Sediments were collected June 15th.*

Treatment	Oxygen consumption rate (mol C m^{-3} s^{-1})	Sulfate reduction rate (mol C m^{-3} s^{-1})	Total turnover (mol C m^{-3} s^{-1})
Untreated	4.79×10^{-5}	8.28×10^{-7}	4.87×10^{-5}
CAT+SOD	1.93×10^{-4}	1.39×10^{-6}	1.94×10^{-4}

Table S2: *Interference of various compounds with the hydrogen peroxide microsensor. Interference (in %) is calculated as: sensitivity/H_2O_2 sensitivity × 100.*

	Tested concentration range (µM)	Sensitivity (pA µM^{-1})	Interference (%)
Ammonium	0 - 40	9×10^{-7}	1
Nitrite	0 - 60	1×10^{-5}	11
Nitrate	0 - 30	2×10^{-6}	2
Formate	0 - 20	1×10^{-6}	1
Acetic acid	0 - 40	5×10^{-7}	0.6
Ascorbate	0 - 40	1×10^{-4}	111
Fe^{2+}	0 - 430	1×10^{-5}	11
Fe^{2+} (sensor with ferrozine)		none	

Conspicuous smooth and white egg-shaped sulfur structures on a deep-sea hydrothermal vent formed by sulfide-oxidizing bacteria

Marit R. van Erk[a]#, Viola Krukenberg[b], Pia Bomholt Jensen[c], Sten Littmann[a], Dirk de Beer[a]

[a]Max Planck Institute for Marine Microbiology, Bremen, Germany
[b]Montana State University, Bozeman, USA
[c]Aarhus University, Aarhus, Denmark

corresponding author
Running title: Notable biologically formed deep-sea sulfur structures
Keywords: sulfide oxidation, *Arcobacter*, sulfur filaments, hydrothermal vent

Abstract

Conspicuous, egg-shaped, white, and smooth structures were observed at a hydrothermal vent site in the Guaymas Basin, Gulf of California. The gelatinous structures decomposed within hours after sampling. Scanning electron microscopy (SEM) and light microscopy showed that the structure consisted of filaments of less than 0.1 µm thickness, which are similar to those observed for "*Candidatus* Arcobacter sulfidicus". SEM-energy-dispersive X-ray spectroscopy (EDS) showed that the filaments were sulfur rich. According to 16S rRNA gene amplicon and fluorescence in situ hybridization (FISH) analysis, *Arcobacter*, a sulfide oxidizer that is known to produce filamentous elemental sulfur, was among the dominant species in the structure and likely responsible for its formation. *Arcobacter* normally produces woolly snowflake like structures in opposed gradients of sulfide and oxygen. In the laboratory, we observed sulfide consumption in the anoxic zone of the structure, suggesting an anaerobic conversion. The sulfide oxidation and decomposition of the structure in the laboratory could be explained by dissolution of the sulfur filaments by reaction with sulfide under formation of polysulfides.

Importance

At the deep-sea Guaymas Basin hydrothermal vent system, sulfide-rich hydrothermal fluids mix with oxygenated seawater, thereby providing a habitat for microbial sulfur oxidation. Microbial sulfur oxidation in the deep-sea involves a variety of organisms and processes, and can result in the excretion of elemental sulfur. Here, we report on conspicuous, white, and smooth gelatinous structures found on hot vents. These strange egg-shaped structures were often observed on previous occasions in the Guaymas Basin, but their composition and formation process were unknown. Our data suggest that the notable and highly ephemeral structure was likely formed by the well-known sulfide-oxidizing *Arcobacter*. While normally *Arcobacter* produces loose flocs or woolly layers, here smooth gel-like structures were found.

Introduction

The release of hydrothermal fluids in oxic seawater generates strong thermodynamic disequilibria that fuel the abundant chemoautotrophic microorganisms typical for hydrothermal vent systems. Hydrothermal fluids are generally highly reduced, oxygen-free, and enriched in compounds such as CO_2, H_2S, CH_4, H_2, and iron (1). Sulfide, as a common constituent of hydrothermal fluids, is a source of energy for chemosynthesis (2). Microbial sulfur oxidation rarely proceeds directly to sulfate but results in a range of oxidized sulfur intermediates, including elemental sulfur and polysulfides (3).

Sulfur oxidizers are well known for their production of elemental sulfur, which is either internally stored or excreted. Produced elemental sulfur has been observed in the form of globules and filaments, and can serve as energy reserve. The excretion process can form thick white mats within a relatively short period of time (4). It was suggested that the sulfur filaments can be used by organisms as an anchor, to position themselves optimally in the chemical gradients present in their habitat (5). An example of a reported responsible organism (both in situ and in laboratory incubations) is the epsilonproteobacterium *Arcobacter* (6, 7). Material discovered at several hydrothermal vent sites appeared similar to filamentous sulfur formed by a coastally derived organism, for which filamentous sulfur formation was first described (6, 8), which led to the suggestion that microbial filamentous sulfur is a common product in hydrothermal environments (7). Especially distinct examples are those of the so-called snowblower events, first observed by (8). Snowblower events were described as the release of flocculent white bacterial mat fragments into the seawater by venting fluids after eruption (e.g. (8)).

Essentially all marine sediments harbor sulfur oxidizers, including a large diversity of *Alpha*-, *Gamma*-, and *Epsilonproteobacteria* (reviewed in (9)). Well-known forms of sulfur excreted by aerobic marine sulfur oxidizers include white mats (e.g. (4)). Such mats were described to be gelatinous, mushroom-like (10), consisting of cotton-ball precipitates (11), or rather consisting of the producing organisms within a matrix of sulfur-rich mucous (12).

Here, we report on conspicuous, unusually smooth, white gelatinous egg-shaped structures with a diameter of several centimeter that were observed in the hydrothermal vent system of the Guaymas Basin, Gulf of California. We used microscopy, microsensor measurements, sediment

extraction methods, and microbial community composition analyses to describe the sampled structure, the sulfide oxidizing process, and determine the inhabiting microorganisms.

Results

Observations

White gelatinous flat mats and egg-shaped structures were observed on and next to a hot smoker at Cathedral Hill, Guaymas Basin (Fig. 1A). The semi-transparent egg-shaped structures were up to several centimeters in diameter. Some were also growing on tube worms. The unusual smooth gelatinous appearance made the structures very notable.

A structure next to the hot smoker was sampled intact together with the underlying sediment using a push core. The structure had a diameter of a few centimeters (Fig. 1B), and likely recently fell of the hot smoker or tube worm where it was attached to. In situ sediment temperatures were 13 °C at 5 cm depth, and increased up to 99 °C at 50 cm depth. Microsensor measurements and subsequent subsampling for the other analyses were conducted before the structure fell apart within a few hours.

Microsensor measurements

Microsensor profiles showed some distinctive features within the structure compared to the overlying seawater and underlying sediment (Fig. 2). Oxygen diffused into the structure from the overlying seawater, and penetrated a few millimeters. Sulfide diffused into the structure from the underlying sediment. The oxygen and sulfide profiles showed consumption of both compounds within the structure. However, oxygen and sulfide were consistently spatially separated by 0.5 centimeter. Hence, sulfide consumption occurred without oxygen being involved.

The pH values in the overlying seawater were stable (7.5), but pH values gradually decreased with depth within the structure and underlying sediment.

The electrical potential was negative throughout the measured interval, and only showed small differences (<0.005) between the seawater, structure, and sediment.
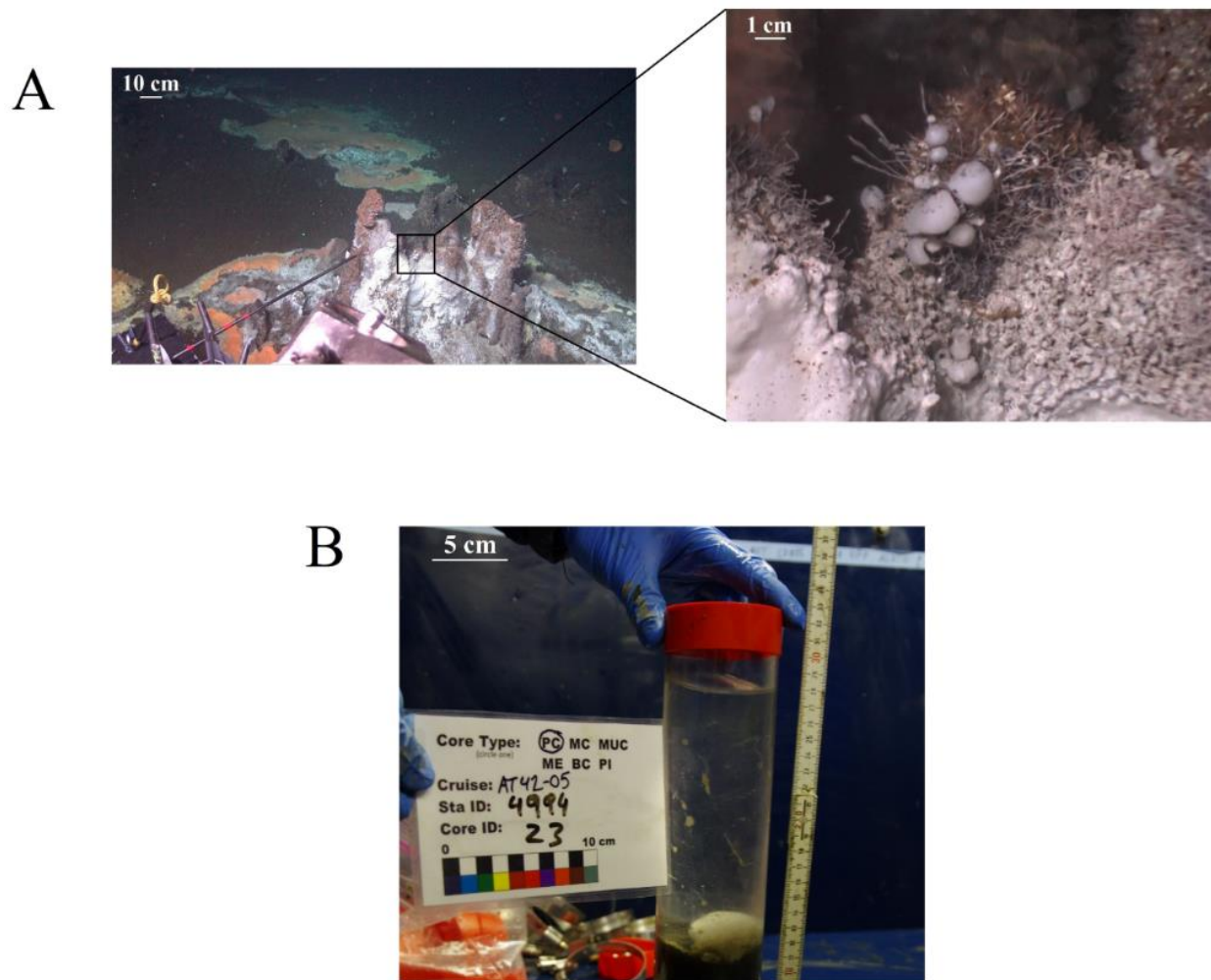
Figure 1: *The structures on a hydrothermal vent site at Cathedral Hill (A); and the sampled structure on board of the ship (B). Structures covered the smoker, and were abundant on surrounding sediments. The structure shown in (B) was sampled from the surrounding sediments.*
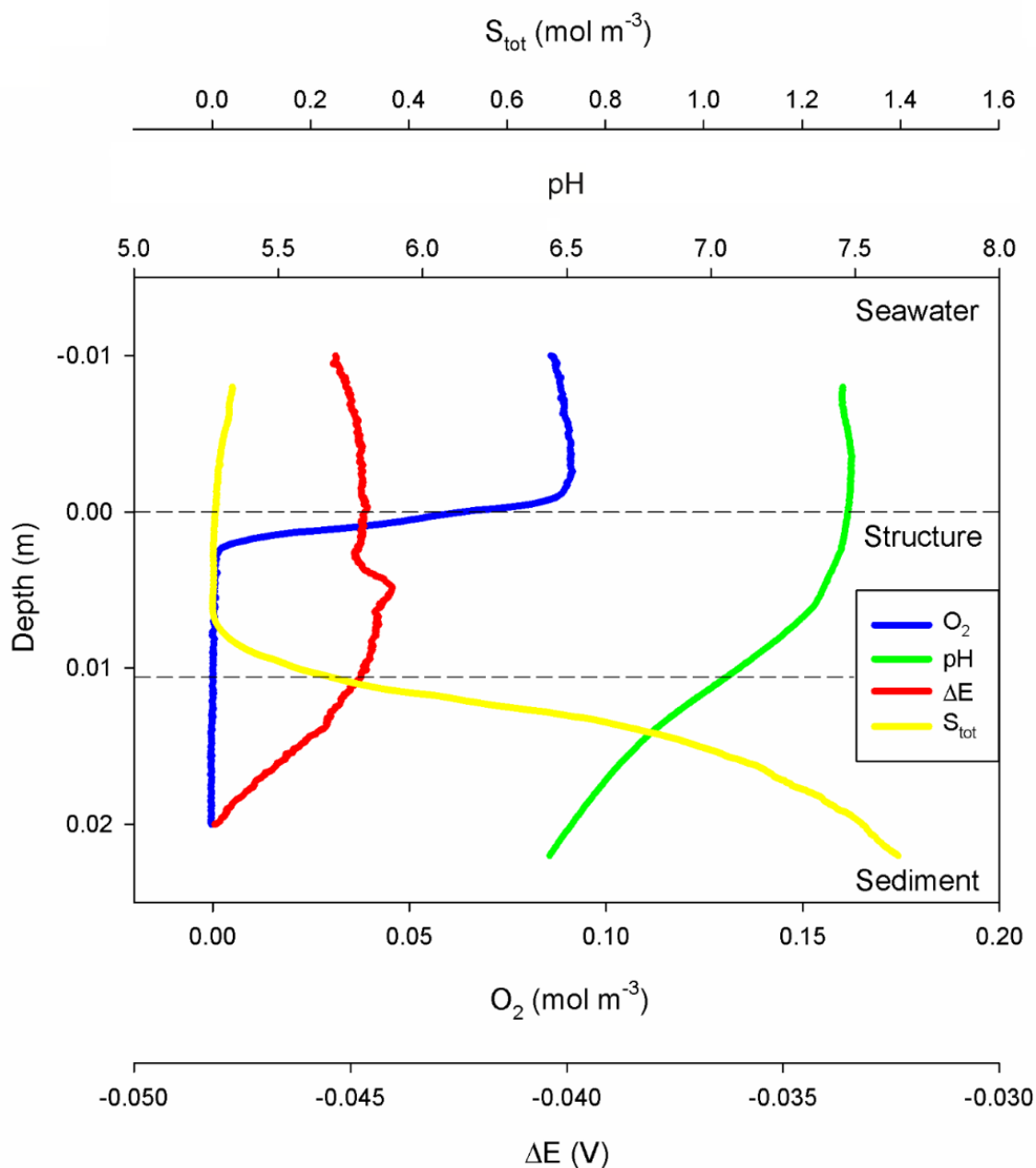
Figure 2: *Microsensor profiles measured on the ship from the overlying seawater through the structure (0.00 to 0.01 m depth) into the sediments. Oxygen (in blue) only penetrated a few millimeters into the structure from above, while sulfide (in yellow) penetrated from below. Both were consumed within the structure. No notable change in the electrical potential (ΔE; in red) was observed. pH (in green) was stable within the seawater, and decreased with depth within the structure and sediment.*

Microscopic observations

The structure was composed of a fibrous mesh of irregular whitish filaments (Fig. 3) with variable length and thickness of maximum 0.1 µm (Fig. 4). Upon squeezing between slide and coverslip, the filaments fragmented and completely disappeared. The filaments were rather electron transparent and no septa were visible (Fig. 4).

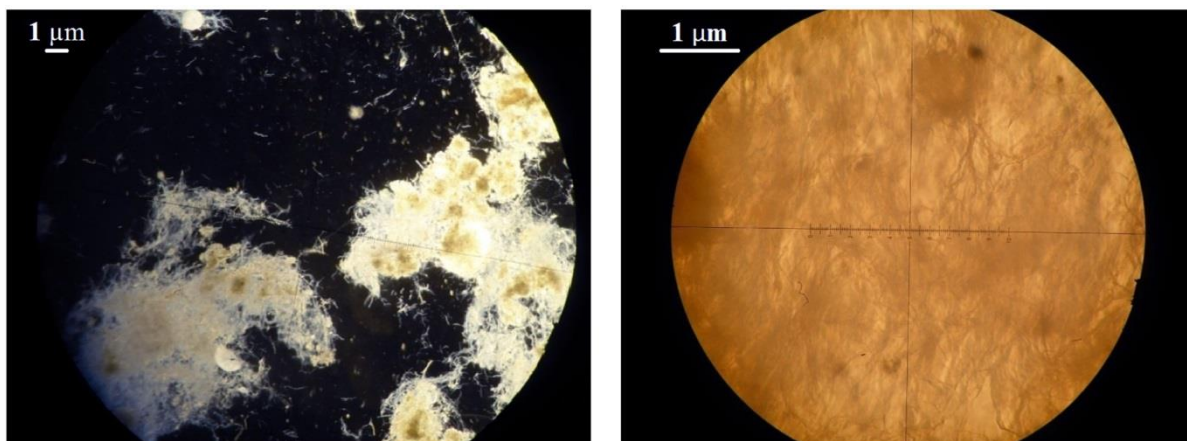***Figure 3:*** *Light microscope images showing a mesh of white filaments with magnifications of 100× (left) and 400× (right). The length and thickness of the filaments are variable.*
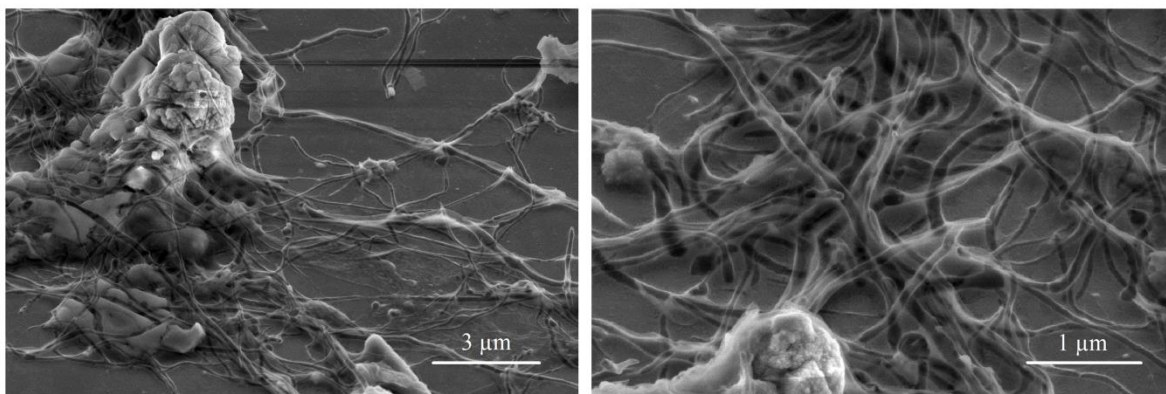

Figure 4: *Secondary electron (SE) micrographs from SEM of the filaments. Filaments have a diameter of 0.1 µm or less. No septa are visible.*

Elemental composition

The white appearance of the structure indicated sulfur accumulation. The dissolution of the filaments in methanol further suggested the presence of sulfur. Iron concentrations, determined by sediment extraction, were low (<0.1 %).

The elemental composition, as determined by combined scanning electron microscopy (SEM) and energy-dispersive X-ray spectroscopy (EDS), showed the filaments to be sulfur rich (Fig. 5A), while other elements, such as carbon, were not enriched (Fig. 5B).
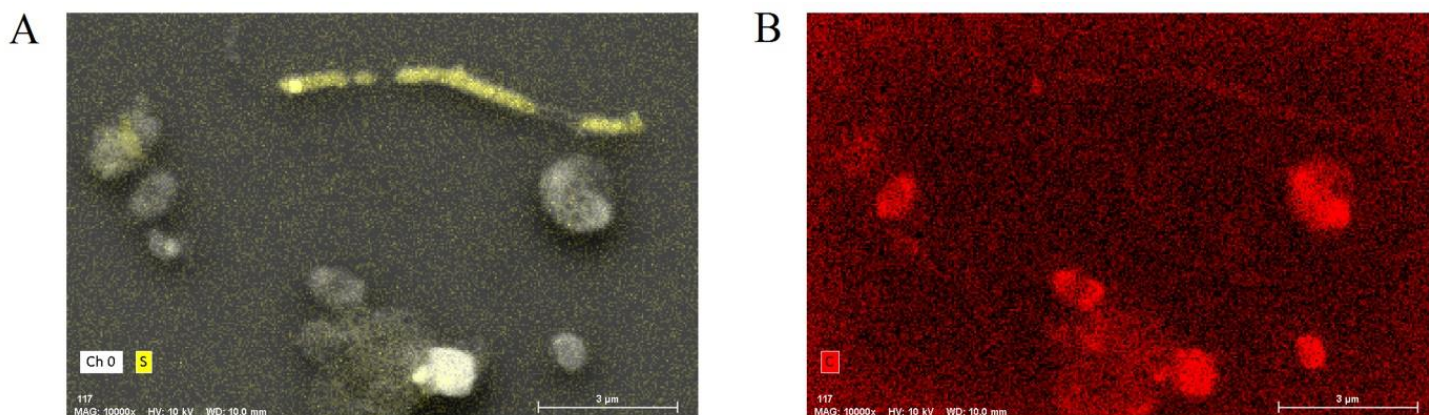

Figure 5: *SEM-EDS images showing that filaments (top right) are enriched in sulfur (A), but low in carbon (B) in comparison to cells. Yellow indicates the presence of sulfur (A), red indicates the presence of carbon (B). The intensity of these colors in the elemental mapping images is correlated to the abundance of these elements in the sample in mass percent.*

Microbial community composition

The analysis of the microbial community inferred from 16S rRNA gene amplicon sequencing indicated prevalence of Bacteria (96%) composed of primarily *Epsilonproteobacteria* (67%), with smaller contributions of *Gammaproteobacteria* (8%) and *Deltaproteobacteria* (6%). Within the *Epsilonproteobacteria* sulfide-oxidizing genera *Arcobacter* and *Sulfurimonas* each accounted for about half of the reads. *Sulfurovum*, *Desulfobulbaceae*, *Beggiatoaceae* and *Methanomicrobia* were detected at low overall frequency (<2%).

On the level of amplicon sequence variants (ASVs), the 15 most frequent ASVs (detected with >300 reads) accounted for about 67% of all reads and were dominated by roughly equal numbers of *Arcobacter* and *Sulfurimonas*. Other taxa (<2%) represented among the most frequent ASVs

were *Methylococcales*, *Desulfobulbaceae*, ANME-1 (*Methanomicrobia*), *Sulfurovom* and *Bacteroidetes.*

Bright field and epifluorescence microscopy on a nucleic acid stained sample visualized cells associated with the filamentous sulfur structure.

Catalyzed reporter deposition fluorescence in situ hybridization (CARD-FISH) with the *Arcobacter* specific oligonucleotide probe Arc94 (13) confirmed the presence of *Arcobacter* cells, which were observed as coccoid to oval shaped single cells often connected to the sulfur filaments (Fig. 6).
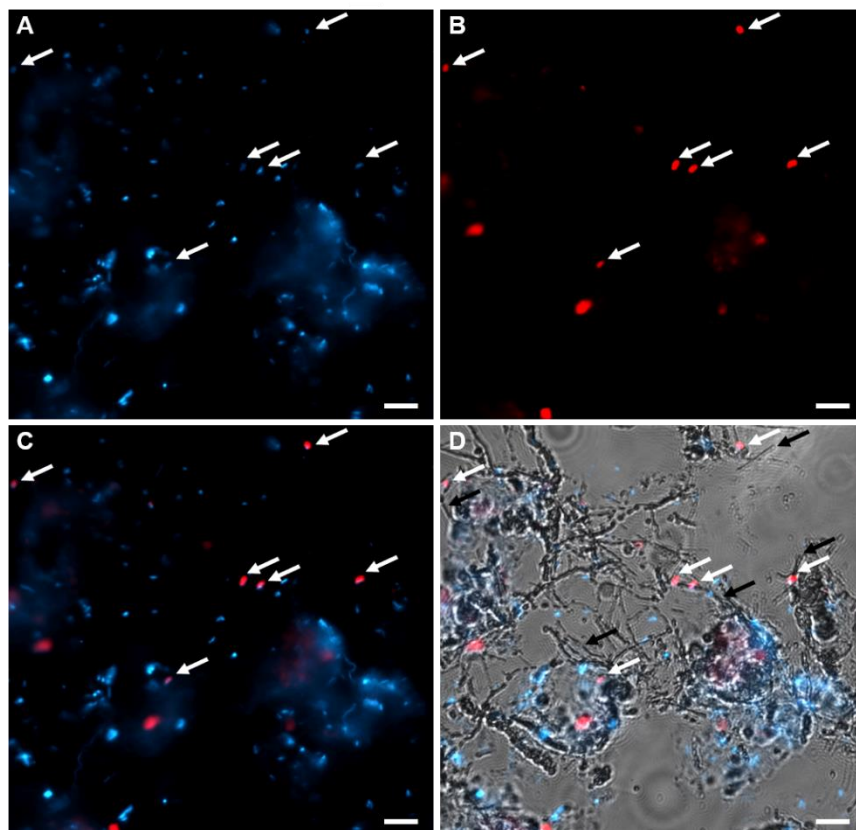
Figure 6: *Fluorescence micrographs of cells and filaments. Cells stained with DAPI in blue (A) and cells labeled with CARD-FISH using probe Arc94 targeting Arcobacter in red (B). Overlay of DAPI and CARD-FISH signals (C) and fluorescence channels overlayed with bright field image showing the filaments (D). White arrows indicate cells labeled with probe Arc94 while black arrows highlight filaments in the proximity of labeled cells. Scale bar, 5 µm.*

Discussion

The conspicuous, smooth, and gelatinous transparent structures we report on here have been observed previously (A. Teske, S. Wankel, personal communication), but were not further investigated. Other remarkable sulfur structures have been observed previously in deep sea environments. Mushroom-like mats produced by *Thiobacterium*, a gammaproteobacterium, were reported in sulfidic marine habitats (10). The structures in the mats were much less smooth and smaller than the structures we report on here, and were inhabited by different organisms. Also, white mats consisting of small granules were observed at the surface of a brine seep in the Eastern Mediterranean. While with a similar fibrous microstructure and inhabiting organism (likely organisms related to "*Candidatus* Arcobacter sulfidicus") (11), these structures were irregular, consisting of cotton ball-like precipitates instead of the smooth structure described here. Other sulfur-rich structures include flocculent material composed of filaments observed in a laboratory reactor (6), which was similar to flocculent material released during snowblower events, and hydrothermal filamentous sulfur mats (4), of which a morphologically comparable mat was dominated by *Arcobacter* (12). In the latter, well described, example, the organism was similar on 16S rRNA gene level to the *Arcobacter* sp. found in this study. However, the here studied structure had a different macroscopic appearance, probably because formation conditions differed.

PCR-based community analyses suffer several well-known biases and should be considered as indicative, rather than quantitative (14, 15). Our analysis of the microbial community indicated that 16S rRNA gene amplicons related to *Arcobacter* and *Sulfurimonas* accounted for a substantial proportion. However, as *Arcobacter* but not *Sulfurimonas* is known to produce filamentous sulfur, we focused further on *Arcobacter*. The detected *Arcobacter* population was dominated by a single amplicon sequence variant (ASV) which was similar to environmental sequences recovered from deep sea and seep environments, and the 16S rRNA gene of "*Candidatus* Arcobacter sulfidicus", a sulfide oxidizer known to form filaments of elemental sulfur (7). The presence of *Arcobacter* cells was detected with CARD-FISH, which indicated that cells were associated with the sulfur filaments. Although the microstructure of the filaments observed by light microscopy and SEM was very similar to the microstructures that "*Candidatus* Arcobacter sulfidicus" produced in laboratory cultures (7), the macroscopic structure was entirely different. The formation of filaments is thought to help the cells find and maintain an optimal position in opposing chemical gradients of oxygen and sulfide (5). Similar as the well-known 'run and tumble' behaviour of swimming

bacteria to orient themselves optimally in a substrate gradient (16) sudden direction changes of cells growing a sulfur wire, explain the strange curvature of the sulfur filaments (Fig. 4).

The SEM-EDS analysis showed that the filaments consist of almost pure sulfur, without important contribution of metals or carbon. This was confirmed by the observed disappearance of filaments after exposure to methanol, which dissolves elemental sulfur. Our data suggests that the sulfur filaments are likely produced by bacteria related to *Arcobacter*, which live at the interface between oxygen and sulfide and produce elemental sulfur by aerobic sulfide oxidation, as found for "*Candidatus* Arcobacter sulfidicus" (7).

Also *Sulfurimonas* seem abundant in the structure, as observed by the microbial community analysis. *Sulfurimonas* can oxidise a range of reduced sulfur compounds, such as sulfide, elemental sulfur, and thiosulfate (17). Known *Sulfurimonas* are able to oxidize sulfide usually completely to sulfate (17), and produce crystalline sulfur only as intermediate product under low oxygen conditions (18). We therefore regarded it likely that *Arcobacter* is responsible for the formation of the abundant and structured filaments.

However, the sulfide consumption observed within the structure cannot be explained by the oxidative activity of *Arcobacter*, as *Arcobacter* needs an overlap of oxygen and sulfide to perform sulfide oxidation. Other processes were considered to explain the gap between the oxic and sulfidic zone, e.g. oxidation by nitrate, Fe(II), nitrate-storing *Beggiatoa*, or cable bacteria.

The giant vacuolated *Gammaproteobacteria* of the family *Beggiatoaceae* forms mats on sulfidic sediments. The family contains a variety of metabolic potential, with autotrophic, mixotrophic, and heterotrophic organisms being isolated (19-21). *Beggiatoa* have vacuoles in which they can store nitrate in mmol L^{-1} concentrations (22), which allows them to oxidize sulfide and survive for days to weeks under anoxic conditions (23). The first step of sulfide oxidation leads to the formation of elemental sulfur (24), which can be stored internally, and is used as electron donor when the external sulfide concentration decreases.

Another sulfide oxidizer that thrives in sediments with separated oxic and sulfidic zones is a filamentous *Desulfobulbaceae* (also referred to as 'cable bacteria') (25). Electric currents couple the sulfide oxidation to the reduction of oxygen (26) or nitrate (27), through microbial cables stretching between the different zones (25). Cable bacteria can be found in a wide variety of

environments (28), but these clearly distinguishable and robust filaments were not observed in the investigated structure. Also, sequences related to *Desulfobulbaceae* were only detected at low frequency.

Such indirect oxidation by oxygen is unlikely as the stoichiometry of sulfide and oxygen fluxes (S_{tot}:O_2 was approximately 5) do not match with aerobic sulfide oxidation to elemental sulfur (S(0)), with a stoichiometry of 2 ($O_2 + 2\ HS^- \rightarrow 2\ S(0) + 2\ OH^-$). Thus the sulfide consumption cannot be explained by the oxygen flux. Moreover, aerobic sulfide oxidation of HS^- (the dominant sulfide species at pH 7.5) to elemental sulfur would lead to a pH maximum where sulfide disappears, which was not observed.

Also sulfide oxidation by nitrate is not responsible for the observed sulfide consumption in our structure. The highest possible nitrate flux from the water column to the sulfidic zone, is 5.1×10^{-9} mol m^{-2} s^{-1}, two orders of magnitude too low to explain the observed sulfide consumption. Nitrate storing giant *Beggiatoa* were highly abundant in Guaymas Basin sediments but not observed inside the structure by microscopy. Furthermore, sequences affiliated with *Beggiatoaceae*, the family containing the genus *Beggiatoa*, were detected with low frequency in the amplicon dataset.

Further cable bacteria that directly transfer electrons from sulfide to oxygen via electrical conductance (25, 26) can be excluded as explanation for the observed gap. Both by light microscopy and SEM the characteristic filaments with nodes and longitudinal thin ridges typical for cable bacteria (25) were not observed, and observed filaments were much too thin (0.1 μm instead of the typical 0.4-1.7 μm for cable bacteria (29)). Furthermore, the cable bacteria are highly robust, while the investigated filaments disappeared when squeezed under microscopic cover glass. The filaments almost completely consisted of sulfur, a poor conductor. Also, the typical pH profile for cable bacteria, with a pH peak in the oxic zone (26) was not observed, and furthermore electrical potential measurements differed from those typical for the presence of cable bacteria (30).

The observed sulfide consumption in our laboratory experiments may be explained by the incubation conditions that differed from the in situ situation. In situ, the structures grow attached to branches of tubeworms, exposed to oxygen and sulfide from the surrounding water, hence oxygen and sulfide are provided from the same direction. Indeed, sulfide is abundant in vent fluids

of the Guaymas Basin (31). Because in situ sulfide and oxygen penetrated the structure from the same direction, sulfide would be rapidly consumed at the surface by sulfide-oxidizing bacteria and be absent inside the structure. Under such conditions the sulfur filaments would not dissolve. The situation of oxygen and sulfide coming from the same direction might also have led to the smooth appearance, instead of woolly flocs. In situ the concentration of oxygen probably exceeded that of sulfide, as upon retrieval the waterphase was no longer sulfidic. Thus in situ sulfide was efficiently oxidised to sulfur at the surface and could not penetrate the structure. In contrast, in our laboratory experiment, the sulfur structure was located in opposing gradients of sulfide from the sediment and oxygen from the water column. Hence the filaments of sulfur were exposed to sulfide that penetrated from below which would react with the filaments before meeting the oxygen penetrating the structures from above. Because sulfide penetrated the structure from the sediments below, it could react with the filaments to form polysulfides ($n/8\ S_8 + HS^- \rightarrow S_{n+1}^{2-} + H^+$ (32)), resulting in dissolution of the filaments and decomposition of the structure within hours. Our H_2S microsensors do not detect polysulfides. In opposing gradients as is normally the case in other environments, sulfur filaments are constantly exposed to sulfide, and the cells will have a more complicated pattern to find the optimal location in the oxygen-sulfide gradients as the exposed surfaces are limited in either oxygen or sulfide. This might lead to a more irregular flocculent and woolly assembly of the individual filaments forming the structure.

Materials and methods

Site description and sample collection

Sampling took place during a research cruise with RV *Atlantis* and DSV *Alvin* in the Guaymas Basin (Gulf of California) in November 2018. Structures were observed on and next to a hot smoker at the Cathedral Hill hydrothermal vent system (27°00.696 N, 111°24.254 W) (33). One of the structures next to the hot smoker was sampled by the *Alvin* submersible using a push corer. On board, the push core with the structure was brought to a cold room (4 °C) for description of sediment characteristics.

Microsensor measurements

The push core with the structure was placed in a water bath, which was set at a constant temperature of 3 °C. Microsensor profiles for O_2, pH, H_2S, and electric potential were measured through the structure, overlying seawater, and underlying sediment. The microsensors for O_2, pH,

H_2S, and electric potential were produced as described previously (30, 34-36). The interface between the structure and the seawater was set as zero position. Depth profiles were measured using a micromanipulator equipped with a motor. The O_2 microsensors were 2-point calibrated with air-saturated seawater (100%) and 1 mol L^{-1} Na ascorbate solution, pH 11 (0%). The pH microsensors were calibrated in standard buffers. The H_2S microsensors were calibrated by incremental addition of a Na_2S stock solution to acidified seawater (pH < 2). Concentrations of total sulfide (S_{tot}) ($S_{tot} = H_2S + HS^- + S^{2-}$) were calculated using the corresponding H_2S concentrations and pH values (34) for each depth, using a pK1 of 6.635 (37). Subsamples for microscopic, chemical, and community analyses were taken after microsensor measurements were finished.

Fluxes of oxygen and sulfide were calculated by multiplication of the molecular diffusion coefficient of oxygen (D_0), with the porosity of the structure (38), resulting in fluxes of 4.9×10^{-8} mol m^{-2} s^{-1} for oxygen ($D_s(O_2) = 1.98 \times 10^{-9}$ m^2 s^{-1}) and 2.2×10^{-7} mol m^{-2} s^{-1} for sulfide ($D_s(S_{tot}) = 0.64 \times D_s(O_2)$ (39, 40)), respectively. The highest possible nitrate flux was calculated using the combined nitrate and nitrite concentration in bottom water of 20 μmol L^{-1} (33), and a D_0 of 1.61×10^{-9} m^2 s^{-1} (41).

Microscopy and elemental analysis

Subsamples of the structure were taken for light microscopy, scanning electron microscopy (SEM), and energy-dispersive X-ray spectroscopy (EDS) analysis. Light microscopy was conducted on board. Samples for SEM were fixed on board using a fixative solvent of paraformaldehyde 2.5%/glutaraldehyde 2.5%/Na-cacodylate 0.1 mol L^{-1}. The objective of fixation is to retain cellular components in their native compartments and to present cells with a distinct and detailed microscopically appearance. The sample was rinsed/diluted in water 1:1 and one drop of this solution was added to a fresh drop of water on a piece of silicon wafer, left for drying out, at room temperature. SEM analysis was performed on a Verso 3D, with scanning parameters: 5 kv,13 pA, with an angle of 45 degrees.

For SEM-EDS the samples were prepared on chips of silicon wafer material. Secondary electron micrographs were recorded using FEI Quanta 250 FEG (Thermo Fisher Scientific, Eindhoven, The Netherlands) scanning electron microscope with an accelerating of 2 and 5 kV for the electron beam. The energy-dispersive X-ray spectroscopy were performed with an accelerating voltage of 10 kV on the SEM and Bruker EDS double detector system equipped with XFlash 6/30 detectors

(Bruker Nano GmbH, Berlin, Germany) with an energy resolution <123 eV at MnKα. EDS data were processed with the Bruker Quantax Esprit software package.

Solid-phase iron extractions

Subsamples for solid-phase iron extractions were fixed in 5% (w/v) ZnAc and stored at -20 °C on board. The subsamples were transported cooled and were stored at -20 °C in the home laboratory. Extraction of solid-phase iron occurred on around 50 mg material, for 0.5 hours using 0.5 mol L^{-1} HCl. Solid-phase iron concentrations were determined on the filtered (0.2 μm PTFE syringe filters) extract using the ferrozine method (42).

DNA extraction, 16S rRNA gene amplicon sequencing and bioinformatic analysis

A subsample was preserved for DNA extraction by spinning down 1 mL material, removing the supernatant and storing the pellet at -20 °C. An aliquot was used for DNA extraction with the FastDNA Spin Kit for Soil (MP Biomedicals) following the manufacturers guidelines and DNA was quantified with the Qubit assay. The 16S rRNA gene of Archaea and Bacteria was amplified using the universal primers 515F (5'-GTGYCAGCMGCCGCGGTAA-3) and 806R (5'-GGACTACNVGGGTWTCTAAT-3') following the Earth Microbiome protocol (43-45). PCR reactions consisted of 10 μL Invitrogen Platinum Taq II 2X Master Mix, 0.5 μL 515F primer (10 μmol L^{-1}), 0.5 μL 806R primer (10 μmol L^{-1}), 9 μL nuclease-free water, and 5 μL of template DNA (5 ng μL^{-1}). PCR was performed with the following thermocycler conditions: 94 °C for 3 min followed by 28 cycles of 94 °C for 45 sec, 50 °C for 60 sec, and 72 °C for 90 sec and a final elongation step at 72 °C for 10 min. PCR products were checked for the expected length on an agarose (1%) gel and were purified using AMPure XR beads (Beckman Coulter) following the manufacturers protocol. Subsequently, the gene amplicons were prepared for Illumina MiSeq sequencing following Illumina's 16S Library Preparation Protocol as previously described (46). Illumina MiSeq sequencing with 2×250 bp paired end read chemistry was performed by Laragen Inc. (Culver City, CA). Demultiplexed sequence reads were processed using QIIME 2 (version 2020.2; (47)). In short, primer sequences were removed using cutadapt with an error rate of 0.12 and reads were further processed in DADA2. Forward and reverse reads were truncated to 140 bp and filtering, denoising, merging and chimera removal was performed with default settings. After data preprocessing 56518 reads of 74938 raw reads (75%) remained in the dataset. The resulting amplicon sequence variants (ASVs) were taxonomically classified using the classify-sklearn method and the SILVA SSU database release 128. The dataset was further curated by removing ASVs occurring in negative controls (i.e., PCR and DNA extraction blanks, 100 ASVs),

classified as Unassigned on domain level (9 ASVs) or present as singletons (1 ASV). The ASVs in the final dataset (752 ASVs represented by 55187 reads) were collapsed at different taxonomic levels to infer relative sequence abundances. The dominant ASVs of interest were further analysed by Blastn comparison against the NCBI nt/nr and ref-seq database (July 2021) and other selected reference sequences (i.e. "*Candidatus* Arcobacter sulfidicus") to identify similarity to environmental sequences and cultured representatives.

Catalyzed reporter deposition fluorescence in situ hybridization (CARD-FISH)

A subsample was fixed in 2% paraformaldehyde for 2 h at room temperature, washed twice with 1×phosphate buffered saline (PBS; pH 7.4) and aliquots were stored in 1×PBS at 4°C or in 1×PBS/EtOH at -20°C. Aliquots of the fixed sample were spotted onto wells of Teflon-coated microscopy slides, dried and briefly washed in 80% ethanol. CARD-FISH was performed as previously described (48). In short, for cell wall permeabilization, samples were incubated in lysozyme solution (10 mg mL^{-1} lysozyme powder, 0.1 mol L^{-1} Tris–HCl, 0.05 mol L^{-1} EDTA, pH 8) for 30 min at 37 °C. Endogenous peroxidases were inactivated by incubation in 0.01 mol L^{-1} HCl for 30 min at room temperature. The oligonucleotide probe ARC94 (5'TGCGCCACTTAGCTGACA3') was applied with a formamide concentration of 20% in hybridization buffer (13). The catalyzed reporter deposition step was done with Alexa Fluor 594 labelled tyramides. As we observed that the filaments dissolved during treatment with methanol, we omitted any incubation in methanol (i.e., inactivation of endogenous peroxidases was done with HCl instead of methanol plus H_2O_2) and limited all ethanol washing steps. Cells were stained with DAPI (4,6-diamidino-2-phenylindole) and micrographs were obtained with an epifluorescence microscope (DM4B; Leica).

Data availability

Sequences have been deposited at NCBI GenBank under BioProject ID PRJNA691673.

Acknowledgements

microsensor construction and their assistance during expedition preparation. This study was funded by the Max Planck Society and the U.S. National Science Foundation (MCB-1817428 award to Roland Hatzenpichler). We declare no conflict of interest.

References

1. Von Damm KL. 1995. Controls on the chemistry and temporal variability of seafloor hydrothermal fluids. *In* Humphris SE, Zierenberg RA, Mullineaux LS, Thomson RE (ed), Seafloor hydrothermal systems: physical, chemical, biological, and geological interactions. American Geophysical Union.
2. Jannasch HW. 1983. Microbial processes at deep sea hydrothermal vents. *In* Rona PA, Boström K, Laubier L, Smith KL (ed), Hydrothermal processes at seafloor spreading centers. Springer, Boston, MA.
3. Kamyshny Jr. A, Borkenstein CG, Ferdelman TG. 2009. Protocol for quantitative detection of elemental sulfur and polysulfide zero-valent sulfur distribution in natural aquatic samples. Geostand Geoanal Res 33:415-435.
4. Taylor CD, Wirsen CO, Gaill F. 1999. Rapid microbial production of filamentous sulfur mats at hydrothermal vents. Appl Environ Microbiol 65:2253-2255.
5. Sievert SM, Wieringa EBA, Wirsen CO, Taylor CD. 2007. Growth and mechanism of filamentous-sulfur formation by *Candidatus* Arcobacter sulfidicus in opposing oxygen-sulfide gradients. Environ Microbiol 9:271-276.
6. Taylor CD, Wirsen CO. 1997. Microbiology and ecology of filamentous sulfur formation. Science 277:1483-1485.
7. Wirsen CO, Sievert SM, Cavanaugh CM, Molyneaux SJ, Ahmad A, Taylor LT, DeLong EF, Taylor CD. 2002. Characterization of an autotrophic sulfide-oxidizing marine *Arcobacter* sp. that produces filamentous sulfur. Appl Environ Microbiol 68:316-325.
8. Haymon RM, Fornari DJ, Von Damm KL, Lilley MD, Perfit MR, Edmond JM, Shanks III WC, Lutz RA, Grebmeier JM, Carbotte S, Wright D, McLaughlin E, Smith M, Beedle N, Olson E. 1993. Volcanic eruption of the mid-ocean ridge along the East Pacific Rise crest at 9°45-52´N: Direct submersible observations of seafloor phenomena associated with an eruption event in April, 1991. Earth Planet Sci Lett 119:85-101.
9. Wasmund K, Mußmann M, Loy A. 2017. The life sulfuric: microbial ecology of sulfur cycling in marine sediments. Environ Microbiol Rep 9:323-344.
10. Grünke S, Lichtschlag A, De Beer D, Kuypers MM, Lösekann-Behrens T, Ramette A, Boetius A. 2010. Novel observations of *Thiobacterium*, a sulfur-storing gammaproteobacterium producing gelatinous mats. ISME J 4:1031-1043.
11. Omoregie EO, Mastalerz V, De Lange G, Straub KL, Kappler A, Røy H, Stadnitskaia A, Foucher J-P, Boetius A. 2008. Biogeochemistry and community composition of iron- and sulfur-precipitating microbial mats at the Chefrun mud volcano (Nile Deep Sea Fan, Eastern Mediterranean). Appl Environ Microbiol 74:3198-3215.

12. Moussard H, Corre E, Cambon-Bonavita M-A, Fouquet Y, Jeanthon C. 2006. Novel uncultured *Epsilonproteobacteria* dominate a filamentous sulphur mat from the 13°N hydrothermal vent field, East Pacific Rise. FEMS Microbiol Ecol 58:449-463.

13. Snaidr J, Amann R, Huber I, Ludwig W, Schleifer K-H. 1997. Phylogenetic analysis and in situ identification of bacteria in activated sludge. Appl Environ Microbiol 63:2884-2896.

14. Muyzer G, Smalla K. 1998. Application of denaturing gradient gel electrophoresis (DGGE) and temperature gradient gel electrophoresis (TGGE) in microbial ecology. Antonie van Leeuwenhoek 73:127-141.

15. Amann RI, Binder BJ, Olson RJ, Chisholm SW, Devereux R, Stahl DA. 1990. Combination of 16S rRNA-targeted oligonucleotide probes with flow cytometry for analyzing mixed microbial populations. Appl Environ Microbiol 56:1919-1925.

16. Tailleur J, Cates ME. 2008. Statistical mechanics of interacting run-and-tumble bacteria. Phys Rev Lett 100:218103.

17. Han Y, Perner M. 2015. The globally widespread genus *Sulfurimonas*: versatile energy metabolisms and adaptations to redox clines. Front Microbiol 6:989.

18. Wang S, Jiang L, Hu Q, Cui L, Zhu B, Fu X, Lai Q, Shao Z, Yang S. 2021. Characterization of *Sulfurimonas hydrogeniphila* sp. nov., a novel bacterium predominant in deep-sea hydrothermal vents and comparative genomic analyses of the genus *Sulfurimonas*. Front Microbiol 12:626705.

19. Nelson DC, Castenholz RW. 1981. Organic nutrition of *Beggiatoa* sp. J Bacteriol 147:236-247.

20. Nelson DC, Jannasch HW. 1983. Chemoautotrophic growth of a marine *Beggiatoa* in sulfide-gradient cultures. Arch Microbiol 136:262-269.

21. Hagen KD, Nelson DC. 1997. Use of reduced sulfur compounds by *Beggiatoa* spp.: Enzymology and physiology of marine and freshwater strains in homogeneous and gradient cultures. Appl Environ Microbiol 63:3957-3964.

22. McHatton SC, Barry JP, Jannasch HW, Nelson DC. 1996. High nitrate concentrations in vacuolate, autotrophic marine *Beggiatoa* spp. Appl Environ Microbiol 62:954-958.

23. Preisler A, De Beer D, Lichtschlag A, Lavik G, Boetius A, Jørgensen BB. 2007. Biological and chemical sulfide oxidation in a *Beggiatoa* inhabited marine sediment. ISME J 1:341-353.

24. Nelson DC, Jørgensen BB, Revsbech NP. 1986. Growth pattern and yield of a chemoautotrophic *Beggiatoa* sp. in oxygen-sulfide microgradients. Appl Environ Microbiol 52:225-233.

25. Pfeffer C, Larsen S, Song J, Dong M, Besenbacher F, Meyer RL, Kjeldsen KU, Schreiber L, Gorby YA, El-Naggar MY, Leung KM, Schramm A, Risgaard-Petersen N, Nielsen LP. 2012. Filamentous bacteria transport electrons over centimetre distances. Nature 491:218-221.

26. Nielsen LP, Risgaard-Petersen N, Fossing H, Christensen PB, Sayama M. 2010. Electric currents couple spatially separated biogeochemical processes in marine sediment. Nature 463:1071-1074.

27. Marzocchi U, Trojan D, Larsen S, Meyer RL, Revsbech NP, Schramm A, Nielsen LP, Risgaard-Petersen N. 2014. Electric coupling between distant nitrate reduction and sulfide oxidation in marine sediment. ISME J 8:1682-1690.

28.	Burdorf LDW, Tramper A, Seitaj D, Meire L, Hidalgo-Martinez S, Zetsche E-M, Boschker HTS, Meysman FJR. 2017. Long-distance electron transport occurs globally in marine sediments. Biogeosciences 14:683-701.

29.	Schauer R, Risgaard-Petersen N, Kjeldsen KU, Bjerg JJT, Jørgensen BB, Schramm A, Nielsen LP. 2014. Succession of cable bacteria and electric currents in marine sediment. ISME J 8:1314-1322.

30.	Damgaard LR, Risgaard-Petersen N, Nielsen LP. 2014. Electric potential microelectrode for studies of electrobiogeophysics. J Geophys Res Biogeosci 119:1906-1917.

31.	Campbell AC, Bowers TS, Measures CI, Falkner KK, Khadem M, Edmond JM. 1988. A time series of vent fluid compositions from 21°N, East Pacific Rise (1979, 1981, 1985), and the Guaymas Basin, Gulf of California (1982, 1985). J Geophys Res Solid Earth 93:4537-4549.

32.	Schauder R, Müller E. 1993. Polysulfide as a possible substrate for sulfur-reducing bacteria. Arch Microbiol 160:377-382.

33.	Teske A, De Beer D, McKay LJ, Tivey MK, Biddle JF, Hoer D, Lloyd KG, Lever MA, Røy H, Albert DB, Mendlovitz HP, MacGregor BJ. 2016. The Guaymas Basin hiking guide to hydrothermal mounds, chimneys, and microbial mats: complex seafloor expressions of subsurface hydrothermal circulation. Front Microbiol 7:75.

34.	Jeroschewski P, Steuckart C, Kühl M. 1996. An amperometric microsensor for the determination of H_2S in aquatic environments. Anal Chem 68:4351-4357.

35.	Revsbech NP. 1989. An oxygen microsensor with a guard cathode. Limnol Oceanogr 34:474-478.

36.	De Beer D, Schramm A, Santegoeds CM, Kühl M. 1997. A nitrite microsensor for profiling environmental biofilms. Appl Environ Microbiol 63:973-977.

37.	Millero FJ, Plese T, Fernandez M. 1988. The dissociation of hydrogen sulfide in seawater. Limnol Oceanogr 33:269-274.

38.	Kühl M, Glud RN, Ploug H, Ramsing NB. 1996. Microenvironmental control of photosynthesis and photosynthesis-coupled respiration in an epilithic cyanobacterial biofilm. J Phycol 32:799-812.

39.	Jørgensen BB, Revsbech NP, Blackburn TH, Cohen Y. 1979. Diurnal cycle of oxygen and sulfide microgradients and microbial photosynthesis in a cyanobacterial mat sediment. Appl Environ Microbiol 38:46-58.

40.	Wieland A, Kühl M. 2000. Short-term temperature effects on oxygen and sulfide cycling in a hypersaline cyanobacterial mat (Solar Lake, Egypt). Mar Ecol Prog Ser 196:87-102.

41.	Li Y-H, Gregory S. 1974. Diffusion of ions in sea water and in deep-sea sediments. Geochim Cosmochim Acta 38:703-714.

42.	Viollier E, Inglett PW, Hunter K, Roychoudhury AN, Van Cappellen P. 2000. The ferrozine method revisited: Fe(II)/Fe(III) determination in natural waters. Appl Geochem 15:785-790.

43.	Thompson LR, Sanders JG, McDonald D, Amir A, Ladau J, Locey KJ, Prill RJ, Tripathi A, Gibbons SM, Ackermann G, Navas-Molina JA, Janssen S, Kopylova E, Vázquez-Baeza Y, González A, Morton JT, Mirarab S, Xu ZZ, Jiang L, Haroon MF, Kanbar J, Zhu Q, Song SJ, Kosciolek T, Bokulich NA, Lefler J, Brislawn CJ, Humphrey G, Owens SM, Hampton-Marcell J, Berg-Lyons D, McKenzie V, Fierer N, Fuhrman JA, Clauset A, Stevens RL,

Shade A, Pollard KS, Goodwin KD, Jansson JK, Gilbert JA, Knight R, TEMC. 2017. A communal catalogue reveals Earth´s multiscale microbial diversity. Nature 551:457-463.

44. Parada AE, Needham DM, Fuhrman JA. 2016. Every base matters: assessing small subunit rRNA primers for marine microbiomes with mock communities, time series and global field samples. Environ Microbiol 18:1403-1414.

45. Apprill A, McNally S, Parsons R, Weber L. 2015. Minor revision to V4 region SSU rRNA 806R gene primer greatly increases detection of SAR11 bacterioplankton. Aquat Microb Ecol 75:129-137.

46. Reichart NJ, Jay ZJ, Krukenberg V, Parker AE, Spietz RL, Hatzenpichler R. 2020. Activity-based cell sorting reveals responses of uncultured archaea and bacteria to substrate amendment. ISME J 14:2851-2861.

47. Bolyen E, Rideout JR, Dillon MR, Bokulich NA, Abnet C, Al-Ghalith GA, Alexander H, Alm EJ, Arumugam M, Asnicar F, Bai Y, Bisanz JE, Bittinger K, Brejnrod A, Brislawn CJ, Brown CT, Callahan BJ, Caraballo-Rodríguez AM, Chase J, Cope EK, Da Silva R, Diener C, Dorrestein PC, Douglas GM, Durall DM, Duvallet C, Edwardson CF, Ernst M, Estaki M, Fouquier J, Gauglitz JM, Gibbons SM, Gibson DL, Gonzalez A, Gorlick K, Guo J, Hillmann B, Holmes S, Holste H, Huttenhower C, Huttley GA, Janssen S, Jarmusch AK, Jiang L, Kaehler BD, Kang KB, Keefe CR, Keim P, Kelley ST, Knights D, Koester I, Kosciolek T, Kreps J, Langille MGI, Lee J, Ley R, Liu Y-X, Loftfield E, Lozupone C, Maher M, Marotz C, Martin BD, McDonald D, McIver LJ, Melnik AV, Metcalf JL, Morgan SC, Morton JT, Naimey AT, Navas-Molina JA, Nothias LF, Orchanian SB, Pearson T, Peoples SL, Petras D, Preuss ML, Pruesse E, Rasmussen LB, Rivers A, Robeson II MS, Rosenthal P, Segata N, Shaffer M, Shiffer A, Sinha R, Song SJ, Spear JR, Swafford AD, Thompson LR, Torres PJ, Trinh P, Tripathi A, Turnbaugh PJ, Ul-Hasan S, van der Hooft JJJ, Vargas F, Vázquez-Baeza Y, Vogtmann E, von Hippel M, Walters W, Wan Y, Wang M, Warren J, Weber KC, Williamson CHD, Willis AD, Xu ZZ, Zaneveld JR, Zhang Y, Zhu Q, Knight R, Caporaso JG. 2019. Reproducible, interactive, scalable and extensible microbiome data science using QIIME 2. Nat Biotechnol 37:852-857.

48. Pernthaler A, Pernthaler J, Amann R. 2002. Fluorescence in situ hybridization and catalyzed reporter deposition for the identification of marine bacteria. Appl Environ Microbiol 68:3094-3101.

III. Discussion

6.1 Discussion

This study focused on marine systems that are unusually far from thermodynamic equilibrium. I investigated intertidal sediments and phenomena at a hot smoker in a hydrothermal vent system. The studied systems were: a beach on Helgoland on which large amounts of kelp are deposited regularly; an intertidal sandflat in the Wadden Sea where reduced material escapes to the surface via porewater seeps at the low tide waterline; and the Guaymas Basin hydrothermal vent system with hot smokers and hydrothermal seepage through the sediment (Teske et al. 2014). These systems are far out of equilibrium since strongly concentrated flows of reduced compounds are transported into an oxic ecosystem. The hydrothermal vent differs from the intertidal sediments in that part of the sulfide is not biogenic, but rather originates from thermal degradation of organic material.

While most of the general hypotheses of this study could be confirmed, several interesting and surprising observations were made that will be further discussed.

6.1.1 Microbial mineralization in intertidal sediments with large amounts of kelp detritus

First, it was remarkable that the addition of the kelp material instantly resulted in strongly enhanced microbial degradation. Kelp is complex organic material composed of a variety of potential substrates with different lability, including a mix of polysaccharides and proteins, whose proportion varies with factors such as species and season (Schiener et al. 2015). As structural polysaccharides, which are optimized for rigidity and resistance to degradation, make up a large proportion of the organic material in kelp, much of the kelp biomass is rather recalcitrant. Many enzymes are needed in order to degrade complex polysaccharides. Yet, the deposition of kelp detritus on beaches fuels a highly active microbial community in underlying sediments. Microbial degradation of kelp starts immediately. The particular composition of kelp thus leads to the development of communities adapted to its degradation. Probably, deeply buried kelp fragments that are plentiful in the beach maintain low activity of the microbial community that is specialized in hydrolysing the polysaccharides in kelp. Therefore, the hydrolysing enzymes are continuously active at low levels, and input of fresh kelp detritus directly results in increasing community activity, without the occurrence of a lag period. An immediate response to complex polysaccharides is advantageous, as kelp deposits are dynamic and frequently move. Organisms that need to express a new degradation pathway after fresh material is deposited are at disadvantage and will

be outcompeted, as much of the fresh kelp is washed away at the next tide; a significant portion of the window of opportunity for degradation would therefore be wasted in boosting cellular processes.

A further interesting observation was that the community in sediments characterized by kelp deposition is strongly specialized to the degradation of polysaccharides from kelp. Clearly, structural polymers should be resistant to both biotic and abiotic degradation, yet the community in the sediments could quickly start degrading them. An interesting question for further research is whether organisms specialize on a specific polysaccharide, or if they use polysaccharides sequentially. Specialization on a specific polysaccharide results in parallel degradation, and the sum of respiration rates associated with the different polysaccharides will be equal to the total respiration on the mix of polysaccharides. Alternatively, degradation of the complex kelp material occurs sequentially. It was shown previously that polysaccharide-degrading organisms could indeed use these compounds in a certain order, where a secondary substrate was only used after exhaustion of the preferred substrate (Koch et al. 2019). In Chapter 3, the sum of all aerobic respiration rates for the different substrates exceeds respiration rates on kelp fragments. Nevertheless, the aerobic degradation rates on kelp fragments was the highest observed compared to individual polysaccharides. This could indicate that both parallel and sequential degradation occurs by different organisms.

An exciting observation was that often polysaccharides provoked higher aerobic respiration rates than monomers. This was contrary to expectation, as polysaccharides need to be hydrolysed to fragments sufficiently small to be taken up by microorganisms (Weiss et al. 1991, Reintjes et al. 2017). In Chapter 3, we hypothesized that the quick response and high respiration rates on polysaccharides could be explained by bacterial selfish uptake, but this remains to be tested. Selfish uptake leads to an advantage for microorganisms, as they do not have to share hydrolysis products with other microorganisms, nor do they lose these products via diffusion or advection in the porewater or seawater (Reintjes et al. 2017). Microscopy on fluorescently labeled substrates could be used to test if selfish uptake occurs, as fluorescent substrates taken up selfishly by microorganisms should be visible in the periplasmic space of the cell (Reintjes et al. 2017).

6.1.2 The effect of oxygen exposure and ROS on mineralization in intertidal surface sediments

An unexpected outcome was that sulfate reduction in the intertidal sandflat studied in Chapter 4 did not occur in the presence of oxygen. Even with the use of a silver wire in the incubations, a method especially designed to detect sulfate reduction in oxic environments, no sulfate reduction could be detected during the oxic period (Chapter 4). However, the presence of oxygen did not eliminate the sulfate-reducing bacteria, as sulfate reduction resumed immediately upon anoxia without a lag phase. The absence of sulfate reduction in the presence of oxygen was contrary to our expectations, as other anaerobic processes (fermentation and dissimilatory nitrate reduction) in permeable sediments were active during the oxic period (Marchant et al. 2014, Kessler et al. 2019), and sulfate reduction was measured in the presence of oxygen in microbial mats (Visscher et al. 1992) .

Remarkably, despite the inhibition of sulfate reduction by the presence of oxygen, the oxygenated period was beneficial for sulfate-reducing bacteria. An oxic pretreatment boosted sulfate reduction in the subsequent anoxic period. This might be explained by oxygen-stimulated hydrolysis of macromolecules. This stimulation of hydrolysis, which already plays a role at low oxygen concentrations, has previously been reported for bioreactors (Niu et al. 2016). Enhanced sulfate reduction after transient oxygenation could also have a large impact on systems such as the beach with kelp deposition on Helgoland, as oxygen-stimulated hydrolysis of the macromolecular kelp material could play an important role for the sulfate-reducing bacteria that are dominant during the anoxic period.

Intertidal permeable sediments are crucial for coastal carbon cycling, thus the observation that ROS affect microbial mineralization in the intertidal sandflat studied in Chapter 4 was very exciting. Additions of the ROS-removing enzymes catalase and superoxide dismutase led to a strong increase in both aerobic and anaerobic mineralization rates, which indicated that ROS are present and reduce microbial mineralization. We also analyzed porewaters for hydrogen peroxide, and indeed, hydrogen peroxide was present in high levels. The formation process of ROS in the intertidal flat remains an open question, but it could be speculated that the frequent oxygenation in combination with the intense iron and sulfur cycling plays an important role.

The set of experiments described in Chapter 4 did not allow for conclusions on whether ROS have a direct or indirect effect on microbial mineralization. An indirect effect would occur via competition between ROS and microorganisms for organic material. Studies focusing on possible upregulation of heat shock proteins due to oxidative stress of microorganisms (Lindquist 1986) in the presence of ROS could be used to discriminate between these two mechanisms. Regardless of the exact mechanism responsible, this study showed that ROS could play a very important role in the carbon cycle in intertidal permeable sediments. Further exploration is necessary to determine the presence and production mechanisms of ROS in coastal environments, including environments other than intertidal sandflats.

6.1.3 Sulfide export and the role of hydrodynamics in shaping niches

First, although beaches characterized by kelp deposits and deep-sea hydrothermal vents seem profoundly different, they show crucial similarities. In both systems reduced compounds are transported into the oxic seawater. This export results from a higher supply of reductant than of oxygen. The export of reduced compounds illustrates the thermodynamic disequilibrium prevailing in these environments, which leads to very rich and distinct microbial communities.

In the three systems that were investigated in this study sulfur played a major role, though sulfide oxidation was performed by sulfur oxidizers with profoundly different strategies. In the Janssand intertidal sediments studied in Chapter 4 sulfide is hardly present in surface sediments, except in sulfidic seeps at the low tide waterline (Jansen et al. 2009). In these seeps the hydrodynamics were unsuitable for most organisms, and much of the sulfide escaped to the water column or atmosphere. However, in sulfidic streams on the sandlfat algae were covered by filamentous *Thiotrix*-like organisms, and extensive *Arcobacter* mats rapidly developed on sulfidic sediments in the laboratory (Jansen et al. 2009). Higher up the intertidal flat most sulfide was scavenged by iron chemistry (Jansen et al. 2009), although a diversity of single cell sulfur oxidizers was also found (Pjevac et al. 2014, Dyksma et al. 2016).

The domination of kelp mineralization in sandy beach sediments by sulfate reduction leads to enhanced sulfur cycling and to sulfide export (Chapter 2). Although the exact proportion of sulfate reduction to total carbon degradation could not be exactly constrained due to the uncertainty in oxygen respiration, the portion of carbon degraded by sulfate reduction was much higher than the 0.3 and 25% determined for other intertidal environments (Billerbeck et al. 2006, Werner et al.

2006). The very large ratio of kelp to oxygen input for beach sediments leads to rapid depletion of oxygen, while leaving ample reductant for sulfate reduction, to such an extent that sulfate concentrations were significantly decreased to approximately 10 mM. The sulfide produced from sulfate reduction was partly oxidized by microorganisms within the sediments. Sulfide oxidizers below and next to kelp deposits mainly consisted of *Thiothrix*, *Sulfurovum* and *Sulfurimonas*. The export of sulfide even changed the adjacent ecosystem which accommodates a filamentous sulfide-oxidizing community consisting of mainly *Thiothrix* and *Sulfurovum*, which were attached to green algae on rocks. The presence of *Sulfurovum* is remarkable, as these organisms are mostly known from micro-oxic and anoxic environments (Nakagawa et al. 2005, Meyer et al. 2013). These attached filaments are optimally adapted to life in a high-energy sulfidic environment. Their attachment prevents them from being washed away by the turbulent seawater, while their filamentous networks are easily flushed by oxic and sulfidic water. Sulfur oxidizing filamentous bacteria were also observed in e.g. sulfidic creeks and sulfidic caves (Hamilton et al. 2015) and on crabs that live near hot smokers (Tsuchida et al. 2011). As the large majority of cells in sediments are attached to sand grains (Rusch et al. 2003, Gobet et al. 2012), the different conditions at the low waterline and in the sediments in Chapter 2 selected for different dominant species of *Sulfurovum.*

Conversely, the hydrothermal vent system of the Guaymas Basin has a large variety of sulfide oxidizers (Teske et al. 2016), including attached filamentous organisms, endosymbiotic sulfur oxidizers, large mats of nitrate-storing migratory *Beggiatoa* on top of sulfidic sediments, and a variety of single cell sulfide oxidizers. These single cell sulfide oxidizers were the organisms observed in the sulfur structures described in Chapter 5. The existence of these sulfur structures relies on calm hydrodynamics in a diffusion-dominated system. The sulfide oxidizers likely thrive on a very narrow zone where both sulfide and oxygen are present. This narrow overlap would not allow for the development of filamentous bacteria. In contrast to the more common situation in marine sediments where sulfide diffuses from the sediments below and oxygen from the water column above, around the sulfur structures sulfide and oxygen come from the same direction. This might explain the gelatinous smooth surface of the structure. Hydrothermal systems represent oases of life within the oligotrophic deep-sea (Teske et al. 2016). The variety in sulfide supply and presence of both oxygen and nitrate make hydrothermal vent systems such as the Guaymas Basin a true paradise for those interested in sulfur biogeochemistry. However, the greatly enhanced sulfur cycle and their accessibility also make beaches with kelp deposition attractive study sites.

6.2 Future perspectives

This study addressed how changes in the availability of electron donors and acceptors influence microbial activity. The sudden increase of organic material available for degradation, in this study in the form of kelp detritus, has a profound effect on the biogeochemistry and microbial community of intertidal sands. Especially the reductive sulfur cycle is greatly enhanced, resulting in high sulfide concentrations. The specialization of the highly active community was remarkable. The community could immediately start degrading kelp biomass. Further studies should elucidate the strategies of the kelp-degrading sedimentary community, as these strategies have profound effects on coastal carbon cycling. The degradation strategy of the microbial community (sequential versus parallel use) could be explored by addition of a mix of substrates: if the substrates are consumed sequentially by one group of organisms, the addition of two substrates will prolong the mineralization at equal rates, while if substrates are consumed in parallel by different groups of organisms, the rates will increase. Additionally, the occurrence of bacterial selfish uptake as a strategy for polysaccharide degradation should be tested.

Intertidal permeable sediments are crucial for coastal carbon and nutrient cycling, thus factors influencing microbial mineralization in these sediments are of high interest. This study showed that ROS are likely to have an important role in coastal sediment biogeochemistry. However, it remains unclear if production of ROS is universal in intertidal sediments, and what the exact formation processes are. An important next step is to determine in situ concentrations of hydrogen peroxide and superoxide over a tidal cycle. The dynamics of Fe(III) and both solid-phase and dissolved Fe(II), sulfide, as well as oxygen must be determined in parallel.

6.3 References

Billerbeck, M., U. Werner, L. Polerecky, E. Walpersdorf, D. De Beer & M. Huettel (2006). Surficial and deep pore water circulation governs spatial and temporal scales of nutrient recycling in intertidal sand flat sediment. *Mar Ecol Prog Ser,* 326, 61-76.

Dyksma, S., K. Bischof, B. M. Fuchs, K. Hoffmann, D. Meier, A. Meyerdierks, P. Pjevac, D. Probandt, M. Richter, R. Stepanauskas & M. Mußmann (2016). Ubiquitous *Gammaproteobacteria* dominate dark carbon fixation in coastal sediments. *ISME J,* 10, 1939-1953.

Gobet, A., S. I. Böer, S. M. Huse, J. E. E. Van Beusekom, C. Quince, M. L. Sogin, A. Boetius & A. Ramette (2012). Diversity and dynamics of rare and of resident bacterial populations in coastal sands. *ISME J,* 6, 542-553.

Hamilton, T. L., D. S. Jones, I. Schaperdoth & J. L. Macalady (2015). Metagenomic insights into S(0) precipitation in a terrestrial subsurface lithoautotrophic ecosystem. *Front Microbiol,* 5, 756.

Jansen, S., E. Walpersdorf, U. Werner, M. Billerbeck, M. E. Böttcher & D. De Beer (2009). Functioning of intertidal flats inferred from temporal and spatial dynamics of O_2, H_2S and pH in their surface sediment. *Ocean Dyn,* 59, 317-332.

Kessler, A. J., Y.-J. Chen, D. W. Waite, T. Hutchinson, S. Koh, M. E. Popa, J. Beardall, P. Hugenholtz, P. L. M. Cook & C. Greening (2019). Bacterial fermentation and respiration processes are uncoupled in anoxic permeable sediments. *Nat Microbiol,* 4, 1014-1023.

Koch, H., A. Dürwald, T. Schweder, B. Noriega-Ortega, S. Vidal-Melgosa, J.-H. Hehemann, T. Dittmar, H. M. Freese, D. Becher, M. Simon & M. Wietz (2019). Biphasic cellular adaptations and ecological implications of *Alteromonas macleodii* degrading a mixture of algal polysaccharides. *ISME J,* 13, 92-103.

Lindquist, S. (1986). The heat-shock response. *Annu Rev Biochem,* 55, 1151-1191.

Marchant, H. K., G. Lavik, M. Holtappels & M. M. M. Kuypers (2014). The fate of nitrate in intertidal permeable sediments. *PLoS ONE,* 9, e104517.

Meyer, J. L., N. H. Akerman, G. Proskurowski & J. A. Huber (2013). Microbiological characterization of post-eruption "snowblower" vents at Axial Seamount, Juan de Fuca Ridge. *Front Microbiol,* 4, 153.

Nakagawa, S., K. Takai, F. Inagaki, H. Hirayama, T. Nunoura, K. Horikoshi & Y. Sako (2005). Distribution, phylogenetic diversity and physiological characteristics of epsilon-*Proteobacteria* in a deep-sea hydrothermal field. *Environ Microbiol,* 7, 1619-1632.

Niu, T., Z. Zhou, X. Shen, W. Qiao, L.-M. Jiang, W. Pan & J. Zhou (2016). Effects of dissolved oxygen on performance and microbial community structure in a micro-aerobic hydrolysis sludge *in situ* reduction process. *Water Res,* 90, 369-377.

Pjevac, P., A. Kamyshny Jr., S. Dyksma & M. Mußmann (2014). Microbial consumption of zero-valence sulfur in marine benthic habitats. *Environ Microbiol,* 16, 3416-3430.

Reintjes, G., C. Arnosti, B. M. Fuchs & R. Amann (2017). An alternative polysaccharide uptake mechanism of marine bacteria. *ISME J,* 11, 1640-1650.

Rusch, A., M. Huettel, C. E. Reimers, G. L. Taghon & C. M. Fuller (2003). Activity and distribution of bacterial populations in Middle Atlantic Bight shelf sands. *FEMS Microbiol Ecol,* 44, 89-100.

Schiener, P., K. D. Black, M. S. Stanley & D. H. Green (2015). The seasonal variation in the chemical composition of the kelp species *Laminaria digitata*, *Laminaria hyperborea*, *Saccharina latissima* and *Alaria esculenta*. *J Appl Phycol,* 27, 363-373.

Teske, A., A. V. Callaghan & D. E. LaRowe (2014). Biosphere frontiers of subsurface life in the sedimented hydrothermal system of Guaymas Basin. *Front Microbiol,* 5, 362.

Teske, A., D. De Beer, L. J. McKay, M. K. Tivey, J. F. Biddle, D. Hoer, K. G. Lloyd, M. A. Lever, H. Røy, D. B. Albert, H. P. Mendlovitz & B. J. MacGregor (2016). The Guaymas Basin hiking guide to hydrothermal mounds, chimneys, and microbial mats: complex seafloor expressions of subsurface hydrothermal circulation. *Front Microbiol,* 7, 75.

Tsuchida, S., Y. Suzuki, Y. Fujiwara, M. Kawato, K. Uematsu, T. Yamanaka, C. Mizota & H. Yamamoto (2011). Epibiotic association between filamentous bacteria and the vent-associated galatheid crab, *Shinkaia crosnieri* (Decapoda: Anomura). *J Mar Biol Assoc U K,* 91, 23-32.

Visscher, P. T., R. A. Prins & H. Van Gemerden (1992). Rates of sulfate reduction and thiosulfate consumption in a marine microbial mat. *FEMS Microbiol Lett,* 86, 283-293.

Weiss, M. S., U. Abele, J. Weckesser, W. Welte, E. Schiltz & G. E. Schulz (1991). Molecular architecture and electrostatic properties of a bacterial porin. *Science,* 254, 1627-1630.

Werner, U., M. Billerbeck, L. Polerecky, U. Franke, M. Huettel, J. E. E. Van Beusekom & D. De Beer (2006). Spatial and temporal patterns of mineralization rates and oxygen distribution in a permeable intertidal sand flat (Sylt, Germany). *Limnol Oceanogr,* 51, 2549-2563.

Acknowledgements

First, I would like to thank Dirk de Beer for the opportunity to do my PhD studies in the Microsensor Group, and for introducing me to the world of microsensors. Thank you for all your advice, support and enthousiasm!

Thank you Tim Ferdelman for reviewing this thesis, and Kai Bischof and Tilmann Harder for agreeing on being members of the examination committee. Also thank you to Olivia and Kati for being members of the committee.

A big thank you to Ingeborg Bussmann for hosting me and having a place for all the equipment I brought for the sampling on Helgoland. Also thanks to everyone at the AWI Helgoland for their hospitality.

Thanks to Andreas Teske for the opportunity to join the cruise to the Guaymas Basin, and all crew members and scientists.

I am grateful to the co-authors of the manuscripts in this thesis; to lab rotation students Matija Lagator, Marwa Baloza and Chyrene Moncada; and to Nicole Dubilier, Gunter Wegener, Ingeborg Bussmann, and Tim Ferdelman for their advice during thesis committee meetings.

I would also like to thank the people that proofread parts of this thesis.

Thank you to all past and present members of the Microsensor Group. I really enjoyed working with you the last years! Especially thank you to Gaby, Vera, Anja, Ines, Cäcilia and Karin. Not only for building all the microsensors I needed, but also for spending time distilling radioactive samples, the talks in the tea kitchen, and your flexibility. Also thank you to Ulrike for travel organization.

Olivia - thank you for the exciting times studying sediment slurries in the middle of the night.

Elisa, Andrea, and Miriam, thank you for the great times at and outside of work.
Elisa – thank you for joining me for sampling on Helgoland and Janssand, I know who to ask now when I need a pretty sediment core. And thanks for translating this thesis' Zusammenfassung.

Andrea – thank you so much for your fast English-to-Spanish-and-back translations.

Miriam – thank you for the nice weeks on Sylt.

Thanks for our Mensa lunches, bike tours, theater visits, dinners, for watching my field hockey games, etc… and for letting me talk about again another "fun sport fact" and pretending to listen.

I am happy to have met many wonderful people in Bremen. Friends, roommates and field hockey teammates. Vielen Dank! Also a big thank you to friends and family back in The Netherlands for being so interested in everything I have been doing in Bremen the last years, and for the great times when I was back in The Netherlands.

Papa, mama, Elin – thank you for being such a loving and supportive family!

Appendices

Contributions to manuscripts

Manuscript 1: Kelp deposition changes mineralization pathways and microbial communities in a sandy beach (Chapter 2)

This manuscript is published in Limnology and Oceanography.
doi: 10.1002/lno.11574

Contribution:

Experimental concept and design: 85%

Data acquisition and experimental work: 80%

Data analysis and interpretation: 75%

Preparation of figures and tables: 75%

Drafting of the manuscript: 90%

Manuscript 2: Microbial communities in intertidal permeable sediments are optimized for the degradation of kelp polysaccharides (Chapter 3)

This manuscript is a summary of preliminary results

Contribution:

Experimental concept and design: 90%

Data acquisition and experimental work: 85%

Data analysis and interpretation: 85%

Preparation of figures and tables: 100%

Drafting of the manuscript: 90%

Manuscript 3: Reactive oxygen species affect mineralization processes in permeable intertidal flats (Chapter 4)

This manuscript is in preparation

Contribution:

Experimental concept and design: 45%

Data acquisition and experimental work: 45%

Data analysis and interpretation: 40%

Preparation of figures and tables: 50%

Drafting of the manuscript: 45%

Manuscript 4: Conspicuous smooth and white egg-shaped sulfur structures on a deep-sea hydrothermal vent formed by sulfide-oxidizing bacteria (Chapter 5)

This manuscript is accepted by Microbiology Spectrum

Contribution:

Experimental concept and design: 50%

Data acquisition and experimental work: 30%

Data analysis and interpretation: 70%

Preparation of figures and tables: 45%

Drafting of the manuscript: 90%

Contributed work

Sediment acidification and temperature increase in an artificial CO_2 vent

Dirk de Beer, Anna Lichtschlag, Anita Flohr, Marit Rianne van Erk, Soeren Ahmerkamp, Moritz Holtappels, Matthias Haeckel, James Strong

Status: published in International Journal of Greenhouse Gas Control (2021)

Defining a biogeochemical baseline for sediments at Carbon Capture and Storage (CCS) sites: An example from the North Sea (Goldeneye)

A.W. Dale, S. Sommer, A. Lichtschlag, D. Koopmans, M. Haeckel, E. Kossel, C. Deusner, P. Linke, J. Scholten, K. Wallmann, M.R. van Erk, J. Gros, F. Scholz, M. Schmidt

Status: published in International Journal of Greenhouse Gas Control (2021)

Limitation of microbial processes at saturation-level salinities in a microbial mat covering a coastal saltflat

Dimitri V. Meier, Andreas J. Greve, Arjun Chennu, Marit R. van Erk, Thirumahal Muthukrishnan, Raeid M.M. Abed, Dagmar Woebken, Dirk de Beer

Status: published in Applied and Environmental Microbiology (2021)

Sediment acidification and temperature increase in an artificial CO$_2$ vent

Dirk de Beer[a], Anna Lichtschlag[b], Anita Flohr[b,c], Marit Rianne van Erk[a], Soeren Ahmerkamp[a], Moritz Holtappels[d], Matthias Haeckel[e], James Strong[b]

[a] Max-Planck-Institute for Marine Microbiology, Celciusstrasse 1, 28359, Bremen, Germany
[b] National Oceanography Centre, European Way, Southampton, SO14 3ZH, United Kingdom
[c] University of Southampton, Waterfront Campus, European Way, Southampton, SO14 3ZH, UK
[d] Alfred Wegener Institute for Polar and Marine Research, Am Handelshafen 12, 27570, Bremerhaven, Germany
[e] GEOMAR Helmholtz Centre for Ocean Research Kiel, Wischhofstr. 1-3, 24148, Kiel, Germany

Contribution Marit R. van Erk: Sulfate reduction determination

Abstract

We investigated the effect of an artificial CO_2 vent ($0.0015-0.037$ mol s^{-1}), simulating a leak from a reservoir for carbon capture and storage (CCS), on the sediment geochemistry. CO_2 was injected 3 m deep into the seafloor at 120 m depth. With increasing mass flow an increasing number of vents were observed, distributed over an area of approximately 3 m. *In situ* profiling with microsensors for pH, T, O_2 and ORP showed the geochemical effects are localized in a small area around the vents and highly variable. In measurements remote from the vent, the pH reached a value of 7.6 at a depth of 0.06 m. In a CO_2 venting channel, pH reduced to below 5. Steep temperature profiles were indicative of a heat source inside the sediment. Elevated total alkalinity and Ca^{2+} levels showed calcite dissolution. Venting decreased sulfate reduction rates, but not aerobic respiration. A transport-reaction model confirmed that a large fraction of the injected CO_2 is transported laterally into the sediment and that the reactions between CO_2 and sediment generate enough heat to elevate the temperature significantly. A CO_2 leak will have only local consequences for sediment biogeochemistry, and only a small fraction of the escaped CO_2 will reach the sediment surface.

Defining a biogeochemical baseline for sediments at Carbon Capture and Storage (CCS) sites: An example from the North Sea (Goldeneye)

A.W. Dale[a], S. Sommer[a], A. Lichtschlag[b], D. Koopmans[c], M. Haeckel[a], E. Kossel[a], C. Deusner[a], P. Linke[a], J. Scholten[d], K. Wallmann[a], M.R. van Erk[c], J. Gros[a], F. Scholz[a], M. Schmidt[a]

[a] GEOMAR Helmholtz Centre for Ocean Research Kiel, Wischhofstrasse 1–3, 24148, Kiel, Germany

[b] National Oceanography Centre Southampton, University of Southampton Waterfront Campus, European Way, Southampton, SO14 3ZH, UK

[c] Max Planck Institute for Marine Microbiology, Celsiusstraße 1, Bremen, 28359, Germany

[d] Institute of Geosciences, Christian-Albrechts-Universität zu Kiel (CAU), Otto-Hahn-Platz 1, 24118, Kiel, Germany

Contribution Marit R. van Erk: Sulfate reduction determination

Abstract

Injection of carbon dioxide (CO_2) into subseafloor reservoirs is gaining traction as a strategy for mitigating anthropogenic CO_2 emissions to the atmosphere. Yet, potential leakage, migration and dissolution of externally-supplied CO_2 from such reservoirs are a cause for concern. The potential impact of CO_2 leakage on the biogeochemistry of sediments and overlying waters in the North Sea was studied during a controlled subsurface CO_2 release experiment in 2019 at a potential carbon capture and storage site (Goldeneye). This study describes the natural (unperturbed) biogeochemistry of sediments. They are classified as muddy sand to sandy mud with low organic carbon content ($\sim$0.6 %). Distributions of dissolved inorganic carbon (DIC) and total alkalinity (TA) in sediment porewaters are reported in addition to in situ benthic fluxes of dissolved nutrients and oxygen between the sediments and the overlying water. Oxygen fluxes into the sediment, measured using benthic chambers and eddy covariance, were 6.18 ± 0.58 and 5.73 ± 2.03 mmol m^{-2} d^{-1}, respectively. Diagnostic indicators are discussed that could be used to detect CO_2 enrichment of sediments due to reservoir leakage at CCS sites. These include the ratio TA and ammonium to sulfate in sediment porewaters, benthic fluxes and chloride-normalized cation distributions. These indicators currently suggest that the organic carbon at Goldeneye has an oxidation state below zero and is mainly degraded via sulfate reduction. Carbonate precipitation is apparently negligible, whereas decreases in Mg^{2+} and K^+ point toward ongoing alteration of lithogenic sediments by reverse weathering processes.

Limitation of microbial processes at saturation-level salinities in a microbial mat covering a coastal saltflat

Dimitri V. Meier[1,†], Andreas J. Greve[2], Arjun Chennu[2,3], Marit R. van Erk[2], Thirumahal Muthukrishnan[4], Raeid M.M. Abed[4], Dagmar Woebken[1], Dirk de Beer[2]

[1] Department of Microbiology and Ecosystem Science, Centre for Microbiology and Environmental Systems Science, University of Vienna, Aithanstrasse 14, 1090 Vienna, Austria
[2] Max-Planck-Institute for Marine Microbiology, Celsiusstrasse 1, 28359 Bremen, Germany
[3] Leibnize Centre for Tropical Marine Research, Fahrenheitsstrasse 6, 28359 Bremen, Germany
[4] Biology Department, College of Science, Sultan Qaboos University, Al-Khoud 123, Muscat, Sultanate of Oman

[†] current address: Institute of Biogeochemistry and Pollutant Dynamics, Swiss Federal Institute of Technology, Zurich (ETH Zurich), Universitätsstrasse 16, Zurich, 8092 Switzerland

Contribution Marit R. van Erk: Sulfate reduction, salinity, porosity and sulfate determination

Abstract

Hypersaline microbial mats are dense microbial ecosystems capable of performing complete element cycling and are considered analogs of Early Earth and hypothetical extraterrestrial ecosystems. We studied the functionality and limits of key biogeochemical processes, such as photosynthesis, aerobic respiration, and sulfur cycling in salt crust-covered microbial mats from a tidal flat at the coast of Oman. We measured light, oxygen, and sulfide microprofiles as well as sulfate-reduction rates at salt saturation and in flood conditions and determined fine-scale stratification of pigments, biomass, and microbial taxa in the resident microbial community.

The salt crust did not protect the mats against irradiation or evaporation. Although some oxygen production was measurable at salinity ≤ 30% (w/v) *in situ*, at saturation-level salinity (40%), oxygenic photosynthesis was completely inhibited and only resumed two days after reducing the pore water salinity to 12%. Aerobic respiration and active sulfur cycling occurred at low rates under salt saturation and increased strongly upon salinity reduction. Apart from high relative abundances of *Chloroflexi*, photoheterotrophic *Alphaproteobacteria*, *Bacteroidetes*, and *Archaea*, the mat contained a distinct layer harboring filamentous *Cyanobacteria*, which is unusual for such high salinities.

Our results show that the diverse microbial community inhabiting this saltflat mat ultimately depends on periodic salt dilution to be self-sustaining and is rather adapted to merely survive salt saturation than to thrive under the salt crust.

Importance

Due to their abilities to survive intense radiation and low water availability hypersaline microbial mats are often suggested to be analogs of potential extraterrestrial life. However, even on Earth the limitations imposed on microbial processes by saturation-level salinity have rarely been studied *in situ*. While abundance and diversity of microbial life in salt-saturated environments is well documented, most of our knowledge on process limitations stems from culture-based studies, few *in situ* studies, and theoretical calculations. Especially oxygenic photosynthesis has barely been explored beyond 5M NaCl (28% w/v). By applying a variety of biogeochemical and molecular methods we show that despite abundance of photoautotrophic microorganisms, oxygenic photosynthesis is inhibited in salt-crust covered microbial mats at saturation salinities, while rates of other energy generation processes are decreased several fold. Hence, the complete element cycling required for self-sustaining microbial communities only occurs at lower salt concentrations.

Ort, Datum: Bremen, 05.08.2021

<u>Versicherung an Eides Statt</u>

Ich, Marit Rianne van Erk
28203 Bremen
.   Matrikelnummer: 3244112

versichere an Eides Statt durch meine Unterschrift, dass ich die vorstehende Arbeit selbständig und ohne fremde Hilfe angefertigt und alle Stellen, die ich wörtlich dem Sinne nach aus Veröffentlichungen entnommen habe, als solche kenntlich gemacht habe, mich auch keiner anderen als der angegebenen Literatur oder sonstiger Hilfsmittel bedient habe.
Ich versichere an Eides Statt, dass ich die vorgenannten Angaben nach bestem Wissen und Gewissen gemacht habe und dass die Angaben der Wahrheit entsprechen und ich nichts verschwiegen habe.
Die Strafbarkeit einer falschen eidesstattlichen Versicherung ist mir bekannt, namentlich die Strafandrohung gemäß § 156 StGB bis zu drei Jahren Freiheitsstrafe oder Geldstrafe bei vorsätzlicher Begehung der Tat bzw. gemäß § 161 Abs. 1 StGB bis zu einem Jahr Freiheitsstrafe oder Geldstrafe bei fahrlässiger Begehung.

_____
Bremen, 05.08.2021